1st Faculty of Medicine, Department of Paediatrics
Charles University, Prague, Czech Republic

HEMOPROTEIN NITRIC OXIDE SYNTHASE IN *APLYSIA CALIFORNICA*

PhD thesis

MUDr. Michaela Buganová

Prague 2008

To my dear parents
To Mat and Pat

LIST OF ORIGINAL COMMUNICATIONS

This thesis is based on the following publications, which will be referred to in the text by capital letters (A-G). Impact Factors (IF) and citation frequency as at May 2008 are shown.

A. **Bodnárová M**, Martásek P, Moroz LL : Calcium/calmodulin-dependent nitric oxide synthase activity in the CNS of *Aplysia californica*: Biochemical characterization and link to cGMP pathways. J Inorg Biochem. 2005;99(4):922-8. IF= 2.423, 6 citations

B. Moroz LL, **Buganová M,** Sadreev R, Uvarov P, Martásek P, Panchin Yu: Cloning and localization of nitric oxide synthase in the CNS of *Aplysia californica.* (manuscript in preparation).

C. **Buganová M,** Sung Y-J, Ambron RT , Walters ET, Moroz LL: Nerve injury in *Aplysia* reduces nitric oxide synthase mRNA levels in neuronal somata while increasing mRNA levels in axoplasm. (Program No. 497.11. *2004 Abstract Viewer.* Washington, DC: Society for Neuroscience, 2004. Online.)

D. Jezzini SH*, **Bodnárová M***, Moroz LL: Two-color in situ hybridization in the CNS of *Aplysia californica.* J Neurosci Methods. 2005;149(1):15-25. *authors contributed equally to the publication, IF= 1.784, 7 citations

E. Walters ET, **Bodnárová M,** Billy AJ, Dulin MF, Diaz-Rios M, Muller M, Moroz LL: Somatotopic organization and functional properties of mechanosensory neurons expressing sensorin-A mRNA in *Aplysia* californica. J Comp Neurol. 2004 Mar 29;471(2):219-40. IF= 2.200, 14 citations

F. Heyland A, Price DA, **Bodnárová M**, Moroz LL.: Thyroid hormone metabolism and peroxidase function in two non-chordate animals. J Exp Zoolog B Mol Dev Evol. 2006 May 31. IF= 2.756, 1 citation

G. Lee DS, Flachsová E, **Bodnárová M**, Demeler B, Martásek P, Raman CS.: Structural basis of hereditary coproporphyria. Proc Natl Acad Sci U S A. 2005 Oct 4;102(40):14232-7. IF= 10.231, 8 citations

ABSTRACT

Nitric oxide (NO) plays a crucial role in neuronal signaling in a variety of eukaryotic and prokaryotic organisms. Nitric oxide synthases (NOS) are heme-containing monooxygenases that catalyze the oxygen dependent oxidation of L-arginine to NO and L-citrulline. The NO produced by NOS activity is a gaseous molecule that diffuses easily through membranes and acts inter or intracellularly. NO activates metal-containing enzymes, including soluble guanylate-cyclase (sGC) that increase levels of the messenger molecule cyclic 3,5-guanosine monophosphate (cGMP) (Arnold et al., 1977, Bredt and Snyder, 1989), which in turn mediate various pathophysiological or physiological functions in neurons. Nevertheless, many aspects of nitrergic neurons and NO function in the central nervous system (CNS) are unclear.

The aim of research described in this thesis was to characterize neuronal NOS, proteins metabolically linked to NOS and NO signaling pathways in the CNS of *Aplysia californica (Aplysia)*, a popular experimental model in cellular and system neuroscience. The biochemical characteristics of *Aplysia* NOS *(Ac*NOS*)* described here revealed its calcium-/calmodulin-(Ca/CaM) and NADPH dependence. A representative set of inhibitors for mammalian NOS isoforms also suppressed NOS activity in *Aplysia.* Polyclonal anti-rat nNOS antibodies hybridized with a putative purified *Ac*NOS (160 kDa protein) from partially purified CNS homogenates in Western blot studies. This thesis reports *Ac*NOS activity about six times lower than activity detected in the mammalian cerebellum (Bredt and Snyder, 1990), but was comparable with average values reported for the insect brain (Regulski and Tully, 1995, Elphick et al., 1993). Basal levels of cGMP production in *Aplysia* CNS were determined. Stimulation with NO donors and incubation with PDE (phosphodiesterase) inhibitors significantly increased cGMP levels. A specific inhibitor of sGC reduced basal cGMP levels by half and prevented a rise of cGMP in the presence of NO, confirming that NO may indeed function as molluscan CNS messenger, and that cGMP is one of its effectors.

The full length gene of *Ac*NOS was cloned and found to contain all of the conserved sites characteristic of a functional NOS in vertebrates. Nitrergic neurons in *Aplysia* CNS were mapped and localized; around 2% of all central neurons were shown to be nitrergic by means of *in situ* hybridization (ISH) and immunohistochemistry.

A two-color ISH protocol for whole-mount *Aplysia* ganglia was optimized for this thesis work and used to identify neurons and directly correlate functional and protein expression data The complete topographic organization of *Aplysia* mechanosensory neurons expressing neuropeptide sensorin-A was thus assembled.

The effect of unilateral pedal nerve crush on the level of expression of NOS mRNA in *Aplysia* pedal neurons was investigated, to look at the functional implications of NO in nerve regeneration and neuropathic pain. ISH and densitometry showed that the number of neurons and the intensity of neuronal staining following unilateral pedal nerve crush was significantly reduced in cells on the injured side, whereas a concurrent and significant increase of *Ac*NOS mRNA was detected in pedal nerve axoplasm by RT-PCR.

Part of the thesis work concentrated on the identification of another functionally important putative heme-containing enzyme, the *Aplysia* thyroid peroxidase gene (*Ac*TPO). After cloning and localization of *Ac*TPO in the *Aplysia* CNS, several transcripts from the thyroid hormone (TH) signaling pathway were identified suggesting the presence of TH-like signaling in molluscs as well.

The thesis theme of heme enzymes continued with an investigation of the protein necessary for the sixth step of the heme synthesis pathway, coproporphyrinogen oxidase (CPO). CPO was cloned from *Aplysia* and other organisms *(Chlorophlexus aurantiacus, E.coli)*. The cloned CPO genes were used to optimize protein crystallization conditions, leading to the first reported crystal structure of human CPO. The crystal structure enabled some elucidation of the catalytic mechanism of CPO and an understanding at the molecular level of the observed decrease in CPO enzymatic activity in certain pathological mutations of hereditary coproporphyria.

Key words: nitric oxide synthase, cyclic 3,5-guanosine monophosphate, *Aplysia californica*, CNS, heme protein, coproporphyrinogen oxidase, *in situ* hybridization

LIST OF ABBREVIATIONS

*Ac*NOS	*Aplysia* nitric oxide synthase
AG	abdominal ganglion
ALA	δ-aminolevulinic acid
AP	alkaline phosphatase
ATP	adenosin triphosphate
BG	buccal ganglion
BH4	tetrahydrobiopterin
BSA	bovine serum albumin
Ca/CaM	Calcium/Calmodulin
CB G250	coomassie blue
CG	cerebral ganglion
cGMP	cyclic guanosine monophosphate
CNS	central nervous system
COPRO	coproporphyrin
COPROgen	coproporphyrinogen
CPO	coproporphyrinogen oxidase
CYPOR	NADPH dependent cytochrome P450 oxidoreductase
DEA/NONOate	Diethylammonium (Z)-1-(N,N-diethylamino)diazen-1-ium-1,2 diolate
DMSO	dimethyl sulfoxide
D-NAME	N-nitro-d-arginine methyl ester
EDRF	endothelium derived relaxing factor
EDTA	ethylenediaminetetraacetic acid
EGTA	ethylene glycol bis(2-aminoethyl ether)-N,N,N'N'-tetraacetic acid
eNOS	endothelial nitric oxide synthase
EST	expressed gene tag
FAD	flavin adenine dinucleotide
FAM	flavin mononucleotide
FSW	filtered sea water
HAC	acetic acid
HCP	hereditary coproporphyria
HEPES	4-(2-hydroxyethyl)-1-piperazineethanesulfonic acid
IBMX	3-isobutyl-1-methylxanthine
iNOS	inducible nitric oxide synthase
ISH	*in situ* hybridization
L-NAME	N-nitro-l-arginine methyl ester
L-NIL DIHYDROCHLORIDE	L-N6-(1-iminoethyl)lysine dihydrochloride
MeOH	methanol
MFSW	Millipore filtered sea water
mRNA	messenger ribonucleic acid
$NAD(P)^+$	nicotinamide adenine dinucleotide (phosphate)
NADPH	nicotinamide adenine dinucleotide phosphate, reduced form
NBT/BCIP	nitroblue tetrazolium/bromochloroindolyl
NMDA	*N*-methyl-D-aspartate

nNOS	neuronal nitric oxide synthase
NO	nitric oxide
NONOate	1-Substitutes Diazen-1-ium-1,2-diolates, NO-Releasing Polymers Containing the [N(O)NO]- Group
NOS	nitric oxide synthase
ODQ	1H-[1,2,4] oxadiazolo [4,3-a] quinoxaline-1-one
PBG	deaminase porphobilinogen deaminase
PDE	phosphodiesterase
PeG	pedal ganglion
pGEX vectors	glutathione S-transferase gene fusion system
PlG	pleural ganglion
Psdn	peroxidasin
PVDF	polyvinylidene fluoride
RIA	radioimmunoassay
RT PCR	real time polymerase chain reaction
SDS	Sodium dodecyl sulphate
SDS-PAGE	Sodium dodecyl sulphate- polyacrylamide gel electrophoresis
S-ETHYL-ITU HBr	S-Ethylisothiourea hydrobromide
sGC	soluble guanylate cyclase
SNAP	S-nitroso-N-acetylpenicillamine
T3	3,3",5-Triiodo- L –thyronine
T4	L-Thyroxin
TBS	Tris buffered saline
TH	thyroid hormone
TLC	thin layer chromatography
TRIS-HCL	Tris (hydroxymethyl) aminomethane Hydrochloride
tRNA	transfer ribonucleic acid
TTBS	TBS buffer containing Tween 20
VC	ventrocaudal clusters
W7 HYDROCHLORIDE	N-(6-amino-hexyl)-5-chloro-1-naphthalene-sulfonamide hydrochloride

CONTENTS

LIST OF ORIGINAL COMMUNICATIONS 4

ABSTRACT 5

LIST OF ABBREVIATIONS 6

CONTENTS 8

AIMS OF THE THESIS 10

INTRODUCTION 11

CHAPTER I. 14

CLONING, LOCALIZATION AND CHARACTERIZATION OF NITRIC OXIDE SYNTHASE IN *APLYSIA CALIFORNICA* 14

BACKGROUND 14

Nitric oxide and its reactivity 16

Structure of NOS 18

NOS mammalian isoforms 21

Function of NO 22

NOS in molluscs- function and detection 25

Advantage of the *Aplysia* model 28

METHODS 30

Animals 30

Preparation of amplified cDNA. 31

Cloning. 32

In situ hybridization (ISH) 32

Dye injection 34

Measurement of NOS activity 34

cGMP assay 35

Western Blot 36

Nerve crush 36

RT-PCR 37

Iodine Incorporation and TH synthesis 37

TH measurements in sea urchin larvae and *Aplysia* haemolymph 38

Phylogenetic analysis 38

Data Analysis 39

RESULTS AND DISCUSSION I. 39

A. Characterization of *Aplysia*NOS 39

NOS present in the CNS of *Aplysia* is calcium dependent 39

PDE inhibitors and NO donors both increase cGMP in the CNS of *Aplysia* 41

Western blot and immunohistochemistry 42

C. Nerve injury in *Aplysia* reduces nitric oxide synthase mRNA levels in neuronal somata while increasing mRNA levels in axoplasm 52

D. Protocol for double chromophorelabeled in situ hybridization 55

Probe synthesis 55

E. Somatotopic Organization and Functional Properties of Mechanosensory Neurons Expressing Sensorin-A mRNA in *Aplysia californica* 59
Number and distribution of sensorin-A-expressing neurons 59
Somatotopic organization of sensorin-A expressing neurons 60
Functions of sensorin-A-expressing neurons 61
F. Cloning of an *Aplysia* hemoprotein,Thyroid Peroxidase, and Characterization of Thyroid Hormone-like signaling in *Aplysia* 63
Iodine incorporation and TH synthesis in *Aplysia* is inhibited by thiourea 63
Cloning of TPO from molluscs 64
CONCLUSIONS FOR CHAPTER I. 68

CHAPTER II. 70

COPORPHYRINOGEN III OXIDASE (CPO) ENZYME –CLONING, LOCALIZATION OF CPO IN *APLYSIA CALIFORNICA* AND CRYSTALLIZATION OF HUMAN CPO 70
Heme 70
Porphyrias 70
Metabolism of heme 72
CPO 74
METHODS II. 75
Animals 75
Cloning 76
In situ hybridization 76
Sequence analysis and phylogenetic tree construction 78
Protein Preparation and Crystallization 78
Structural Determination 79
RESULTS II. 80
Cloning of coproporphyrinogen oxidase gene from the cDNA of *Aplysia californica* 80
Crystallization of human CPO 83
The Protein Fold 83
CPO Functions as a Homodimer 84
CPO Structure Lacks a Transition Metal Center 84
The Active Site 85
Catalytic Mechanism 86
Structural Basis of Disease 86
CONCLUSIONS FOR CHAPTER II. 87

ABSTRAKT ČESKY (ABSTRACT IN CZECH) 87

ACKNOWLEDGEMENTS 88

REFERENCES 90

SUPPLEMENTS 99

Original publications A-G 99

NCBI submission file for AcCPX (CPX, AF510850.1, GI:30515681) 99

AIMS OF THE THESIS

The overall aim of this thesis was to characterize heme protein nitric oxide synthase (NOS) and proteins linked to metabolism and signaling pathway of NOS in the central nervous system of *Aplysia californica* (*Aplysia*), a popular experimental model in neurocellular and neuronsystem science, in order to better understand the role of NO as a physiological neuromodulator and its pathogenesis in a variety of neuronal disturbances and degenerative CNS afflictions. The specific aims of the thesis are listed below.

- to characterize the enzymatic activity of *Ac*NOS and provide biochemical evidence for NO-cGMP signaling in molluscs,(Paper A).

- to clone *Ac*NOS and map NOS-containing (nitrergic) neurons in the *Aplysia* CNS (Paper B).

- to investigate the effect of unilateral pedal nerve crush on expression levels of *Ac*NOS mRNA in *Aplysia* pedal neurons (Paper C), to determine NO contribution to nerve regeneration and neuropathic pain.

- to examine the topographic organization of sensorin-A expressing central neurons in the *Aplysia* mechanosensory system (Paper D), using ISH protocols, and utilizing other techniques (staining by nerve backfill, soma injection and electrophysiological methods) to define the spatial relationship between soma, peripheral axons and receptive fields.

- to optimize a two-color ISH protocol for use on whole-mount *Aplysia* ganglia, in conjunction with intracellular dye labeling to identify and directly correlate functional phenotype with specific gene expression (Paper E)

- to identify another functionally important, putative heme enzyme: *Aplysia* thyroid peroxidase (*Ac*TPO) by cloning and localization, and to assemble evidence of TH-like signaling in mollusks (Paper F).

- to clone the sixth protein from the heme biosynthetic pathway- coproporphyrinogen oxidase from *Aplysia* and to help characterize the crystal structure of its human counterpart (Paper G).

INTRODUCTION

Nitric oxide (NO) plays a crucial role in neuronal signaling in variety of eukaryotic and prokaryotic organisms. NO produced by nitric oxide synthase (NOS) enzymes is a gaseous molecule that diffuses easily through membranes and acts inter or intracellularly.

Unlike the classical neurotransmitters, NO does not require storage vesicles or exocytosis, and is produced on demand. Tightly regulated NO production is critical for its action ('right amount at the right time at the right place', (Kone *et al.*). NO is released in small amounts; it acts locally as a signaling molecule, activating mainly the second messenger cyclic guanosine monophosphate (cGMP) (Garthwaite et al., 1988), and further various of its effectors. Besides a cGMP activation role, NO has an electron pair that makes a radical molecule able to directly act on ion channels (Koh et al., 1995, Lynch, 1998, Summers et al., 1999)}; interact with, or nitrosylate proteins (Lipton et al., 1993, Stamler et al., 1992) and cyclic nucleotide gated channels (Savchenko *et al.*). The unregulated release of large amounts of NO leads to pathological conditions in sepsis, carcinogenesis and multiple sclerosis. Underproduction of NO also triggers pathological conditions including hypertension, artherosclerosis, septic shock and ischemic reperfusion injury.

In the human central nervous system (CNS), nitrergic (NOS containing) neurons account for roughly 1% of neurons in the cerebral cortex. NO is implicated in neural signaling, neurotoxicity (Huang et al., 1994), in modulating synaptic plasticity (e.g. long-term potentiation is considered a synaptic correlate of learning and memory, where glutamate binds to N-methyl-D-aspartate (NMDA) receptor and activates NOS), brain development (Okere and Kaba, 2000), visual processing (Cudeiro and Rivadulla, 1999), food and drinking behavior (Calapai et al., 1992), circadian rhytm (Watanabe et al., 1995), and in nociceptive neural responses (Mao, 1999). NO plays a role in neurological disorders such as Alzheimer's disease, Parkinson's disease, secondary neuronal cell death after trauma, demyelination disorders (multiple sclerosis). Increased NO levels are also seen in infections like meningitis, affecting the disruption of the blood-brain barrier (Brian et al., 1995, Zheng et al.), or in AIDS dementia (Adamson et al., 1996).

Three NOS isoforms have been described in mammals. An iNOS isoform is inducible (inducible NOS type II), and is synthesized in response to elevated cytokine production, inflammatory mediators etc. Two other NOS isoforms are constitutively expressed (neuronal type I, nNOS and endothelial type III, eNOS) and their activity depends on increased calcium levels. The presence of NOS and NOS-like proteins has been documented in different phyla, from bacteria and plants to mammals, but biochemical characterization of NOS in molluscs has been limited. This thesis concentrates on investigating nNOS in the mollusc *Aplysia* that is widely used to model human neurophysiology.

Nitric oxide synthases are hemoproteins that catalyze the production of nitric oxide and L-citrulline by oxidation of L-arginine. NOS functions as a homodimer. Each NOS monomer contains a N-terminal oxygenase domain binding heme, tetrahydrobiopterin and arginine; and a C-terminal reductase domain binding for FAD, FMN, and NADPH. The two domains are linked by a calmodulin (CaM) binding region.

Heme (protoporphyrin IX) with its bound iron, acts as a prosthetic group for a number of proteins ("hemoproteins") with a wide range of biological functions (including nitric oxide synthase, cytochrome P450, catalases, peroxidases, and guanyl cyclase enzymes). Heme biosynthesis, comprised of eight sequential enzymatic reactions, is one of the essential biochemical pathways of life, and occurs in all metabolically active cells. The porphyrin molecules are colored with unique photochemical features (the conjugated double-bond system makes porphyrins resonating compounds, with a typical dark red color and characteristic absorption spectra consisting of a major band near 400 nm, the Soret band, and multiple smaller bands (depending upon the solvent), between 500 and 630 nm).

A partial aim of this study from a biochemical point of view was to approach NOS not only as an enzyme, but also as a heme protein family member. In humans deficiency of individual heme biosynthetic enzymes can lead to the clinical presentation of specific porphyrias (see Table 2, page 71 of thesis). This thesis examines hereditary coporphyria caused by deficiencies of coproporphyrinogen oxidase. Defining the crystal structure of heme biosynthetic enzymes will enable the understanding of catalytic mechanisms of heme synthesis, and very likely of the molecular basis of porphyrias.

The overall aim of the thesis was to characterize neuronal nitric oxide synthase and proteins linked to metabolism and signaling pathway of NOS in the central nervous system of an opistobranch mollusc *Aplysia californica*. *Aplysia* is an effective model organism, widely used in the neuroscience field to study isolated cell interactions as well as for linking together neuronal function and complex behavior. The advantage of *Aplysia* as a model stems from the robustness and ease of identification of its neurons, as well as the relative ease of isolation and detailed characterisation of known neurons and neural networks linked to behavior. Cell culture techniques for isolated molluscan neurons allow researchers to (Lovell and Moroz, 2006) better define the external variables, and study transmitter – receptor interactions and the action of NO directly on isolated neurons. *Aplysia's* large and identifiable neurons have been used to study the molecular basis of learning and memory (Kandel, 2001, Brembs et al., 2004, Sharma and Carew, 2004), cellular correlates of motivational states (Teyke et al., 1991, Proekt and Weiss, 2003, Proekt et al., 2004), nerve injury and regeneration (Bedi and Glanzman, 2001, Sung and Ambron, 2004, Weragoda et al., 2004), and motor pattern generation and modulation (Cropper et al., 2004).

Aplysia data on isolated and reconstructed sensory-motor synapses is being extrapolated and linked to results from other species, from invertebrates to humans (Lovell and Moroz, 2006). During the writing of this thesis, genomic information representing 50-70% of the total *Aplysia* transcriptome was sequenced and published (Moroz et al., 2006), giving this project the chance to systematically use a genetic basis for better understanding biochemical characteristics and physiological functions in *Aplysia's* neural system.

CHAPTER I.

CLONING, LOCALIZATION AND CHARACTERIZATION OF NITRIC OXIDE SYNTHASE IN *APLYSIA CALIFORNICA*

BACKGROUND

Nitric oxide (NO) is an important signaling molecule proposed to play role in neuronal transmission, vascular tone modulation (Palmer *et al.*) and in the immune system (Hibbs et al., Stuehr et al.).

Amyl nitrite was used from 1867 to alleviate pain caused by angina pectoris (Sir Thomas Lauder Brunton and Conan Doyle credited Sherlock Holmes with that knowledge in *The Case of the Resident Patient*) on the basis of empirical rather than biochemical knowledge. During the World War I, doctors noticed that workers packing shells with nitroglycerine in ammunition factories had very low blood pressure. The observation led to the development of drugs containing nitroglycerine, but not an understanding of their mechanism of action.

Furchgott and Zawadski showed that when intact lengths of blood vessels were bathed in an organ bath and chemically stimulated, the blood vessels relaxed. If the endothelium of a vessel was absent or damaged, the smooth muscles of the blood vessel lost their capacity to expand. This showed that a previously unidentified substance must exist that regulated the tone of the smooth muscles of blood vessels, termed endothelium dependent relaxing factor, EDRF. The mystery was solved in 1987 when EDRF was identified as NO (Ignarro et al., 1987, Palmer et al., 1987, Bredt and Snyder, 1990), which aroused great scientific interest in the molecule. After identification of NO, the biochemistry of NO formation from the amino acid L-arginine to L-citrulline by the action of one of the enzymes from the family of nitric oxide synthase enzymes, was reported.

NO was demonstrated to be a neuronal messenger in the mammalian CNS (Garthwaite et al., 1988), released by the action of glutamate on the *N*-methyl-D-aspartate (NMDA) receptors. Nitric oxide was chosen as the cover story by Science for its "Molecule of the Year" in 1992. In 1998, the Nobel Prize for Medicine and Physiology was awarded to Furchgott, Ignarro and Murad for their contribution to unraveling the function of NO in the cardiovascular system.

It is now well characterized that endogenous NO is produced by nitric oxide synthases (NOS), a family of hemoproteins. Besides the three mammalian isoforms described below, NO synthesis has been documented in recent years among vertebrates, invertebrates, yeast, bacteria and plants, suggesting the evolutionary importance and hence conservation of nitric oxide activity across species. All known isoforms of NOS enzymes use NADPH as an electron donor and catalyze a five electron oxidation of guanidine group of L-arginine to yield NO and L-citrulline (Figure 1).

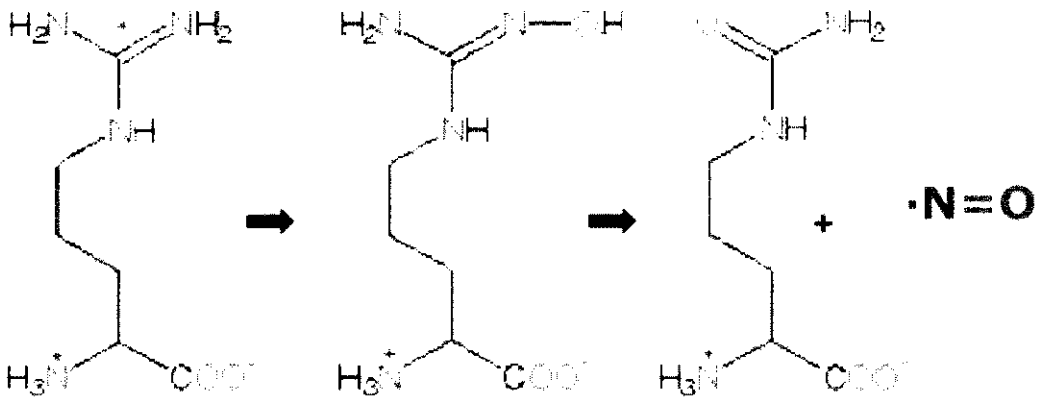

Figure1. Production of NO. NOS enzymes catalyze the formation of NO from L-arginine through two sequential monooxygenation reactions.

The reaction is similar to monooxygenation catalyzed by cytochromes P450. NOS functions as a homodimer, with each monomer consisting of a N-terminal oxygenase domain (NOSoxy) containing binding sites for heme and tetrahydrobiopterin (BH4), linked to a calmodulin-binding domain and a C-terminal reductase domain (NOSred), binding flavine adenine dinucleotide (FAD), flavine mononucleotide (FMN), and NADPH. Structurally NOS shares the heme and the reductase domain with cytochrome P450. Within this family two

groups of enzymes have been defined as Ca^{2+}-independent (inducible) and Ca^{2+}-dependent (or constitutive). Activities of constituvely expressed enzymes, including neuronal NOS (nNOS, NOS1) and endothelial NOS (eNOS, NOS3), are increased by rise in intracellular calcium. On the other hand inducible NOS (iNOS, NOS2) is expressed through activation of cytokines.

Nitric oxide and its reactivity

Nitric oxide is a colorless odorless gaseous diatomic molecule with one atom of oxygen and one of nitrogen. Although nitric oxide is a free radical it is relatively stable. The hexavalent oxygen atom and pentavalent nitrogen leave NO with one unpaired electron, which reacts mostly just with molecules that have an unpaired electron, which are typically other free radicals (O_2^- *-superoxide ion-*, OH. *-hydroxyl ion-*) or transition metals like heme iron (hemoglobin, myoglobin, cytochromes).

The physical properties of NO determine reactivity of NO. The half-life of NO, although still being debated, is very short, counted in milliseconds to seconds in biological tissues. NO is only slightly soluble in water. Due to its hydrophobicity and greater solubility in organic solvents, NO is enabled to concentrate in lipid reach areas, and rapidly diffuses across cell membranes in biological systems and mediate reactions through a vast number of its reactive forms and its targets such as haem groups, cysteine residues, iron and zinc clusters.

Under physiological conditions the reactivity of NO depends on its concentration (which is relatively low, less than 1 μM), and the main target of NO is soluble guanylyl cyclase (sGC) and other metal centers of metalloproteins such as hemoglobin, protoporphyrin and cytochrome P450 (Davis and Homsi, 2001, Wink et al.).

At higher concentrations such as during inflammatory reaction, when the inducible NOS is stimulated, NO is more prone to react with oxygen and nitrogen species and causes oxidative and nitrosative stress (Figure 2). Higher concentrations (nanomolar) of NO also compete with oxygen and reversibly inhibit cytochrome oxidase in mitochondria, thus affecting the respiratory chain and energy production in the cells (Beltran et al., 2002).

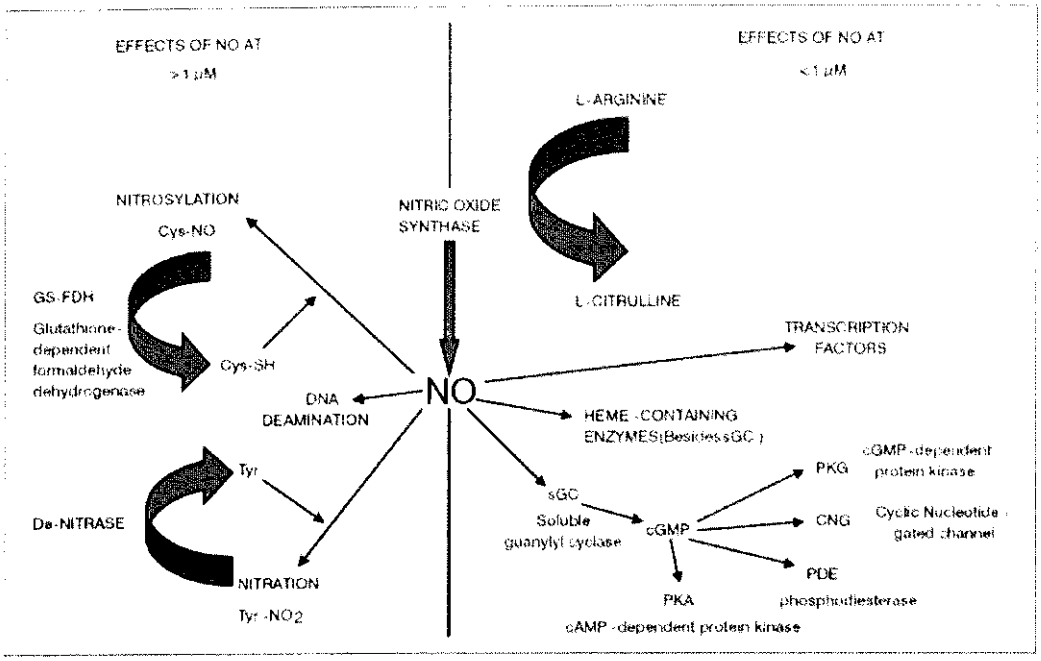

Figure 2. Summary of NO transduction and its effect at high and low concentrations. Adapted from: (Hanafy et al., 2001).

NO reacts with molecular oxygen to produce nitrogen dioxide (NO_2), or with superoxide to produce peroxynitrite (OONO-) (Figure 3); both are stonger oxidizing agents than NO. Peroxynitrite can further cause nitration by reacting with tyrosine (via addition of NO_2 to an aminoacid with a phenol moiety) to form nitrotyrosine, possibly affecting the protein function (e.g. in prostacyclin synthase this results in decreased activity, (Zou et al., 1998)).

Nitric oxide may autooxidize to produce N_2O_3 (dinitrogen trioxide), the main mediator of nitrosylation (formation of nitrosothiols from cysteines). S-nitrosylation (Stamler et al., 1992 Lipton, Nature, 1993) was shown to alter function of several proteins including transcription factors and signaling molecules (e.g. NF κB, (Klatt et al., 1999)).

NO targets a wide number of different systems that utilize nitric oxide as a regulatory factor. As a result pathological NO upregulation or downregulation affects many essential reactions in the normally regulated organism.

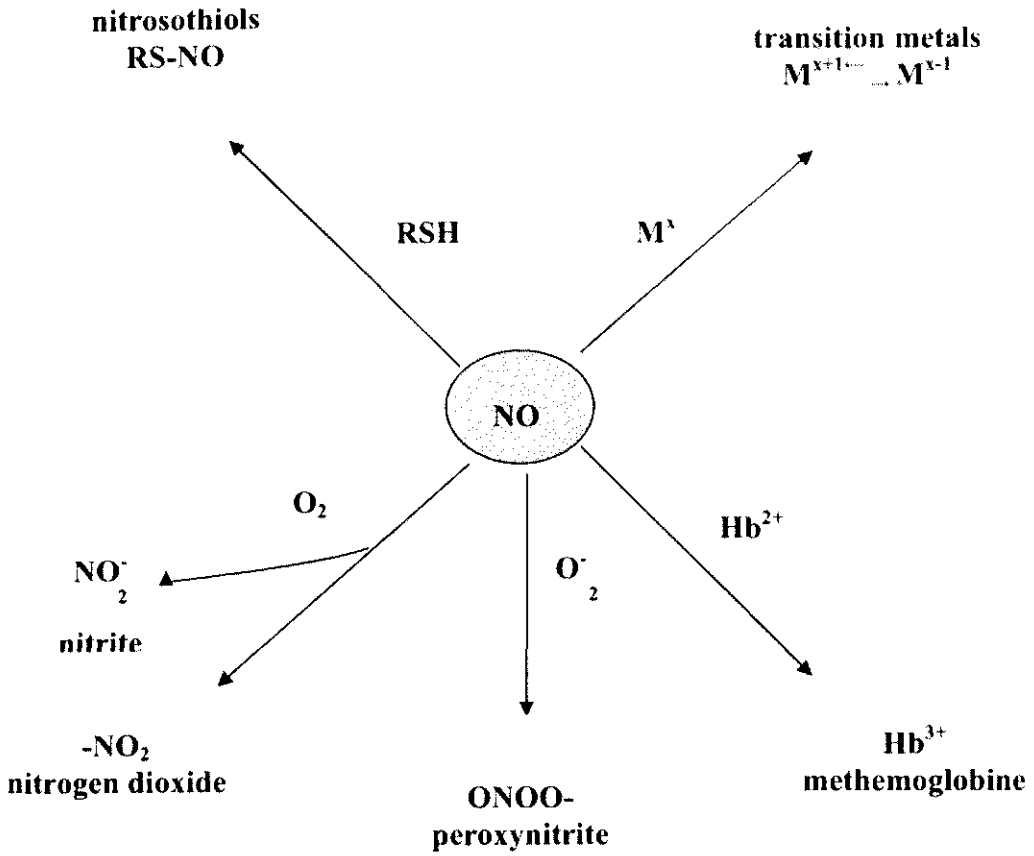

Figure 3. Common chemical reactions of nitric oxide. Nitric oxide (·NO) reacts with a variety of targets to mediate its effects. Nitric oxide reacts with transition metals (M) to alter their valence (x). An example of this reaction is the conversion of ferrous iron (Fe^{2+}) in the heme moiety of hemoglobin (Hb^{2+}) to ferric iron (Fe^{3+}), forming methemoglobin (Hb^{3+}). ·NO reacts at rapid rates with superoxide anion to form $ONOO^-$. In solution, ·NO reacts with O_2 to form the inactive metabolite nitrite (NO_2^-, whereas in the gas phase, ·NO reacts with oxygen to produce the oxidizing gas NO_2. ·NO also reacts with thiol groups (RSH) to produce nitrosothiols (RS-NO). The reactive pathway followed by ·NO is determined by the biochemical characteristics of the various components of the system. Adapted from: (Hart, 1999)

Structure of NOS

Functional NOS protein is formed as a homodimer. Each identical NOS molecule (subunit) contains an N-terminal oxygenase domain, a C-terminal reductase domain and a calmodulin-binding domain inbetween (Figure 4). NOS requires a set of cofactors- two flavine cofactors (FAD, FMN), NADPH, tetrahydrobiopterin and calmodulin (CaM)- for catalysis of the reaction

of L-arginine to L-citrulline and NO. The reaction is similar to monooxygenation catalyzed by cytochromes P450. Structurally, NOS isoforms share the reductase domain and heme moiety with P450 enzymes.

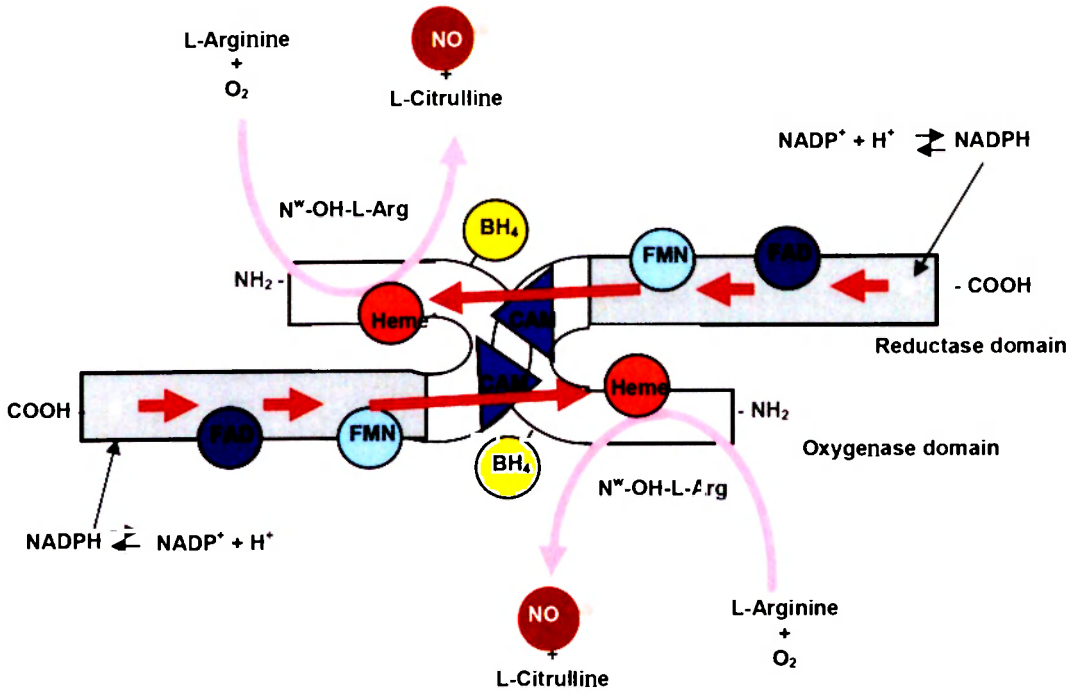

Figure 4. NOS dimer schematic structure, a representation of the NOS catalytic machinery. Oxygenase domain (white in the figure) represents the catalytic heme domain dimer which is the site of NO production and reductasedomain (grey) corresponds to the flavoprotein reductase domain from which the electrons are transferred to the heme domain. The locations of the heme prosthetic group, cofactor and substrate have also been shown. See nearby text for details. (Adapted from (Forstermann)).

1) The reductase domain: this domain contains the FAD and FMN moieties and a binding site for the electron donor NADPH that transfes electrons to the oxygenase domain of the opposite subunit of the dimer, and not to the domain on the same subunit to which it binds. The flavins enable the reductase domain to transfer electrons to artificial electron acceptors, being independent on the oxygenase domain (e.g. 2,6-dichlorophenol indophenol (DCIP), potassium ferricyanide ($K_3Fe(CN)_6$).

While the sequence homology of NOS reductase domain with P450 reductase domain is around 58% (Bredt et al., 1991), the dependence on calcium-calmodulin binding is unique (Abu-Soud et al., 1994). In the Masters lab it was shown that nNOS FAD binding domain has a very similar

folding to NADPH-dependent cytochrome P450 oxidoreductase (CYPOR)(Zhang et al., 2001). The NOS catalytic mechanism has been proposed on the basis of the CYPOR catalysis (Sheta et al., 1994).

2) Calmodulin binding: the binding of calcium- calmodulin (Ca++/CaM) is required for the activity of all the NOS isoforms and the flow of electrons from the reductase to the oxygenase domain (Abu-Soud et al., 1994). It detects changes in intracellular calcium levels, although its precise function is slightly different in each of the three isoforms.

When the CaM/Ca binds, the electrons are channelled from the NADPH through the flavine cofactors FAD and FMN to the heme domain. After the reduction of heme and binding of oxygen, with the assistance of BH4 the NO and citrulline are produced (Griffith and Stuehr, 1995).

3) The oxygenase domain (also called the heme domain): this domain contains a heme (iron protoporphyrin IX) prosthetic group and the binding sites for tetrahydrobiopterin (H4B) and physiological substrate L-arginine (McMillan and Masters, 1993). The oxygenase domain has a cysteine thiolate-liganded heme, as in cytochrome P450 and catalyses the conversion of arginine into citrulline and NO.

NOS isoforms contain the heme and the flavin mononucleotide and flavine dinucleotide as does cytochrome P450. Tetrahydrobiopterin as a cofactor is found only in NOSes. The crystal structure of the oxygenase domain of all three isoforms is similar with identical α/β folds (Raman et al., 1998). Due to the different character of substrates being catalyzed (NOS isoforms catalyze the reaction of a polar substance, while the substrates of P450 are non-polar), NOS and P450 have a very different substrate binding channel. Cytochrome P450 has a hydrophobic channel (to accommodate hydrophobic substances) while there is a strong polarity around the L-arginine pocket (Poulos et al., 1998). The structure of iNOS was published first (Crane et al., 1998), followed shortly after by the eNOS structure (Raman et al., 1998) and both documented the presence of one Zn atom bound to two cysteine residues from each monomer. A similar importance of Zn binding was shown in nNOS (Raman et al., 1998), possibly for stabilizing the enzyme structure.

NOS mammalian isoforms

NO in mammals is produced by at least three different isoforms of NOS, each encoded by a different gene. Activities of constitutive NOSes (eNOS and nNOS) under physiological conditions depend on calcium concentrations, which enable the binding of calmodulin and facilitate the flow of electrons for NO production. In contrast iNOS calcium-calmodulin is tightly bound, and is not influenced by fluctuating calcium concentrations.

nNOS: Human *nNOS* gene was the first to be cloned and sequenced. *nNOS* was detected on human chromosome 12. Neuronal NOS is constitutively expressed and is regulated by the dynamics of cytoplasmic Ca^{2+} concentration being increased through the NMDA subtype of a glutamate receptor (Figure 5). nNOS is mainly localized in the central and peripheral nervous system, but is also present in other tissues like skeletal muscle, macula densa, and placenta. Although soluble, nNOS is localized to the membrane through protein/protein interactions via a PDZ domain at the carboxy-terminal of the protein. The PDZ domain is circa 100 amino acids long and anchors proteins to cytoskeletal elements such as synaptic densities and related membrane associated guanylate cyclases (Tomita et al., 2001). The PDZ domain interacts with postsynaptic density protein PSD95 in the nervous system (binding the NMDA receptor as well) and with the syntrophin/dystrophin complex in the muscle. nNOS produces NO in picomolar amounts *in vivo*.

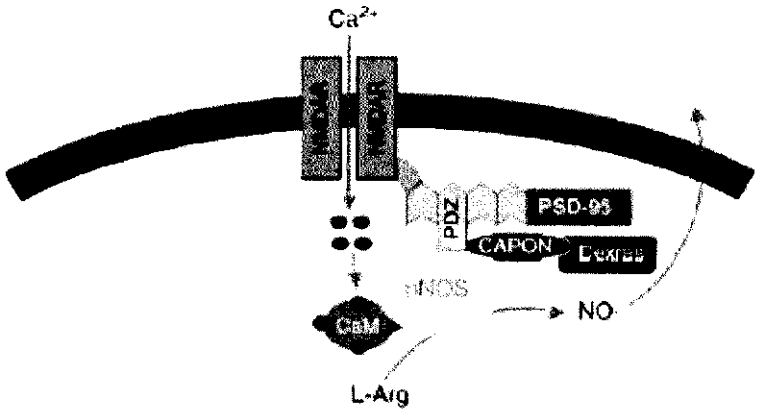

Figure 5. Interaction of neuronal (n) NOS with the *N*-methyl-D-aspartate (NMDA) receptor (NMDAR) and PDZ domain-containing proteins at neuronal synapses. nNOS binds via PDZ-PDZ domain interactions to postsynaptic density (PSD)-95, and PSD-95 associates with the NMDAR. The resultant ternary signal complex efficiently couples Ca2+ entry through the NMDAR to activation of nNOS. (Adapted from (Kone et al.)).

iNOS: The human *inducible NOS* (*iNOS*) gene was mapped to chromosome 17. *iNOS* is not constitutively expressed and can be synthesized *de novo* due to stimulation by various immunological stimuli, such as endotoxins and cytokines. iNOS is located primarily in the cytosol of macrophages and neutrophils, where it exerts its primarily cytotoxic function via peroxynitrite formation, DNA cleavage and deamination, nitrosation of proteins, and inhibition of heme proteins. Calmodulin is tightly bound to iNOS, and thus the Ca^{2+} levels have no effect on the enzyme. iNOS produces NO in nanomolar amounts *in vivo*.

eNOS: *Endothelial NOS* gene has been mapped to human chromosome 7. eNOS is constitutive, Ca^{2+}/calmodulin dependent, and acts as a vasodilator and inhibitor of platelet adhesion and aggregation. eNOS is expressed in endothelial cells, in cardiac myocytes (Balligand et al., 1993), and cardiac conduction tissue (Schulz et al., 1991). Endothelial NOS is activated through receptor-mediated activation of G proteins, by substances as catecholamines, vasopressin, bradykinin, histamine, ADP, serotonin (Boulanger and Vanhoutte, 1997), and by shear stress (Nishida et al., 1992). eNOS is targeted intracellularly for transport to the membrane due to post-translational myristoylation and palmitoylation of the N-terminus. The spatial distribution of eNOS plays its role in activation as well, placing the eNOS in plasmalemmal caveolae (Shaul et al., 1996) close to the G protein mediators and enabling inhibition of eNOS through interaction with caveolin (coat proteins in caveloae) (Garcia-Cardena et al., 1997). Unlike iNOS, eNOS is active at the calcium concentration found in resting endothelial cells (around 100nM) (Presta et al., 1997), documented on eNOS inhibitors vasoconstricting the vessels (Rees et al., 1989). NO produced by eNOS is in the picomolar range *in vivo*.

Function of NO

In mammals NO functions in a variety of biological processes including neurotransmission in the CNS and peripheral nervous system ((Bredt and Snyder, 1990); (Garthwaite et al., 1988), regulation of vascular tone (Moncada et al., 1988) and plays a role in anti inflammatory and defence mechanisms (Nathan, 1997).

The well documented effect of NO is through activating guanylate cyclase (sGC). sGC is a heme containing cytosolic protein. Activation of sGC by binding of NO to its heme domain converts GTP to cGMP, which is a second messenger that regulates many cell signaling events,

including activation of protein kinases, ion channels and phosphodiesterases (Hardman and Sutherland, 1969) (Figure 6).

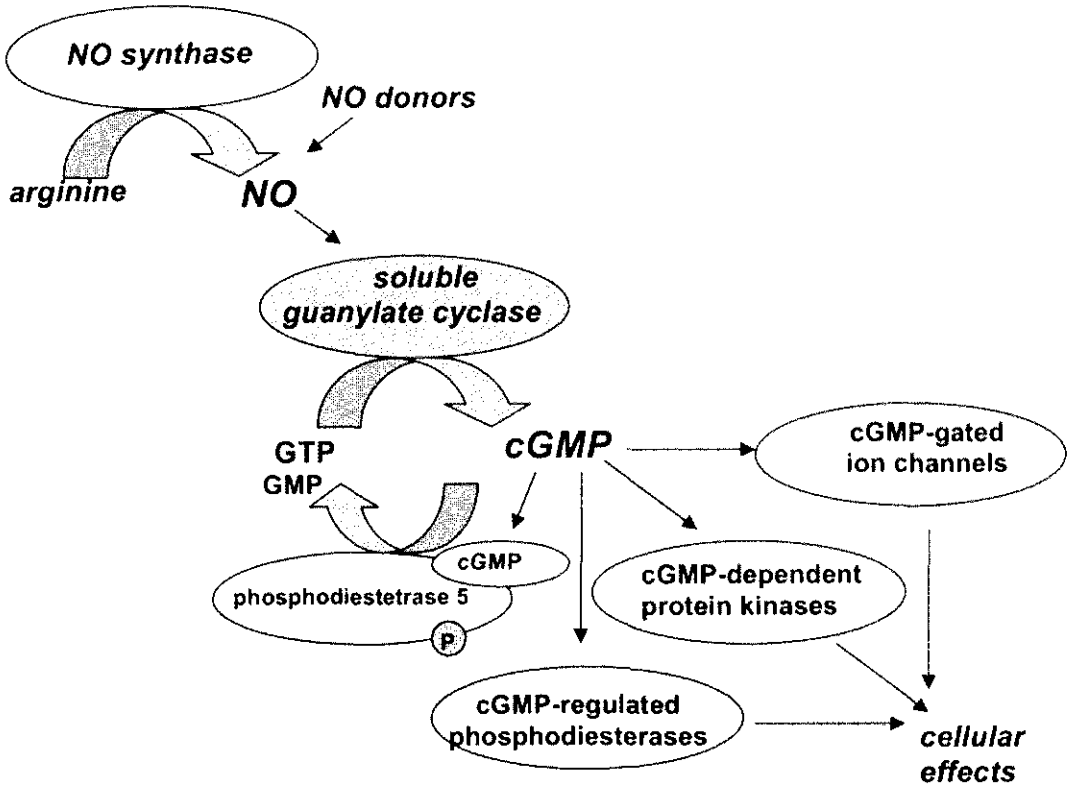

Figure 6. NO/cGMP signaling cascade. NO endogenously produced by NO synthases or released from exogenously applied NO donors activates NO-sensitive sGC and leads to increased synthesis of cGMP. This intracellular messenger in turn modulates the activity of cGMP-dependent kinases, cGMP-gated ion channels, and cGMP-regulated phosphodiesterases. These effectors are involved in the regulation of several physiological functions in the cardiovascular and nervous systems (modified after (Friebe and Koesling, 2003)).

NO in the nervous system: In the human CNS, nitrergic (NOS containing) neurons account for roughly 1% of neurons in the cerebral cortex. The population of nitrergic neurons is very heterogeneous as to their morphology and chemical characteristics. NO diffuses from the nitrergic neurons for a distance of 40-300 μm and acts on neuronal and non-neuronal cells. NO is implicated in neural signaling (Garthwaite et al., 1988), in modulating synaptic plasticity as a retrograde messenger. For example long-term potentiation is considered a synaptic correlate of learning and memory, glutamate binds to NMDA and activates NOS (Kandel, 2001). Inhibition

of NOS was documented to produce amnesia (Holscher and Rose), and to alter olfactory memory (Kendrick et al., 1997) and spatial learning (Bohme *et al.*). NO is also reported to play a role in brain development (Okere and Kaba, 2000), visual processing (Cudeiro and Rivadulla, 1999), food and drinking behavior (Calapai et al., 1992), circadian rhythm (Watanabe et al., 1995), and in nociceptive neural responses (Mao, 1999). A physiological function of NO was proposed in modulating release of neuroendocrine hormones. NO was shown to account for neurotoxicity (Huang et al., 1994), and inhibiton of nNOS was shown to reduce the infarct size, and reduce its toxic effects (Tominaga et al., 1993), more over the ischemic neuronal damage was attenuated in nNOS knock out mice (Huang et al., 1994). Nitric oxide levels are poorly regulated in several severe neurological disorders: Alzheimer's disease, Parkinson's disease, secondary neuronal cell death after trauma, demyelination disorders (multiple sclerosis) and levels of NO are increased in infections like meningitis, disrupting the blood-brain barrier (Brian et al., 1995, Zheng et al.), or in AIDS dementia (Adamson et al., 1996). NO has been shown to be involved in regulating apoptosis in neurons. Nitrergic nerves releasing NO in the peripheral nervous system (PNS) are also characterized as inhibitory non-adrenergic, non-cholinergic nerves (NANC) (Gillespie et al., 1989, Li and Rand, 1989), contributing to smooth muscle relaxation. Much attention in recent years has concerned the role of NO in penile erection, where the stimulated nitrergic neurons inervating the penile vessels and the corpus cavernosum lead to erection. Thus, a potent selective inhibitor of phosphodiesterase-5 (e.g. sildenafil (Bivalacqua et al., 2000)), prolongs the local action of NO by inhibiting cGMP deactivation. Impaired local production of NO can also lead to motility disorders in the gastrointestinal tract (e.g. oesophagial achalasia (Mearin et al., 1993), pyloric stenosis (Vanderwinden et al., 1992), Hirschprung's disease (Vanderwinden et al., 1993), diabetic gastroparesis (Takahashi et al., 1997). NO underproduction contributes to pathological conditions in the respiratory tract such as hyperreactivity and increased bronchial tone in asthma (Belvisi et al., 1995). In the vascular system nNOS contributes to local vasorelaxation and exerts regional cerebral blood flow control (Estrada and DeFelipe, 1998). Lack of nNOS in skeletal muscles is associated with pathological dystrophin (as in Duschenne muscular dystrophy (Chao et al., 1996)). Isoform specific nNOS inhibitors could play an effective role in alleviating the symptoms of many CNS and PNS afflictions related to NO dysbalance.

NO in the immune system: NO can be produced by a number of cells (macrophage-monocyte lineage cells, microglia, Kupffer cells) involved in immune responses. In particular cytokine-activated macrophages can produce concentrations of NO in order to kill target cells such as bacteria, parasites, viruses or tumour cells. NO-mediated cytotoxicity is often associated with the

formation of nitrosyl-thiol complexes in enzymes within the target cell. NO has been shown to kill cells by disrupting enzymes involved in the Kreb's cycle, DNA synthesis and mitochondrial function, so stimulation of iNOS has to be tightly regulated. Overstimulation of iNOS can be linked to the promotion of tissue injury in septic shock, bacterial and viral infections, autoimmune and inflammatory disorders (rheumatoid arthritis, Crohns disease, asthma, multiple sclerosis, systemic lupus erythematosus and glomerulonephritis). NO from iNOS also modulates both anti and pro-apoptotic effects in cell of the immune system (Rathmell and Thompson, 1999).

NO in vascular system: The endothelium plays a crucial role in regulating vascular tone. NO is one of the key vasodilatory substances (Furchgott and Zawadzki, 1980) through the activation of sGC and G-protein coupled receptors, and has been shown to inhibit smooth muscle cell proliferation, as well as monocyte adherence to endothelia (Kubes *et al.*), platelet adherence and aggregation (Radomski et al., 1991). Endothelial dysfunction observed in various pathological conditions such as atherosclerosis, hypertension, preeclampsia, hyperglycemia, adult respiratory distress syndrome (ARDS), pulmonary hypertension of newborns, erectile dysfunction and reperfusion injury can all be linked to the altered availability of NO.

NOS in molluscs- function and detection

In recent years NOS-like activity has been detected in bacteria (Chen and Rosazza, 1995, Choi et al., 1997, Hong et al., 2003, Adak et al., 2002), slime mold (Werner-Felmayer et al., 1994, Golderer et al., 2001), fungi (Ninnemann and Maier, 1996), plants (Cueto et al., 1996 1996, Delledonne et al. 1998). Invertebrate NOS has been documented in the brain of insects :manduca (Stengl and Zintl, 1996 locust, cricket, cockroaches Ott 1999, apis Muller 1994)); and in the brain of some crustaceans (Johansson and Carlberg); *Sepia officinalis* (Chichery and Chichery, 1994), crayfish (Lee *et al.*) *Loligo beekeri* (Kimura et al., 1997); *Pacifastacus* (Schuppe et al., 2001); *Gecarcinus lateralis* (Kim et al., 2004)) and several molluses (see below). Among nonmammalian animals, NOS has been shown to be present in birds (Lin and Leise, 1996), fish{(Laing et al., 1996, Saeij et al., 2000)).

Molluscan NO has been shown to participate in neurotransmission, and was shown to act as an orthograde (Jacklet, 1995) and retrograde messenger (Park et al., 1998), in modulation of neurotransmitter release (Meulemans et al., 1995) and in neuronal plasticity (Katzoff et al., 2002). NO plays an important role in activation of the feeding network in *Lymnaea* (Moroz et al., Park et al., 1998, Jacklet, 1995, Korneev et al., 1998); *Pleurobranchae* (Moroz and Gillette, 1996); *Aplysia* (Katzoff et al., 2002); in modulation of oscillatory dynamics due to odor stimulation (Gelperin *et al.*); in slug olfactory processing (Fujie et al., 2002) and in the inhibition of NOS disrupted neural processing of slime trail stimuli (Clifford et al., 2003). NO is implicated in modulation of locomotion (Moroz et al., 2000 2002), contribution to long term memory formation (Lewin and Walters, 1999), in learning (Lechner and Byrne, 1998), in conditioning (Teyke, 1996) and development (Lin and Leise).

Direct detection and localization of NO production is very cumbersome firstly because NO is a relatively small and volatile molecule. Secondly, being a radical molecule, nitric oxide easily reacts with a wide range of substances, accounting for its short half time. Thirdly, the levels of NO produced in vivo are low, ranging from nanomolar to picomolar values. Although several reports of a stable model for direct NO determination have been published in molluscs (NO sensitive electrodes (Meulemans et al., 1995, Moroz et al., 1996), EPR (Moroz et al., 1998), capillary electrophoresis with laser induced fluorescence –NO sensor (Kim et al., 2006), they are not being widely used due to above mentioned hindrances. The disadvantages of direct NO production are partially overcome by the indirect NO measurements, which lack specificity hence quantification of NO metabolites might not necessarily reflect production solely by NO, but from different sources as well. The indirect measurements of NO production that are widely used are: detection of NO degradation products like nitrates and nitrites (spectrophotometry with Griess reaction), measurement of the conversion of arginine to citrulline by NOS , or second messenger products (cGMP), and assessment of the degree of protein nitrosylation (nitrosylated proteins can be determined with HPLC, fluorimetric methods, gas chromatography, mass spectrometry).

To link the distribution of nitrergic cells with the NOS function in species other than mammals, histochemical techniques have been primarily engaged to identify NO releasing structures. The NADPH-diaphorase (NADPH-d) histochemistry in formaldehyde-fixed tissue, (Vincent and Kimura, 1992) for mammalian CNS (Vincent and Kimura, Hope et al., 1991),

provides an effective tool for localizing nitrergic cells in most life forms. This technique is resistant to fixation, and deactivates other NADPH-d reactive enzymes. However, the NADPH-d histochemistry is difficult to quantify, and is not necessarily specific for NOS, as several enzymes show diaphorase activity due to inappropriate fixation techniques (Wolf, 1997).

For immunolabeling in invertebrates, antisera against mammalian NOS and a universal anti-NOS antibody directed against a conserved peptide sequence in the reductase domain, have been previously reported. By using the NADPH-d histochemistry and immunohistochemistry, NOS has been localized from a few mostly unidentified neurons, to the CNS of many molluscan genera (*Aplysia californica*(Jacklet and Gruhn, 1994, Moroz, 2006), *Melibe leonine* (Newcomb and Watson, 2001), *Limax maximus* (Gelperin, 1994), *Helix pomatia* (Huang et al., 1997), *Pleurobranchaea californica* (Moroz and Gillette, 1996), 1997}, *Lymnaea stagnalis* (Moroz et al., 1993, Moroz et al., 1994), *Clione limacine* (Moroz et al., 2000). The pattern of NADPH-d biochemistry does not always correspond to the immunohistochemistry staining, which could be accounted for by a non-specific cross reactivity with other NOS-like proteins in invertebrates or yields poor results (Elphick et al., 1995).

Molecular biology has offered the next step in the possibility of identifyingNOS genes and utilizing NOS for *in situ* hybridization (ISH) in order to get a detailed description of the distribution of NOS containing neurons. ISH is very useful for analyzing low abundant transcripts, it is highly specific and sensitive, preserving the tissues and neuronal morphology, and it can be used on sections as well as on whole mount preparations.

A rough distribution of nitrergic neurons has been established in various molluscan brains, nevertheless there is a lack of evidence on the molecular, functional, and pharmacological characteristics of NO producing enzymes.

Advantage of the *Aplysia* model

NO signaling has been shown to serve several functions in the nervous system, but little is known about the physiology of individual nitrergic neurons. To address this issue it is necessary to identify and characterize individual NO releasing neurons. However, nitrergic neurons are cumbersome to isolate and identify in the mammalian brain.

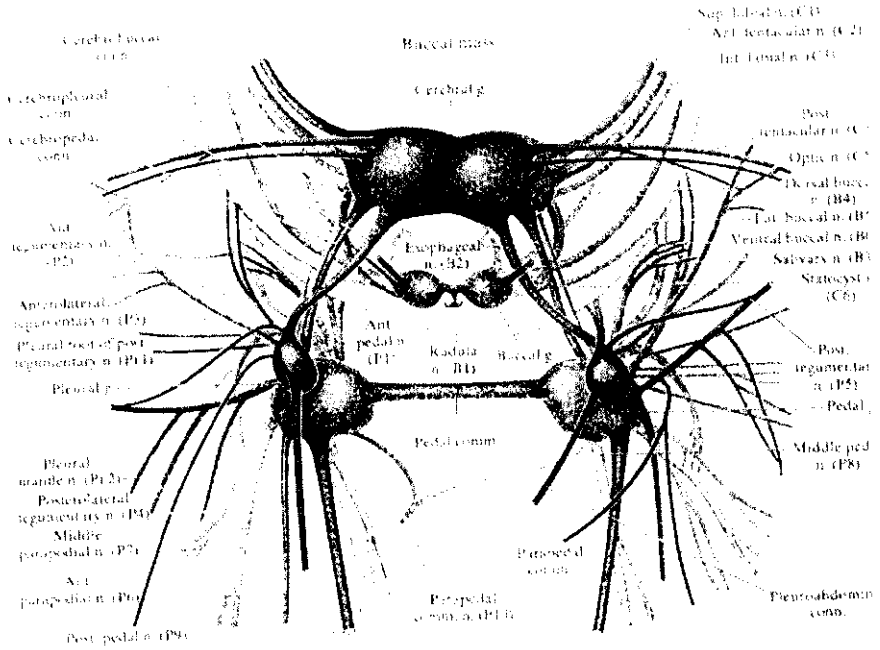

Figure 7. Schematic diagram of *Aplysia* CNS – showing the major ganglia (cerebral ganglia, buccal ganglia, pedal and pleural ganglia, abdominal ganglion) and nerves
(adapted from Jahan-Parwar from Behavioral Biology of *Aplysia*, Kandel)

In order to be able to further characterize neuronal nitric oxide synthese and nitrergic neurons, we chose a gastropod mollusc *Aplysia californica* (a giant marine slug), as a model system for several reasons. *Aplysia* is already a well characterized functional model in neuroscience, with widely studied behavioral patterns, and for learning and memory studies (Kandel, 1976, Kandel, 2001) (Figure 7). The large size of neurons that can range up to 500µm (Figure 8A,B), and a relatively low number of neurons in the CNS- only around 20.000 neurons-

are advantageous for research. Also important is the relative ease of accessibility to neurons that can be isolated and penetrated with multiple electrodes. *Aplysia* neurons are amenable to direct single-cell microchemical/microarray analysis (Moroz et al., 2000), and the identifiability of neurons from animal to animal or even between relative species is quite straightforward. *Aplysia* is a feasible model for linking biochemistry with genomic data and physiological function, because it has been extensively studied and the function of specific neurons within neural networks and their link to behavior has been described. For introducing chemical substances e.g. novel isoform-specific NOS inhibitors, *Aplysia* is valuable because 60% of body volume – haemolymph – is fully exchanged in 15 minutes. Very important in this genomic age is that the genome is being sequenced in the Moroz and Kandel labs and has already been partially published (Moroz et al., 2006).

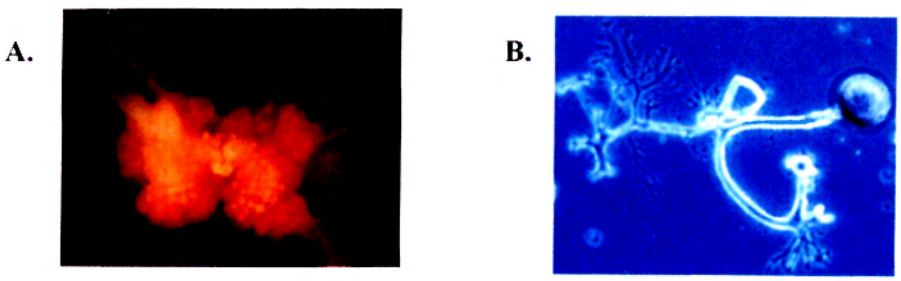

Figure 8. A. An exposed desheathed cerebral ganglia of *Aplysia californica*, depicting the individual neurons –dorsal view. B. An example of an isolated neuron in the media from the CNS of *Aplysia*.

METHODS

Animals

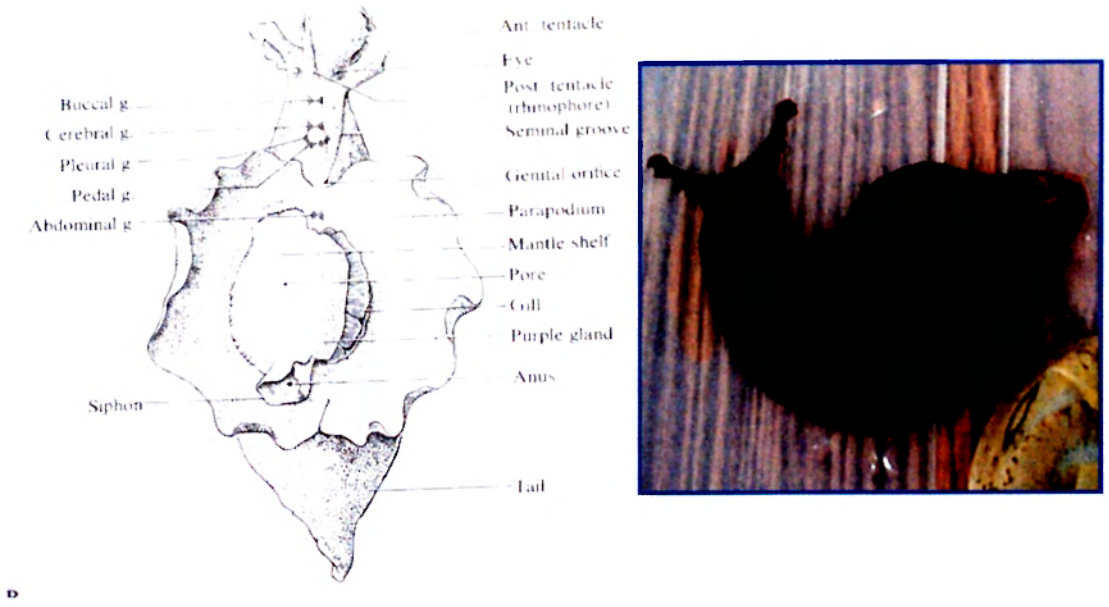

A. **B.**

Figure 9. A. Schematic view of *Aplysia* (Kandel, 1976)
B. Adult *Aplysia* californica (Figure courtesy of Prof.Moroz)

Aplysia californica (50-200 g) (Figure 9) were supplied by Marinus (Long Beach, CA), and the NIH-*Aplysia* Resource Facility (Miami, FL). Animals were kept in aquaria containing filtered sea water (FSW) at 15-18°C on a 12:12 light:dark cycle. They were regularly fed on live *Gracilaria* seaweed or dried seaweed laver. Prior to dissection, animals were anesthetized by injecting a volume of isotonic $MgCl_2$ (337 mM) equivalent to 50-60% of their weight. For testing thyroid hormone (TH) and TH metabolite effects on sea urchin development and metamorphosis we collected adult *Lytechinus variegatus* at Jupiter inlet Florida (26° 57' 28.41'' N; 80° 04' 40.03'' W) in October and November 2002 at low tide and from the Keys Marine Laboratory on Long Key, Florida in February and October 2003. Upon collection, animals were maintained in the laboratory at 21-24°C in flow-through seawater. We received developmentally

staged juvenile and adult *Aplysia* californica from the experimental hatchery in Miami (The University of Miami Experimental Hatchery of the Rosenstiel School of Marine and Atmospheric Science (RSMAS).

To obtain sea urchin larval cultures, we induced spawning by injection of 1ml 0.55M KCl solution in the gonad of adult urchins. Eggs were collected in MFSW (millipore-filtered seawater; 0.2μm) and sperm were collected dry. After eggs had settled, excess water was replaced once with fresh MFSW and a 1:10,000 solution of concentrated sperm was added. One minute later eggs were viewed under the compound microscope to check for fertilization envelopes. Fertilization success was estimated by counting the number of successfully fertilized eggs out of 50 randomly sampled eggs. We only considered the fertilization as successful if fertilization success was more than 95% (successfully fertilized/50). Larvae were maintained in gallon jars filled with 3.8 liter MFSW at a concentration of 1 larva/5ml MFSW. Hatching occurred within 12 hours after fertilization. Larvae were then fed 4 cells/μl of the unicellular alga *Rhodomonas lens* or 12 cells/ul *T-iso*. Water in cultures was changed every 2 days by reverse filtration (see Strathmann, 1987). Fresh food was added at each water-change.

Preparation of amplified cDNA.

cDNA library preparation was carried out exactly according to (Matz, 2002) (Method A) (Clonetech Kit) or as described in (Kacharmina et al., 1999) (Ambion Kit) from the whole CNS of Aplysia. In short: We amplified a representative cDNA sample from microamounts of starting material, a technique which was initially developed for amplifying cDNA from vertebrates (Chenchik et al., 1996) and which was further optimized for invertebrate animals. Specifically, we used an invertebrate-optimized adapter-primer set, which resolves background problems usually encountered with a conventional (human-optimized) oligonucleotide set, and makes it possible to carry out 5'- and 3'-RACEs starting from the amplified cDNA. Briefly, total RNA was extracted using the modified guanidine thiocyanate method (Chomczynski and Sacchi, 1987) performing all the procedures at neutral pH instead of originally suggested acidic pH. The first strand of cDNA was synthesized by SuperScript II reverse transcriptase with an oligo(dT) primer Trsa (5'-CGC AGT CGG TAC (T)13-3') . Then the second strand cDNA was synthesized using a kit (Marathon, CLONTECH Laboratories). The double-stranded cDNA was treated with T4 DNA polymerase, purified by ethanol precipitation and ligated to pseudo-double-stranded adaptor (the mixture of two complementary oligonucleotides, 5'-CGA CGT GGA CTA

TCC ATG AAC GCA ACT CTC CGA CCT CTC ACC GAG TAC G -3' and 5'-C GTA CTC GGT-3'). Then cDNA was purified with Qiaquick kit (Qiagen), and amplified using Advantage polymerase mix (CLONTECH Laboratories) under the following conditions: 94°C, 30 s; 66°C, 1 min; 72°C, 2 min 30 s; 15 cycles. The PCR primers for the amplification were Trsa and Lu4 (5' CGACGTGGACTATCCATGAACGCA 3'). As estimated from the cycling parameters of the amplification (Luk'ianov et al., 1996), the sequence complexity of the cDNA samples was no less than 0.3x109 for the whole CNS.

Cloning.

Cloning of *Ac*NOS was done from the amplified cDNA from the CNS of *Aplysia*. RNA isolation and preparation of amplified cDNA by reverse transcription-PCR was done as previously described (Matz et al., 2003). The original starting sequence of *Ac*NOS was done using degenerate primers 5' GGNTGYCCNGCNGAYTGGRTNTGG 3' and 5' NGGNGGRTCNCCRTTNCCRAANGT 3'. Cycling parameters for PCR were as follows: (30 s 94°C; 1 min 55° C; 2 min 30 s 72° C) x 30. 450 bp PCR product was cloned and sequenced, which showed a significant similarity to the corresponding fragments of known NOS. The sequence was extended by the RACE (Rapid Amplification of cDNA Ends, /Matz et al.}). We obtained the full-length cDNA Ac clone (GeneBank accession number: AF 288780) using terminal primers: Aca0 5' GGGAGACACCCG CAGCAGCC 3', and ApEND, 5' CTGGGCCGTCGCTGATTGGT 3'. Several full length clones of *Ac*NOS were isolated and sequenced. Sequencing was done by the Whitney Laboratory molecular core facility.

In situ hybridization (ISH)

In situ hybridization experiments were performed using whole mount preparations of the *Aplysia* CNS. Plasmid containing the full length *Aplysia* californica nitric oxide synthase (NOS) sequence (GeneBank accession number: AF288780) were subcloned in pGEM-T vector (Promega)(Sadreyev R. *et al,* 2002) in JM-109 E.coli cells. The plasmid was isolated, purified and sequenced to obtain the orientation of the gene. The plasmid was linearized with specific restriction enzymes (*NotI* for the anti-sense probe using T7 polymerase, *ApaI* for the sense probe with Sp6 polymerase) and used as a template for the preparation of specific anti-sense and sense digoxigenin-labeled RNA probes following the Roche protocol for probe preparation with DIG RNA labeling kit (Sp6/T7). Sense probes were used as nonspecific controls and in none of the

control preparations using sense probes (twelve preparations) produced any specific staining in the CNS under identical conditions and labeling protocols.

Our *in situ* hybridization protocol was based on previously published reports (Bogdanov Yu et al., 1996) with several modifications. Briefly, central ganglia were isolated from *Aplysia* and were treated with 1% protease IX (Sigma) in filtered sea water (FSW) for 45-60 minutes at 34°C, Followed by a 15 minute rinse in FSW. The ganglia were pinned to a Sylgard dish in FSW and fixed overnight in 4% paraformaldehyde in 0.2 M PBS (pH 7.2) at 4°C. Preparations were washed in PBS and connective tissues of the ganglionic sheath were carefully removed from all ganglia. The ganglia were washed in PTW (0.1% Tween 20 in PBS) 3 times for 5 minutes, followed by 10 minute incubation in increasing amounts of methanol (3:1 PTW:MetOH, 1:1, 1:3, and 100% MetOH) where the ganglia were preserved for up to one week. In most experiments, ganglia were transferred back to PTW in the same fashion by repetitive substitution of methanol by PTW (10 minute washes with 1:3 PTW/MetOH, 1:1, 3:1, PTW, followed by a 10 minute wash with 0.3% Triton in PBS, PTW for 5 min). After incubation with proteinase K (10 µg/ml) in PTW at room temperature for 1 hr, the ganglia were postfixed with 4% paraformaldehyde in PBS for 20 minutes at 4°C, and washed (2X, 5 min) in each solution of the following solutions: glycine (2mg/ml PTW), PTW, 0.1M triethanolamine hydrochloride (TEA HCl, pH 8.0), and anhydrous acetate (2.5 µl/ ml) in TEA HCL. The ganglia were then repeatedly washed in PTW. All subsequent steps were done with moderate shaking, including prehybridization in hybridization buffer (50% formamide, 5 mM EDTA, 5x SSC, 1x Denhardt solution (0.02% ficoll, 0.02% polyvinylpyrrolidone, 0.02% BSA), 0.1% Tween 20, 0.5 mg/ml yeast tRNA (GIBCO BRL)) for 6-8 hours at 55°C. Digoxigenin labeled full length RNA probes (2µl/ml) has undergone alkaline hydrolysis in order to yield shorter length probes for better penetration and were added to ganglia and incubated further for 10-12 h. Hybridization was followed by 30 min washing at 60°C in 50% formamide/ 5x SSC/ 1% SDS, then 50% formamide/ 2x SSC/ 1% SDS, then 0.2x SSC, twice for 30 min at 55°C. After 3 washes in PBT (1xPBS, 0.1%Triton x100, 2mg/ml BSA), ganglia were treated with 10% normal goat serum in PBT at 4°C for up to 90min and left overnight with 1: 1350 dilution of alkaline phosphatase-conjugated DIG-antibodies (Boehringer) in 1% goat serum in PBT at 4°C. Unbound antibodies were washed out in several PBT incubations at 4°C (at least 2-3 hours total). After two 5 min incubations in detection buffer (100mM NaCl, 50 mM $MgCl_2$, 100 mM NaCl, 100 mM Tris/Cl pH 9.5, 0.01% Tween 20, 1mM levamisol), NBT/BCIP color substrates (DIG Nucleic Acid Detection Kit, Boehringer) were added to detect the hybridized probes. At this stage ganglia were kept at 4°C in the dark with

periodic visual assessment of the staining intensity. Following the detection procedure (usually 30-60 minutes), ganglia were postfixed in 4% paraformaldehyde in methanol for up to 1 hour, and washed twice in 100% ethanol. Permanent preparations were produced by incubating ganglia in methylsalycilate and embedding in Permount (Fisher) on microscopic slides. Examination and analysis of staining was conducted on an upright Nikon Optiphot-2 or an Olympus SZX 12 dissecting microscope. Images were acquired with a Nikon Coolpix 4500 digital camera, and initially saved as JPEG files.

Dye injection

Sensory neurons were impaled with sharp microelectrodes filled with 4% LuciferYellow in 0.1% lithium chloride (LiCl). The same type electrodes had resistances of 5–9Ω when filled with 3M potassium acetate and ~25–40 Ω when filled with 0.1% LiCl. Dye was iontophoretically injected into sensory neurons for 25 min using a continuous train of −2 to −5 nA current pulses with a 600 ms interpulse interval and a 50% duty cycle. After injection ganglia were fixed by flooding the dish with 4% formaldehyde in PBS and left for at least 4 h, but not longer than overnight at 4°C. Following fixation the preparations were rinsed and desheathed as described above.

Measurement of NOS activity

Following dissection, ganglia were homogenized in approximately 5 vol. of buffer containing 25mM Tris-HCl (pH 7.4), 1mM EDTA, 10 mM EGTA with a tissue homogenizer on ice. The homogenate was centrifuged at 14,000x g for 5 min. at 4°C and the pellet was discarded. NOS activity was determined according to the method described previously (Bredt and Snyder, 1990). Briefly, homogenate was added into a reaction mixture containing L-[^{14}C]arginine (specific activity 0.30Ci/mmol, PerkinElmer), NADPH (10 mM), free calcium ions ($CaCl_2$, 6 mM), and TRIS-HCl buffer(50mM) at pH 7.4 with tetrahydrobiopterin (BH_4, 6μM), flavin adenine dinucleotide (FAD, 2μM) and flavin adenine mononucleotide (FAM, 2μM), where final volume was 50μl. Samples were incubated for 1 hour at room temperature. Reaction was terminated by addition of HEPES (50 mM) containing EDTA (5mM). L-[^{14}C]Citrulline was separated by passing through a 0,1 ml equilibrated cation-exchange resin and radioactivity of the flow-through was measured by liquid scintilation spectrometry in 6ml of scintillation coctail. Samples of rat cerebellum were analyzed simultaneously in all experiments as a positive control. Total protein content in the homogenates was determined by the Bradford method (Bradford, 1976).

The total NOS activity (in pmol/mg protein/min) was determined as the difference between the total activity L-[^{14}C]Citrulline in control samples and a reaction lacking homogenate. Other experiments were performed in the presence of 5mM W 7 (hydrochloride (N-(6-Aminohexyl)-5-chloro-1-naphthalenesulfonamide, HCl) a potent Ca/CaM-dependent phosphodiesterase inhibitor, from Calbiochem, San Diego, CA, USA) (Itoh and Hidaka, 1984), various concentrations of L-NAME (a competitive NOS inhibitor), or D-NAME (its less active enantiomer), 5 mM S-Ethyl-ITU hydrobromide (selective inhibitor of all vertebrate NOS isoforms, Alexis Biochemicals)(Garvey et al., 1994), 5mM L-NIL dihydrochloride (L-N6-(1-iminoethyl)lysine , iNOS inhibitor) (Moore et al., 1994), L-thiocitrulline 5mM (an inhibitor of nNOS and iNOS){(Narayanan and Griffith, 1994)) . Calcium independent activity was the activity measured in the incubation mixture lacking $CaCl_2$; chelating agent EGTA (10mM) was added to the media prior to all experiments. Student's *t*-test was used for statistical analysis of the observed differences. All data are presented as mean ±SEM values.

cGMP assay

Following dissection the *Aplysia* CNS was transferred into microcentrifuge vials (1.5ml, Eppendorf) with FSW for treatment with PDE inhibitors and NO donors. Central ganglia were incubated for 1 h with IBMX (3-isobutyl-1-methylxanthine, non-specific PDE inhibitor, from Calbiochem, San Diego, CA, USA)(Beavo et al., 1970) dissolved in DMSO (dimethyl sulfoxide, 1mM, from Fischer) at RT, and/or with 1H-[1,2,4] oxadiazolo [4,3-a] quinoxaline-1-one (ODQ, 1mM) (Garthwaite et al., 1995). The control group was incubated with 1% DMSO. Then the CNS was incubated for 10 min with NO donors SNAP (*S*-nitroso-*N*-acetylpenicillamine, dissolved in DMSO, 1mM) or with DEA/NONOate (Diethylammonium (Z)-1-(N,N-diethylamino)diazen-1-ium-1,2-diolate, 1mM){(Morley et al., 1993)). After incubation ganglia were transferred into a boiling acetate buffer (400 µl at pH 5.8, 0.5 M), and incubated for 3 min.at 100°C, then mechanically homogenized and spun at 13000xg for 10 min at 4°C {(Huang et al., 1998). The homogenate was diluted 10x in the acetate buffer and the cGMP levels were assessed using the RIA cGMP[^{125}I] assay from Amersham Biosciences following the manufacturer's protocol. Duplicate 100µl aliquots in glass tubes were prepared both from the standard and experimental vials. 100µl of antiserum and 100µl of tracer cGMP[^{125}I] were added into all assay tubes, vortexed thoroughly and incubated for 18 h at 4°C. Amerlex-M second antibody 500µl was added to each tube, vortexed thoroughly and incubated for 10 min. at RT. The antibody bound fraction was separated by centrifugation at 2500g for 10 min at 4°C, the

supernatant was discarded and the radioactivity of the pellet was determined in each tube by counting in a gamma scintillation counter. Total protein content in the homogenates was determined by the Bradford method (Bradford, 1976) and the readings were recalculate to fmol per µg of protein.

Western Blot

SDS-PAGE was performed as first described by Laemmli (Laemmli, 1970). 1-3 µg of the denatured protein was applied per lane to an SDS gel (10%T, 2.6%C) and separated in a Bio Rad mini-gel apparatus at 20 mA for about one hour or until the dye front approached the bottom of the gel. Gels were removed and either stained in coomassie blue or transferred to a PVDF membrane. Coomassie staining was performed for about 30 minutes at room temperature in a solution of 2% CB G250, 7.5% HAc, and 50% MeOH. Destaining was carried out in 7.5% HAc, 15% MeOH. Electrotransfer (Towbin et al., 1979) to a 0.2 µ PVDF membrane was performed in a Bio Rad Mini Trans-Blot apparatus following manufacturer's instructions. The transfer buffer was 24 mM TRIS, 19.5mM Glycine, pH9.2, and the running conditions were 100 volts for one hour. Detection was performed with a polyclonal antibody raised against rat neuronal NOS (rabbit) and visualized with alkaline phosphatase color reagent. Briefly, the membrane was blocked with 1% non-fat dry milk, 1% BSA, in TBS (20 mM TRIS/HCl, pH 7.4, 0.5 M NaCl) for one hour. The membrane was then incubated for one hour with a 1: 2-3000 dilution of antibody in TTBS (as TBS, plus 0.05% Tween 20). After extensive washing in TTBS, goat anti-mouse IgG alkaline phosphatase conjugate (ZYMED, 81-6522) was used as a secondary antibody, again for one hour. Visualization was accomplished by gentle rocking in NBT/BCIP reagent.

Nerve crush

After injecting isotonic $MgCl_2$ solution (equivalent to about 30% of body weight) with the animal suspended in a chamber containing FSW a small incision was made in the skin to expose the pedal ganglia. Peripheral left or right pedal nerves were crushed using fine forceps at a distance of approximately 1 cm from the pedal ganglion The incision was sutured immediately after all the ipsilateral peripheral nerves from the pedal ganglion had been crushed (Walters et al., 1991).

RT-PCR

cDNA made from each sample was used to amplify specific fragments by PCR (40 cycles), using specific primer sets for the following: (1) neuronal nitric oxide synthase (NOS) (GenBank accession numberAAK83069), nt 3610-4049; (2) SN-specific neuropeptide sensorin A (GenBank accession number X56770), nt 43-331; (3) beta-thymosin (GenBank accession number AF454398, nt 61-195. All the reactions were assembled, amplified, and analyzed at the same time.

Iodine Incorporation and TH synthesis

We exposed larvae at the developmental stage when adult spicules had formed (see also above) for 8 hours in 12 well plates to experimental treatments. Prior to this exposure we cultured larvae for 24 hours in the complete absence of food to drain the stomachs from any algal food. We placed 50 randomly chosen larvae into each well, containing 4ml of solution (10^{-3}M thiourea and the buffer-only control respectively). All solutions were made up in SW^{125} (MPFSW with I^{125} at 51937 dpm; Carrier free specific activity of I^{125} was 642.8GBq/mg). For each treatment we used 6 wells. After the exposure, larvae from three wells were pooled together in one test tube resulting in two independent replicates per treatment (150 larvae per replicate). Specimens were washed 5 times with fresh MFSW until the radioactivity in the supernatant was below 30dpm (counted on ssMPD instrument see below). Between each wash, larvae were centrifuged at 1980g for 3 minutes and kept on ice. *Aplysia* juveniles were processed in a similar way except that we used 10^{-2}M thiourea in the inhibitor treatment.

To test whether I^{125} that the larvae had incorporated was built into T4, we prepared samples for thin layer chromatography (TLC). We added 1ml of ice cold MeOH to each sample after the sample was counted [samples containing I^{125} were counted on a ssMPD instrument (BioTraces, Inc., Herndon, VA) in standard mode. In standard mode, digital signal processing is used to distinguish the I^{125} decay specific characteristics from those of background events to give a background equivalent to 5 DPM of I^{125} with about 45% efficiency] and let it stand at 4°C over night. After vortexing all samples at full strength for 2 minutes we centrifuged them at 1980g for 10 minutes and collected the supernatant. Then we spiked the samples with 100µl non-radioactive 10^{-4}M T4 (thyroxine; Sigma-Aldrich T-1774) and T3 (3,3",5-Triiodo- L –thyronine; Sigma: T2877) and then concentrated in a speed-vac to complete dryness. The dry pellet was redissolved in 30µl 0.01N NaOH. Note that usually not all the salt crystals redissolved. All 30ul

(excluding the crystals) were loaded on a TLC plate (Whatman LK5D silica gel 150A with fluorescence marker; Whatman #4851-840) and run for 1.5 hours in a 2-methylbutanol/*t*-butyl alcoholy/25%NH3/acetone, 7:14:14:56, v/v solvent. We visualized the cold T4 and T3 markers under UV light on a BioRad™ Fluor-S MultiImager system and radioactive bands on a Molecular Dynamics™ Phosphorimager SI. Overlaying the UV image with the one from the phosphor imager allowed us to compare the radioactive bands to our TH standards.

TH measurements in sea urchin larvae and Aplysia haemolymph

We collected *Aplysia* haemolymph samples and sea urchin larval samples (40 larvae per sample). In case samples were not immediately processed we kept them at -80°C. Note that samples were never kept longer at -80°C than 2 months. Samples were defrosted on ice, and 5 volumes of 100% ice-cold MeOH was added. Extraction was done at 4°C overnight. We then centrifuged samples at 3000rpm for 10 minutes at 4°C. We decanted the liquid upper phase and kept the pellet for protein analysis. The upper phase was brought to complete dryness in a Speed-Vac and then resuspended in 50ul 0.01N NaOH. The pellet was redissolved in 100µl 1N HCl at 60°C for one hour and then vortexed at full strength for 1 minute per sample.

For TH analysis we used the ELISA KIT (Total Thyroxine (Total T4) ELISA Kit Alpha Diagnostic International, Inc.; TX, USA) following the manufacturer's instructions. Note that in addition to the standards provided in the kit we used our own standards made up in 0.01N NaOH for better comparison. For Protein analysis we used Pierce micro BCA kit as per manufacturer's instructions.

Phylogenetic analysis

The alignment was done using ClustalX (EBI European Bioinformatics Institute (Oxford, United Kingdom) (Thompson et al., 1997) with default parameters, all gaps were removed manually in GeneDoc prior to tree construction. Sequence analysis and phylogenetic tree building was done in the program TREEPUZZLE (http://www.tree-puzzle.de) with the default parameters and 10,000 iterations of the maximum likelihood algorithm. The tree itself was drawn with Treeview. The conserved domains were confirmed using Swissprot and Prosite databases (for further details see methods in attached paper E).

Data Analysis

Data were organized and analyzed in Excel and SPSS. Statistical comparisons between the experimental treatments and the controls were done using Student's t-test, ANOVA with simple contrast or MANOVA. For all analyses we used SPSS. Results are presented as: mean difference (treatment value minus control value) ± one S.E.; p-value. If the mean difference is positive this means that the value in the experimental treatment was larger than the value in the control. All p-values are from null hypotheses testing that the mean difference mentioned above equals 0. Information on *Aplysia* ESTs was derived from the *Aplysia* neuronal transcriptome (Moroz , unpublished data). EST and genomic information from the sea urchin *Strongylocentrotus purpuratus* was derived from NCBI.

RESULTS AND DISCUSSION I.

A. Characterization of *Aplysia*NOS

Our goal was to characterize NOS from *Aplysia*. We examined the effect of calcium chelators and cofactors on NOS from the CNS of *Aplysia* and tested well known mammalian, isoform-specific NOS inhibitors on *AcNOS*. The connection to functional importance was tested by assessing the NO induced cyclic guanosine monophosphate (cGMP) upregulation, with or without the presence of phosphodiesterase inhibitors. Some pharmacological evidence, together with an effect on evoked excitatory postsynaptic potential (EPSPs) for signaling mediated by NO via cGMP in the metacerebral cells (MCC, a pair of serotonergic modulatory neurons in the cerebral ganglia) of *Aplysia* has been already provided by Jacklet, 1998.

NOS present in the CNS of Aplysia is calcium dependent

The relative NOS activity and the role of cofactors in the CNS of *Aplysia* is shown in Figure 10 as an L-[14C]arginine/L-[14C]citrulline conversion. The production rate of L-[14C] citrulline from homogenized ganglia was 22.2 ± 4.0 pmol/mg of protein/min. Importantly, Figure 10 illustrates that *Ac*NOS activity was shown to be Ca-dependent; the documented values for Ca-

free conditions in the media containing EGTA were below 40% of the control NOS. Exclusion of NADPH from the reaction caused a reduction in *Ac*NOS activity to less than 35%. Addition of W-7 hydrochloride, a Ca/CaM-dependent phosphodiesterase (PDE) inhibitor, also significantly reduced L-[14C]citrulline production to less than 60%.

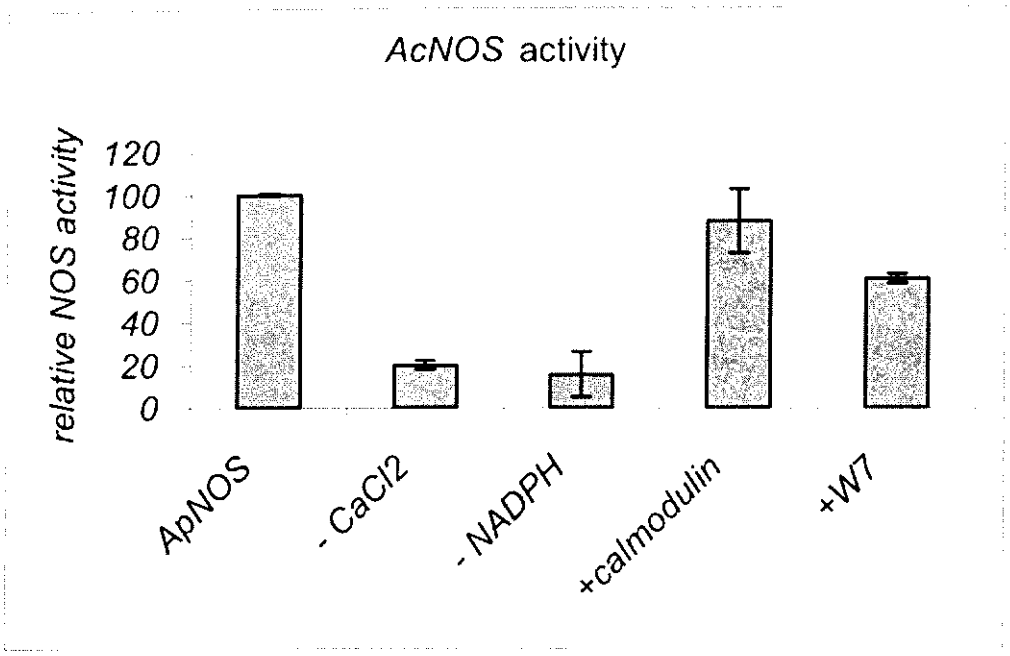

Figure 10. Co-factor dependence of *AcNOS*. Relative NOS activity is shown as a percentage of *AcNOS* activity (L-[14C]arginine/L-[14C]citrulline conversion in homogenates of the CNS of *Aplysia*). Contr, control conditions with all co-factors; _CaCl2, without CaCl2; NADPH, without NADPH; in the presence of calmodulin (+CaM); +W7, in the presence of 5 mM W 7hydrochloride (a potent Ca/CaMdependent phosphodiesterase inhibitor). Student's t-test was used for statistical analysis of the observed differences. Data are the mean of three experiments ±SEM values. See additional details in the text.

The effects of vertebrate isoform specific NOS inhibitors on *Aplysia* NOS were studied and the most potent inhibitor proved to be L-thiocitrulline (an inhibitor of mammalian nNOS and iNOS) which reduced theNOS activity by 95% ($P < 0.005$). All other tested NOS inhibitors caused a significant reduction in L-[14C]citrulline production: S-Ethyl-ITU hydrobromide (a selective inhibitor of all vertebrate NOS isoforms) by 85% ($P < 0.050$) and L-NIL dihydrochloride (iNOS inhibitor) by 78% ($P < 0.05$). The competitive NOS inhibitor L-NAME suppressed the NOS activity by almost 60%.

PDE inhibitors and NO donors both increase cGMP in the CNS of Aplysia

The cGMP levels from the RIA cGMP[125I] assay are shown as converted per 1 lg of total homogenized protein (Figure 11). The basal level of cGMP in the CNS was 44.47 fmol/µg. Incubation with the NO donor DEA/NONOate (1 mM) increased the cGMP activity almost 3.5 times, whereas incubation with non specific PDE inhibitors increased the cGMP levels 26 times. Following 1 h incubation with IBMX (1 mM) the increase of cGMP was 58–61 times higher compared with the basal level of cGMP. Further, selective inhibition of soluble guanylyl cyclase with ODQ (1 mM) incubated simultaneously with the NO donor DEA/NO (1 mM) even reduced the cGMP activity compared with basal cGMP levels. The co-incubation of ODQ, DEA/NO and IBMX still kept the cGMP activity 2.4 times below normal.

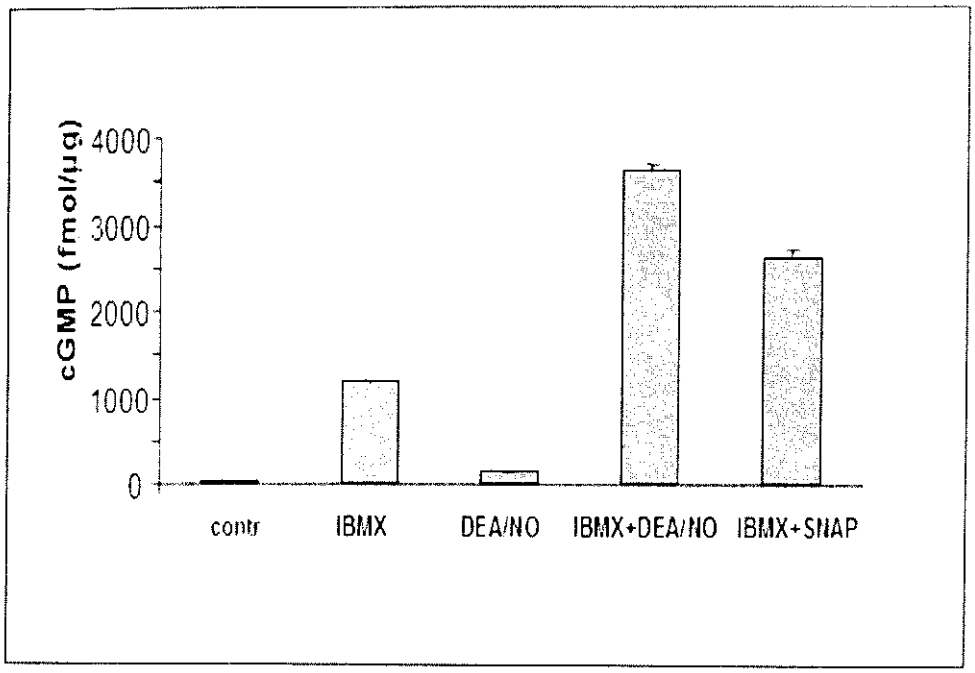

Figure 11. Pharmacology of *AcNOS*. Relative NOS activity is shown as a percentage of L-[14C]arginine/L-[14C]citrulline conversion in the presence of several inhibitors of mammalian NOSs. Contr, control conditions with all co-factors; + L-NAME, in the presence of 500 IM L-NAME (a competitive NOS inhibitor); + D-NAME, in the presence of 500 IM D-NAME (less active enantiomer of L-NAME), + L-NIL, in the presence of 5 mM L-NIL dihydrochloride (iNOS inhibitor); +thiourea, in the presence of 5 mM S-Ethyl-ITU hydrobromide (selective inhibitor of all vertebrate NOS isoforms); and with 5 mM L-thiocitrulline (an inhibitor of nNOS and iNOS).

Western blot and immunohistochemistry

(Figure 12). Partially purified *Ac*NOS run on SDS-PAGE gel, then reblotted and hybridized with a preadsorbed polyclonal rabbit anti-rat nNOS antibody showed a clear band around 160 kDa. A similar immunopositive band at 150 kDa was detected in our control rat cerebellum homogenate.

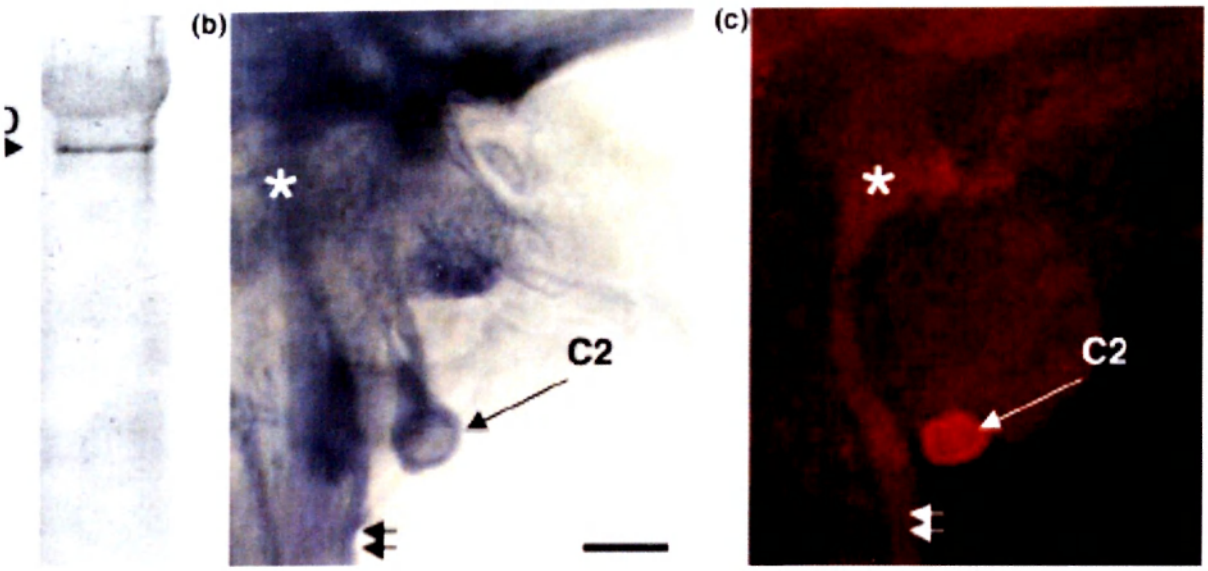

Figure 12. Western blot and immunostaining in the CNS of *Aplysia*. (a) Partially purified *Ac*NOS is from the CNS cross reacted with a preadsorbed polyclonal antibody to rat neuronal NOS and is recognized as a protein with molecular mass of cca 160 kDa (a). (b) NADPH-diaphorase histochemistry in the lateral part of the cerebral ganglion (E-cluster area); (c) NOS immunoreactivity with rat polyclonal NOS antibodies reveals similar patterns of labeling in the same region of the cerebral ganglion. Large arrows in (b and c) indicate the position of the identified neuron (C2) also know to be nitrergic and located in this area of the cerebral ganglion. Small arrows mark specific labeling in nerves and (*) point out the staining in ganglionic neuropil.

In this study we documented that functionally active NOS is present in the CNS of *Aplysia californica* and for the first time it is shown to be calcium dependent. *Aplysia* NOS shares common enzymatic characteristics with constitutive mammalian and insect neuronal NOS (Bredt and Snyder, 1990) as a calmodulin and NADPH dependent enzyme. Thus, the observed Ca-

dependence of *Aplysia* NOS confirms an earlier hypothesis that the rise of intracellular Ca^{2+} (either following activation of transmembrane Ca-channels or from intracellular stores) might act as a physiological regulator of NO synthesis in the molluscan CNS. In this repect, *Ac*NOS was similar to the NOS described in two representatives of pulmonate molluscs, *Lymnaea stagnalis* (Elofsson et al., 1993) and *Helix pomatia* (Huang et al., 1997). Interestingly, in *Helix* the level of NOS activity was around 13 times higher than in *Aplysia*, and even three times higher than in the mammalian cerebellum. However, in another marine opisthobranch mollusc, *Pleurobranchaea californica*, NOS activity was about two magnitudes lower (Moroz and Gillette, 1996) than reported here and was shown to be Ca-independent but calmodulin-dependent. Such substantial variations are likely to be related to ecology and the overall metabolic activity of these molluscan species as well as the possible presence of more than one NOS isoform. These issues need to be investigated in the future. NOS activity measured in *Aplysia* was around six to seven times lower than the activity detected in the mammalian cerebellum (Bredt and Snyder, 1990), but it was comparable with the average values reported for the insect brain (Elphick et al., 1993, Regulski and Tully, 1995). Yet, regions of the insect brain involved in chemosensation and known to be enriched with NOS containing elements express 10–20 times higher levels of NOS activity than we detected in *Aplysia* (Muller, 1994, Elphick et al., 1995). The pharmacological profile of *Aplysia* NOS was similar but not identical to NOS described for other species. The *AcNOS* showed closest similarity to mammalian neuronal NOS, although selective inhibitors of two other mammalian isoforms (eNOS and iNOS) had a significant suppressive effect as well. L-thiocitrulline was found to be the most potent inhibitor of *Ac*NOS and suppressed the relative NOS activity to a level of less than 5% of its control value, while the widely used competitive NOS inhibitor L-NAME was less effective. There is relatively little known about the structure of NOS-related proteins in molluscs. For example, partially purified NOS protein from *Aplysia* CNS displayed a band with molecular mass of approximately 160 kDa and a very faint band around 175 kDa. The shorter band is comparable in size with the 150 kDa of denatured rat nNOS protein (Stuehr and Griffith, 1992). The molecular mass of insect NOS protein was around 130–155 kDa (Elphick et al., 1993, Regulski and Tully, 1995), but, surprisingly, the immunoreactive NOS protein in the mollusc *Helix pomatia* with the highest reported enzymatic activity showed only a band of 60 kDa (Huang et al., 1997). The fact that NO induces cGMP synthesis and immunoreactivity through activating soluble guanylyl cyclase has already been shown (Southam and Garthwaite, 1991, Schmidt et al., 1993, Arnold et al., 1977, Aonuma, 2002) for many species including some molluscs (Koh and Jacklet, 2001, Koh and Jacklet, 1999, Fujie et al., 2002).

However, direct biochemical measurements of soluble guanylyl activity in molluscs has been performed only on a representative of land pulmonates, Helix pomatia (Huang et al., 1998). Here, we determined the basal levels of cGMP production in the CNS of *Aplysia* and showed that it significantly increased following stimulation with NO donors (>3-fold), and incubation with PDE inhibitors (>20-fold). Importantly, a specific inhibitor of soluble guanylyl cyclase (ODQ) reduced by half the basal level of cGMP in the CNS of *Aplysia* and prevented the rise of cGMP by NO. These results suggest the substantial tonic production of NO in the intact CNS and its link to cGMP pathways. In summary, we directly showed that enzymatically active Ca-dependent NOS is present in the CNS of *Aplysia* and that it can act via cGMP signaling. Biochemical and pharmacological characterization of these two signaling pathways provide a foundation to further examine their interactions and functional role in neuronal networks using *Aplysia* as a model organism.

This study was performed in cooperation with Prof.Moroz lab at the Whitney Laboratory, Saint Augustine, FL, USA. In this work my contribution was to biochemically characterize the *AcNOS* by measurement of NOS activity, cGMP assay, Western Blot, and immunohistochemistry.

B. Cloning of *Aplysia* NOS and its localization in the CNS

Cloning of Aplysia nitric oxide synthase (AcNOS)

The degenerate primers were designed for the conserved parts of the calmodulin (CaM)-binding site and the neighboring regions of oxygenase and reductase domains of NOS, and a fragment with high sequence similarity to known NOS isoforms was amplified from the cDNA. The cloned and deduced 150-amino acid sequence exhibited 75% identity to NOS from a mollusc, *Lymnaea stagnalis,* and 70% identity to human neuronal NOS. A set of specific primers was designed to perform 3'-RACE and 5'-RACE and to amplify flanking fragments of cDNA. The full-length cDNA was then amplified using the primers designed from the sequences of these flanking fragments.

The cDNA of 4444-bp has been cloned, with an ORF of 4161 bp and conceptual translation yielded a protein of 1387 amino acid residues (*Ac*NOS; GeneBank accession number AF288780). The sequences contain all putative conserved cofactor and substrate binding sites.

Three molluscan full length cDNA sequences of NOS proteins, from *Lymnaea stagnalis* (Korneev 1998) and *Aplysia* (Sadreyev, 2000), and last year a NOS from terrestrial slug *Lehmannia valentiana* (Matsuo, 2007) has been published. The analysis of highest BLAST homology (Altschul et al., 1990) of these molluscan NOS sequences reveals the maximum identity of 73% with *Lehmannia* and 61% with *Lymnea*. From the three vertebrate NOS isoforms, the molluscan sequences share the highest homology with human neuronal NOS (54% with *Aplysia*), suggesting a similar function.

*Ac*NOS sequence contains all putative conserved cofactor and substrate binding sites characteristic of a functional NOS that are implicated in interaction with L-arginine, heme, tetrahydrobiopterin, CaM, FAD, FMN, and NADPH. Amino acid residues critical for the formation of a functional NOS dimer are also present (Crane et al., 1997, Crane et al., 1998, Stuehr, 1999), (Figure 14). At the N-terminal AcNOS has a leader sequence, which is present in neuronal NOS isoforms in mammals. Although the *Aplysia* N-terminal leader sequence lacks the PDZ domains that are found in mammalian nNOS and are suggested to play a role in their intracellular targeting (Stricker et al., 1997). An autoinhibitory loop, which is a stretch of circa 45 amino acids and has been shown to regulate NOS in calcium dependent manner, is present in mammalian constitutive NOS (nNOS and eNOS) in the FMN domain (Salerno et al., 1997),.This region has been shown in *Ac*NOS (residues 760 - 806), suggesting that the *Aplysia* NOS may be a Ca^{2+}-dependent isoform (Figure 14).

The oxygenase domain of AcNOS contains a binding motif for caveolins, which were shown to interact with many different signaling molecules via its scaffolding domain.In mammals, caveolins are shown to bind to NOS and inhibit NO synthesis (Venema et al., 1997, Garcia-Cardena et al., 1997).

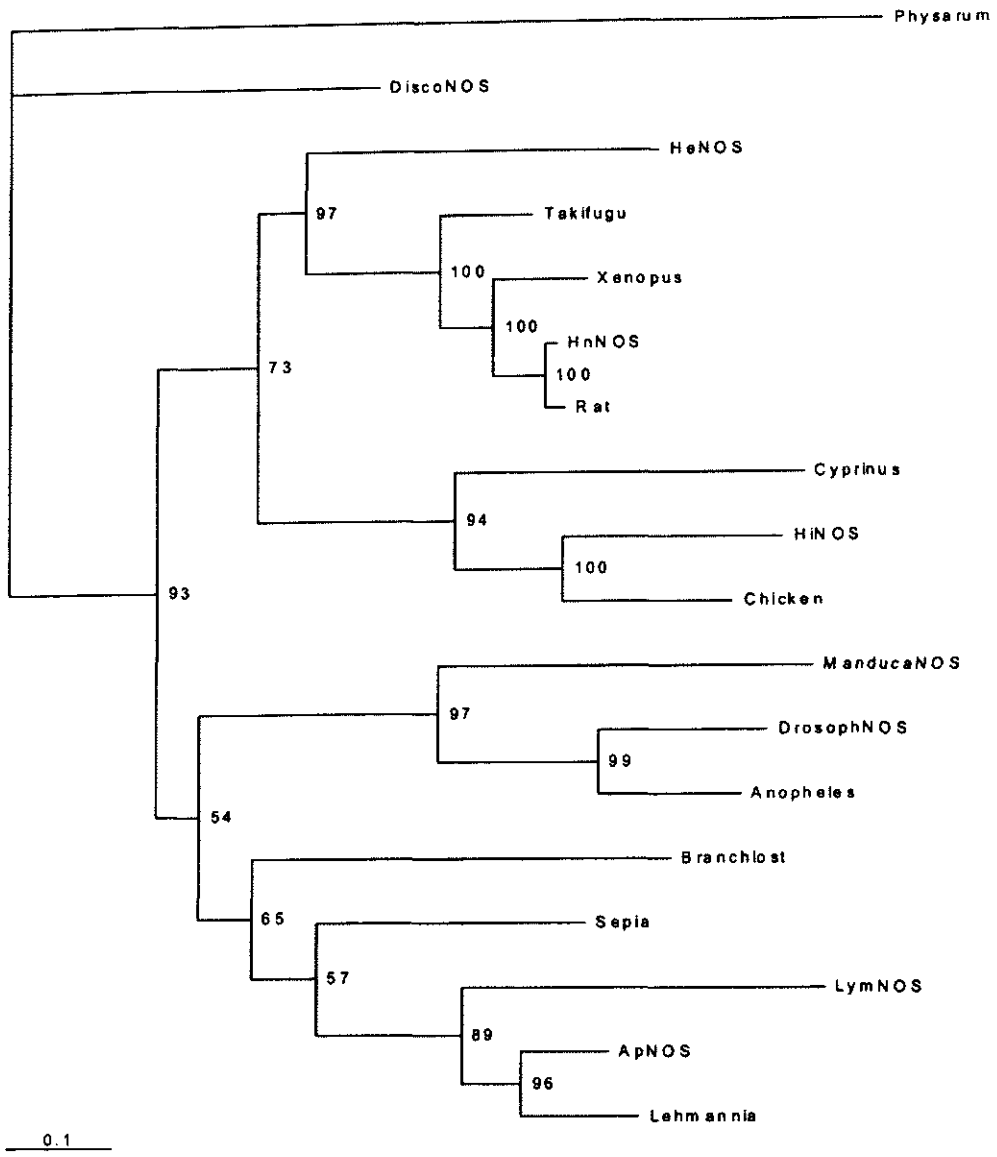

Figure 13. Phylogenetic tree of known vertebrate and invertebrate NOSs. Numbers stand for support values for the branch.

(NOS used for analysis are: NOS from *Aplysia californica*(Accession AAK83069, ApNOS), *Lehmannia Valentina* (Accession BAF73722.1, Lehmannia), *Sepia officinalis*(Accession AAS93626.1,Sepia, neuronal NOS from *Homo sapiens*(Accession AAB60654.1, HnNOS), endothelial NOS from *Homo sapiens*(Accession P29474, HeNOS), inducible NOS from *Homo sapiens*(Accession AAC83553, HiNOS), nNOS from *Rattus norvegicus* (Accession NP_434686.1, Rat), *Takifugu rubripes* (Accession AAL82736.1, Takifugu), *Xenopus laevis* (Accession NP_001079155.1, Xenopus), *Branchiostoma floridae*(Accession AAQ02989.1, Branchiost), *Lymnaea stagnalis* (Accession AAC17487.1, LymNOS, *Drosophila melanogaster*(Accession AAF25682, DrosophNOS), *Manduca sexta* (Accession AAC61262, ManducaNOS), inducible *Cyprinus carpio* (Accession CAB60197, Cyprinus), inducible *Gallus gallus*(Accession NP_990292, Chicken), *Anopheles stephensi* (Accession AAC68577.1, Anopheles), *Discosoma striata* (Accession AAK61379, DiscoNOS), *Physarum polycephalum* (Accession ABO21654,Physarum)).

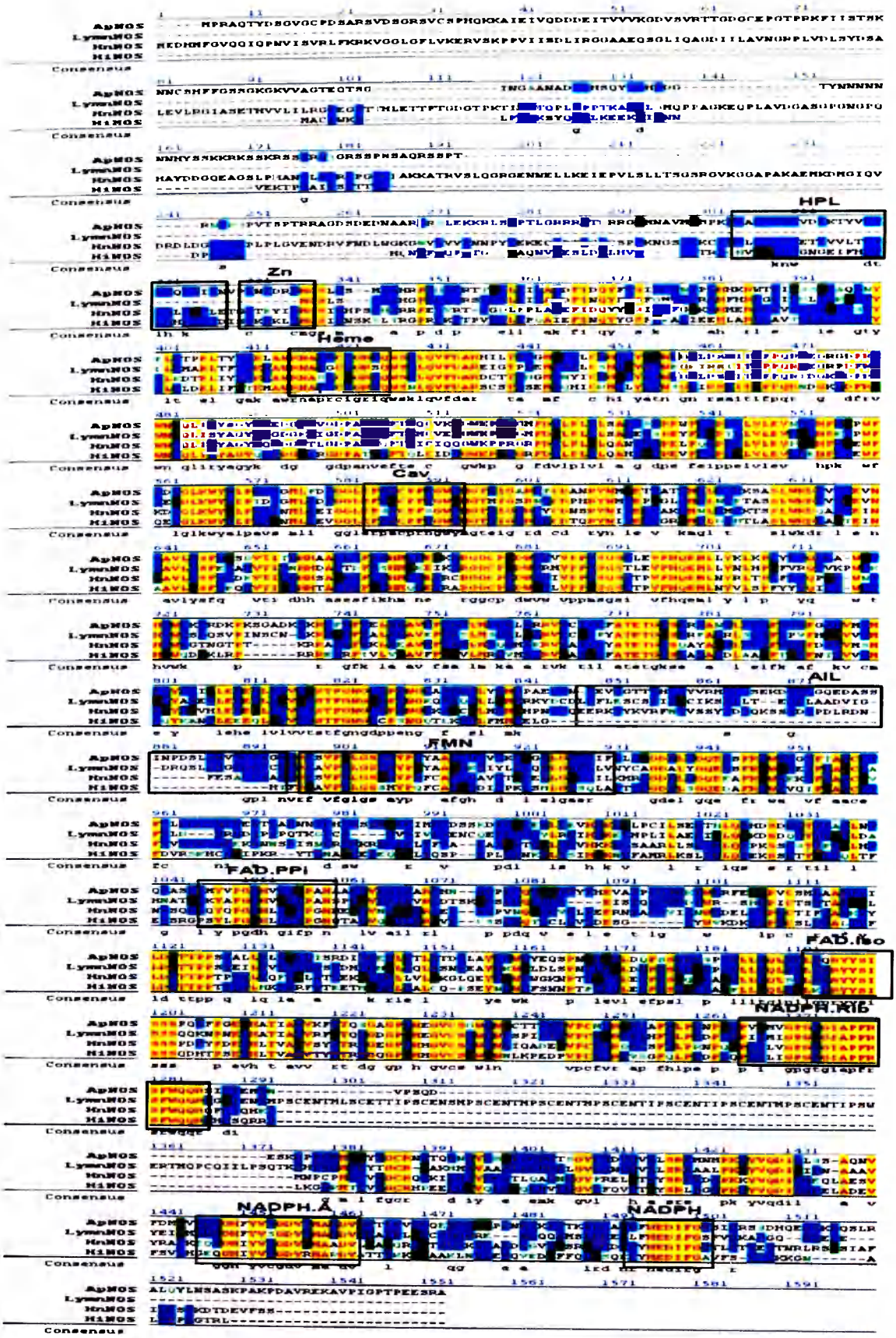
HPL
Zn
Heme
Csv
AIL
FMN
FAD.PPi
FAD.bo
NADPH.A
NADPH

Figure 14. Alignment of molluscan *Ac*NOS 1 and *Lymnaea* NOS, together with human nNOS and iNOS. A conceptual translation of both AcNOS yielded a protein of 1387 amino acid residues. Cofactor-binding sites for heme, calmodulin (CaM), FMN, FAD pyrophosphate (FAD•PPi), FAD isoalloxazine (FAD•Iso), NADPH Ribose (NADPH•Rib), NADPH adenine (NADPH•A), and the C-terminal sequence necessary for NADPH binding are marked, as well as putative N-terminal hairpin loop region (HPL), caveolin-binding consensus sequence (Cav). The proximal heme ligand (C^{420} in HnNOS), the substrate-binding residue (E^{597} in HnNOS), and the cystein residue that was shown to form the bond across the murine iNOS dimer interface (C^{336} in HnNOS, (Crane *et al,* 1998)), are conserved at equivalent positions (•).

In situ hybridization in the CNS of Aplysia californica

To describe a topographic distribution of *Aplysia* nitrergic neurons in the CNS we used the full length clone of *Ac*NOS (see section above) for the in situ hybridization. The staining was specific, with darkly labeled NOS containing neurons. Control animals (labeled with sense mRNA) showed no staining.

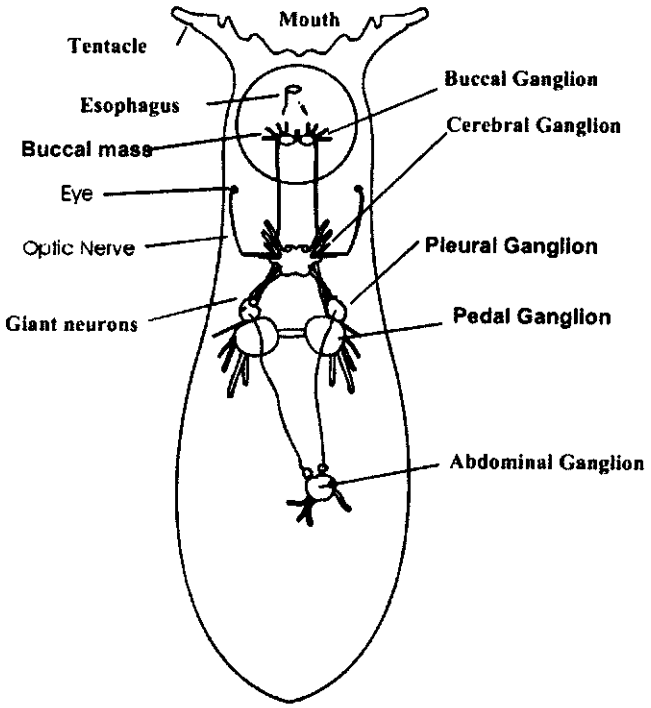

Figure 15. Simple schematic view of *Aplysia* CNS, with major ganglia depicted (a pair of buccal, cerebral, plural, pedal ganglia and abdominal ganglion).

AcNOS distribution in the CNS of Aplysia

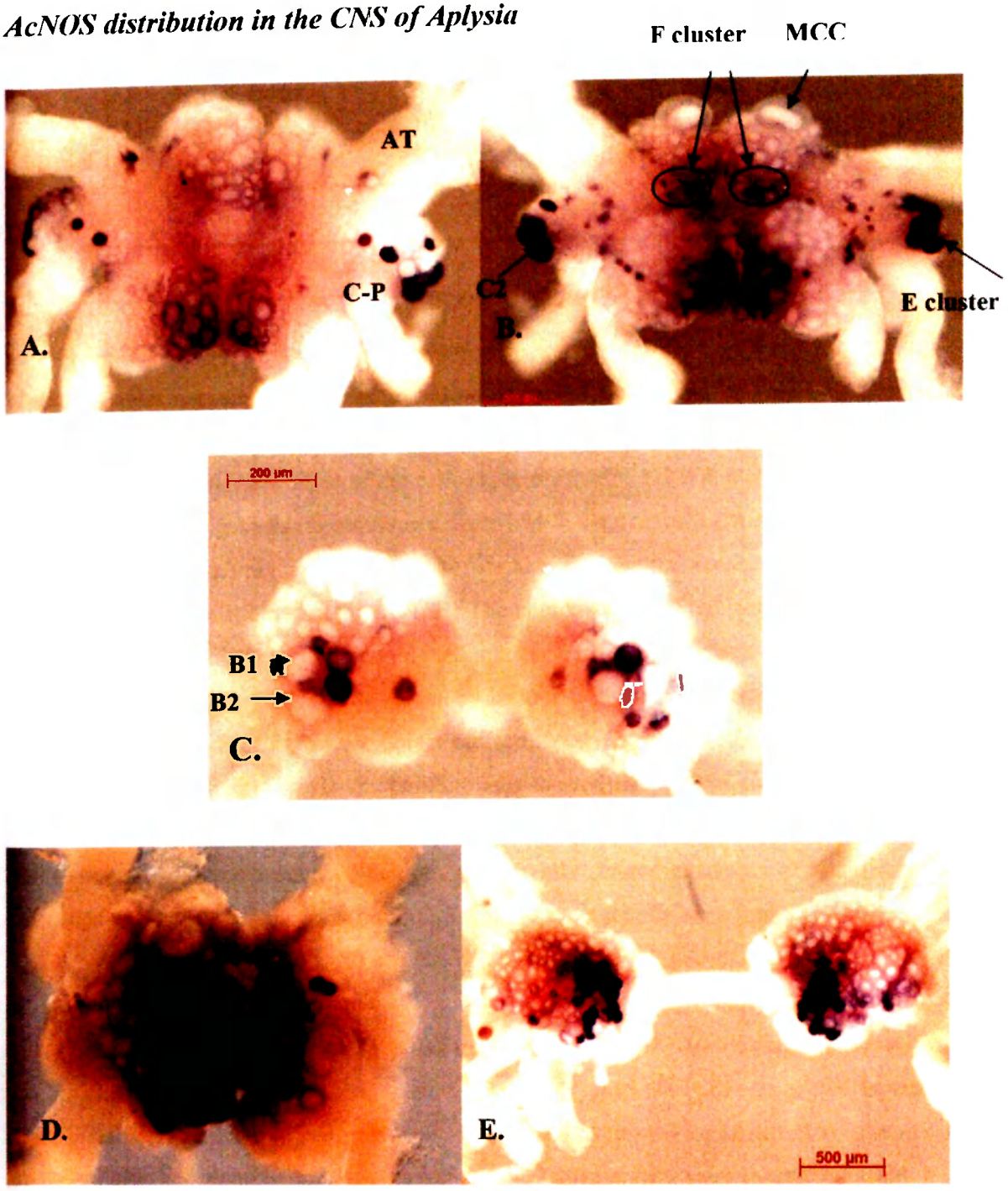

Figure 16. In situ hybridization with antisense full/length RNA probes with DIG-labelled NTPs to *Ac*NOS mRNA produced intense and specific labeling throughout the CNS. (A) Ventral view of the cerebral ganglia (B) Dorsal view of the cerebral ganglia. (C) Caudal view of the buccal ganglion. (D) Ventral view of the abdominal ganglion. (E) Dorsal view of the pedal ganglia.

Anterior tentacular nerve (AT), the cerebro-pedal (C-P) nerve, metacerebral cell (MCC), B1,B2,C2-neurons.

ganglion	number of nitrergic cells (n=4-10)	cell size
CG	2x(13-30) in F cluster 2x(7-15) in E cluster 2x(7-10) in B cluster 2x(25-38) isolated n.	(9-186)
BG	2x31-53	(15-129)
AG	17-26	
PeG	2x(12-29)	(15-101)
PlG	2x(1-4)	(10-33)

Table 1. Counts and soma size of nitrergic neurons in the *Aplysia* ganglia

Cerebral ganglion. Most of the cells expressing NOS mRNA were localized to the dorsal side of the cerebral ganglia: to previously described F cluster (two symetrical clusters located in lateral part of each hemiganglion dorsal surface near the cerebral commissure, Rubakhin,1999, j neurophys.) and the E cluster (Figure 16B) The neurons in the F cluster were relatively smaller 20- 40 μm (soma diameter) compared to E cluster cells ranging from 40 to 180 μm. The C2 neuron (member of the E cluster described by Jacklet 1995} was consistently labeled very darkly in all preparations. Further on the dorsal surface lightly lstained cells in the area of cluster B were labeled and several small unidentified cells located outside the clusters A and C clusters. Consistently with Jacklets work (Jacklet, 1995), the MCC (metacerebral cells) were not labeled. On the ventral surface around 10 neurons were lightly stained in the are of K cluster (Ono and McCaman, 1980) and in all preparation 2-5 darkely stained cells were found at the place between the anterior tentacular nerve (AT) and the cerebro-pedal (C-P) nerve, closer to the origin of the C-P nerve (Figure 16A).

Buccal ganglia. The NOS positive neurons were found surrounding the B1 and B2 cells on the caudal side of the ganglion, around 7-9 cells (Figure 16C), in one or two layers. Further lightly stained smaller size neurons were located next to the sensory neurons on the rostral side in the middle, additionally circa two darker stained larger somata were located adjacent to the n5, n6 nerves.

Pedal ganglia. The staining in the pedal ganglia revealed a strong labeling in a morphologically uniform population of 20-30 rather larger neurons (60-100μm) on the antero-lateral region of the ganglia, situated between the pedal-pleural and pedal-pedal connectives and pleural ganglia.

Pleural ganglia. One to four small somata (10-33μm) were labeled in pleural ganglia, located between the pedal-pleural (PePl) and cerebral-pleural (CPl) connectives. No staining was observed in the VC cluster of mechanosensory cells.

Abdominal ganglion. Nitrergic cells (10-100μm) were present at the left rostral quarter ganglion on the ventral surface, 3-5 neurons (Figure 16D) (described as L29 in Antoniov 2007, Moroz 2006}. Further a cluster of neurons around the R16, on the ventral side (right caudal quarter ganglion) was lightly stained. Additionaly in the abdominal ganglion several smaller size cells hidden in the lower layer were observed.

Periphery. Due to high pigment content of the peripheral tissue, it was difficult to discern ISH labeling of nitrergic neurons from the natural pigmentation. In smaller animals the ISH labeling was consistent with the NADPH-labeling (Moroz) and documented high intensity staining in the mouth area, followed by tentacles and rhinophores.

To study the role of NO on the level of individual neurons we cloned the nitric oxide synthase from a model organism *Aplysia* and mapped NOS-containing (nitrergic) neurons in the CNS using *in situ* hybridization and immunocytochemistry. A similar pattern of NOS expression was observed with both techniques and matched the known distribution of NADPH-d reactive neurons in the CNS. Up to 390 central neuronal somata were found to be labeled with NOS selective RNA-probes including several identified neurons, which corresponds to 1-2% of nitrergic neurons described in mammals. The majority of nitrergic neurons were located in the cerebral (~145) and buccal (~84) ganglia followed by pedal (~41), abdominal (~21) ganglion and pleural (~8) ganglia. NOS containing cells were detected at the periphery in chemosensory areas such as the mouth area, rhinophores, tentacles. The intensity of the staining between distinct populations of neurons varied considerably even within one ganglion, but the pattern of intensity of staining together with the localization of stained somata was preserved between individuals. A gradual scale of intensity of staining corresponds with the NADPH-d labeling published earlier, where the NOS-positive cells in the E-cluster and the pleural ganglia were the darkest (Moroz, 2006). NOS specific antibodies and NADPH-d activity (Moroz) labeled primarily neuronal processes and the ganglionic neuropil; with neuronal somata showing relatively weak staining intensity. This finding suggests that the major NOS activity is associated with neurites. Furthermore, in situ hybridization also confirms the presence and transport of NOS-specific mRNAs to distant processes (unpublished observation, Buganova and Moroz). In addition, NOS

containing cells were detected in the neuropil and at the periphery. Patterns of NOS distribution implies an important role for this enzyme in diverse networks including feeding & locomotion.

The cloned *Aplysia* NOS gene sequence contains all of the conserved sites characteristic of a functional NOS; these sites are implicated in interactions with L-arginine, heme, tetrahydrobiopterin, calmodulin (CaM), FAD, FMN, and NADPH, in Zn2+ binding and in dimerization.

This study was performed in cooperation with Prof. Moroz lab at Whitney Laboratory, Saint Augustine, FL, USA. My contribution was to cooperate on cloning the full length *AcNOS* gene, and utilize it for *ISH* to localize and map the *AcNOS* mRNA in the *Aplysia* brain.

C. Nerve injury in *Aplysia* reduces nitric oxide synthase mRNA levels in neuronal somata while increasing mRNA levels in axoplasm.

Nitric oxide (NO) signaling in mammals is thought to contribute to nerve regeneration and neuropathic pain. *Aplysia* sensory and motor neurons with axons in pedal nerves have proven useful for investigating similar responses to nerve injury, including sensory hyperexcitability involving the NO-cGMP pathway. Here we describe alterations in nNOS mRNA expression in pedal ganglion neurons and injured pedal nerves following nerve crush.

ISH of control pedal ganglia showed that neuronal somata expressing nNOS mRNA form a discrete cluster of 25-50 cells situated between the pedal-pleural and pedal-pedal connectives and pleural ganglia (Figure 18A). After unilateral pedal nerve crush, the number of pedal neuron somata expressing nNOS mRNA was significantly decreased 3 or more days after ipsilateral pedal nerve crush (14.6± 1.6 cells per pedal ganglion, tested at 3, 5, 6, 10, and 21 days) compared to contralateral control ganglia (34.3 ± 2.1 cells) or to ipsilateral ganglia tested 1 day after crush (30.7 ± 0.7 cells). In addition, densitometry analysis showed (Figure 18B) that the intensity of staining was reduced in cells on the injured side. In contrast, a significant increase of nNOS mRNA was detected from pedal nerve axoplasm by RT-PCR 3 days after nerve crush (Figure 17), and preliminary evidence using in situ hybridization suggests that this mRNA accumulates at the crush site. A tentative hypothesis to explain this altered pattern of

expression is that nNOS mRNA in the soma decreases because of its translocation to the injury site for peripheral translation during adaptive responses to nerve injury.

Axonal AcNOS upregulation after nerve crush

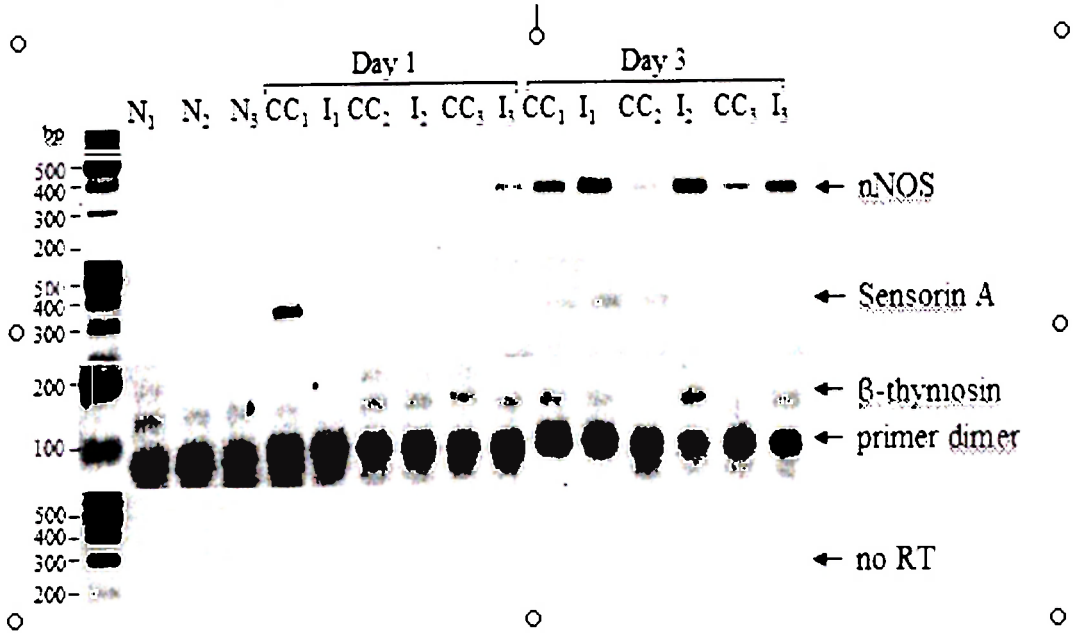

Figure 17. *Detection of AcNOS mRNA in axoplasm by RT-PCR.* Peripheral nerves p5-p9 were crushed on one side. At the indicated times, 1-day or 3-days after injury, axoplasm was extruded from the crush site of the injured nerves (I) and contralateral control (CC) side nerve segments. Axoplasm was also collected from animals that had never been exposed to surgery (N). Total RNA was extracted from the axoplasm and cDNA was then synthesized. Appropriate size fragments were amplified with primer sets for *Ac*NOS, sensorin A, and the β-thymosin from the cDNA. The results from three animals (N1-3, CC1-3 and I1-3) are shown. The size of the synthesized fragments detected by ethidium bromide staining on 2% agarose gels were identical to those predicted from the known sequences in the GenBank database. Sensorin A is a sensory neuron-specific marker; its mRNA was previously shown to be in the axon. β-thymosin mRNA has previously been shown to be present in neurites of cultured sensory neurons. There was no amplification in the absence of reverse transcriptase, indicating the RNA preparations were not contaminated with genomic DNA (bottom panel). Positions of molecular markers are indicated on the left.

cDNA made from each sample was used to amplify specific fragments by PCR (40 cycles), using specific primer sets for the following: (1) neuronal nitric oxide synthase (NOS) (GenBank accession number AAK83069), nt 3610-4049; (2) SN-specific neuropeptide sensorin A (GenBank accession number X56770), nt 43-331; (3) beta-thymosin (GenBank accession number AF454398, nt 61-195. All the reactions were assembled, amplified, and analyzed at the same time.

Soma AcNOS mRNA decreases after nerve crush

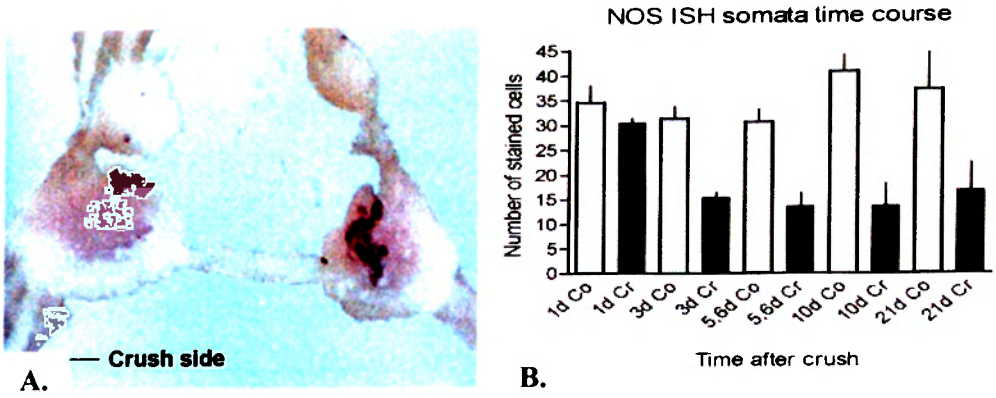

Figure 18. A. *In situ* hybridization of anti-NOS RNA probes in pedal ganglia visualized with NBT/BCIP. Shown are pedal ganglia following nerve crush (Cr) dissected after different time intervals (5 days here) vs. control pedal ganglia with uncrushed nerve (Co).

B. After unilateral pedal nerve crush, the number of pedal neuron somata expressing nNOS mRNA was significantly decreased 3 or more days after ipsilateral pedal nerve crush (Cr, 14.6± 1.6 cells per pedal ganglion, tested at 3, 5, 6, 10, and 21 days), compared to contralateral control ganglia (Co, 34.3 ± 2.1 cells) or to ipsilateral ganglia tested 1 day after crush (30.7 ± 0.7 cells), Cr- cruched, grey bars, Co- control, black bars.

This study was performed in cooperation with Prof.Leonid Moroz laboratory at Whitney Laboratory, Saint Augustine, FL, USA, Department of Integrative Biology and Pharmacology, University of Texas-Houston Medical School, Houston, TX, USA and Department of Anatomy and Cell Biology, Columbia University, New York, NY, USA. My contribution to this study was to perform the ISH and densitometry, and evaluate the results.

D. Protocol for double chromophorelabeled *in situ* hybridization

The non radioactive *in situ hybridization* allows for simultaneous detection of two different transcripts in the same molluscan brain using different colours, with the opportunity to use the protocol to identify colocalization of neurotransmitters, or other substances. The excellent preservation of morphology in whole mount preparations together with the high sensitivity for mRNA detection warrant the use of the protocol in systemic studies of expression patterns of different mRNA, and following electrophysiology experiments with intracellular dye labeling, making it possible to
couple localization of transcripts with electrophysiological studies in positively identified neurons. (Antonov et al., 2007).

Probe synthesis

Antisense probes were synthesized to four different full-length cDNAs. Two encoded neuropeptides sensorin (X56770) and FMRFamide (gi|155762), one encoded the putative potassium channel AcK2p1 (gi|24528452), and one encoded the protein fasciclin (Bastiani et al., 1987) (gi|20799319). Sensorin is relatively short at 541 bp and encodes a peptide that is specific to mechanosensory neurons (Brunet et al., 1991). The FMRFamide transcript encodes a longer prepropeptide and is ~2.4 kb in length (Schaefer et al., 1985). The coding region of the AcK2p1 RNA transcript is ~2.5 kb and the coding region for the fasciclin transcript is ~2.3 kb.

We found it necessary to empirically determine the optimum amount of probe to be used whenever a new probe was synthesized because yields of probe during synthesis
and abundance of different transcripts were both variable. It was also necessary to empirically determine whether crushed or uncrushed probe produced more intense cell-specific staining. When probe synthesis reactions produced a bright band on a 1% agarose gel, 2.0 µl of probe per 1.0 ml of hybridization buffer was used for the first test and often produced good results. Such probes typically contained 100–400 ng/µl of labeled RNA. For example the concentration of DIG labeled probes for the neuropeptides used in this study was 115 ng/µl for FMRFamide and 380 ng/µl for sensorin.

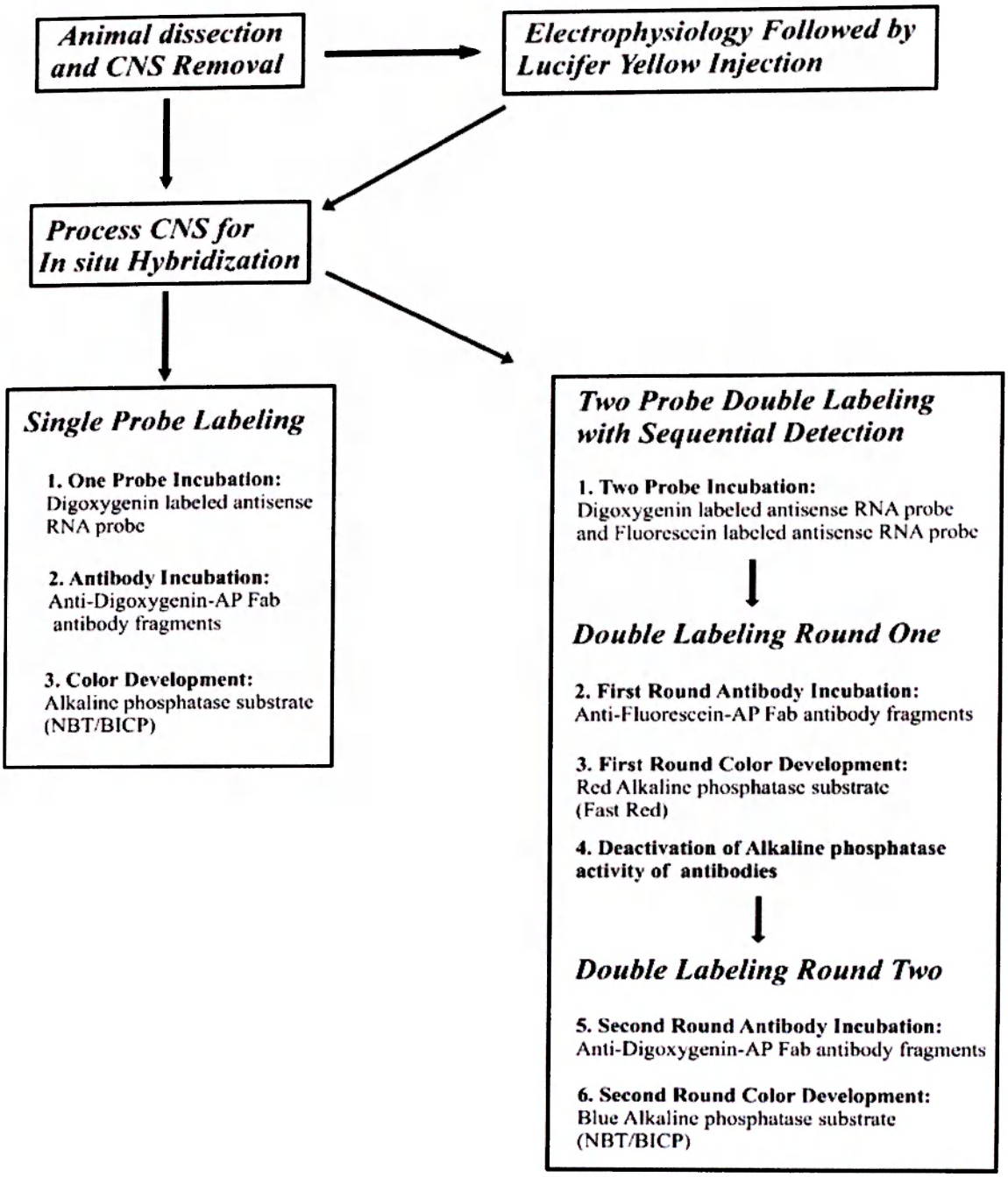

Figure 19. An overview of the *in situ* hybridization protocol. The left side outlines the basic steps of the in situ hybridization. Optional variations are shown on the right. Lucifer Yellow may be injected prior to fixation of ganglia to specifically mark neurons after electrophysiological tests. For two-color *in situ* labeling, two probes are hybridized at the same time and detected separately by sequential antibody incubations and color development reactions on separate days. Each probe and antibody incubation is done overnight, thus the procedure takes at least 3 days to complete for single labeling and 4 days for double labeling.

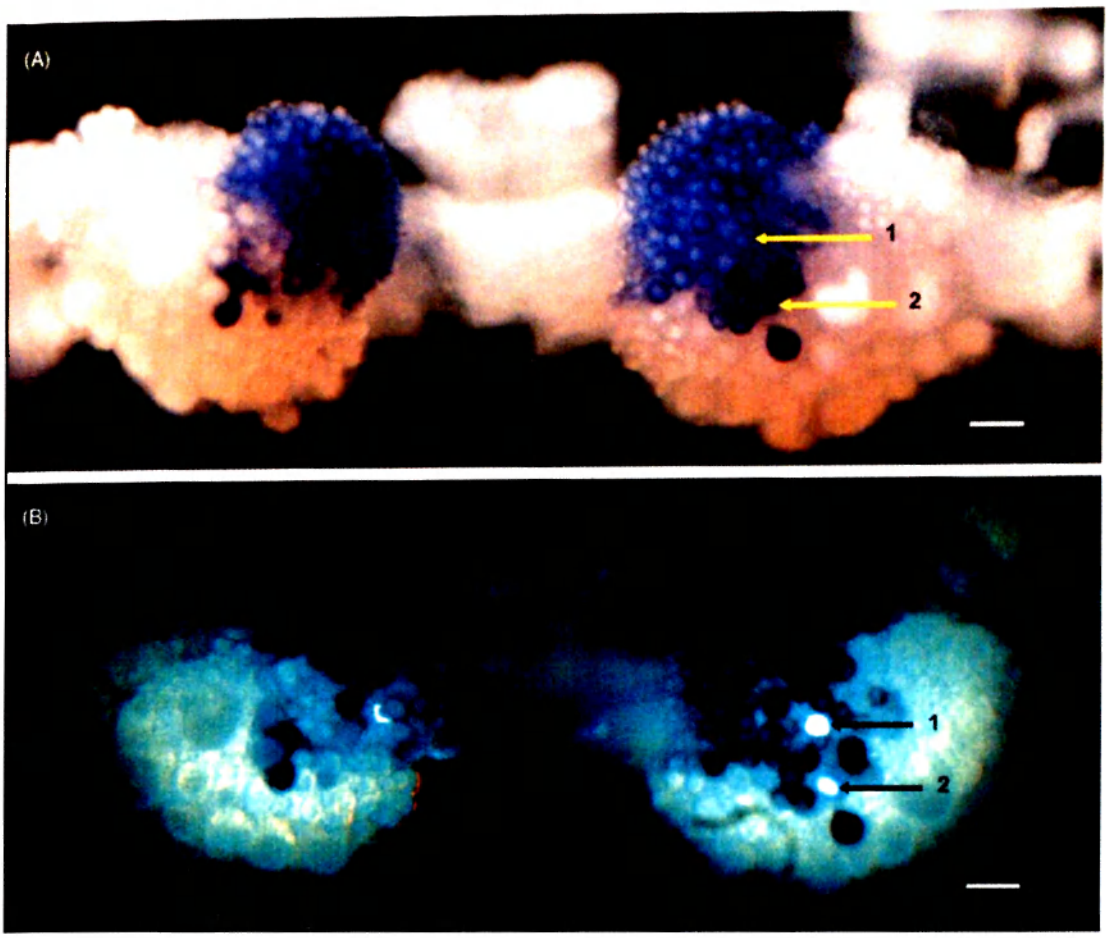

Figure 20. Lucifer Yellow is retained after *in situ* hybridization. (A) Sensorin darkly labels sensory clusters of the buccal ganglion. Arrows indicate cells that were labeled with Lucifer Yellow prior to fixation. (B) Fluorescent image of the same preparation as in (A). The white appearance of the Lucifer Yellow injected neurons is due to digital contrast enhancement done in Adobe Photoshop. Scale bars = 100 μm.

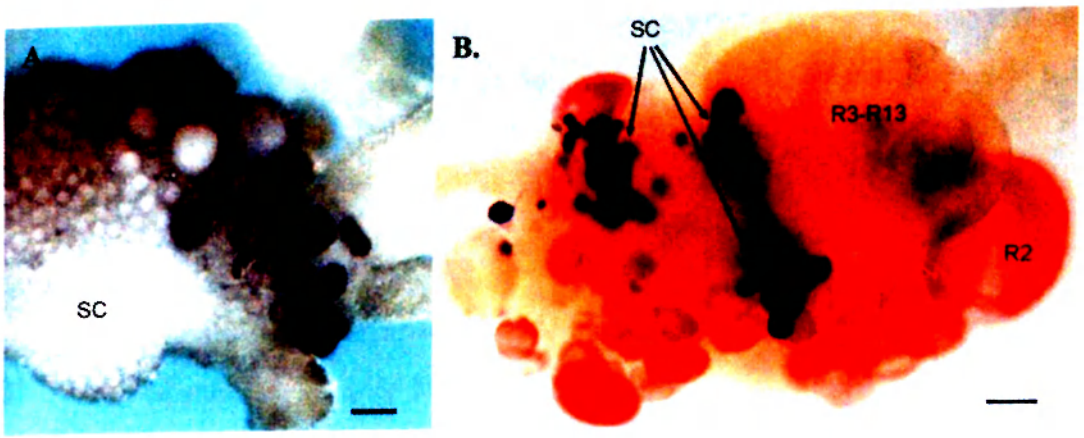

Figure 21. (A) Chromogenic *in situ* hybridization allowed detection of low abundance transcript-fasciclin expression in the right caudal buccal ganglion imaged in a 100% ethanol bath..
(B) Double labeling for sensorin (dark blue precipitate- the substrate of AP is NBT/BICP) and FMRFamide (red- substrate for AP is FAST Red) indicates the respective positions of sensory clusters and cells expressing FMRFamide. Dorsal view of the abdominal ganglion. The giant cell R2, which is the contra-lateral homolog of LPl 1 is intensely stained while the cluster containing cells R3–R13 is not. The ganglia in were imaged in a glycerol bath. SC, sensory clusters. Scale bars = 100μm.

Several *in situ hybridization* protocols have previously been applied to the CNS of *Aplysia* (McAllister et al., 1983, Brunet et al., 1991, Ono and McCaman, 1992, Levenson et al., 2000) but most were adapted to sectioned tissues or cultured neurons (Moccia et al., 2003). Ono and McCaman (1992) described an alkaline phosphatase-based in situ hybridization method for whole mount *Aplysia* ganglia; however, the protocol was not able to consistently detect expression of the abundant transcript for the neuropeptide FMRFamide (Figure 21B) in identified cells such as R2 where it is known to be expressed. The described protocol differs from previous *Aplysia* protocols in that it is optimized for processing whole ganglia, produces consistent staining for neuropeptides, and is sensitive enough to detect less abundant transcripts. Expression patterns of two highly abundant neuropeptide transcripts, sensorin (Brunet et al., 1991) (Figure 20) and FMRFamide (Price and Greenberg, 1977, Schaefer et al., 1985), and one relatively low abundant transcript, fasciclin (Bastiani et al., 1987) (Figure 21A) are shown as illustrative examples. Some parts of this protocol have been published previously (Vilim et al., 2001, Jezzini and Moroz, 2004, Walters et al., 2004).

This study was performed in cooperation with Prof. Moroz lab at Whitney Laboratory, Saint Augustine, FL, USA. My contribution was to introduce the double-chromophore labeling in *Aplysia*, and together with Dr. Sami Jezzini to optimalize the *in situ* hybridization protocol for whole mountpreparations and as well as following electrophysiology experiments.

E. Somatotopic Organization and Functional Properties of Mechanosensory Neurons Expressing Sensorin-A mRNA in *Aplysia californica*

Sensorin- A, a neuropeptide, was identified in the pleural VC cluster of *Aplysia*, by Brunet and colleagues (1991). Physiological experiments demonstrated that sensorin-A, could act as an inhibitory cotransmitter at VC cell synapses and imaging experiments showed that sensorin-A is selectively expressed in all of the known mechanosensory clusters in the central ganglia of *Aplysia* and appeared to be absent from all other cells of the CNS (Brunet et al., 1991). However, except for this brief, preliminary description of sensorin-A staining in previously defined mechanosensory clusters by Brunet et al. (Brunet et al.), sensorin-A expression was not examined systematically. In this study, we describe the central and peripheral organization of mechanosensory neurons and show that the receptive fields of the sensorin-A-expressing clusters cover the entire surface of the animal's body. Detailed mapping of a population of mechanosensory neurons in *Aplysia* will enhance the tools for exploring mechanisms of axonal regeneration (Steffensen et al., 1995), changes in gene expression after nerve injury (Noel et al., 1995), and expression and stability of neuropeptide mRNA during synapse formation and synaptic plasticity (Santarelli et al., 1996, Schacher et al., 1999, Hu et al., 2002).

Number and distribution of sensorin-A-expressing neurons

In adult *Aplysia*, all of the somata labeled by sensorin-A antisense probes in our whole mount preparations were in central ganglia; none were in peripheral ganglia or other tissues. The labeled somata correspond to previously described mechanosensory clusters (Brunet et al.) in the abdominal, pleural, cerebral, and buccal ganglia.

Approximately 1000 cells express sensorin-A mRNA in young adult animals (10-30 g) and 1200 cells in larger adults (100-300 g). Thus, sensorin-A-expressing neurons represent 5-10% of all neurons in the CNS (Cash and Carew, 1989, Kandel).All of the labeled somata are in

the CNS, primarily in the abdominal left E cluster ((Byrne et al., 1974) , right E (RE), right F (RF), and rostral LE (rLE) clusters (Byrne et al., 1974, Dubuc and Castellucci, 1991), pleural ventrocaudal (VC) clusters (Walters et al., 1983), and the J and K clusters in the cerebral ganglia (Rosen et al., 1979), and buccal S clusters (Fiore and Geppetti, 1985) (for detailed pictures see the attached original publication). Expression also occurs in some sparsely distributed cells in most ganglia.

Somatotopic organization of sensorin-A expressing neurons

The results complete the macroscopic map of the peripheral receptive fields of sensorin-A-expressing cell clusters. Our study confirms earlier descriptions of receptive fields in *Aplysia* (Byrne et al., 1974, Rosen et al., 1979, Fiore and Geppetti, 1985, Walters et al., 1983, Dubuc and Castellucci, 1991) and provides new information about coverage of the midbody and anterior body by the pleural VC clusters, of the rhinophores and propodium by the cerebral J clusters, and of the lip region and buccal mass by the buccal S clusters. When all of this information is combined, sensorin-A-expressing cells are seen to provide a centrally distributed map of the entire surface of the body (see Figs in the attached original paper).

A clear (albeit rough) topographic relationship was demonstrated between the location of each sensory neuron soma in the VC cluster (Figure 23B) and both the location of its peripheral receptive field (Figure 22) and the nerve carrying its primary axon (Figure 22A; see also Zhang *et al,* 1993}. Thus, each VC cluster forms a somatotopic map of most of the ipsilateral body surface- an "aplunculus" (Figure 23B,C). Although somatotopic mapping of the body surface onto topographically organized populations of central neurons (e.g., the sensory homunculus in sensory cortex) is a common feature of mammalian sensory systems, and somatotopic organization of afferent terminals is well known in arthropods (Murphey et al., 1981 1981, Peterson and Weeks, 1988), this remains the only known invertebrate somatotopic mapping of peripheral receptive fields onto a discrete cluster of central neuronal somata. (Walters et al., 1983).

Functions of sensorin-A-expressing neurons

Neurons in all of the clusters have relatively high mechanosensory thresholds, responding preferentially to threatening or noxious stimuli. Synaptic outputs to target cells having defensive functions support a nociceptive function, although additional functions are likely in some clusters.

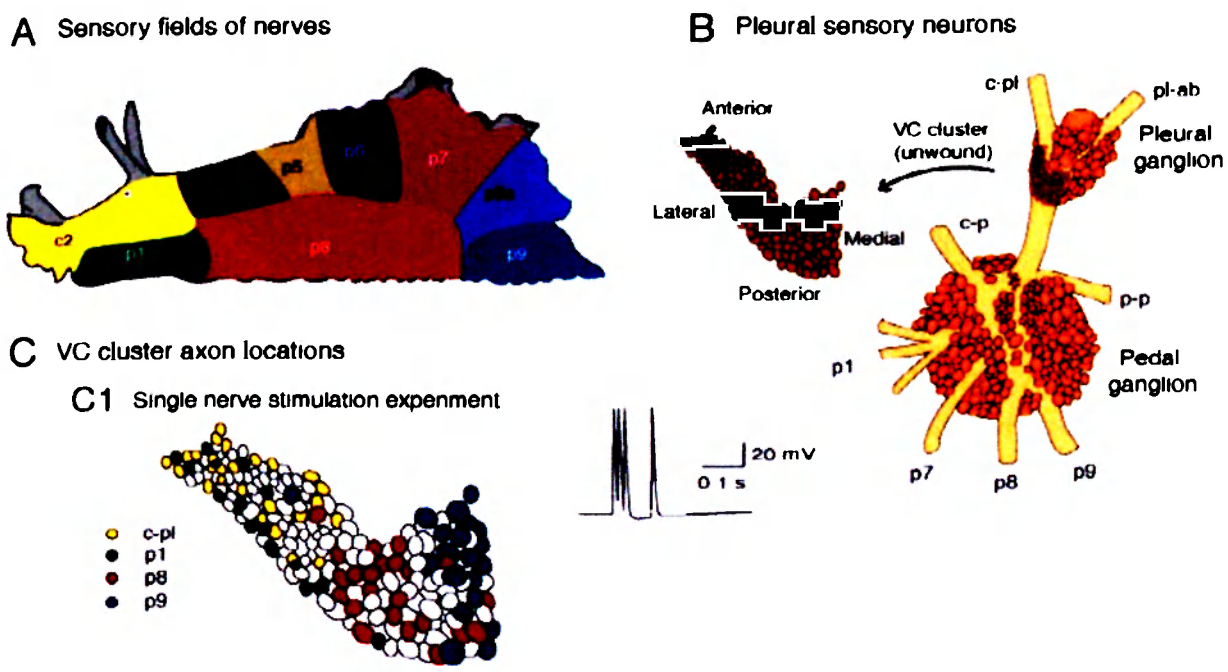

Figure 22. Relationship between positions of the somata in the VC cluster and axonal projections into peripheral nerves. **A:** Simplified map of the major sensory fields of left pedal nerves and a left cerebral nerve, c2 (anterior tentacular nerve). The extensive overlap of different fields is not indicated on this map. **B:** Schematic drawing of VC cluster in left pleural ganglion. The entire cluster is represented two-dimensionally by unwinding it (left) from the cylindrical tract extending from the pl-p to the c-pl connectives. The right VC cluster is very similar (not shown). **C:** The inset shows a spike evoked by a 2-msec shock delivered to nerve p9. **C1:** Positions and relative sizes recorded in a single experiment of cells in left VC cluster that responded with spikes to stimulation of axons in the indicated nerves.

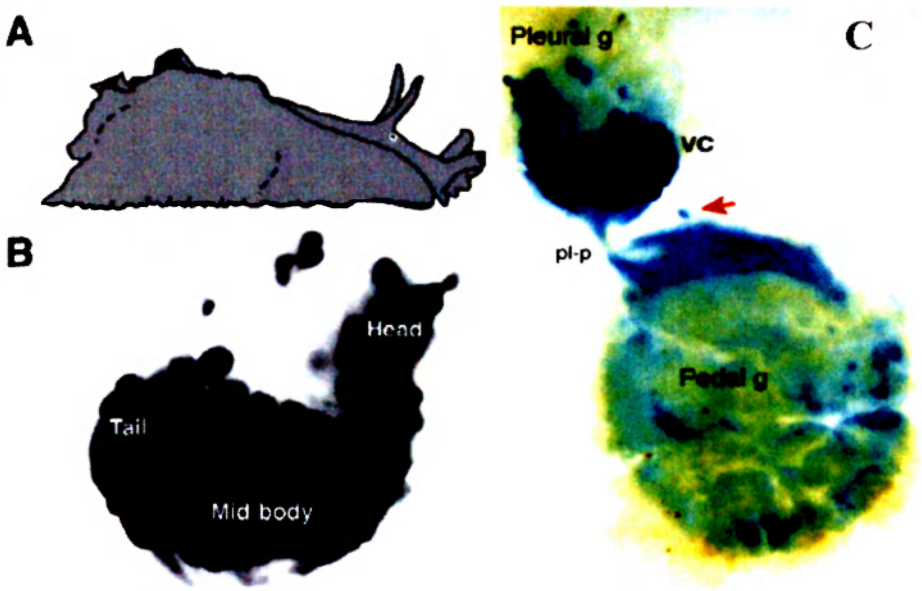

Figure 23. Somatotopic representation of mechanosensory receptive fields in the VC cluster.

A: Drawing of the right side of an *Aplysia* facing the right. ***Somata in pleural, and pedal ganglia labeled by in situ hybridization with antisense probe to sensorin-A mRNA***

B: A micrograph of the right VC cluster. The regions within the cluster having somata with receptive fields on the head, midbody, and tail are indicated. The anterior side of the cluster is at the top of the image, and the medial and lateral sides are indicated

(see Figure 22). Scale bar 100 μm. **C:** Relatively deep focus on a whole-mount preparation of the right pleural and pedal ganglia from a 30 g animal after clearing and embedding. This revealed labeled cells throughout the VC cluster and a smaller, more lightly labeled cell in the pedal ganglion (arrow). Note the intense labeling of neurites in the pleural–pedal connective (pl-p) and the neuropil throughout the pedal ganglion.

This study was performed in cooperation with Prof. Moroz lab at the Whitney Laboratory, Saint Augustine, FL, USA and Department of Integrative Biology and Pharmacology, University of Texas-Houston Medical School, Houston, TX, USA. My contribution to this study was to perform the in situ hybridization and densitometry, with evaluation of the results, together with the mapping of sensorin-A expressing neurons.

F. Cloning of an *Aplysia* hemoprotein,Thyroid Peroxidase, and Characterization of Thyroid Hormone-like signaling in *Aplysia*

The aim was to identify other functional, putative heme enzymes. The putative thyroid peroxidase gene sequence from *Aplysia* (*Aca*TPO) showed high sequence similarity with peroxidasin and thyroid peroxidases, which are the critical thyroid hormone (TH) synthesis enzymes found in all vertebrates. Spatial and temporal expression patterns of these transcripts suggest a role for *Aca*TPO in a variety of processes such as developmental metamorphosis and regulation of the animal's energy metabolism.

TH signaling is critically involved in metabolism, differentiation and homeostasis. Moreover it is well known that these hormones are critically involved in nervous system development in a variety of vertebrate taxa. Specifically they are important for synapse formation and are potentially involved in neurite growth.

Our results revealed the presence of thyroid peroxidase transcripts in the *Aplysia* F-cluster, a putative neuro-endocrine center located in the cerebral ganglion. The in frame translation of *Aca*TPO yielded a protein of 576 AA. TPO belongs to the animal peroxidase superfamily and catalyzes three reactions critical for thyroid hormone (TH) synthesis. The presence of this gene in the CNS of *Aplysia* along with several other transcripts from the TH signaling pathway (thyroid-stimulating hormone beta subunit, thyrotropin receptor, thyroxine deiodinase, thyroid hormone binding protein and others) suggest the presence of TH like signaling in molluscs as well. Here we provide further evidence or the presence of this signaling pathway by showing that *Aplysia* synthesizes both T4 (thyroxine) and T3 (triiodotyrosine) endogenously using ELISA. We then confirmed uptake of radioactive iodine by juvenile *Aplysia* and showed that this iodine is incorporated into T3. Finally we were able to clone newly identified regulatory genes upstream of thyroid hormone synthesis indicating that a large part of the TH signaling machinery might be present in the sea hare. These findings have strong implications for the evolution of TH signaling among metazoa and moreover may elucidate some of the critical regulators involved in brain development and synapse formation.

Iodine incorporation and TH synthesis in Aplysia is inhibited by thiourea

We exposed juvenile *Aplysia* to I^{125} in order to test whether 1) iodine is incorporated and 2) incorporated iodine is used for TH synthesis (thyroxine and triiodotyrosine). Our results from the

thin layer chromatograms confirm that *Aplysia* juveniles used incorporated 1125 to make THs (Figure 24B). Interestingly, *Aplysia* juveniles primarily synthesize T3. Thiourea inhibited TH synthesis in *Aplysia* (Figure 24B). Finally, we were able to detect T4 and T3 in haemolymph of adult *Aplysia* (Figure 24A.) using ELISA. Note that all measurements are standardized to the protein content of the samples.

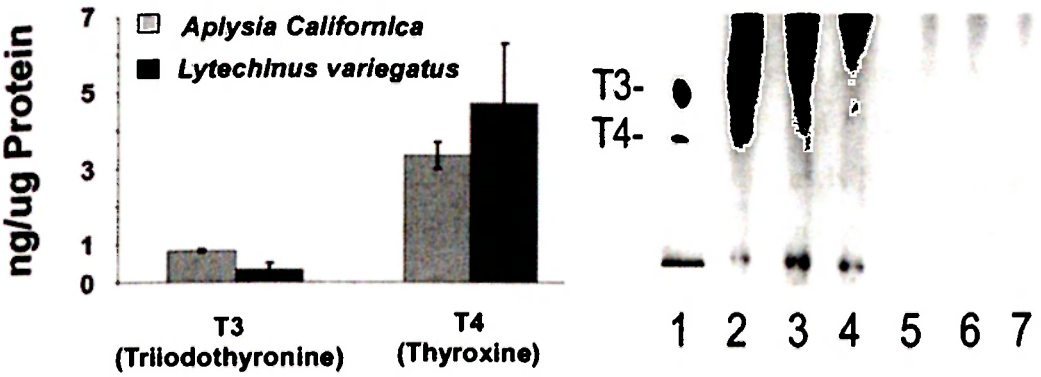

Figure 24. *Lytechinus variegatus* larvae and *Aplysia californica* juveniles incorporate 1125 and build THs with it. Both species contain measurable TH levels. A) We measured T4 and T3 in sea urchin larvae and *Aplysia* juveniles using ELISA and found both hormones present in both species at different concentration. Note that all measurements are standardized to the protein content of the samples. T4 was present at higher concentrations in both species. DPM: decays per minute, B). Incorporated iodine is used to synthesize T3 in *Aplysia* and neither T4 nor T3 was detected when juveniles were exposed to thiourea before extraction. (B; control: lane 2-4, standard: lane 1, +thiourea (10-2) :lane 5-7

Cloning of TPO from molluscs

As a first step to elucidate the mechanisms of TH-like synthesis in non-chordate animals we cloned two partial sequences of peroxidases closely related to peroxidasin and thyroid peroxidase from *Aplysia* (*Aca*TPO) (Figure 26) and the sea urchin *Lytechinus variegatus* (LvTPO) .

For the phylogenetic analysis we used fungal peroxidase (*Gaeumannomyces graminis* lineolate diol synthase: GgLDS) as the outgroup (Figure 25A). We used parsimony with subsequent bootstrap analysis. Numbers above the branches are bootstrap values (100 replicates). Bootstrap values below 50% are not shown. The phylogenetic tree in Figure 25A reveals clustering of LvTPO together with several deuterostome thyroid peroxidases (BbTPO: *Brachiostoma belcheri*

thyroid peroxidase; CiTPO: *Ciona intestinalis* thyroid peroxidase; HrTPO: *Halocynthia roretzi* thyroid peroxidase) and peroxidasin (Psdn) from the round worm *C. elegans* (cluster D). AcaTPO on the other hand clusters together with peroxidasin from *Drosophila melanogaster* (DmPsdn) and Humans (HsPsdn) (cluster C). Note, that neither LvTPO nor *Aca*TPO clusters together with human or rat thyroid peroxidase (cluster B). Cluster A consists of other peroxidases with various functions.

Figure 25B is a schematic representation of the domain structure derived from the complete alignment of *Drosophila melanogaster* peroxidasin and several thyroid peroxidases. *Aca*TPO is 576 amino acids long and has also all major domains necessary for peroxidase function conserved. These are proximal and distal histidine in positions 25 and 273, Ca2+ binding domain in positions 104 (T), 106 (F), 108 (D) and 110 (S). Finally arginine is found in position 77 and asparagines in position 357. While Human (HsTPO) and *Ciona* thyroid peroxidases have complement control protein (CCP) modules (also known as short consensus repeats SCRs or SUSHI repeats) towards the 3 prime end of the gene, LvTPO, BbTPO, DmPsdn and *Aca*TPO do not have such a motive. A second calcium-binding EGF-like domain present in CiTPO and HsTPO are lacking in these genes. In addition, LvTPO, BbTPO and AcaTPO are significantly shorter than CiTPO and HsTPO. Thus, *Aca*TPO and LvTPO can be characterized as peroxidases based on their conserved residues. Based on their sequence similarities and topology of the phylogenetic tree we suggest that both *Aca*TPO and LvTPO can be classified as possible thyroid peroxidase orthologues. The fact that peroxidasins from *Drosophila melanogaster* (DmPsdn), *C. elegans* (CePsdn) and humans (HsPsdn) have the ability to crosslink tyrosines and iodinate protein (Nelson et al., 1994) might explain their apparent similarities to *Aca*TPO and LvTPO compare to other cloned vertebrate thyroid peroxidases.

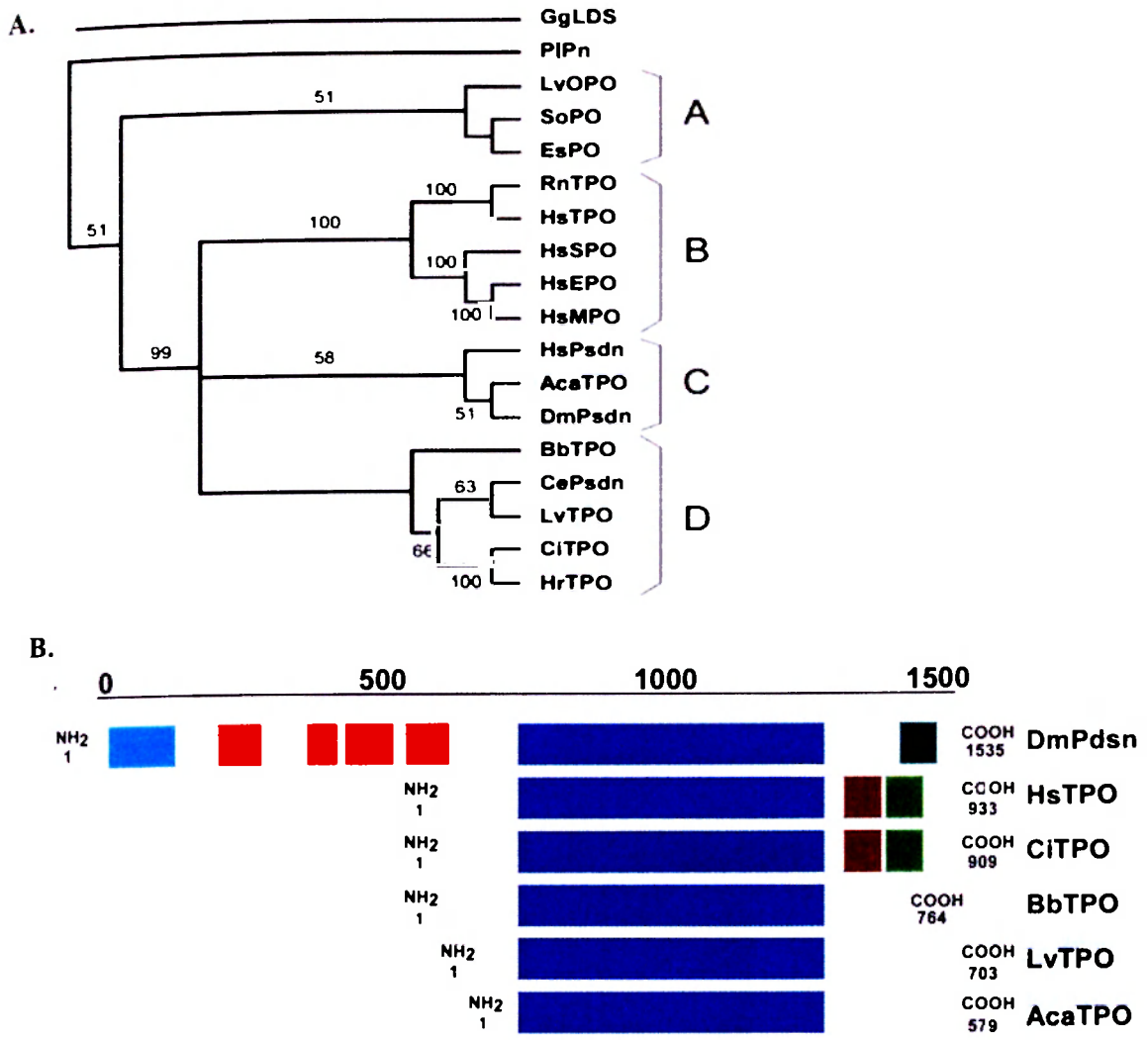

Figure 25. Thyroid hormone-like function has been proposed for a variety of metazoan phyla but its mechanisms are poorly investigated in the majority of taxa except chordates. We identified two putative thyroid peroxidase (TPO) genes, the enzyme critical for thyroid hormone (TH) synthesis, from the mollusc *Aplysia californica* (AcaTPO) and the echinoderm *Lytechinus variegatus* (LvTPO). **A)** Phylogenetic analysis using nucleotide sequence of catalytic domains confirms AcaTPO and LvTPO as peroxidases. Peroxidasin from Drosophila melanogaster appears to be similar to thyroid peroxidases. Note also that neither LvTPO nor AcaTPO clusters together with human or rat thyroid peroxidase (cluster B) **B)** Schematic result of sequence alignment with indicated domain structure. Only the catalytic domain of AcaTPO and LvTPO is present and the overall length of the gene is significantly reduced compared to chordate and urochordate peroxidases. (Peroxidases used for analysis are: fungal (*Gaeumannomyces graminis*) lineolate diol synthase (Accession: AF124979; GgLds); Peroxinectine from the signal crayfish *Pacifastacus leniusculus* (Accession: JC4397; PlPn); Ovoperoxidase from the sea urchin *Lytechinus variegatus* (Accession: AF03581; LvOPO); Ink gland peroxidase from the cuttlefish *Sepia officinalis* (Accession: 2320157A; SoPO); Light organ peroxidase from the squid *Euprymna scolopes* (Accession: PN0667; EsPO); Salivery peroxidase from *Homo sapiens* (Accession: JC4935; HsSPO); Eosinophil peroxidase from *Homo sapiens* (Accession: P11678; HsEPO); Myeloperoxidase from *Homo sapiens* (Accession: P05164; HsMPO); Peroxidasin from *Homo sapiens* (Accession: D86983; HsPsdn); Peroxidasin from *Drosophila melanogaster* (Accession: S46224; DmPsdn) and Peroxidasin from the round worm *Caenorhabditis elegans* (Accession: CEF59F3; CePsdn); Thyroid peroxidase from *Rattus norvegicus* (Accession: P14650; RnTPO); Thyroid peroxidase from *Homo sapiens* (Accession: P07202; HsTPO); Putative thyroid peroxidase from the lancelet *Brachiostoma belcheri* (Accession: AB028841; BbTPO); Putative thyroid peroxidase from *Ciona intestinalis* (Accession: AB022196; CiTPO); Putative thyroid peroxidase from *Halocynthia roretzi* (Accession: AB022197; HrTPO)).

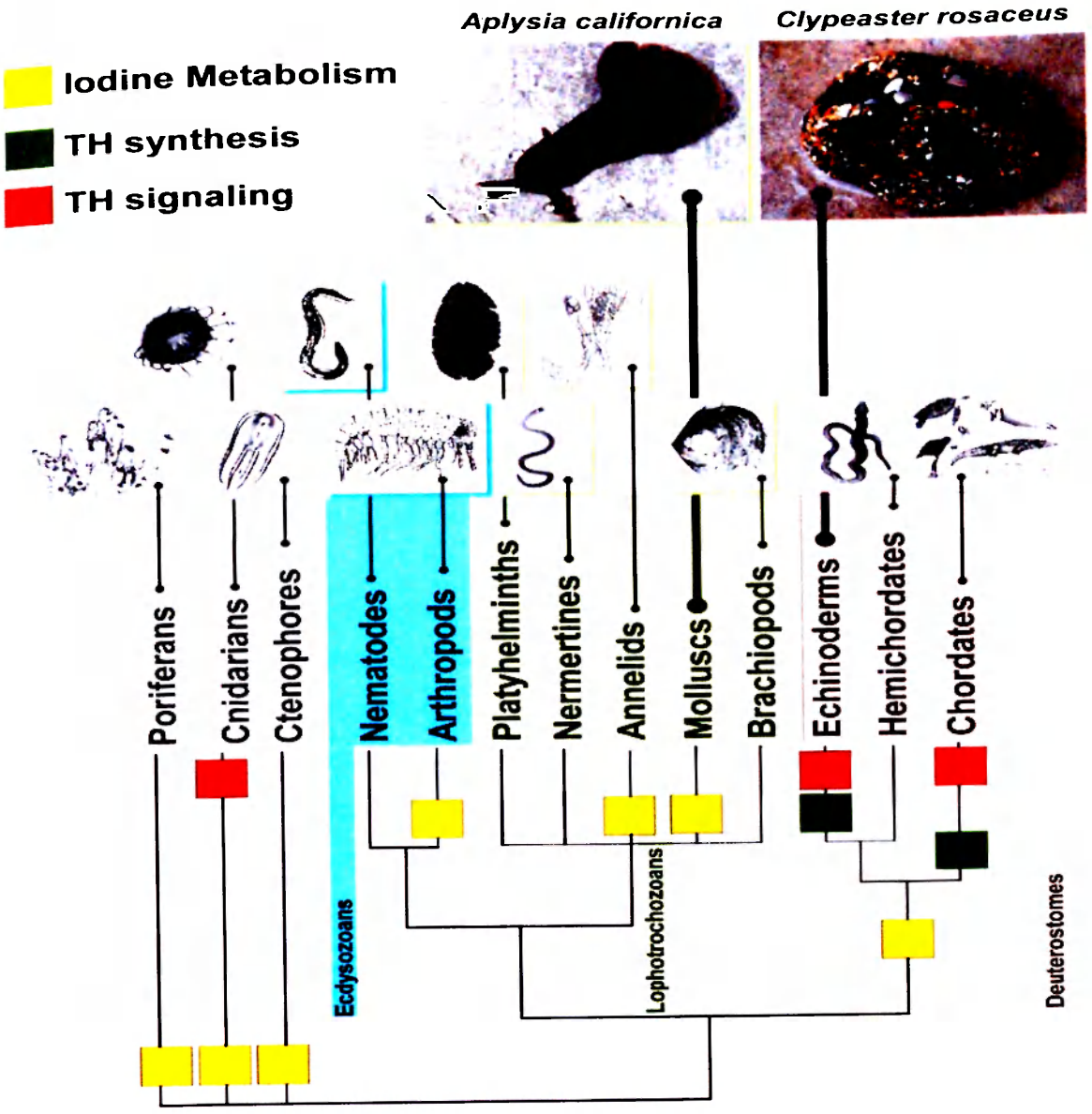

Figure 26. Evidence for TH and TH related function among the Metazoa: Iodine metabolism and TH-like function are potentially widespread in the animal kingdom. While many phyla were never investigated for their ability to use TH as a signaling molecule, recent findings on Echinoderms (Chino et al., 1994 Hodin et al. 2001) suggest an important role of TH-like molecules in echinoderm larval development and metamorphosis. (Adoutte *et al.*). (A) Metazoan phylogeny (Peterson and Eernisse): Except ctenophores, Nematodes and Echiurans, all metazoan taxa appear to have Iodine and or TH-like function (data compiled from Eales et al. 1997). E: Ecdysozoa; L: Lophotrochozoa; D: Deuterostomata; The mechanistic basis of TH action however is only known in chordates (red)

This study was performed in cooperation with Prof.Moroz lab at the Whitney Laboratory, Saint Augustine, FL, USA. My contribution to this study was to identify and clone peroxidasin and thyroid peroxidase from *Aplysia* (*AcaTPO*)., to localize the TH in *AcNOS* CNS using *in situ* hybridization, and to perform the phylogenetic analysis.

CONCLUSIONS FOR CHAPTER I.

A. Publication A provided evidence that functionally active NOS is present in the CNS of the mollusc *Aplysia californica* and for the first time it was shown to be calcium dependent. *Ac*NOS activity was around six times lower than that in the mammalian cerebellum [1], but was comparable with the average values reported for the insect brain [7]. The basal levels of cGMP production in the CNS of *Aplysia* were determined and found to be significantly increased following stimulation with NO donors and incubation with PDE inhibitors. Importantly, a specific inhibitor of sGC (ODQ) reduced the basal level of cGMP in *Aplysia* CNS by half and prevented the NO-induced rise of cGMP. These results suggest the substantial tonic production of NO in the intact CNS and its link to cGMP pathways.

B. We cloned the full length gene of *AcNOS* from the model organism *Aplysia* and mapped nitrergic neurons in its CNS using *in situ* hybridization and immunocytochemistry. A similar pattern of NOS expression was observed with both techniques, with up to 390 nitrergic neurons labeled with NOS selective RNA-probes including several identified neurons, which corresponds to 1-2% of all central neurons. The majority of nitrergic neurons were located in the cerebral (~145) and buccal (~84) ganglia followed by pedal (~41), abdominal (~21) ganglion and pleural (~8) ganglia. A conceptual translation of the *Ac*NOS cloned gene yielded a protein of 1387 amino acid residues. *Ac*NOS is structurally similar to neuronal NOS (NOS-I type in mammals) and contains all of the conserved sites characteristic of a functional NOS.

C. In order to examine the functional implications of NO in nerve regeneration and neuropathic pain, the effect of unilateral pedal nerve crush on the level of expression of NOS mRNA in *Aplysia* pedal neurons was studied in paper C. ISH and densitometry showed that the number of neurons and the intensity of neuronal staining following unilateral pedal nerve crush was significantly reduced in cells on the injured side. In contrast, a significant increase of *Ac*NOS mRNA was detected in pedal nerve axoplasm by RT-PCR within the same timeframe. Complimentary experiments need to be done to confirm the hypothesis whereby the diminished expression pattern of *Ac*NOS mRNA in the soma can be explained by its translocation to the injury site for peripheral translation during adaptive responses to nerve injury.

D. A highly sensitive protocol for double chromophore labeled ISH has been developed and optimized for whole-mount preparations of *Aplysia* CNS. It has been successfully used for *Aplysia* weighing between 10 and 300 g. This procedure can also be used for molecular mapping of expressed genes in combination with electrophysiological mapping of identified neurons. Lucifer Yellow labeling of specific cells following electrophysiology is retained during ISH, thus the identity of a cell can be positively matched with any particular gene it may express.

E. The presented study adapted and utilized in situ hybridization, staining by nerve back-fill and soma injection, and electrophysiological methods to characterize the locations, numbers, and functions of sensorin-A-expressing neurons and to define the relationships between soma locations and the locations of peripheral axons and receptive fields. Approximately 1,000 cells express sensorin-A mRNA. All of the labeled somata are in the CNS, primarily in the abdominal LE, rLE, RE and RF, pleural VC, cerebral J and K, and buccal S clusters. Together, receptive fields of all these mechanosensory clusters cover the entire body surface. Each VC cluster forms a somatotopic map of the ipsilateral body, a "sensory aplunculus." Neurons in all of the clusters appeared to have relatively high mechanosensory thresholds, responding preferentially to threatening or noxious stimuli. Synaptic outputs to target cells having defensive functions support a nociceptive role, as does peripheral sensitization following noxious stimulation, although additional functions are likely in some clusters.

F. We identified and cloned a new heme enzyme from *Aplysia,* a putative thyroid peroxidase (*Aca*TPO). The *Aplysia* peroxidase gene showed high sequence similarity with peroxidasin and thyroid peroxidases, the critical TH synthesis enzymes found in all vertebrates. Data presented in the paper provide evidence for thyroid hormone-related signaling in *Aplysia* and evidence of endogenous TH synthesis. Furthermore, spatial and temporal expression patterns of these transcripts suggest a role of *Aca*TPO in a variety of processes such as developmental metamorphosis and regulation of the animal's energy metaboli

CHAPTER II.

COPORPHYRINOGEN III OXIDASE (CPO) ENZYME –CLONING, LOCALIZATION OF CPO IN *APLYSIA CALIFORNICA* AND CRYSTALLIZATION OF HUMAN CPO

Heme

Heme (iron protoporphyrin IX) plays a crucial role in variety of biological reactions as a prosthetic group of several hemoproteins, such as haemoglobin in oxygen metabolism, cytochromes in electron transport and respiration, P450 enzymes for drug metabolism and detoxification, as well as being part of signaling pathways as a component of guanylyl cyclase and nitric oxide synthases. Heme is responsible for the color of hemoglobin in red blood cells, and is an essential part of myoglobin, cytochromes, and hemoproteins - including NOS.

Heme is produced in the bone marrow and liver through a complex step by step process of eight different enzymes. As production of heme is tightly regulated, several different intermediate compounds (heme precursors) are created and modified, and only small amounts of precursors in a healthy organism are released through urine and feces. Deficiency of one of the enzymes responsible for the heme production leads to accumulation of heme precursors in tissues (especially in the bone marrow or liver), and its excess presence in the blood, leading to excretion in urine or stools.

Porphyrias

Porphyrias are a group of mainly inborn errors of enzymes involved in heme biosynthesis. Disease is manifested by either autosomal dominant or autosomal recessive inheritance. Human porphyrias have been assigned different names during the years, the most accurate classification system is based on the specific enzyme deficiency. Another system divides porphyrias into hepatic and erythropoetic, based on the major organ overproducing and storing porphyrins (Table 2). The third and clinically relevant classification divides porphyrias as being chronic (cutaneous porphyrias) or acute.

Porphyria	Enzyme Defect	Primary Symptom
Erythropoietic Class		
Congenital erythropoietic porphyria, CEP	Uroporphyrinogen III cosynthase	Photosensitivity
Erythropoietic protoporphyria, EPP	Ferrochelatase	Photosensitivity
Hepatic Class		
ALA dehydratase deficiency porphyria, ADP	ALA dehydratase	Neurovisceral
Acute intermittent porphyria, AIP	PBG deaminase	Neurovisceral
Hereditary coproporphyria, HCP	Coproporphyrinogen oxidase	Neurovisceral,some photosensitivity
Variegate porphyria, VP	Protoporphyrinogen oxidase	Neurovisceral, some photosensitivity
Porphyria cutanea tarda, PCT	Uroporphyrinogen decarboxylase	Photosensitivity
Hepatoerythropoietic porphyria, HEP	Uroporphyrinogen decarboxylase	Photosensitivity, some neurovisceral

Table 2. Classification of porphyrias based on the deficiency of the major organ overproducing and storing porphyrins and specific enzyme deficiency.

Metabolism of heme

Heme is produced in eight consecutive steps. The first part of its synthetic pathway is common with lower organisms as bacteria, algae and plants, leading to formation of chlorophyll and vitamin B12 on one hand and to formation of heme on other hand. The first reaction of heme biosynthesis takes place in the mitochondrion and involves the condensation of L-glycine and L-succinylCoA to δ-aminolevulinic acid (ALA) by δ-aminolevulinic acid synthase (ALA synthase), a pyridoxal phosphate-containing enzyme. This is a rate limiting reaction. Mitochondrial ALA is transported to the cytosol, where ALA dehydratase dimerizes 2 molecules of ALA to produce the pyrrole ring compound porphobilinogen. The next reaction involves the head-to-tail condensation of molecules of porphobilinogen to produce hydroxymethylbilane, the linear tetrapyrrole intermediate, catalysed by porphobilinogen deaminase (PBG deaminase or uroporphyrinogen I synthase). Hydroxymethylbilane can be enzymatically converted to uroporphyrinogen III by a holoenzyme comprised of uroporphyrinogen synthase and uroporphyrinogen III cosynthase. Nonenzymatically hydroxymethylbilane is converted into uroporphyrinogen I. Uroporphyrinogen (normal uroporphyrinogen III or abnormal uroporphyrinogen I) contains eight acetate groups which are all decarboxylated by the enzyme uroporphyrinogen decarboxylase in the cytosol.

Products of this reaction have methy groups in place of acetate and are known as coproporphyrinogens, with coproporphyrinogen III being the normal intermediate in heme synthesis. The resulting coproporphyrinogen III is transported into the mitochondria, by yet unknown mechanism, where 2 propionate residues are decarboxylated, yielding vinyl substituents on the 2 pyrrole rings. The colorless product is protoporphyrinogen IX. In the mitochondrion, protoporphyrinogen IX oxidase localized to the cytoplasmic side of the inner mitochondrial membrane, converts protoporphyrinogen IX to protoporphyrin IX (structure shown below in Figure 27). The oxidase reaction requires molecular oxygen and results in the loss of 6 protons and 6 electrons, yielding a completely conjugated ring system, which is responsible for the characteristic red color of heme-containing molecules like hemoglobin. The final reaction in heme synthesis also takes place in the mitochondrion (in the matrix) and involves the insertion of the iron atom into the ring system generating heme. The enzyme catalyzing this reaction is known as ferrochelatase.

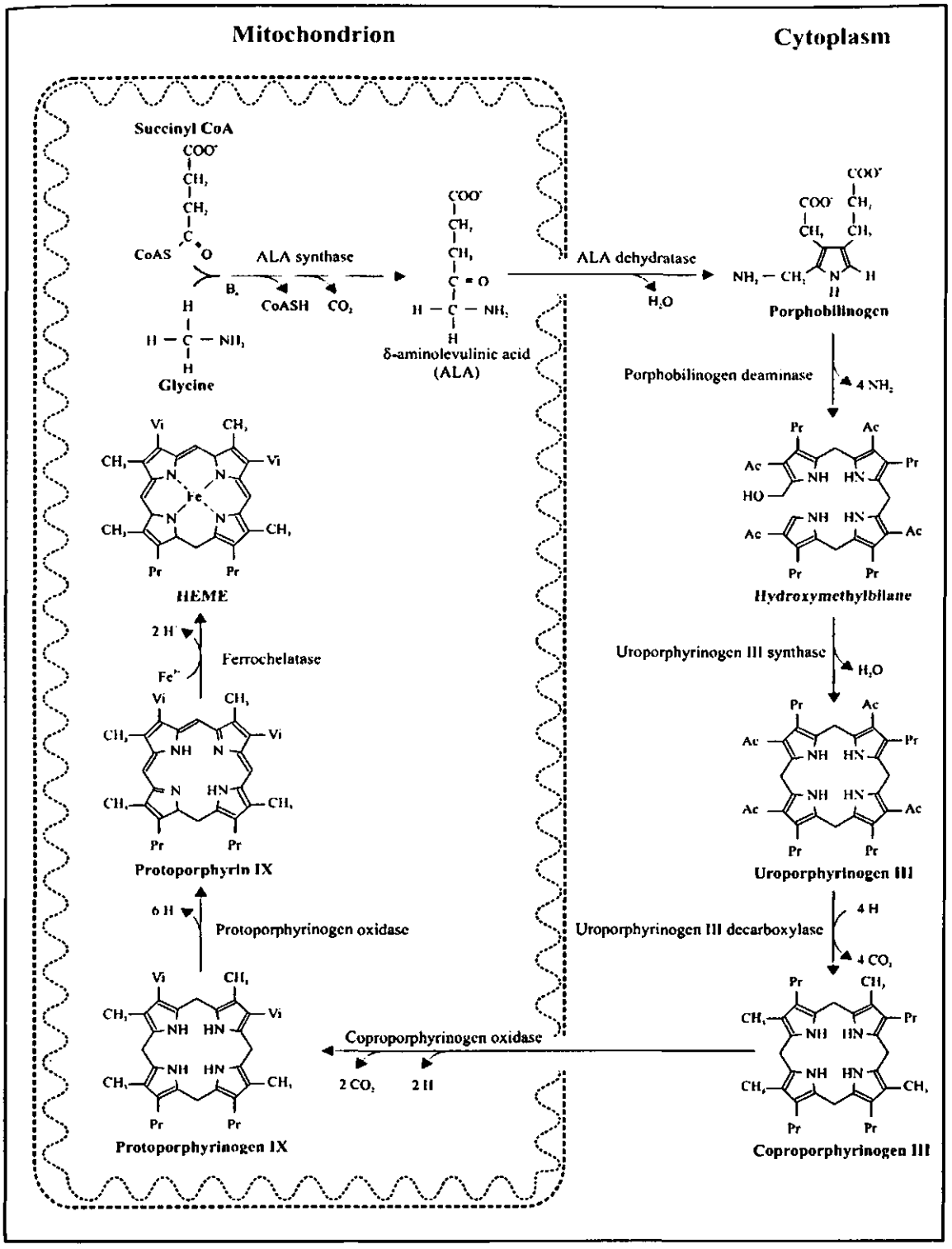

Figure 27. Enzymes and intermediate products in the heme biosynthetic pathway.

Ac= - CH_2COOH, Pr= -CH_2CH_2COOH, Vi= -$CH{=}CH_2$ (Mustajoki, 1999).

CPO

Coproporphyrinogen III oxidase (CPO) is an enzyme catalyzing the sixth step in the heme biosynthesis pathway. It functions as a homodimer, catalyzing the oxidative decarboxylation of coporoporphyrinogen III to protoporphyrinogen IX, without any metals or cofactors. In this reaction the two propionyl groups on the pyrole ring A and B are converted to vinyl groups, through an intermediate known as "harderoporphyrinogen" (Figure 28).

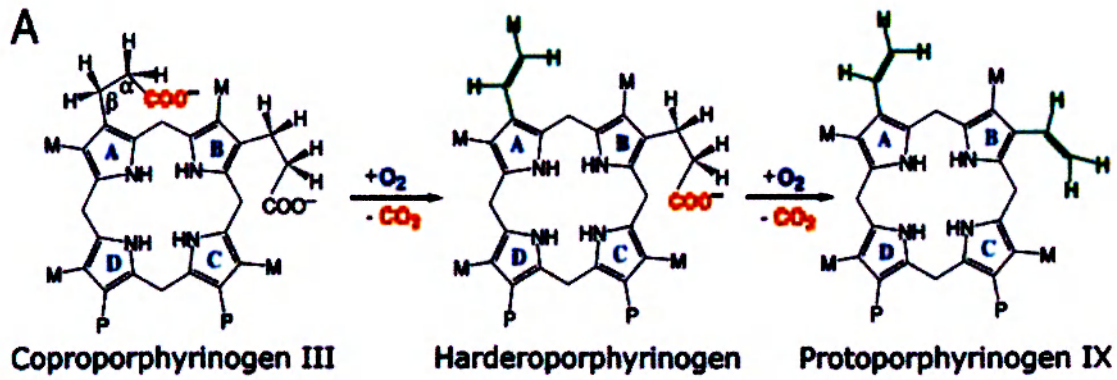

Figure 28. CPO chemistry. (*A*) Reaction catalyzed by CPO involves both oxidation and decarboxylation. CPO sequentially decarboxylates the propionates attached to A and B rings without affecting those on C and D rings. A hydrogen atom from the β-position of the propionate side chain also is removed at each step. The chemical identity of the oxidation end product(s) remains to be elucidated. M = CH3 and P = CH2.CH2.COO- (adapted from Lee et al 2005}

Human CPO gene (EC 1.3.3.3, CPO) is located on chromosome 3q11.2 (Delfau-Larue et al., 1994), cloned by Prof.Martasek (Martasek et al., 1994)}. The CPO gene spans 14kb, and contains 7 exons and encodes an enzyme of 654 amino acids (Abell and Schloss, 1991). In mammals the CPO is localized to the cytoplasmic side of the inner mitochondrial membrane (Grandchamp et al., 1978).

Hereditary coproporphyria (HCP) is an autosomal dominant acute hepatic porphyria, due to mutations in the gene encoding the coproporphyrinogen III oxidase (CPO).

Patients present with an acute neurovisceral crisis provoked by drugs, infection, fasting, stress or menstrual cycle, and clinical manifestation is rarely before puberty (Brodie et al., 1977 Kuhnel A, Gross U 2000). Presentation may be associated with skin lesions as well. Affected individuals excrete lagre amounts of coproporphyrinogen III in urine and feces. A specific and fast diagnosic test for acute attacks of HCP is an intensive red fluorescence of feces under UV light. Diagnosis can be confirmed by measurement of enzymatic activity of CPO in lymphocytes (Blake et al., 1992) and by molecular detection of mutations in the CPO gene (Schmitt et al., 2005 Malonova E, 2005) So far in the CPO gene around 50 mutations (Human Gene Mutation Database, http://www.hgmd.cf.ac.uk/ac/index.php) have been documented in families with hereditary coporporphyria. Acute crisis in HCP may be treated with a high carbohydrate diet and intra venous administration of heme arginine (Tenhunen et al., 1987).

After the cloning of the human CPO gene(Martasek et al., 1994), trials continued for several years to get the crystal structure of the CPO in order to connect the information available on mutations in HCP and clinical manifestation. Cloning of coproporphyrinogen oxidase from other organisms (*Aplysia*, *thermophilus*) helped us find the conserved sequences in the CPO genes and optimize the crystallization conditions for the human CPO protein. With a known CPO crystal structure we can step closer to exploring the understanding of regulation of heme synthesis and specifically the function of CPO in porphyrine synthesis.

METHODS II.

Animals

Live *Aplysia californica* (50-200 g) were supplied by Marinus (Long Beach, CA), and the NIH-*Aplysia* Resource Facility (Miami, FL). Animals were kept in aquaria containing filtered sea water (FSW) at 15-18°C on a 12:12 light:dark cycle. They were regularly fed on live *Gracilaria* seaweed or dried seaweed laver. Prior to dissection, animals were anesthetized by injecting a volume of isotonic $MgCl_2$ (337 mM) equivalent to 50-60% of their weight.

Cloning

Cloning of *Ap*CPX was done from the amplified cDNA from the CNS of *Aplysia*. RNA isolation and preparation of amplified cDNA by reverse transcription-PCR was done as previously described (Matz et al., 1999). The original starting sequence of *Ap*CPX was done using degenerate primers CPX_rev: CCRAAYTTNGTNC CNCKRTCRTA and CPX_dir: ATHGGNGGNATHTTYTTYGAYGA The sequence was extended by the RACE method (Matz et al., 1999), We obtained the full-length cDNA Ac clone (GeneBank accession number: AF 288780) using terminal primers: 5'- ATGGCACAGGTCCTCCGTCAGTGTG -3'and 5'-TCAC ACCCACTCGCGCGGATTCT-3'. Several full length clones of *Ap*CPX were isolated and sequenced.

In situ hybridization

In situ hybridization experiments were performed using whole mount preparations of the CNS of *A. californica*. Plasmid containing the full length *Aplysia* nitric oxide synthase (NOS) sequence (GeneBank accession number: AF288780) were subcloned in pGEM-T vector (Promega)(Sadreyev *et al,* 2002) in JM-109 E.coli cells. The plasmid was isolated, purified and sequenced to obtain the orientation of the gene. The plasmid was linearized with specific restriction enzymes (*NotI* for the anti-sense probe using T7 polymerase, *ApaI* for the sense probe with Sp6 polymerase) and used as a template for the preparation of specific anti-sense and sense digoxigenin-labeled RNA probes following the Roche protocol for probe preparation with DIG RNA labeling kit (Sp6/T7). Sense probes were used as nonspecific controls and none of the control preparations using sense probes (twelve preparations) produced any specific staining in the CNS under identical conditions and labeling protocols.

Our *in situ* hybridization protocol was based on previously published reports (Bogdanov Yu et al., 1996, Jezzini et al.) with several modifications. Briefly, central ganglia were isolated from *Aplysia* and were treated with 1% protease IX (Sigma) in filtered sea water (FSW) for 45-60 minutes at 34°C, Followed by a 15 minute rinse in FSW. The ganglia were pinned to a Sylgard dish in FSW and fixed overnight in 4% paraformaldehyde in 0.2 M PBS (pH 7.2) at 4°C.

Preparations were washed in PBS and connective tissues of the ganglionic sheath were carefully removed from all ganglia. The ganglia were washed in PTW (0.1% Tween 20 in PBS) 3 times for 5 minutes, followed by 10 minute incubation in increasing amounts of methanol (3:1 PTW:MetOH, 1:1, 1:3, and 100% MetOH) where the ganglia were preserved for up to one week. In most experiments, ganglia were transferred back to PTW in the same fashion by repetitive substitution of methanol by PTW (10 minute washes with 1:3 PTW/MetOH, 1:1, 3:1, PTW, followed by a 10 minute wash with 0.3% Triton in PBS, PTW for 5 min). After incubation with proteinase K (10 µg/ml) in PTW at room temperature for 1 hr, the ganglia were postfixed with 4% paraformaldehyde in PBS for 20 minutes at 4°C, and washed (2X, 5 min) in each solution of the following solutions: glycine (2mg/ml PTW), PTW, 0.1M triethanolamine hydrochloride (TEA HCl, pH 8.0), and anhydrous acetate (2.5 µl/ ml) in TEA HCL. The ganglia were then repeatedly washed in PTW. All subsequent steps were done with moderate shaking, including prehybridization in hybridization buffer (50% formamide, 5 mM EDTA, 5x SSC, 1x Denhardt solution (0.02% ficoll, 0.02% polyvinylpyrrolidone, 0.02% BSA), 0.1% Tween 20, 0.5 mg/ml yeast tRNA (GIBCO BRL)) for 6-8 hours at 55°C. Digoxigenin labeled full length RNA probes (2µl/ml) that had undergone alkaline hydrolysis in order to yield shorter length probes for better penetration were added to ganglia and incubated further for 10-12 h. Hybridization was followed by 30 min washing at 60°C in 50% formamide/ 5x SSC/ 1% SDS, then 50% formamide/ 2x SSC/ 1% SDS, then 0.2x SSC, twice for 30 min at 55°C. After 3 washes in PBT (1xPBS, 0.1%Triton x100, 2mg/ml BSA), ganglia were treated with 10% normal goat serum in PBT at 4°C for up to 90min and left overnight with 1: 1350 dilution of alkaline phosphatase-conjugated DIG-antibodies (Boehring) in 1% goat serum in PBT at 4°C. Unbound antibodies were washed out in several PBT incubations at 4°C (at least 2-3 hours total). After two 5 min incubations in detection buffer (100mM NaCl, 50 mM $MgCl_2$, 100 mM NaCl, 100 mM Tris/Cl pH 9.5, 0.01% Tween 20, 1mM levamisol), NBT/BCIP color substrates (DIG Nucleic Acid Detection Kit, Boehringer) were added to detect the hybridized probes. At this stage ganglia were kept at 4°C in the dark with periodic visual assessment of the staining intensity. Following the detection procedure (usually 30-60 minutes), ganglia were postfixed in 4% paraformaldehyde in methanol for up to 1 hour, and washed twice in 100% ethanol. Permanent preparations were produced by incubating ganglia in methylsalycilate and embedding in Permount (Fisher) on microscopic slides.

Examination and analysis of staining was conducted on an upright Nikon Optiphot-2 or an Olympus SZX 12 dissecting microscope. Images were acquired with a Nikon Coolpix 4500 digital camera, and initially saved as JPEG files.

Sequence analysis and phylogenetic tree construction

The alignment was done using ClustalX (EBI European Bioinformatics Institute (Oxford, United Kingdom) (Thompson et al., 1997) with default parameters, all gaps were removed manually in GeneDoc prior to tree construction. Sequence analysis and phylogenetic tree building was done in the program TREEPUZZLE (http://www.tree-puzzle.de) with the default parameters and 10,000 iterations of the maximum likelihood algorithm. The tree itself was drawn with Treeview. The conserved domain was confirmed using Swissprot and Prosite databases.

Protein Preparation and Crystallization

Human CPO homodimer (monomer Mr 39,248) was expressed and purified as described (Martasek et al., 1997). Several attempts to crystallize this protein failed due to time-dependent proteolytic cleavage at residue K230 resulting in two fragments of Mr 13,000 and 26,000. To overcome this, we devised a cross-seeding strategy. First, we obtained crystals of a bacterial CPO (*Chloroflexus aurantiacus*, a thermophilic phototroph). These were grown in sitting drop vapor diffusion setups at 22 °C from a reservoir buffer containing 30% MPD and 100 mM cacodylate buffer, pH 6.5. Crystals obtained under these conditions belong to the hexagonal space group (P6122) with cell dimensions 205.53 x 205.53 x 85.92 Å, $\alpha = 90^{\circ}$, $\beta = 90^{\circ}$, $\gamma = 120^{\circ}$, and easily diffract X-rays to a Bragg spacing of 1.9 Å. Second, seed stocks of *C. aurantiacus* CPO crystals were prepared and used to streak seed into pre-equilibrated solutions containing fresh human CPO (40 mg mL-1), 20% MPD, 0.05 M Tris-HCl pH 7.5, and 10 mM sodium citrate as an additive. Cubic shaped crystals appeared after 48 hours. We used the same strategy to grow crystals of human selenomethionine (Se-Met)-substituted CPO which on their own were not capable of nucleation. Mature crystals were stabilized in a glycerol-containing cryoprotectant prior to flash freezing in liquid nitrogen. The crystals belong to space group P23 with unit cell dimensions of a = b = c = 112.72 Å. There is one molecule in the asymmetric unit corresponding to a solvent content of ~ 60%.

Structural Determination

Data from a native crystal were collected to a Bragg spacing of 1.5 Å using an ADSC Quantum-315 detector at beam line 9-2 of the Stanford Synchrotron Radiation Laboratory. Multiwavelength data on Se-Met human CPO crystals were collected on an ADSC Quantum-4 CCD detector at beamline 5.0.2 of the Advanced Light Source, Berkeley. All data sets were integrated and scaled using the HKL2000 package and the statistics are reported in Table I (which is published as supporting information on the PNAS web site). Human CPO contains seven methionine residues and we were able to identify four of these in native Bijvoet Patterson maps before solving the structure. All seven Se sites, however, were readily interpreted using FPH – FP coefficients as input to the direct methods option of SHELXS. Heavy-atom parameters were refined and phases were calculated at 1.9 Å resolution using SHARP. Solvent flattening with SOLOMON and phase extension to 1.58 Å resolution against structure factor amplitudes from the native crystal produced an electron density map into which majority of residues could be built unambiguously using the program O. The first couple of key refinement steps were performed using the program BUSTER. This was a sine qua non for modeling 4 key loop regions which had no electron density when refined with CNS or REFMAC. All other refinement calculations were performed with CNS and REFMAC (including TLS). Refinement statistics are reported in Table I. ***Equilibrium Analytical Ultracentrifugation.*** 120 μL of wild-type human CPO was sedimented to equilibrium at two different loading concentrations (A280 of 0.32 and 0.4), five different speeds (18.0, 22.1, 23.4, 26.2, and 28.0 krpm) and, at 4 °C in a double-sector, epon-filled centerpieces using an AN60 TI rotor in a Beckman Optima XL-A analytical ultracentrifuge. Scans were taken at 280 nm once equilibrium was established by scanning with 20 averages at a 0.001 cm radial step size setting. Data were globally fitted using the NONLIN software package.

RESULTS II.

Cloning of coproporphyrinogen oxidase gene from the cDNA of Aplysia californica

Several phylogenetically unrelated species from the Gene Bank were chosen that containin the CPO gene. Utilizing the software for analysis of biological sequences (Clustal X, GeneDoc, Jellyfish) we prepared a sequence alignment. From the alignment we chose the most conserved parts of CPX gene and designed degenerate primers for this region. To obtain part of the actual CPO gene fom *Aplysia* californica, we needed to design around 10 primers, from which the CPX_rev: CCRAAYTTNGTNCCNCKRTCRTA and CPX_dir : ATHGGNGGNATHTTYTTY GAYGA showed to be useful in pulling out the ÄpCPX sequence from the *Aplysia* cDNA. The expected product was 210bp long and we directly cloned it the pGEM-T vector, and after ligation, and transformation in JM-109 cells, the plastid was sequenced. With the help of BlastX we were able to check that the cloned part corresponds to the highly conserved part of CPO, making sure that the cloned part coresponds with a high probability with the conserved part of CPX gene. Using the RACE Method (Matz, 2002), designing the nested primers and specific adapter primers ligated at the 3´a 5´ ends of the genes in the cDNA library of the CNS of *Aplysia californica* we obtained the full sequence of APCPX gene. Sequence was submitted to gene bank and the accession numer is AF51085.1 (CPX, AF510850.1, GI:30515681).

In situ hybridization with antisense RNA probe from the full length clone coproporphyrinogen oxidase from *Aplysia* (*Ap*CPX) was localized in the CNS in the cerebral ganglia in th F cluster of neurons (Figure 29). F cluster consists of symetrical clusters located in lateral part of each hemiganglion, on the dorsal surface near the cerebral commissure and morphologically distinct neurons in this region appear to be neuroendocrine cells (Rubakhin et al., 1999).

The sequence alignment with different species (from plants, through bacteria, fish to humans (Figure 31) shows CPO sequence conservation. *Ac*CPO sequence contains all conserved parts important for secondary structure. The analysis of highest BLAST homology (Altschul et al., 1990) of these molluscan CPO sequence reveals the maximum identity of 68% with

Drosophila and 63% with *Homo sapiens*. A simple phylogenetic tree with the representative species from diffrent phyla is depicted in figure 30.

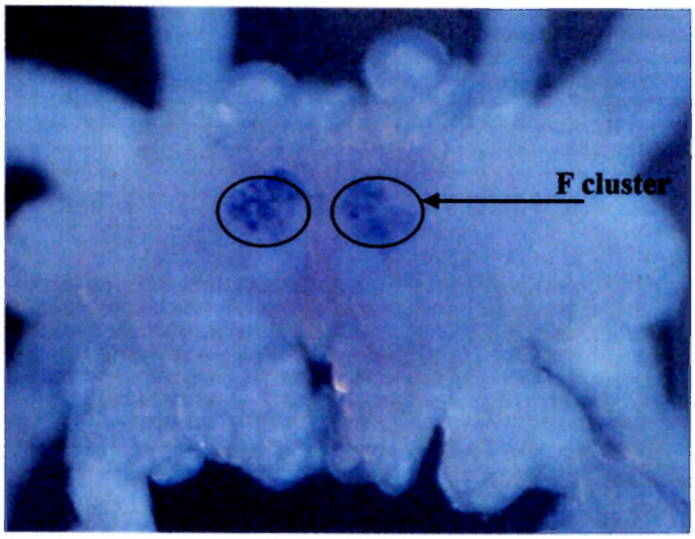

Figure 29. *In situ* hybridization with antisense RNA probe from the full length clone coproporphyrinogen oxidase from *Aplysia californica* (ApCPX). In the CNS of *Aplysia* the ApCPX transcript is localized primarily in the cerebral ganglium (dorsal view), to the F region of neurons, which are connected with metabolism.

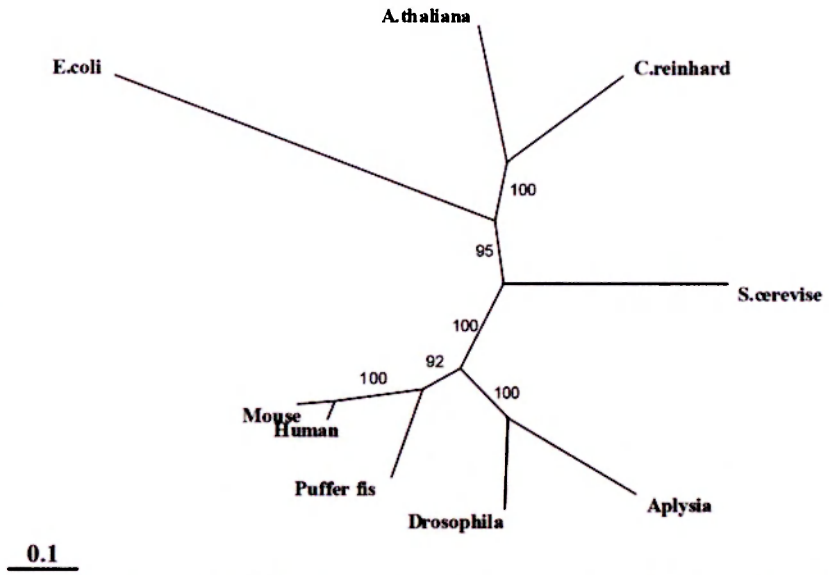

Figure 30. Phylogenetic tree of human, fruit fly, mouse, aplysia, puffer fish, arabidospsis,, chlamydomonas, saccharomyces and E.coli. Numbers stand for support values for the branch.

(Coproporphyrinogen oxidases used for analysis are: CPO from *Homo sapiens* (Accession: AAH23554.1 ; Human); CPO from *Mus musculus* (Accession: NP_031783.2, Mouse); CPO from *Drosophila melanogaster* (Accession: NP_524777; Drosophila), CPO from *Aplysia californica* (Accession. AAP34327.1 ; *Aplysia*), unnamed protein from *Tetraodon nigroviridis* (Accession: CAG08052.1 ; Puffer fish); CPO from *Arabidopsis thaliana* (Accession: NP_171847.1; A.thaliana); CPO from Chlamydomonas reinhardtii (Accession: XP_001701729.1, Ch.reinhardtii); CPO from Saccharomyces cerevisiae (Accession: NP_010329, S.cerevisiae), CPO from *Escherichia coli* (Accession: NP_416931.1; E.coli)) E.coli was used as an outgroup.

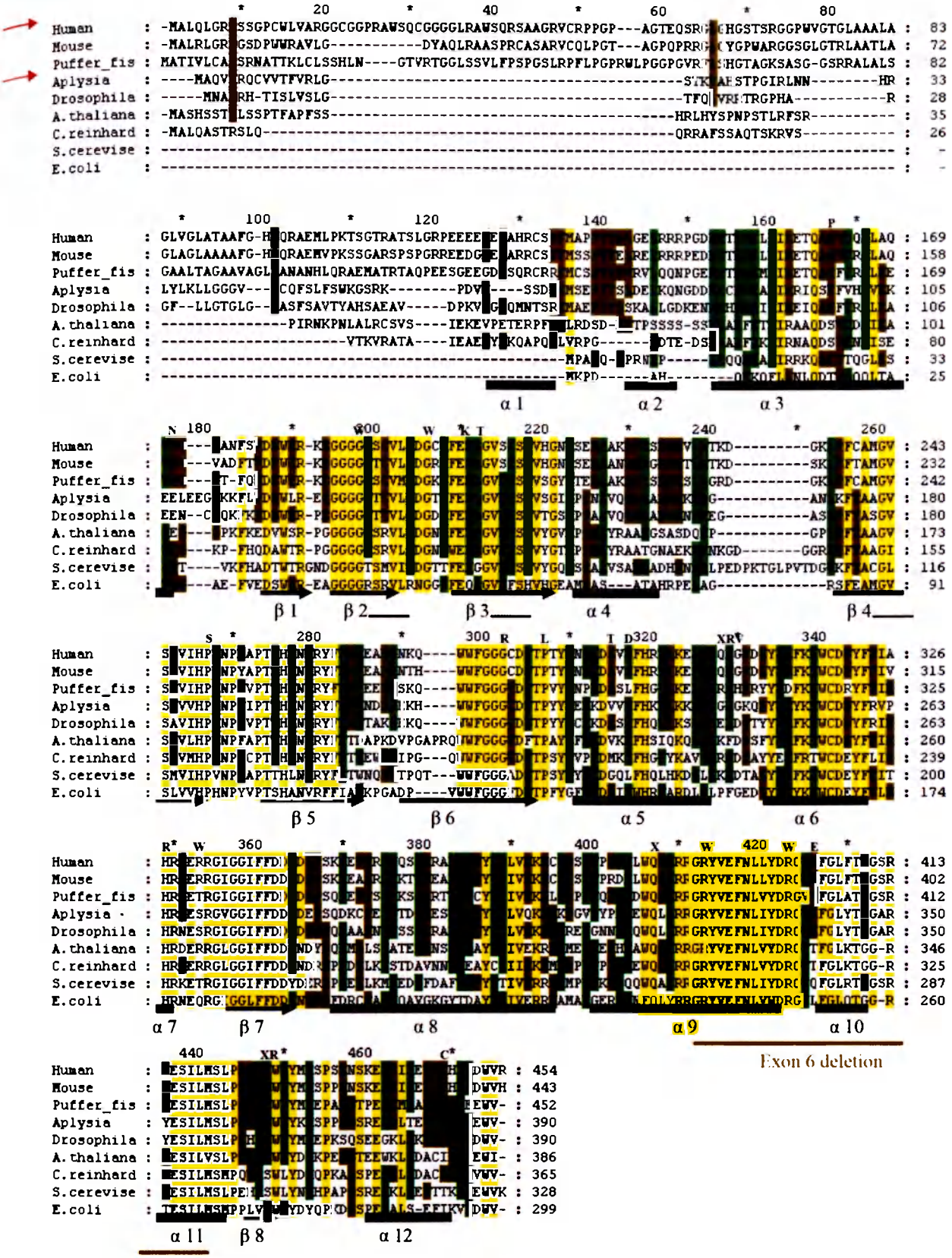
Human
Mouse
Puffer_fis
Aplysia
Drosophila
A.thaliana
C.reinhard
S.cerevise
E.coli
α 1
α 2
α 3
β 1
β 2
β 3
α 4
β 4
β 5
β 6
α 5
α 6
α 7
β 7
α 8
α 9
α 10
Exon 6 deletion
α 11
β 8
α 12

Figure 31. CPO sequence conservation. Sequence alignment, secondary structure, and location of HCP-causing mutations in human CPO. The first 110 amino acids are absent in the mature enzyme, for they are part of a mitochondrial targeting signal that is cleaved upon import. In the alignment (generated by using ClustalX and GeneDoc) yellow represents absolute identity over all sequences present in that part of the alignment. Database of Secondary Structure of Proteins-derived (Kabsch and Sander, 1983) secondary structural assignments are shown directly below the alignment with thick lines indicating α-helices and arrows denoting β-strands. Mutations known to cause HCP are indicated by one letter codes above the human sequence.

(Coproporphyrinogen oxidases used for analysis: see figure 29).

Crystallization of human CPO

The Protein Fold

CPO assumes a previously unknown tertiary topology characterized by a large seven-stranded β-sheet that is flanked on both sides by α-helices (Figure 32*B*). The up-and-down β -strands are similar to porins, but the β-sheet in CPO is flat (Figure 32 B) and does not form a barrel. The flatness of the up-and-down β-sheet in CPO is striking (Figure 32A). In contrast, seven-stranded β -sheet-containing enzymes usually contain a twisted (TauD) (O'Brien et al., 2003) or highly curved (thiol ester dehydrase; ref. 40) β-sheet whose convex or the apolar concave side, respectively, is flanked by helices. The flatness of the CPO sheet is very likely enabled by the abundance of Gly residues found within the β -strands (β 2, β 3, β 4, β 6, and β 7).

A.

B.

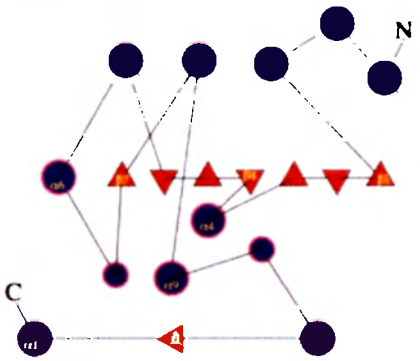

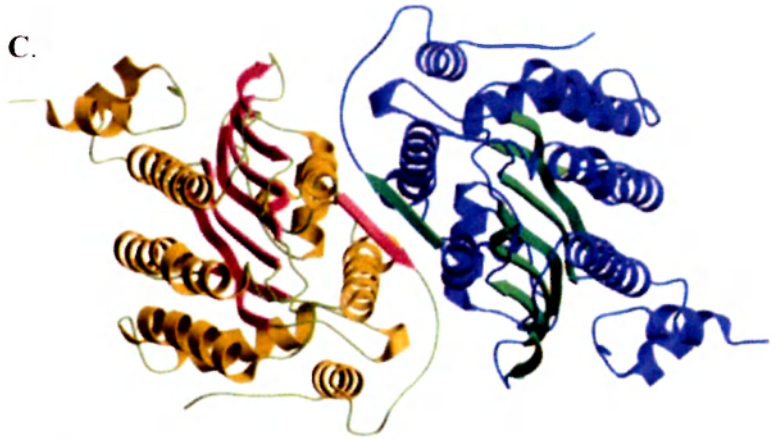

Figure 32. Structure of human CPO. (*A*) Tertiary topology and quaternary structure. (*B*) Topology diagram illustrating the organization of secondary structural elements in human CPO. Filled circles and triangles represent α-helices and β-strands, respectively. (*C*) Dimer interface.

CPO Functions as a Homodimer

The dimensions of the dimer are ≈80 x 60 x 60 Å. The two subunits of the CPO homodimer are related by an ≈40° rotation of one monomer relative to another. This rotation is a hinge-like motion about the crystallographic 2-fold axis located roughly parallel to the β -sheet.

Interestingly, β 8 is not part of the flat β -sheet, but instead pairs up in an antiparallel fashion, with the corresponding β -strand from the second subunit to generate key contacts at the dimer interface (Figure 32C). Overall, the interface is made up of 64% nonpolar atoms and 36% polar atoms. Taken together, the interacting surface on the CPO monomer is a hydrophobic patch. All of the parameters we have used to describe the CPO interface are in excellent agreement with those found in other homodimers (Jones and Thornton, 1995). Thus, it is extremely unlikely that CPO will function as a monomer and we conclude that the homodimer is the biologically relevant form of CPO.

CPO Structure Lacks a Transition Metal Center

We have screened for metal ions bound to CPO by recording anomalous dispersion effects (Hendrickson et al., 1985). We subjected both human and bacterial CPO crystals to fluorescence energy scans at the x-ray absorption edge of Cu, Fe, Mn, and Zn. Furthermore, we have grown CPO crystals in the presence of these metal salts and have collected complete anomalous data sets at the maximal *f* ' values of the absorption edges. Neither the energy scans nor the native anomalous difference Fourier maps provide evidence for bound transition metal ions in CPO.

The Active Site

We discovered that an electropositive cleft (Figure 33A) near the dimer interface had a molecule of citrate (Figure 33 B) bound to it

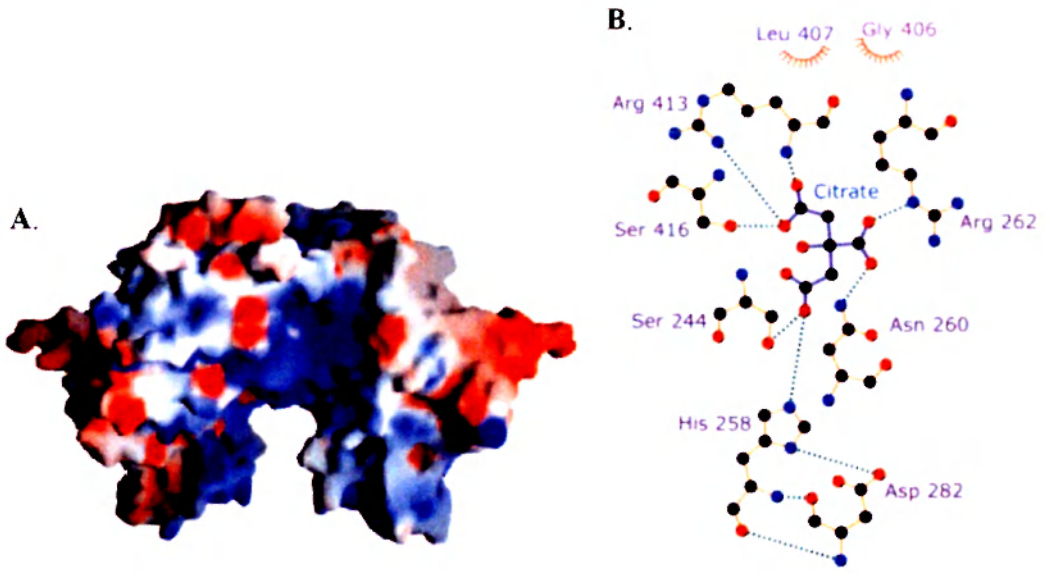

Figure 33. Active site of human CPO. (*A*) Electrostatic potential mapped on to the molecular surface. The electropositive active site cleft is readily visible. The blue and red contours represent positive and negative potential (full saturation = 10 kT), respectively (Figure was generated by using GRASP; (Nicholls et al., 1991)). (*B*) Schematic illustration of the amino acid residues that make direct contact with the bound citrate. Dashed lines indicate H bonds, and nonbonded contacts are represented by an arc with spokes radiating toward the ligand atoms (Figure was generated by using LIGPLOT; (Wallace et al., 1995)).

In proteins, arginine residues are hot candidates for carboxylate recognition (53) and by comparing >500 unique sequences of CPO (>350 of these sequences are from the environmental samples of the Sargasso Sea; ref. 54), we have identified that Arg-262, Arg-328, Arg-332, and Arg-389 are invariant. In addition, there are no conserved Lys residues. Arg-262 forms a key ionic interaction with citrate and Arg-332 is within striking distance. Thus, where coproporphyrinogen III and harderoporphyringen are concerned, we conclude that Arg-262 mediates substrate recognition. The invariant Gly-406 and Leu-407, located in close proximity to a region that affects the second step of CPO catalysis (see below), also make nonbonded contacts with citrate. This part of the active site plays an important role in properly orienting the substrate.

Catalytic Mechanism

CPO catalyzes an unusual metal- and cofactor independent oxidative decarboxylation. It is well established that CPO abstracts the *pro-S* hydrogen from the methylene group adjacent to the pyrrole ring (Figure 28A), leading to the generation of a vinyl group from the remaining three hydrogens and two carbons without rearrangement. Such strong stereoselectivity indicates that CPO strictly constrains the orientation of the substrate in the active site, and our structure provides insights into how this result can be achieved (see above). However, the precise mechanism for hydrogen abstraction is unknown. We favor a mechanism in which oxygen serves as the immediate electron acceptor, and a substrate radical or a carbanion with substantial radical character participates in catalysis.

Structural Basis of Disease

There are several naturally occurring HCP mutations and a majority of these mutations lead to substitution of amino acid residues within the structural framework of CPO (Figure 31). Here we will discuss mutations for which meaningful insights can be provided solely by inspecting the structure of the native enzyme. First, deletion of the region encoded by exon six, comprising residues 392–418, has been reported in a heterozygous patient, and the resulting protein will be unable to dimerize. Indeed, we have confirmed this prediction by expressing the variant in *E. coli*. Trp-427, located on strand β8, makes intersubunit interactions, and, therefore, W427R mutation will also affect dimerization. Second, H327R and R328C will perturb the interaction between helix β 7 and the dimerization helix 9. Third, R331W variant retains sufficient activity to support life in a homozygous setting but can also produce HCP in a heterozygote. Twelve different amino acids are tolerated at position 331 but aromatic residues are not. R331W substitution will abolish the hydrogen bonds between the guanidinium group and the carbonyl of Leu-446 and Arg-447. Interestingly, R447C mutation also results in diminished activity. Finally, K404E causes harderoporphyria, a disease with symptoms unrelated to HCP (Lamoril et al., 2001, Doss et al., 1984, Nordmann et al., 1983, Lamoril et al., 1995). This mutation affects the region that separates helices β 9 and β 10. Lys-404 is not conserved, and the favored residue at this position is Leu. In the human CPO structure, K404 is part of a type I β-turn. Whereas a positively charged residue at this position is not essential for the second decarboxylation step, introducing a negative charge will produce electrostatic repulsion (or steric hindrance), and the enzyme will lose its ability to hold on to harderoporphyrinogen.

This study was performed in cooperation with Prof. Moroz lab at Whitney Laboratory, Saint Augustine, FL, USA and Dr.Raman's lab at the Department of Biochemistry and Molecular Biology, University of Texas Medical School, Houston, TX, USA. My contribution to this study was to identify and clone the coproporphyrinogen oxidase from *Aplysia*, together with submission to NCBI. Then to localize *Ac*CPO transcript in the CNS of *Aplysia*, perform the phylogenetic analysis, further to clone the bacterial CPO from *Chlorophlexus aurantiacus* and *E.coli*, and prepare the CPO expression vectors.

CONCLUSIONS FOR CHAPTER II.

G. The CPO from *Aplysia* has been cloned and we showed its location in the metabolically active part of the CNS of *Aplysia*.

For the first time we report the crystal structure of human CPO at 1.58-Å resolution. The structure reveals a previously uncharacterized tertiary topology comprising an unusually flat seven stranded β-sheet sandwiched by α-helices. Our work has revealed the identity of active site residues in CPO and on the molecular level for several CPO mutations has provided explanation how these alterations diminish enzyme activity.

ABSTRAKT ČESKY (ABSTRACT IN CZECH)

Oxid dusnatý (NO) má nezastupitelnou roli v neuronální signalizaci v řadě eukaryotických a prokaryotických organizmů. NO-syntázy (NOS) jsou hem-obsahující monooxygenázy, které v přítomnosti kyslíku katalyzují oxidaci L-argininu na NO a L-citrulin. NO produkovaný NO-syntázou je plynná molekula, která lehce difunduje přes membrány a zprostředkovává jak mezibuněčnou, tak i vnitrobuněčnou komunikaci. NO aktivuje enzymy vážící kovy včetně solubilní guanylátcyklázy (sGC), a tím zvyšuje hladinu druhého posla cyklického guanosinmonofosfátu (cGMP) (Arnold et al., 1977; Bredt and Snyder, 1989), který dále zprostředkovává řadu fyziologických a patologických procesů v neuronech. Nicméně, detailní charakteristika nitrergních neuronů a funkce NO v centrální nervové soustavě (CNS) není zcela objasněna.

Cílem dizertační práce bylo charakterizovat neuronální NOS, proteiny spojené s metabolismem neuronální NOS a signální dráhu NO v CNS zeje kalifornského (*Aplysia californica*), populárního experimentálního modelu buněčných a systémových neurověd.

Na biochemické úrovni byla zjištěná závislost NOS *Aplysie* (*Ac*NOS) na kalciu- kalmodulinu (Ca-CaM) a NADPH. Řada reprezentativních inhibitorů savčích NOS isoforem též snížila NOS aktivitu u *Aplysie*. Polyklonální protilátky vytvořené proti krysí NOS hybridizovaly na Western blotu s purifikovanou *Ac*NOS (160 kDa protein) z částečně purifikovaných CNS homogenátů.

Aktivita *Ac*NOS popsaná v této práci byla asi šestkrát nižší než zjištěná aktivita NOS v savčím mozečku (Bredt and Snyder, 1990), ale aktivita *Ac*NOS byla srovnatelná s průměrnými hodnotami uváděnými pro nervovou soustavu hmyzu (Regulski and Tully, 1995, Elphick et al., 1993). Stanovili jsme bazální hodnoty produkce cGMP v CNS *Aplysie*. Stimulace NOS donory NO nebo inkubace s inhibitory fosfodiesterázy významně zvýšily hodnoty cGMP. Specifický inhibitor sGC snížil bazální hodnoty cGMP o polovinu a předešel zvýšení cGMP za přítomnosti NO. Na základě těchto výsledků lze předpokládat, že NO funguje jako posel v CNS *Aplysie* a že cGMP je jedním z efektorů NO.

Klonovali jsme *Ac*NOS v jeho plné délce a dokumentovali, že obsahuje všechny konzervované části charakteristické pro funkční NOS u obratlovců. Lokalizovali a zmapovali jsme nitrergní neurony v CNS *Aplysie*. Pomocí *in situ* hybridizace a imunohistochemicky byla prokázána přítomnost NOS v přibližně 2% všech centrálních neuronů.

Optimalizovali jsme protokol pro vícebarevnou *in situ* hybridizaci s použitím celých ganglií („whole mount"), tedy bez nutnosti připravovat řezy. S využitím této nově zavedené metody jsme identifikovali neurony, ve kterých jsme následně korelovali jejich proteinová expresní data a jejich funkci. Tím jsme sestavili i úplnou topografickou mapu uspořádání mechanosensorických neuronů v CNS *Aplysie* exprimujících neuropeptid sensorin-A.

Hodnotili jsme působení jednostranného mechanického poškození „nožního" nervu na úroveň exprese NOS mRNA v neuronech „nožního" ganglia v souvislosti s funkčním významem NO v regeneraci nervů a u neuropatických bolestí. Výsledky *in situ* hybridizace a denzitometrie prokázaly snížení počtu niterních neuronů a intenzity neuronálního zbarvení na straně poškozeného nervu a současné zvýšení *Ac*NOS mRNA v axoplasmě stejnostranného „nožního nervu" pomocí RT-PCR.

Část dizertační práce se soustředila na identifikaci dalšího funkčně významného hemoproteinu, thyroidperoxidázy z *Aplysie* (*Ac*TPO). Po naklonování *Ac*TPO genu a lokalizaci *Ac*TPO transkriptu v CNS *Aplysie* jsme prokázali i přítomnost několika dalších transkriptů. Tyto transkripty přímo souvisejí s thyroidální signalizační dráhou a naznačují funkci a přítomnost látek podobných thyroidálním hormonům i u plžů.

Téma hemoproteinů v této dizertační práci vedlo dále ke studiu hemové syntetické dráhy, konkrétně šestého enzymu této kaskády, koproporphyrinogenoxidázy (CPO). CPO jsme klonovali z *Aplysie* a dalších organismů *(Chlorophlexus aurantiacus, E.coli)*. Klonované CPO jsme použili při optimalizaci krystalizačních podmínek vedoucích k prvnímu publikování krystalové struktury lidské CPO. Krystalová struktura umožnila udělat další krok k pochopení katalytického mechanismu CPO a na molekulární úrovni objasnit snížení enzymatické aktivity u jednotlivých patologických mutací hereditární koproporfyrie.

Klíčová slova: nitric oxid syntáza, cyklický guanosin monofosfát, *Aplysia californica*, CNS, hemoprotein, koproporfyrinogen oxidáza, *in situ* hybridizace

ACKNOWLEDGEMENTS

I would like to express my greatest gratitude to all of you who have been involved in this work in one way or another. It has been my pleasure working together with you, with joyful moments in the lab, as well as outside. Special thanks are due to:

Prof. Pavel Martásek, M.D., DrSc, my supervisor, for giving me the chance to work with him and for the opportunities to cooperate with other labs, further for deepening my insight into the mysteries of nitric oxide synthase, and a broad yet focused view on this area of research.

Prof. Leonid Moroz who was effectively my co-supervisor, for numerous inspiring talks and ideas; and the opportunity to do research and have access to excellent lab facilities at the Whitney Laboratory.

Dr. Jarle Vaage and Dr. Robert Humphries who stood at the beginning of my research trials and showed me the door to yet another world of research in medicine- basic research, together with supportive friends from Karolinska Universitet, Stockholm- Patrick, for always being there for disussion and for reading and commenting the manuscripts and Nora, Chibbe.

Prof. Jiří Zeman, M.D., DrSc, for his supportive attitude towards research has encouraged me and the discussions have influenced my way of working not only as a researcher but also as a practicing physician. My dear friends and colleagues from the Laboratory for Studies of Mitochondrial Disorder - Eva, Alenka, Katka, Hanka, Lenka, Ivan, Danka and Janka for their help during my experimental work and for making a friendly and constructive atmosphere; together with Markéta, to whom I am greatful also for hints and carefull reading of the manuscript.

Friends and colleagues from the Whitney Laboratory, University of Florida, USA- Sami, Thomas, Peter, Andreas, Jim, Christelle for being helpful, friendly and encouraging, and offering an insight into new techniques during my fellowship in their laboratory; and Dr.Yuri Panchin, Naila, Ella and Mike Matz for always having time for discussion of experiments and the beauty of science, or just a good tea.

Dr.Raman from the University of Texas for sharing his positive energy and for giving me the opportunity to cooperate with his lab on several finished and ongoing projects.

And most of all, my patient partner Patrik, for giving me a different perspective on problems, to my son Matej, my parents and my brother, who were always encouraging and provided me with moral support and lots of love.

Acknowledgements: This work was supported by GAČR grants 309/02/1139 to PM and MB, and GAUK grant 10/2002/1.LF to MB.

This PhD thesis was elaborated at the Laboratory for Studies of Mitochondrial Disorders, Department of Pediatrics, 1st Faculty of Medicine in Prague, Czech Republic and in the Whitney Laboratory in Marineland, Florida, USA. The dissertation is based on the results of 5 scientific papers published in the prestigious journals, and 2 manuscripts prior to submission for publication.

REFERENCES

Abell LM, Schloss JV (1991) Oxygenase side reactions of acetolactate synthase and other carbanion-forming enzymes. *Biochemistry,* **30,** 7883-7.

Abu-Soud HM, Yoho LL, Stuehr DJ (1994) Calmodulin controls neuronal nitric-oxide synthase by a dual mechanism. Activation of intra- and interdomain electron transfer. *J Biol Chem,* **269,** 32047-50.

Adak S, Bilwes AM, Panda K, et al. (2002) Cloning, expression, and characterization of a nitric oxide synthase protein from Deinococcus radiodurans. *Proc Natl Acad Sci U S A,* **99,** 107-12.

Adamson DC, Wildemann B, Sasaki M, et al. (1996) Immunologic NO synthase: elevation in severe AIDS dementia and induction by HIV-1 gp41. *Science,* **274,** 1917-21.

Adoutte A, Balavoine G, Lartillot N, de Rosa R (1999) Animal evolution. The end of the intermediate taxa? *Trends Genet,* **15,** 104-8.

Altschul SF, Gish W, Miller W, Myers EW, Lipman DJ (1990) Basic local alignment search tool. *J Mol Biol,* **215,** 403-10.

Antonov I, Ha T, Antonova I, Moroz LL, Hawkins RD (2007) Role of nitric oxide in classical conditioning of siphon withdrawal in Aplysia. *J Neurosci,* **27,** 10993-1002.

Aonuma H (2002) Distribution of NO-induced cGMP-like immunoreactive neurones in the abdominal nervous system of the crayfish, Procambarus clarkii. *Zoolog Sci,* **19,** 969-79.

Arnold WP, Mittal CK, Katsuki S, Murad F (1977) Nitric oxide activates guanylate cyclase and increases guanosine 3':5'-cyclic monophosphate levels in various tissue preparations. *Proc Natl Acad Sci U S A,* **74,** 3203-7.

Balligand JL, Kelly RA, Marsden PA, Smith TW, Michel T (1993) Control of cardiac muscle cell function by an endogenous nitric oxide signaling system. *Proc Natl Acad Sci U S A,* **90,** 347-51.

Bastiani MJ, Harrelson AL, Snow PM, Goodman CS (1987) Expression of fasciclin I and II glycoproteins on subsets of axon pathways during neuronal development in the grasshopper. *Cell,* **48,** 745-55.

Beavo JA, Hardman JG, Sutherland EW (1970) Hydrolysis of cyclic guanosine and adenosine 3',5'-monophosphates by rat and bovine tissues. *J Biol Chem,* **245,** 5649-55.

Bedi SS, Glanzman DL (2001) Axonal rejoining inhibits injury-induced long-term changes in Aplysia sensory neurons in vitro. *J Neurosci,* **21,** 9667-77.

Beltran B, Quintero M, Garcia-Zaragoza E, O'Connor E, Esplugues JV, Moncada S (2002) Inhibition of mitochondrial respiration by endogenous nitric oxide: a critical step in Fas signaling. *Proc Natl Acad Sci U S A,* **99,** 8892-7.

Belvisi M, Barnes PJ, Larkin S, et al. (1995) Nitric oxide synthase activity is elevated in inflammatory lung disease in humans. *Eur J Pharmacol,* **283,** 255-8.

Bivalacqua TJ, Champion HC, Hellstrom WJ, Kadowitz PJ (2000) Pharmacotherapy for erectile dysfunction. *Trends Pharmacol Sci,* **21,** 484-9.

Blake D, McManus J, Cronin V, Ratnaike S (1992) Fecal coproporphyrin isomers in hereditary coproporphyria. *Clin Chem,* **38,** 96-100.

Bogdanov Yu D, Balaban PM, Zakharov IS, Poteryaev DA, Belyavsky AV (1996) Identification of two novel genes specifically expressed in the D-group neurons of the terrestrial snail CNS. *Invert Neurosci,* **2,** 61-9.

Bohme GA, Bon C, Lemaire M, et al. (1993) Altered synaptic plasticity and memory formation in nitric oxide synthase inhibitor-treated rats. *Proc Natl Acad Sci U S A,* **90,** 9191-4.

Boulanger CM, Vanhoutte PM (1997) G proteins and endothelium-dependent relaxations. *J Vasc Res,* **34,** 175-85.

Bradford MM (1976) A rapid and sensitive method for the quantitation of microgram quantities of protein utilizing the principle of protein-dye binding. *Anal Biochem,* **72,** 248-54.

Bredt DS, Hwang PM, Glatt CE, Lowenstein C, Reed RR, Snyder SH (1991) Cloned and expressed nitric oxide synthase structurally resembles cytochrome P-450 reductase. *Nature,* **351,** 714-8.

Bredt DS, Snyder SH (1989) Nitric oxide mediates glutamate-linked enhancement of cGMP levels in the cerebellum. *Proc Natl Acad Sci U S A,* **86,** 9030-3.

Bredt DS, Snyder SH (1990) Isolation of nitric oxide synthetase, a calmodulin-requiring enzyme. *Proc Natl Acad Sci U S A,* **87,** 682-5.

Brembs B, Baxter DA, Byrne JH (2004) Extending in vitro conditioning in Aplysia to analyze operant and classical processes in the same preparation. *Learn Mem,* **11,** 412-20.

Brian JE, Jr., Heistad DD, Faraci FM (1995) Dilatation of cerebral arterioles in response to lipopolysaccharide in vivo. *Stroke,* **26,** 277-80; discussion 281.

Brodie MJ, Thompson GG, Moore MR, Beattie AD, Goldberg A (1977) Hereditary coproporphyria. Demonstration of the abnormalities in haem biosynthesis in peripheral blood. *Q J Med,* **46,** 229-41.

Brunet JF, Shapiro E, Foster SA, Kandel ER, Iino Y (1991) Identification of a peptide specific for Aplysia sensory neurons by PCR-based differential screening. *Science,* **252,** 856-9.

Byrne J, Castellucci V, Kandel ER (1974) Receptive fields and response properties of mechanoreceptor neurons innervating siphon skin and mantle shelf in Aplysia. *J Neurophysiol,* **37,** 1041-64.

Calapai G, Squadrito F, Altavilla D, et al. (1992) Evidence that nitric oxide modulates drinking behaviour. *Neuropharmacology,* **31,** 761-4.

Cash D, Carew TJ (1989) A quantitative analysis of the development of the central nervous system in juvenile Aplysia californica. *J Neurobiol,* **20,** 25-47.

Clifford KT, Gross L, Johnson K, Martin KJ, Shaheen N, Harrington MA (2003) Slime-trail tracking in the predatory snail, Euglandina rosea. *Behav Neurosci,* **117,** 1086-95.

Crane BR, Arvai AS, Gachhui R, et al. (1997) The structure of nitric oxide synthase oxygenase domain and inhibitor complexes. *Science,* **278,** 425-31.

Crane BR, Arvai AS, Ghosh DK, et al. (1998) Structure of nitric oxide synthase oxygenase dimer with pterin and substrate. *Science,* **279,** 2121-6.

Cropper EC, Evans CG, Jing J, et al. (2004) Regulation of afferent transmission in the feeding circuitry of Aplysia. *Acta Biol Hung,* **55,** 211-20.

Cudeiro J, Rivadulla C (1999) Sight and insight--on the physiological role of nitric oxide in the visual system. *Trends Neurosci,* **22,** 109-16.

Cueto M, Hernandez-Perera O, Martin R, et al. (1996) Presence of nitric oxide synthase activity in roots and nodules of Lupinus albus. *FEBS Lett,* **398,** 159-64.

Davis MP, Homsi J (2001) The importance of cytochrome P450 monooxygenase CYP2D6 in palliative medicine. *Support Care Cancer,* **9,** 442-51.

Delfau-Larue MH, Martasek P, Grandchamp B (1994) Coproporphyrinogen oxidase: gene organization and description of a mutation leading to exon 6 skipping. *Hum Mol Genet,* **3,** 1325-30.

Doss M, von Tiepermann R, Kopp W (1984) Harderoporphyrin coproporphyria. *Lancet,* **1,** 292.

Dubuc B, Castellucci VF (1991) Receptive fields and properties of a new cluster of mechanoreceptor neurons innervating the mantle region and the branchial cavity of the marine mollusk Aplysia californica. *J Exp Biol,* **156,** 315-34.

Elofsson R, Carlberg M, Moroz L, Nezlin L, Sakharov D (1993) Is nitric oxide (NO) produced by invertebrate neurones? *Neuroreport,* **4,** 279-82.

Elphick MR, Green IC, O'Shea M (1993) Nitric oxide synthesis and action in an invertebrate brain. *Brain Res,* **619,** 344-6.

Elphick MR, Kemenes G, Staras K, O'Shea M (1995) Behavioral role for nitric oxide in chemosensory activation of feeding in a mollusc. *J Neurosci,* **15,** 7653-64.

Estrada C, DeFelipe J (1998) Nitric oxide-producing neurons in the neocortex: morphological and functional relationship with intraparenchymal microvasculature. *Cereb Cortex,* **8,** 193-203.

Fiore L, Geppetti L (1985) Input-output relationships of identified buccal neurones involved in feeding control in Aplysia. *Behav Brain Res,* **16,** 37-45.

Forstermann U (1994) Biochemistry and molecular biology of nitric oxide synthases. *Arzneimittelforschung,* **44,** 402-7.

Friebe A, Koesling D (2003) Regulation of nitric oxide-sensitive guanylyl cyclase. *Circ Res,* **93,** 96-105.

Fujie S, Aonuma H, Ito I, Gelperin A, Ito E (2002) The nitric oxide/cyclic GMP pathway in the olfactory processing system of the terrestrial slug Limax marginatus. *Zoolog Sci,* **19,** 15-26.

Furchgott RF, Zawadzki JV (1980) The obligatory role of endothelial cells in the relaxation of arterial smooth muscle by acetylcholine. *Nature,* **288,** 373-6.

Garcia-Cardena G, Martasek P, Masters BS, et al. (1997) Dissecting the interaction between nitric oxide synthase (NOS) and caveolin. Functional significance of the nos caveolin binding domain in vivo. *J Biol Chem,* **272,** 25437-40.

Garthwaite J, Charles SL, Chess-Williams R (1988) Endothelium-derived relaxing factor release on activation of NMDA receptors suggests role as intercellular messenger in the brain. *Nature,* **336,** 385-8.

Garthwaite J, Southam E, Boulton CL, Nielsen EB, Schmidt K, Mayer B (1995) Potent and selective inhibition of nitric oxide-sensitive guanylyl cyclase by 1H-[1,2,4]oxadiazolo[4,3-a]quinoxalin-1-one. *Mol Pharmacol,* **48,** 184-8.

Garvey EP, Oplinger JA, Tanoury GJ, et al. (1994) Potent and selective inhibition of human nitric oxide synthases. Inhibition by non-amino acid isothioureas. *J Biol Chem,* **269,** 26669-76.

Gelperin A (1994) Nitric oxide mediates network oscillations of olfactory interneurons in a terrestrial mollusc. *Nature,* **369,** 61-3.

Gelperin A, Flores J, Raccuia-Behling F, Cooke IR (2000) Nitric oxide and carbon monoxide modulate oscillations of olfactory interneurons in a terrestrial mollusk. *J Neurophysiol,* **83,** 116-27.

Gillespie JS, Liu XR, Martin W (1989) The effects of L-arginine and NG-monomethyl L-arginine on the response of the rat anococcygeus muscle to NANC nerve stimulation. *Br J Pharmacol,* **98,** 1080-2.

Golderer G, Werner ER, Leitner S, Grobner P, Werner-Felmayer G (2001) Nitric oxide synthase is induced in sporulation of Physarum polycephalum. *Genes Dev,* **15,** 1299-309.

Grandchamp B, Phung N, Nordmann Y (1978) The mitochondrial localization of coproporphyrinogen III oxidase. *Biochem J,* **176,** 97-102.

Griffith OW, Stuehr DJ (1995) Nitric oxide synthases: properties and catalytic mechanism. *Annu Rev Physiol,* **57,** 707-36.

Hanafy KA, Krumenacker JS, Murad F (2001) NO, nitrotyrosine, and cyclic GMP in signal transduction. *Med Sci Monit,* **7,** 801-19.

Hardman JG, Sutherland EW (1969) Guanyl cyclase, an enzyme catalyzing the formation of guanosine 3',5'-monophosphate from guanosine trihosphate. *J Biol Chem,* **244,** 6363-70.

Hart CM (1999) Nitric oxide in adult lung disease. *Chest,* **115,** 1407-17.

Hendrickson WA, Smith JL, Sheriff S (1985) Direct phase determination based on anomalous scattering. *Methods Enzymol,* **115,** 41-55.

Hibbs JB, Jr., Taintor RR, Vavrin Z, Rachlin EM (1988) Nitric oxide: a cytotoxic activated macrophage effector molecule. *Biochem Biophys Res Commun,* **157,** 87-94.

Holscher C, Rose SP (1992) An inhibitor of nitric oxide synthesis prevents memory formation in the chick. *Neurosci Lett,* **145,** 165-7.

Hong IS, Kim YK, Choi WS, et al. (2003) Purification and characterization of nitric oxide synthase from Staphylococcus aureus. *FEMS Microbiol Lett,* **222,** 177-82.

Hope BT, Michael GJ, Knigge KM, Vincent SR (1991) Neuronal NADPH diaphorase is a nitric oxide synthase. *Proc Natl Acad Sci U S A,* **88,** 2811-4.

Hu JY, Meng X, Schacher S (2002) Target interaction regulates distribution and stability of specific mRNAs. *J Neurosci,* **22,** 2669-78.

Huang S, Kerschbaum HH, Engel E, Hermann A (1997) Biochemical characterization and histochemical localization of nitric oxide synthase in the nervous system of the snail, Helix pomatia. *J Neurochem,* **69,** 2516-28.

Huang S, Kerschbaum HH, Hermann A (1998) Nitric oxide-mediated cGMP synthesis in Helix neural ganglia. *Brain Res,* **780,** 329-36.

Huang Z, Huang PL, Panahian N, Dalkara T, Fishman MC, Moskowitz MA (1994) Effects of cerebral ischemia in mice deficient in neuronal nitric oxide synthase. *Science,* **265,** 1883-5.

Chao DS, Gorospe JR, Brenman JE, et al. (1996) Selective loss of sarcolemmal nitric oxide synthase in Becker muscular dystrophy. *J Exp Med,* **184,** 609-18.

Chen Y, Rosazza JP (1995) Purification and characterization of nitric oxide synthase (NOSNoc) from a Nocardia species. *J Bacteriol,* **177,** 5122-8.

Chenchik A, Diachenko L, Moqadam F, Tarabykin V, Lukyanov S, Siebert PD (1996) Full-length cDNA cloning and determination of mRNA 5' and 3' ends by amplification of adaptor-ligated cDNA. *Biotechniques,* **21,** 526-34.

Chichery R, Chichery MP (1994) NADPH-diaphorase in a cephalopod brain (Sepia): presence in an analogue of the cerebellum. *Neuroreport,* **5,** 1273-6.

Chino Y, Saito M, Yamasu K, Suyemitsu T, Ishihara K (1994) Formation of the adult rudiment of sea urchins is influenced by thyroid hormones. *Dev Biol,* **161,** 1-11.

Choi WS, Chang MS, Han JW, Hong SY, Lee HW (1997) Identification of nitric oxide synthase in Staphylococcus aureus. *Biochem Biophys Res Commun,* **237,** 554-8.

Chomczynski P, Sacchi N (1987) Single-step method of RNA isolation by acid guanidinium thiocyanate-phenol-chloroform extraction. *Anal Biochem,* **162,** 156-9.

Ignarro LJ, Buga GM, Wood KS, Byrns RE, Chaudhuri G (1987) Endothelium-derived relaxing factor produced and released from artery and vein is nitric oxide. *Proc Natl Acad Sci U S A,* **84,** 9265-9.

Itoh H, Hidaka H (1984) Direct interaction of calmodulin antagonists with Ca2+/calmodulin-dependent cyclic nucleotide phosphodiesterase. *J Biochem (Tokyo),* **96,** 1721-6.

Jacklet JW (1995) Nitric oxide is used as an orthograde cotransmitter at identified histaminergic synapses. *J Neurophysiol,* **74,** 891-5.

Jacklet JW, Gruhn M (1994) Co-localization of NADPH-diaphorase and myomodulin in synaptic glomeruli of Aplysia. *Neuroreport,* **5,** 1841-4.

Jezzini SH, Bodnarova M, Moroz LL (2005) Two-color in situ hybridization in the CNS of Aplysia californica. *Journal of Neuroscience Methods,* **149,** 15-25.

Jezzini SH, Moroz LL (2004) Identification and distribution of a two-pore domain potassium channel in the CNS of Aplysia californica. *Brain Res Mol Brain Res,* **127,** 27-38.

Johansson KU, Carlberg M (1994) NADPH-diaphorase histochemistry and nitric oxide synthase activity in deutocerebrum of the crayfish, Pacifastacus leniusculus (Crustacea, Decapoda). *Brain Res,* **649,** 36-42.

Jones S, Thornton JM (1995) Protein-protein interactions: a review of protein dimer structures. *Prog Biophys Mol Biol,* **63,** 31-65.

Kabsch W, Sander C (1983) Dictionary of protein secondary structure: pattern recognition of hydrogen-bonded and geometrical features. *Biopolymers,* **22,** 2577-637.

Kacharmina JE, Crino PB, Eberwine J (1999) Preparation of cDNA from single cells and subcellular regions. *Methods Enzymol,* **303,** 3-18.

Kandel ER (1976) *Cellular Basis of Behavior,* W.H. Freeman and Company, San Francisco.

Kandel ER (2001) The molecular biology of memory storage: a dialogue between genes and synapses. *Science,* **294,** 1030-8.

Katzoff A, Ben-Gedalya T, Susswein AJ (2002) Nitric oxide is necessary for multiple memory processes after learning that a food is inedible in aplysia. *J Neurosci,* **22,** 9581-94.

Kendrick KM, Guevara-Guzman R, Zorrilla J, et al. (1997) Formation of olfactory memories mediated by nitric oxide. *Nature,* **388,** 670-4.

Kim HW, Batista LA, Hoppes JL, Lee KJ, Mykles DL (2004) A crustacean nitric oxide synthase expressed in nerve ganglia, Y-organ, gill and gonad of the tropical land crab, Gecarcinus lateralis. *J Exp Biol,* **207,** 2845-57.

Kim WS, Ye X, Rubakhin SS, Sweedler JV (2006) Measuring nitric oxide in single neurons by capillary electrophoresis with laser-induced fluorescence: use of ascorbate oxidase in diaminofluorescein measurements. *Anal Chem,* **78,** 1859-65.

Kimura T, Shouno O, Matsumoto G (1997) NADPH-diaphorase containing cells and fibers in the central nervous system of squid, Loligo bleekeri keferstein. *Life Sci,* **61,** 2375-81.

Klatt P, Molina EP, Lamas S (1999) Nitric oxide inhibits c-Jun DNA binding by specifically targeted S-glutathionylation. *J Biol Chem,* **274,** 15857-64.

Koh HY, Jacklet JW (1999) Nitric oxide stimulates cGMP production and mimics synaptic responses in metacerebral neurons of Aplysia. *J Neurosci,* **19,** 3818-26.

Koh HY, Jacklet JW (2001) Nitric oxide induces cGMP immunoreactivity and modulates membrane conductance in identified central neurons of Aplysia. *Eur J Neurosci,* **13,** 553-60.

Koh SD, Campbell JD, Carl A, Sanders KM (1995) Nitric oxide activates multiple potassium channels in canine colonic smooth muscle. *J Physiol,* **489 (Pt 3),** 735-43.

Kone BC, Kuncewicz T, Zhang W, Yu ZY (2003) Protein interactions with nitric oxide synthases: controlling the right time, the right place, and the right amount of nitric oxide. *Am J Physiol Renal Physiol,* **285,** F178-90.

Korneev SA, Piper MR, Picot J, Phillips R, Korneeva EI, O'Shea M (1998) Molecular characterization of NOS in a mollusc: expression in a giant modulatory neuron. *J Neurobiol,* **35,** 65-76.

Kubes P, Suzuki M, Granger DN (1991) Nitric oxide: an endogenous modulator of leukocyte adhesion. *Proc Natl Acad Sci U S A,* **88,** 4651-5.

Laemmli UK (1970) Cleavage of structural proteins during the assembly of the head of bacteriophage T4. *Nature,* **227,** 680-5.

Laing KJ, Grabowski PS, Belosevic M, Secombes CJ (1996) A partial sequence for nitric oxide synthase from a goldfish (Carassius auratus) macrophage cell line. *Immunol Cell Biol,* **74,** 374-9.

Lamoril J, Martasek P, Deybach JC, Da Silva V, Grandchamp B, Nordmann Y (1995) A molecular defect in coproporphyrinogen oxidase gene causing harderoporphyria, a variant form of hereditary coproporphyria. *Hum Mol Genet,* **4,** 275-8.

Lamoril J, Puy H, Whatley SD, et al. (2001) Characterization of mutations in the CPO gene in British patients demonstrates absence of genotype-phenotype correlation and identifies relationship between hereditary coproporphyria and harderoporphyria. *Am J Hum Genet,* **68,** 1130-8.

Lee CY, Zou HS, Yau SM, Ju YR, Liau CS (2000) Nitric oxide synthase activity and immunoreactivity in the crayfish Procambarus clarkii. *Neuroreport,* **11,** 1273-6.

Lechner HA, Byrne JH (1998) New perspectives on classical conditioning: a synthesis of Hebbian and non-Hebbian mechanisms. *Neuron,* **20,** 355-8.

Levenson J, Sherry DM, Dryer L, Chin J, Byrne JH, Eskin A (2000) Localization of glutamate and glutamate transporters in the sensory neurons of Aplysia. *J Comp Neurol,* **423,** 121-31.

Lewin MR, Walters ET (1999) Cyclic GMP pathway is critical for inducing long-term sensitization of nociceptive sensory neurons. *Nat Neurosci,* **2,** 18-23.

Li CG, Rand MJ (1989) Evidence for a role of nitric oxide in the neurotransmitter system mediating relaxation of the rat anococcygeus muscle. *Clin Exp Pharmacol Physiol,* **16,** 933-8.

Lin MF, Leise EM (1996) NADPH-diaphorase activity changes during gangliogenesis and metamorphosis in the gastropod mollusc Ilyanassa obsoleta. *J Comp Neurol,* **374,** 194-203.

Lipton SA, Choi YB, Pan ZH, et al. (1993) A redox-based mechanism for the neuroprotective and neurodestructive effects of nitric oxide and related nitroso-compounds. *Nature,* **364,** 626-32.

Lovell P, Moroz LL (2006) The largest growth cones in the animal kingdom: an illustrated guide to the dynamics of Aplysia neuronal growth in cell culture

10.1093/icb/icl042. *Integr. Comp. Biol.*, **46**, 847-870.

Luk'ianov KA, Gurskaia IG, Matts MV, et al. (1996) [A method for obtaining the normalized cDNA libraries based on the effect of suppression of polymerase chain reaction]. *Bioorg Khim*, **22**, 686-90.

Lynch JW (1998) Nitric oxide inhibition of the rat olfactory cyclic nucleotide-gated cation channel. *J Membr Biol*, **165**, 227-34.

Mao J (1999) NMDA and opioid receptors: their interactions in antinociception, tolerance and neuroplasticity. *Brain Res Brain Res Rev*, **30**, 289-304.

Martasek P, Camadro JM, Delfau-Larue MH, et al. (1994) Molecular cloning, sequencing, and functional expression of a cDNA encoding human coproporphyrinogen oxidase. *Proc Natl Acad Sci U S A*, **91**, 3024-8.

Martasek P, Camadro JM, Raman CS, et al. (1997) Human coproporphyrinogen oxidase. Biochemical characterization of recombinant normal and R231W mutated enzymes expressed in E. coli as soluble, catalytically active homodimers. *Cell Mol Biol (Noisy-le-grand)*, **43**, 47-58.

Matz M, Shagin D, Bogdanova E, et al. (1999) Amplification of cDNA ends based on template-switching effect and step-out PCR. *Nucleic Acids Res*, **27**, 1558-60.

Matz MV (2002) Amplification of representative cDNA samples from microscopic amounts of invertebrate tissue to search for new genes. *Methods Mol Biol*, **183**, 3-18.

Matz MV, Alieva NO, Chenchik A, Lukyanov S (2003) Amplification of cDNA ends using PCR suppression effect and step-out PCR. *Methods Mol Biol*, **221**, 41-9.

McAllister LB, Scheller RH, Kandel ER, Axel R (1983) In situ hybridization to study the origin and fate of identified neurons. *Science*, **222**, 800-8.

McMillan K, Masters BS (1993) Optical difference spectrophotometry as a probe of rat brain nitric oxide synthase heme-substrate interaction. *Biochemistry*, **32**, 9875-80.

Mearin F, Mourelle M, Guarner F, et al. (1993) Patients with achalasia lack nitric oxide synthase in the gastro-oesophageal junction. *Eur J Clin Invest*, **23**, 724-8.

Meulemans A, Mothet JP, Schirar A, Fossier P, Tauc L, Baux G (1995) A nitric oxide synthase activity is involved in the modulation of acetylcholine release in Aplysia ganglion neurons: a histological, voltammetric and electrophysiological study. *Neuroscience*, **69**, 985-95.

Moccia R, Chen D, Lyles V, et al. (2003) An unbiased cDNA library prepared from isolated Aplysia sensory neuron processes is enriched for cytoskeletal and translational mRNAs. *J Neurosci*, **23**, 9409-17.

Moncada S, Palmer RM, Higgs EA (1988) The discovery of nitric oxide as the endogenous nitrovasodilator. *Hypertension*, **12**, 365-72.

Moore WM, Webber RK, Jerome GM, Tjoeng FS, Misko TP, Currie MG (1994) L-N6-(1-iminoethyl)lysine: a selective inhibitor of inducible nitric oxide synthase. *J Med Chem*, **37**, 3886-8.

Morley D, Maragos CM, Zhang XY, Boignon M, Wink DA, Keefer LK (1993) Mechanism of vascular relaxation induced by the nitric oxide (NO)/nucleophile complexes, a new class of NO-based vasodilators. *J Cardiovasc Pharmacol*, **21**, 670-6.

Moroz LL (2006) Localization of putative nitrergic neurons in peripheral chemosensory areas and the central nervous system of Aplysia californica. *J Comp Neurol*, **495**, 10-20.

Moroz LL, Edwards JR, Puthanveettil SV, et al. (2006) Neuronal Transcriptome of Aplysia: Neuronal Compartments and Circuitry. *Cell*, **127**, 1453-1467.

Moroz LL, Gillette R (1996) NADPH-diaphorase localization in the CNS and peripheral tissues of the predatory sea-slug Pleurobranchaea californica. *J Comp Neurol*, **367**, 607-22.

Moroz LL, Chen D, Gillette MU, Gillette R (1996) Nitric Oxide Synthase Activity in the Molluscan CNS. *J Neurochem*, **66**, 873-876.

Moroz LL, Norby SW, Cruz L, Sweedler JV, Gillette R, Clarkson RB (1998) Non-enzymatic production of nitric oxide (NO) from NO synthase inhibitors. *Biochem Biophys Res Commun*, **253**, 571-6.

Moroz LL, Norekian TP, Pirtle TJ, Robertson KJ, Satterlie RA (2000) Distribution of NADPH-diaphorase reactivity and effects of nitric oxide on feeding and locomotory circuitry in the pteropod mollusc, Clione limacina. *J Comp Neurol,* **427,** 274-84.

Moroz LL, Park JH, Winlow W (1993) Nitric oxide activates buccal motor patterns in Lymnaea stagnalis. *Neuroreport,* **4,** 643-6.

Moroz LL, Winlow W, Turner RW, Bulloch AG, Lukowiak K, Syed NI (1994) Nitric oxide synthase-immunoreactive cells in the CNS and periphery of Lymnaea. *Neuroreport,* **5,** 1277-80.

Muller U (1994) Ca2+/calmodulin-dependent nitric oxide synthase in Apis mellifera and Drosophila melanogaster. *Eur J Neurosci,* **6,** 1362-70.

Murphey RK, Johnson SE, Walthall WW (1981) The effects of transplantation and regeneration of sensory neurons on a somatotopic map in the cricket central nervous system. *Dev Biol,* **88,** 247-58.

Mustajoki S (1999

) Molecular genetics of acute intermittent porphyria in Finland. . In *Institute of Clinical Medicine, Faculty of Medicine,*), pp. 1-79. Helsinki: University of Helsinki

Narayanan K, Griffith OW (1994) Synthesis of L-thiocitrulline, L-homothiocitrulline, and S-methyl-L-thiocitrulline: a new class of potent nitric oxide synthase inhibitors. *J Med Chem,* **37,** 885-7.

Nathan C (1997) Inducible nitric oxide synthase: what difference does it make? *J Clin Invest,* **100,** 2417-23.

Nelson RE, Fessler LI, Takagi Y, et al. (1994) Peroxidasin: a novel enzyme-matrix protein of Drosophila development. *EMBO J,* **13,** 3438-47.

Newcomb JM, Watson WH, 3rd (2001) Identifiable nitrergic neurons in the central nervous system of the nudibranch Melibe leonina localized with NADPH-diaphorase histochemistry and nitric oxide synthase immunoreactivity. *J Comp Neurol,* **437,** 70-8.

Nicholls A, Sharp KA, Honig B (1991) Protein folding and association: insights from the interfacial and thermodynamic properties of hydrocarbons. *Proteins,* **11,** 281-96.

Ninnemann H, Maier J (1996) Indications for the occurrence of nitric oxide synthases in fungi and plants and the involvement in photoconidiation of Neurospora crassa. *Photochem Photobiol,* **64,** 393-8.

Nishida K, Harrison DG, Navas JP, et al. (1992) Molecular cloning and characterization of the constitutive bovine aortic endothelial cell nitric oxide synthase. *J Clin Invest,* **90,** 2092-6.

Noel F, Frost WN, Tian LM, Colicos MA, Dash PK (1995) Recovery of tail-elicited siphon-withdrawal reflex following unilateral axonal injury is associated with ipsi- and contralateral changes in gene expression in Aplysia californica. *J Neurosci,* **15,** 6926-38.

Nordmann Y, Grandchamp B, de Verneuil H, Phung L, Cartigny B, Fontaine G (1983) Harderoporphyria: a variant hereditary coproporphyria. *J Clin Invest,* **72,** 1139-49.

O'Brien JR, Schuller DJ, Yang VS, Dillard BD, Lanzilotta WN (2003) Substrate-induced conformational changes in Escherichia coli taurine/alpha-ketoglutarate dioxygenase and insight into the oligomeric structure. *Biochemistry,* **42,** 5547-54.

Okere CO, Kaba H (2000) Increased expression of neuronal nitric oxide synthase mRNA in the accessory olfactory bulb during the formation of olfactory recognition memory in mice. *Eur J Neurosci,* **12,** 4552-6.

Ono JK, McCaman RE (1980) Identification of additional histaminergic neurons in Aplysia: improvement of single cell isolation techniques for in tandem physiological and chemical studies. *Neuroscience,* **5,** 835-40.

Ono JK, McCaman RE (1992) In situ hybridization of whole-mounts of Aplysia ganglia using non-radioactive probes. *J Neurosci Methods,* **44,** 71-9.

Palmer RM, Ferrige AG, Moncada S (1987) Nitric oxide release accounts for the biological activity of endothelium-derived relaxing factor. *Nature,* **327,** 524-6.

Park JH, Straub VA, O'Shea M (1998) Anterograde signaling by nitric oxide: characterization and in vitro reconstitution of an identified nitrergic synapse. *J Neurosci,* **18,** 5463-76.

Peterson BA, Weeks JC (1988) Somatotopic mapping of sensory neurons innervating mechanosensory hairs on the larval prolegs of Manduca sexta. *J Comp Neurol,* **275,** 128-44.

Peterson KJ, Eernisse DJ (2001) Animal phylogeny and the ancestry of bilaterians: inferences from morphology and 18S rDNA gene sequences. *Evol Dev*, **3**, 170-205.

Poulos TL, Raman CS, Li H (1998) NO news is good news. *Structure*, **6**, 255-8.

Presta A, Liu J, Sessa WC, Stuehr DJ (1997) Substrate binding and calmodulin binding to endothelial nitric oxide synthase coregulate its enzymatic activity. *Nitric Oxide*, **1**, 74-87.

Price DA, Greenberg MJ (1977) Purification and characterization of a cardioexcitatory neuropeptide from the central ganglia of a bivalve mollusc. *Prep Biochem*, **7**, 261-81.

Proekt A, Brezina V, Weiss KR (2004) Dynamical basis of intentions and expectations in a simple neuronal network. *Proc Natl Acad Sci U S A*, **101**, 9447-52.

Proekt A, Weiss KR (2003) Convergent mechanisms mediate preparatory states and repetition priming in the feeding network of Aplysia. *J Neurosci*, **23**, 4029-33.

Radomski MW, Palmer RM, Moncada S (1991) Modulation of platelet aggregation by an L-arginine-nitric oxide pathway. *Trends Pharmacol Sci*, **12**, 87-8.

Raman CS, Li H, Martasek P, Kral V, Masters BS, Poulos TL (1998) Crystal structure of constitutive endothelial nitric oxide synthase: a paradigm for pterin function involving a novel metal center. *Cell*, **95**, 939-50.

Rathmell JC, Thompson CB (1999) The central effectors of cell death in the immune system. *Annu Rev Immunol*, **17**, 781-828.

Rees DD, Palmer RM, Hodson HF, Moncada S (1989) A specific inhibitor of nitric oxide formation from L-arginine attenuates endothelium-dependent relaxation. *Br J Pharmacol*, **96**, 418-24.

Regulski M, Tully T (1995) Molecular and biochemical characterization of dNOS: a Drosophila Ca2+/calmodulin-dependent nitric oxide synthase. *Proc Natl Acad Sci U S A*, **92**, 9072-6.

Rosen SC, Weiss KR, Kupfermann I (1979) Response properties and synaptic connections of mechanoafferent neurons in cerebral ganglion of Aplysia. *J Neurophysiol*, **42**, 954-74.

Rubakhin SS, Li L, Moroz TP, Sweedler JV (1999) Characterization of the Aplysia californica cerebral ganglion F cluster. *J Neurophysiol*, **81**, 1251-60.

Saeij JP, Stet RJ, Groeneveld A, Verburg-van Kemenade LB, van Muiswinkel WB, Wiegertjes GF (2000) Molecular and functional characterization of a fish inducible-type nitric oxide synthase. *Immunogenetics*, **51**, 339-46.

Salerno JC, Harris DE, Irizarry K, et al. (1997) An autoinhibitory control element defines calcium-regulated isoforms of nitric oxide synthase. *J Biol Chem*, **272**, 29769-77.

Santarelli L, Montarolo P, Schacher S (1996) Neuropeptide localization in varicosities of Aplysia sensory neurons is regulated by target and neuromodulators evoking long-term synaptic plasticity. *J Neurobiol*, **31**, 297-308.

Savchenko A, Barnes S, Kramer RH (1997) Cyclic-nucleotide-gated channels mediate synaptic feedback by nitric oxide. *Nature*, **390**, 694-8.

Sharma SK, Carew TJ (2004) The roles of MAPK cascades in synaptic plasticity and memory in Aplysia: facilitatory effects and inhibitory constraints. *Learn Mem*, **11**, 373-8.

Shaul PW, Smart EJ, Robinson LJ, et al. (1996) Acylation targets emdothelial nitric-oxide synthase to plasmalemmal caveolae. *J Biol Chem*, **271**, 6518-22.

Sheta EA, McMillan K, Masters BS (1994) Evidence for a bidomain structure of constitutive cerebellar nitric oxide synthase. *J Biol Chem*, **269**, 15147-53.

Schaefer M, Picciotto MR, Kreiner T, Kaldany RR, Taussig R, Scheller RH (1985) Aplysia neurons express a gene encoding multiple FMRFamide neuropeptides. *Cell*, **41**, 457-67.

Schacher S, Wu F, Panyko JD, Sun ZY, Wang D (1999) Expression and branch-specific export of mRNA are regulated by synapse formation and interaction with specific postsynaptic targets. *J Neurosci*, **19**, 6338-47.

Schmidt HH, Lohmann SM, Walter U (1993) The nitric oxide and cGMP signal transduction system: regulation and mechanism of action. *Biochim Biophys Acta*, **1178**, 153-75.

Schmitt C, Gouya L, Malonova E, et al. (2005) Mutations in human CPO gene predict clinical expression of either hepatic hereditary coproporphyria or erythropoietic harderoporphyria. *Hum Mol Genet*, **14**, 3089-98.

Schulz R, Smith JA, Lewis MJ, Moncada S (1991) Nitric oxide synthase in cultured endocardial cells of the pig. *Br J Pharmacol,* **104,** 21-4.

Schuppe H, Aonuma H, Newland PL (2001) NADPH-diaphorase histochemistry in the terminal abdominal ganglion of the crayfish. *Cell Tissue Res,* **303,** 289-99.

Southam E, Garthwaite J (1991) Intercellular action of nitric oxide in adult rat cerebellar slices. *Neuroreport,* **2,** 658-60.

Stamler JS, Simon DI, Osborne JA, et al. (1992) S-nitrosylation of proteins with nitric oxide: synthesis and characterization of biologically active compounds. *Proc Natl Acad Sci U S A,* **89,** 444-8.

Steffensen I, Dulin MF, Walters ET, Morris CE (1995) Peripheral regeneration and central sprouting of sensory neurone axons in Aplysia californica following nerve injury. *J Exp Biol,* **198,** 2067-78.

Stengl M, Zintl R (1996) NADPH diaphorase activity in the antennae of the hawkmoth Manduca sexta. *J Exp Biol,* **199,** 1063-72.

Strathmann MF (1987) *Reproduction and Larval Development of Marine Invertebrates of the northern Pacific Coast,* University of Washington Press, Seattle.

Stricker NL, Christopherson KS, Yi BA, et al. (1997) PDZ domain of neuronal nitric oxide synthase recognizes novel C-terminal peptide sequences. *Nat Biotechnol,* **15,** 336-42.

Stuehr DJ (1999) Mammalian nitric oxide synthases. *Biochim Biophys Acta,* **1411,** 217-30.

Stuehr DJ, Griffith OW (1992) Mammalian nitric oxide synthases. *Adv Enzymol Relat Areas Mol Biol,* **65,** 287-346.

Stuehr DJ, Gross SS, Sakuma I, Levi R, Nathan CF (1989) Activated murine macrophages secrete a metabolite of arginine with the bioactivity of endothelium-derived relaxing factor and the chemical reactivity of nitric oxide. *J Exp Med,* **169,** 1011-20.

Summers BA, Overholt JL, Prabhakar NR (1999) Nitric oxide inhibits L-type Ca2+ current in glomus cells of the rabbit carotid body via a cGMP-independent mechanism. *J Neurophysiol,* **81,** 1449-57.

Sung YJ, Ambron RT (2004) Pathways that elicit long-term changes in gene expression in nociceptive neurons following nerve injury: contributions to neuropathic pain. *Neurol Res,* **26,** 195-203.

Takahashi M, Tu BL, Leombruni E, Kelly KA (1997) Use of an ileal Roux limb to prevent the Roux stasis syndrome. *J Gastrointest Surg,* **1,** 545-53.

Tenhunen R, Tokola O, Linden IB (1987) Haem arginate: a new stable haem compound. *J Pharm Pharmacol,* **39,** 780-6.

Teyke T (1996) Nitric oxide, but not serotonin, is involved in acquisition of food-attraction conditioning in the snail Helix pomatia. *Neurosci Lett,* **206,** 29-32.

Teyke T, Weiss KR, Kupfermann I (1991) Activity of identified cerebral neuron correlates with food-induced arousal in Aplysia. *Neurosci Lett,* **133,** 307-10.

Thompson JD, Gibson TJ, Plewniak F, Jeanmougin F, Higgins DG (1997) The CLUSTAL_X windows interface: flexible strategies for multiple sequence alignment aided by quality analysis tools. *Nucleic Acids Res,* **25,** 4876-82.

Tominaga T, Sato S, Ohnishi T, Ohnishi ST (1993) Potentiation of nitric oxide formation following bilateral carotid occlusion and focal cerebral ischemia in the rat: in vivo detection of the nitric oxide radical by electron paramagnetic resonance spin trapping. *Brain Res,* **614,** 342-6.

Tomita S, Nicoll RA, Bredt DS (2001) PDZ protein interactions regulating glutamate receptor function and plasticity. *J Cell Biol,* **153,** F19-24.

Towbin H, Staehelin T, Gordon J (1979) Electrophoretic transfer of proteins from polyacrylamide gels to nitrocellulose sheets: procedure and some applications. *Proc Natl Acad Sci U S A,* **76,** 4350-4.

Vanderwinden JM, De Laet MH, Schiffmann SN, et al. (1993) Nitric oxide synthase distribution in the enteric nervous system of Hirschsprung's disease. *Gastroenterology,* **105,** 969-73.

Vanderwinden JM, Mailleux P, Schiffmann SN, Vanderhaeghen JJ, De Laet MH (1992) Nitric oxide synthase activity in infantile hypertrophic pyloric stenosis. *N Engl J Med,* **327,** 511-5.

Venema VJ, Ju H, Zou R, Venema RC (1997) Interaction of neuronal nitric-oxide synthase with caveolin-3 in skeletal muscle. Identification of a novel caveolin scaffolding/inhibitory domain. *J Biol Chem,* **272**, 28187-90.

Vilim FS, Alexeeva V, Moroz LL, et al. (2001) Cloning, expression and processing of the CP2 neuropeptide precursor of Aplysia. *Peptides,* **22**, 2027-38.

Vincent SR, Kimura H (1992) Histochemical mapping of nitric oxide synthase in the rat brain. *Neuroscience,* **46**, 755-84.

Wallace AC, Laskowski RA, Thornton JM (1995) LIGPLOT: a program to generate schematic diagrams of protein-ligand interactions. *Protein Eng,* **8**, 127-34.

Walters ET, Alizadeh H, Castro GA (1991) Similar neuronal alterations induced by axonal injury and learning in Aplysia. *Science,* **253**, 797-9.

Walters ET, Bodnarova M, Billy AJ, et al. (2004) Somatotopic organization and functional properties of mechanosensory neurons expressing sensorin-A mRNA in Aplysia californica. *J Comp Neurol,* **471**, 219-40.

Walters ET, Byrne JH, Carew TJ, Kandel ER (1983) Mechanoafferent neurons innervating tail of Aplysia. I. Response properties and synaptic connections. *J Neurophysiol,* **50**, 1522-42.

Watanabe A, Ono M, Shibata S, Watanabe S (1995) Effect of a nitric oxide synthase inhibitor, N-nitro-L-arginine methylester, on light-induced phase delay of circadian rhythm of wheel-running activity in golden hamsters. *Neurosci Lett,* **192**, 25-8.

Weragoda RM, Ferrer E, Walters ET (2004) Memory-like alterations in Aplysia axons after nerve injury or localized depolarization. *J Neurosci,* **24**, 10393-401.

Werner-Felmayer G, Golderer G, Werner ER, Grobner P, Wachter H (1994) Pteridine biosynthesis and nitric oxide synthase in Physarum polycephalum. *Biochem J,* **304 (Pt 1)**, 105-11.

Wink DA, Osawa Y, Darbyshire JF, Jones CR, Eshenaur SC, Nims RW (1993) Inhibition of cytochromes P450 by nitric oxide and a nitric oxide-releasing agent. *Arch Biochem Biophys,* **300**, 115-23.

Wolf G (1997) Nitric oxide and nitric oxide synthase: biology, pathology, localization. *Histol Histopathol,* **12**, 251-61.

Zhang J, Martasek P, Paschke R, Shea T, Siler Masters BS, Kim JJ (2001) Crystal structure of the FAD/NADPH-binding domain of rat neuronal nitric-oxide synthase. Comparisons with NADPH-cytochrome P450 oxidoreductase. *J Biol Chem,* **276**, 37506-13.

Zheng YM, Schafer MK, Weihe E, et al. (1993) Severity of neurological signs and degree of inflammatory lesions in the brains of rats with Borna disease correlate with the induction of nitric oxide synthase. *J Virol,* **67**, 5786-91.

Zou MH, Klein T, Pasquet JP, Ullrich V (1998) Interleukin 1beta decreases prostacyclin synthase activity in rat mesangial cells via endogenous peroxynitrite formation. *Biochem J,* **336 (Pt 2)**, 507-12.

SUPPLEMENTS

Original publications

NCBI submission file for AcCPX (CPX, AF510850.1, GI:30515681)

NCBI submission file for *AcCPX*

```
LOCUS       AF510850               1315 bp    mRNA    linear   INV 10-MAY-2003
DEFINITION  Aplysia californica coproporphyrinogen oxidase mRNA, complete cds.
ACCESSION   AF510850
VERSION     AF510850.1  GI:30515681
KEYWORDS    .
SOURCE      Aplysia californica (California sea hare)
  ORGANISM  Aplysia californica
            Eukaryota; Metazoa; Mollusca; Gastropoda; Orthogastropoda;
            Apogastropoda; Heterobranchia; Euthyneura; Opisthobranchia;
            Anaspidea; Aplysioidea; Aplysiidae; Aplysia.
REFERENCE   1  (bases 1 to 1315)
  AUTHORS   Bodnarova,M., Kelmanson,I.V., Martasek,P. and Moroz,L.L.
  TITLE     Cloning and distribution of coproporphyrinogen oxidase in Aplysia
            californica
  JOURNAL   Unpublished
REFERENCE   2  (bases 1 to 1315)
  AUTHORS   Bodnarova,M., Kelmanson,I.V., Martasek,P. and Moroz,L.L.
  TITLE     Direct Submission
  JOURNAL   Submitted (09-MAY-2002) Whitney Lab, University of Florida, 9505
            Ocean Shore Blvd., St. Augustine, FL 32086, USA
FEATURES             Location/Qualifiers
     source          1..1315
                     /organism="Aplysia californica"
                     /mol_type="mRNA"
                     /db_xref="taxon:6500"
     CDS             41..1213
                     /codon_start=1
                     /product="coproporphirynogen oxidase"
                     /protein_id="AAP34327.1"
                     /db_xref="GI:30515682"
                     /translation="MAQVLRQCVVTFVRLGSTKVAHSTPGIRLNNHRLYLKLLGGGVL
                     CQFSLFSWKGSRKPDVDSSDSWMSEPITSLDELKQNGDDMKCKMEAMIMRIQSEFVHA
                     VEKEELEEGGKKFLVDRWLREQGGGGITCVLQDGTVFEKAGVNISVVSGILPPNAVQQ
                     MRARGKKMKGANLKFFAAGVSSVVHPRNPHIPTVHFNYRYFEVENDDGEKHWWFGGGT
                     DLTPYYLEEKDVVHFHKTLKKACDGHGKQLYPKYKKWCDDYFRVPHRGESRGVGGIFF
                     DDVDEPSQDKCFEFVTDCAESVVPSYLPLVQKHKKDGVSYPEREWQLLRRGRYVEFNL
                     IYDRGTKFGLYTPGARYESILMSLPLTARWEYKHSPPEGSREAQLTEVLKNPREWV"
ORIGIN
        1 acccttacg tctgagataa aggaggaagt taactccagc atggcacagg tcctccgtca
       61 gtgtgtggtg actttgtcc gtctgggatc caccaaagtt gctcattcta ccccaggcat
      121 taggctgaat aatcacagac tctacttgaa actgttagga ggtggagttt tatgccagtt
      181 ttccttgttc agttggaagg gttccagaaa gcctgatgtg gactccagtg actcttggat
      241 gtctgagccc atcacgtccc ttgatgagtt gaaacagaac ggagatgaca tgaagtgcaa
      301 gatggaagcc atgatcatgc ggattcagtc tgagtttgtt cacgctgtgg agaaagagga
      361 gttagaggag ggtgggaaaa agtttctagt tgacaggtgg ctgcgagagc agggtggtgg
      421 tggaattacg tgtgtcttgc aagacggcac cgtgtttgaa aaggctggag tgaacatctc
      481 tgtggtcagt ggcatcctgc cccccaacgc tgtgcaacag atgagagcca gaggaaagaa
      541 aatgaaggga gcaaacctca agtttttgc tgcgggcgtc agttctgtgg tccatcctcg
      601 caatcctcat ataccaactg ttcacttcaa ctaccgctac tttgaggtgg agaatgatga
      661 tggggagaaa cactggtggt ttggtggagg caccgacctc acgccctact atctagaaga
      721 aaaggatgtc gtccatttcc acaagacctt gaaaaaagca tgcgatggtc acgggaagca
      781 gttgtacccc aagtacaaga agtggtgcga cgattacttc cgcgtgcctc acagaggtga
      841 gagtcgagga gtgggtggaa tcttctttga cgatgttgac gagccatccc aagacaagtg
      901 ttttgagttt gtcactgact gtgccgagtc tgtggtcccg tcatatttgc cccttgtcca
      961 aaaacacaag aaagatggag tcagctatcc tgaaagagag tggcagctgc tgagaagagg
     1021 ccgctatgtt gagttcaatc tgatctatga cagaggaaca aaatttggcc tgtacacccc
     1081 cggagccaga tatgagagca tcttgatgtc cctgcccctc acagcgagat gggagtacaa
     1141 gcactcccct cctgaaggct cccgggaggc tcagctgact gaggttttga agaatccgcg
     1201 cgagtgggtg tgaagacgcg atggaatcag gattagtcag tgtaatgcgg agatgaacaa
888"
```

Available online at www.sciencedirect.com
SCIENCE DIRECT®
Journal of Inorganic Biochemistry 99 (2005) 922–928
Journal of Inorganic Biochemistry
www.elsevier.com/locate/jinorgbio

Calcium/calmodulin-dependent nitric oxide synthase activity in the CNS of *Aplysia californica*: Biochemical characterization and link to cGMP pathways

Michaela Bodnárová [a,b], Pavel Martásek [b], Leonid L. Moroz [a,c,*]

[a] *Whitney Laboratory for Marine Bioscience, University of Florida, 9505 Ocean Shore Blvd., St. Augustine, FL 32080, USA*
[b] *Department of Pediatrics, 1st Medical Faculty, Charles University, Prague, Czech Republic*
[c] *Department of Neuroscience, University of Florida, Gainesville, FL 32611, USA*

Received 7 December 2004; received in revised form 3 January 2005; accepted 21 January 2005
Available online 19 February 2005

Abstract

We characterized enzymatic activity of nitric oxide synthase (NOS) in the central nervous system of *Aplysia californica*, a popular experimental model in cellular and system neuroscience, and provided biochemical evidence for NO-cGMP signaling in molluscs. *Aplysia* NOS (ApNOS) activity, determined as citrulline formation, revealed its calcium-/calmodulin-(Ca/CaM) and NADPH dependence and it was inhibited by 50% with 5 mM of W7 hydrochloride (a potent Ca/CaM-dependent phosphodiesterase inhibitor). A representative set of inhibitors for mammalian NOS isoforms also suppressed NOS activity in *Aplysia*. Specifically, the ApNOS was inhibited by 65–92% with 500 μM of L-NAME (a competitive NOS inhibitor) whereas D-NAME at the same concentration had no effect. *S*-Ethylisothiourea hydrobromide (5 mM), a selective inhibitor of all NOS isoforms, suppressed ApNOS by 85%, L-*N*6-(1-iminoethyl)lysine dihydrochloride (L-NIL, 5 mM), an iNOS inhibitor, by 78% and L-thiocitrulline (5 mM) (an inhibitor of nNOS and iNOS) by greater than 95%. Polyclonal antibodies raised against rat nNOS hybridized with a putative purified ApNOS (160 kDa protein) from partially purified central nervous system homogenates in Western blot studies. Consistent with other studies, the activity of soluble guanylyl cyclase was stimulated as a result of NO interaction with its heme prosthetic group. The basal levels of cGMP were estimated by radioimmunoassay to be 44.47 fmol/μg of protein. Incubation of *Aplysia* CNS with the NO donors DEA/NONOate (diethylammonium (Z)-1-(*N*,*N*-diethylamino) diazen-1-ium-1,2-diolate – 1 mM) or *S*-nitroso-*N*-acetylpenicillamine (1 mM) and simultaneous phosphodiesterase inhibition with 3-isobutyl-1-methylxanthine (1 mM) prior to the assay showed a 26–80 fold increase in basal cGMP levels. Addition of ODQ (1H-[1,2,4]oxadiazolo[4,3-a] quinoxaline-1-one – 1 mM), a selective inhibitor of soluble guanylyl cyclase, completely abolished this effect. This confirms that NO may indeed function as a messenger in the molluscan CNS, and that cGMP acts as one of its effectors.

Keywords: *Aplysia californica*; Nitric oxide synthase; cGMP; Molluscs; Invertebrates

1. Introduction

Nitric oxide (NO) is well recognized as a signaling molecule across the animal kingdom. NO, generated from L-arginine by the family of nitric oxide synthases, can activate soluble guanylyl cyclase leading to the cyclic GMP formation in target cells. Although this is a well established cascade in many mammalian preparations, comparative data from invertebrates and lower chordates are highly controversial and limited to a relatively small number of model organisms. The main focus of the present study is to biochemically characterize both nitric oxide synthase (NOS) and soluble guanylyl cyclase

* Corresponding author. Tel.: +1 904 461 4020; fax: +1 904 461 4052.
E-mail address: moroz@whitney.ufl.edu (L.L. Moroz).

0162-0134/$ - see front matter © 2005 Elsevier Inc. All rights reserved.
doi:10.1016/j.jinorgbio.2005.01.012

sGC) activities in the central nervous system (CNS) of the marine opisthobranch mollusc, *Aplysia californica*. In contrast to many vertebrate preparations, the large size and robustness of many molluscan neurons make these cells easily accessible for isolation and direct microchemical analysis of NOS related metabolites [1,2], while their identifiability allows further characterization of the roles of specific nitrergic neurons in neural networks and behavior. *Aplysia* appears to be an especially suitable preparation in this direction with several reports suggesting both the presence of neuronal NOS [3] and NO-mediated signaling between identified neurons involved in the feeding network [4–6]. In addition, a modulatory role for NO in cholinergic [7–10] and serotonergic transmission [10,11], as well as in neuronal plasticity [12] and excitability has also been reported [13–16].

However, these data were obtained using a variety of pharmacological and immunological tools developed specifically for vertebrate preparations and their selectivity for molluscan NOS and sGC is lacking. Furthermore, neither enzymatic characterization of NOS nor the biochemical examination of NO-dependent cGMP production in *Aplysia* has been performed. Finally, comparative studies of NOS activity in molluscs are controversial, suggesting the presence of either Ca-dependent or Ca-independent NOS activity [3,17]. This situation is strongly contrasted to the studies on other model invertebrates such as insects (e.g., *Drosophila*) where biochemical and pharmacological characterization of Ca-dependent NOS provide a solid platform for further functional analysis of NO signaling in these species [34,36]. The data presented here confirm both calcium-/calmodulin- dependence of Aplysia NOS and its links with cGMP production in the CNS.

2. Experimental

2.1. Animals and chemical materials

Experiments were performed on adult *Aplysia californica* (150–300 g) collected in the wild and supplied by Marinus (Long Beach, CA). Animals were kept in natural sea water at 15–18 °C and fed *Gracilaria* for 2–7 days before experiments. Anesthesia was performed by an injection of isotonic (337 mM) $MgCl_2$ (50% of body weight) into the hemolymph. The CNS of *Aplysia* was dissected and immediately processed for experiments. All chemicals were supplied by Sigma-Aldrich if not specified otherwise.

2.2. Measurement of NOS activity

Following dissection, ganglia were homogenized in approximately 5 volumes of buffer containing 25 mM Tris–HCl (pH 7.4), 1 mM *e*thylene*d*iamine*t*etra*a*cetic acid (EDTA), and 10 mM ethylene glycol bis(2-aminoethyl ether)-*N*,*N*,*N*′*N*′-tetraacetic acid (EGTA) with a tissue homogenizer on ice. The homogenate was centrifuged at 14,000*g* for 5 min at 4 °C and the pellet was discarded. NOS activity was determined according to a method described previously [18]. Briefly, 10 μl of homogenate (from two CNS per test from weight matched molluscs) was added into a reaction mixture containing L-[^{14}C]arginine (sp.act. 0.30 Ci/mmol, from Perkin–Elmer Life and Analytical Sciences), NADPH (10 mM), free calcium ions ($CaCl_2$, 6 mM), Tris–HCl buffer (50 mM) at pH 7.4, tetrahydrobiopterin (BH_4, 6 μM), flavin adenine dinucleotide (FAD, 2 μM) and flavin adenine mononucleotide (FAM, 2 μM), where the final volume was 50 μl. Samples were incubated for 1 h at room temperature. Reaction was terminated by addition of HEPES (50 mM) containing EDTA (5 mM). L-[^{14}C]Citrulline was separated by passing the solution through a 0.1 ml equilibrated cation-exchange resin and radioactivity of the unretained citrulline was measured by liquid scintillation spectrometry in 6 ml of scintillation cocktail. Samples of rat cerebellum were analyzed simultaneously in all experiments as a positive control. Total protein content in the homogenates was determined by the Bradford method [19].

The total NOS activity (in pmol/mg protein/min) was determined as the difference between the total activity of L-[^{14}C]citrulline in control samples and a reaction lacking homogenate. Other experiments were performed in the presence of 5 mM W7 hydrochloride (*N*-(6-Aminohexyl)-5-chloro-1-naphthalenesulfonamide HCl, a potent Ca/CaM-dependent phosphodiesterase inhibitor, (Calbiochem, San Diego, CA, USA)) [20], various concentrations of L-NAME (a competitive NOS inhibitor), or D-NAME (its less active enantiomer), 5 mM *S*-Ethyl-ITU hydrobromide (*S*-Ethylisothiourea HBr, a selective inhibitor of all vertebrate NOS isoforms, (Alexis Biochemicals)) [21], 5 mM L-NIL dihydrochloride (L-*N*6-(1-iminoethyl)lysine dihydrochloride, a vertebrate iNOS specific inhibitor) [22], 5 mM L-thiocitrulline (an inhibitor of vertebrate nNOS and iNOS) [23]. Calcium independent activity was the activity measured in the incubation mixture lacking $CaCl_2$; chelating agent EGTA (10 mM) was added to the media prior to these experiments. Student's *t*-test was used for statistical analysis of the observed differences. All data are presented as mean ±SEM values.

2.3. cGMP assay

Following dissection the *Aplysia* CNS was transferred into 1.5 ml Eppendorf vials with filtered seawater (FSW) for treatment with phosphodiesterase (PDE) inhibitors and NO donors. Central ganglia were incubated for 1 h with 1 mM IBMX (3-isobutyl-1-methyl-

xanthine, a phosphodiesterase inhibitor (Calbiochem, San Diego, CA, USA)) [24] dissolved in 1% DMSO (dimethyl sulfoxide (Fischer)) at room temperature, and/or with 1 mM ODQ (1H-[1,2,4]oxadiazolo[4,3-a] quinoxaline-1-one) also dissolved in 1% DMSO [25]. The control group was incubated with 1% DMSO. Then, the CNS was incubated for 10 min with the NO donors SNAP (*S*-nitroso-*N*-acetylpenicillamine, 1 mM, dissolved in DMSO) or DEA/NONOate (or DEA/NO, diethylammonium (Z)-1-(*N*,*N*-diethylamino)diazen-1-ium-1,2-diolate, 1 mM) [26]. After incubation ganglia were transferred to an acetate buffer (400 µl, 0.5 M, pH 5.8) and incubated for 3 min at 100 °C in a boiling water bath, then mechanically homogenized and spun at 13,000*g* for 10 min at 4 °C [27]. The homogenate was diluted 10× in the acetate buffer and the cGMP levels were assessed using the RIA cGMP[^{125}I] assay from Amersham Biosciences following the manufacturer's protocol. Duplicate 100 µl aliquots in glass tubes were prepared from both the standard and experimental vials. One hundred microliters of antisera and 100 µl of tracer cGMP[^{125}I] were added into all assay tubes, vortexed thoroughly and incubated for 18 h at 4 °C. Five hundred microliters of Amerlex-M second antibody were added to each tube, vortexed thoroughly and incubated for 10 min at room temperature. The antibody bound fraction was separated by centrifugation at 2500*g* for 10 min at 4 °C, the supernatant was discarded and the radioactivity of the pellet in each tube was determined by counting in a gamma scintillation counter. Total protein content in the homogenates was determined by the Bradford method [19] and the readings were recalculated to fmol per µg of protein.

2.4. Western blot and immunostaining

SDS-PAGE was performed as first described by Laemmli [28]. One to three micrograms of the denatured protein was applied per lane to an SDS gel (10%T, 2.6%C) and separated in a Bio Rad mini-gel apparatus at 20 mA for about 1 h or until the dye front approached the bottom of the gel. Gels were removed and either stained in Coomassie Blue or transferred to a PVDF membrane. Coomassie staining was performed for about 30 min at room temperature in a solution of 2% CB G250, 7.5% HAc, and 50% MeOH. Destaining was carried out in 7.5% HAc, 15% MeOH.

Electrotransfer [29] to a 0.2µ PVDF membrane was performed in a Bio Rad Mini Trans-Blot apparatus following the manufacturer's instructions. The transfer buffer was 24 mM TRIS and 19.5 mM glycine, pH 9.2, with running conditions of 100 V for 1 h.

Partial purification of NOS was carried out using a modification of a protocol published before [30]. ApNOS from 20 *Aplysia* CNS has been homogenized in buffer A (50 mM Tris–HCl, pH 7.8, 1 mM EDTA, 1 mM dithiothritol (DTT), 10% glycerol, 150 mM NaCl, 0.1 mM phenylmethylsulfonyl fluoride, 1 µM leupeptin, 1 µM pepstatin) and centrifuged to sediment the cell debris. The supernatant was applied to a 2′, 5′-ADP Sepharose 4B column equilibrated with buffer B (50 mM Tris–HCl, pH 7.8, 1 mM EDTA, 0.1 mM DTT, 150 mM NaCl, 10% glycerol) and the column was washed with 20 column volumes of buffer B and again with 20 column volumes of buffer B containing 600 mM NaCl. Partially purified ApNOS has been eluted with buffer B containing 600 mM NaCl and 5 mM 2′-AMP. Detection was performed with a polyclonal antibody raised against rat neuronal NOS (rabbit) and visualized with alkaline phosphatase color reagent. Briefly, the membrane was blocked with 1% non-fat dry milk and 1% BSA in TBS (20 mM Tris–HCl, pH 7.4, 0.5 M NaCl) for 1 h. The membrane was then incubated for 1 h with a 1:2–3000 dilution of antibody in TTBS (TBS plus 0.05% Tween 20). After extensive washing in TTBS, goat anti-mouse IgG alkaline phosphatase conjugate (ZYMED, 81-6522) was used as a secondary antibody, again for 1 h. Visualization was accomplished by gentle rocking in NBT/BCIP reagent.

We used whole mount preparations of the CNS of *Aplysia* for the immunohistochemistry as described [31]. Ganglia were fixed in fresh fixative (4% paraformaldehyde, 25% sucrose, and 0.1 M NaH_2PO_4, pH 7.6) overnight at 4 °C. During washing with PBS, the ganglia were desheathed. Ganglia were washed overnight in a blocking solution (as wash buffer below with 10% goat serum, 2% Triton X-100, pH 7.4). Polyclonal antibody raised against rat neuronal NOS (rabbit) was used in 1:100 dilution in the blocking solution for 7 days at room temperature. Following the incubation with the primary antibody the CNS was washed overnight (154 mM NaCl, 10 mM Na_2HPO_4, 50 mM EDTA, and 0.01% thimerosal, 1% BSA, at pH 7.4). The secondary antibody (Cy5-conjugated goat anti-rabbit IgG, Jackson ImmunoResearch) was diluted 1:250. The preparations were incubated with this antibody for up to 8 h, washed for several hours and analyzed under a confocal microscope. For controls, the primary antibody was omitted from the incubation solution. NADPH-d staining was performed on whole mount preparations of the CNS as described before [1].

3. Results

3.1. NOS present in the CNS of Aplysia is calcium dependent

The relative NOS activity and the role of cofactors in the CNS of *Aplysia californica* is shown in Figs. 1 and 2

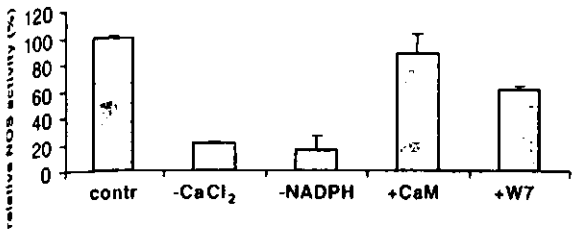

Fig. 1. Co-factor dependence of ApNOS. Relative NOS activity is shown as a percentage of ApNOS activity (L-[^{14}C]arginine/L-[^{14}C]citrulline conversion in homogenates of the CNS of *Aplysia californica*). Contr, control conditions with all co-factors; $-CaCl_2$, without $CaCl_2$; -NADPH, without NADPH; in the presence of calmodulin (+CaM); +W7, in the presence of 5 mM W 7hydrochloride (a potent Ca/CaM-dependent phosphodiesterase inhibitor). Student's *t*-test was used for statistical analysis of the observed differences. Data are the mean of three experiments ±SEM values. See additional details in the text.

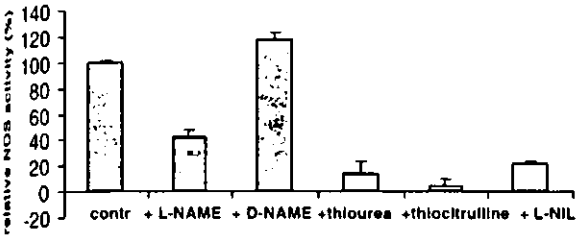

Fig. 2. Pharmacology of ApNOS. Relative NOS activity is shown as a percentage of L-[^{14}C]arginine/L-[^{14}C]citrulline conversion (see text) in the presence of several inhibitors of mammalian NOSs. Contr, control conditions with all co-factors; + L-NAME, in the presence of 500 μM L-NAME (a competitive NOS inhibitor); + D-NAME, in the presence of 500 μM D-NAME (less active enantiomer of L-NAME), + L-NIL, in the presence of 5 mM L-NIL dihydrochloride (iNOS inhibitor); +thiourea, in the presence of 5 mM *S*-Ethyl-ITU hydrobromide (selective inhibitor of all vertebrate NOS isoforms); and with 5 mM L-thiocitrulline (an inhibitor of nNOS and iNOS).

as an L-[^{14}C]arginine/L-[^{14}C]citrulline conversion. The production rate of L-[^{14}C] citrulline from homogenized ganglia was 22.2 ± 4.0 pmol/mg of protein/min.

Importantly, Fig. 1 illustrates that ApNOS activity was shown to be calcium dependent; the documented values for calcium-free conditions in the media containing EGTA were below 40% of the control NOS activity (5.3 ± 1.5 pmol/mg of protein/1/min, $P < 0.05$).

Exclusion of NADPH from the reaction mixture caused a reduction in ApNOS activity to less than 35% (7.2 ± 2.4 pmol/mg of protein/min, $P < 0.005$). Addition of W-7 hydrochloride, a Ca/CaM-dependent phosphodiesterase inhibitor, also significantly reduced L-[^{14}C]citrulline production to less than 60% (16.0 ± 1.0 pmol/mg of protein/1/min). The addition of calmodulin had no significant effect on NOS activity. Thus, in contrast to previously reported data in the gastropod mollusc *Pleurobranchaea*, we demonstrated here that Arg–Cit conversion related to NOS activity in the CNS is Ca-dependent.

3.2. The pharmacological profile of ApNOS is similar but not identical to vertebrate NOS isoforms

The effects of vertebrate isoform specific NOS inhibitors on Aplysia NOS were studied (Fig. 2) and the most potent inhibitor proved to be L-thiocitrulline (an inhibitor of mammalian nNOS and iNOS) which reduced the NOS activity by 95% ($P < 0.005$). All other tested NOS inhibitors caused a significant reduction in L-[^{14}C]citrulline production: *S*-Ethyl-ITU hydrobromide (a selective inhibitor of all vertebrate NOS isoforms) by 85% ($P < 0.050$) and L-NIL dihydrochloride (iNOS inhibitor) by 78% ($P < 0.05$). The competitive NOS inhibitor L-NAME suppressed the NOS activity by almost 60% (11.0 ± 1.0 pmol/mg of protein/min), whereas its less active enantiomer D-NAME was without a significant effect on neuronal NOS activity in *Aplysia*.

3.3. PDE inhibitors and NO donors both increase cGMP in the CNS of Aplysia

To experimentally establish a link between NOS and cGMP pathways, we evaluated the background cGMP activity as well as its sensitivity to NO donors and inhibitors. The cGMP levels from the RIA cGMP[^{125}I] assay are shown as converted per 1 μg of total homogenized protein. The basal level of cGMP in the CNS was 44.47 fmol/μg. Incubation with the NO donor DEA/NONOate (1 mM) increased the cGMP activity almost 3.5 times (154.1 fmol/μg), whereas incubation with non specific PDE inhibitors increased the cGMP levels 26 times (1186.4 fmol/μg). Following 1 h incubation with IBMX (1 mM) the increase of cGMP was 58–61 times higher compared with the basal level of cGMP. This documents that NO indeed functions as a messenger in the CNS, and cGMP is one of its effectors (Fig. 3).

Further, selective inhibition of soluble guanylyl cyclase with ODQ (1 mM) incubated simultaneously with the NO donor DEA/NO (1 mM) even reduced the cGMP activity compared with basal cGMP levels. The

Fig. 3. cGMP concentrations in the CNS of *Aplysia*. NO donors (DEA/NO and SNAP – 1 mM each) and the non specific PDE inhibitor – IBMX (1 mM) significantly increased cGMP concentrations in the CNS. Co-incubation with NO donors and PDE inhibitors further increases the cGMP levels (see details and abbreviations in the text).

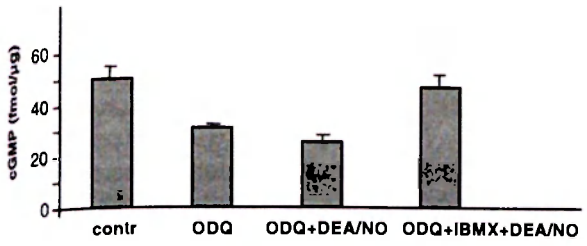

Fig. 4. ODQ decreases cGMP concentrations in the CNS and eliminates effects of NO donors. Selective inhibition of soluble guanylyl cyclase with ODQ (1 mM) incubated simultaneously with the NO donor DEA/NO (1 mM) even reduced the cGMP activity compared with basal cGMP levels. The co-incubation of ODQ, DEA/NO and IBMX still kept the cGMP activity 2.4 times below normal.

co-incubation of ODQ, DEA/NO and IBMX still kept the cGMP activity 2.4 times below normal (Fig. 4).

3.4. Western blot and immunohistochemistry

Partially purified ApNOS run on SDS-PAGE gel, then reblotted and hybridized with a preadsorbed polyclonal rabbit anti-rat nNOS antibody showed a clear band around 160 kDa. A similar immunopositive band at 150 kDa was detected in our control rat cerebellum homogenate. These antibodies selectively labeled approximately several dozen neurons and distinct areas of ganglionic neuropil with a pattern similar to those described for NADPH-diaphorase immunohistochemistry (Fig. 5).

4. Discussion

Here, we have provided evidence that functionally active NOS is present in the CNS of *Aplysia californica* and for the first time it is shown to be calcium dependent. *Aplysia* NOS shares common enzymatic characteristics with constitutive mammalian and insect neuronal NOS [18] as a calmodulin and NADPH dependent enzyme. Thus, the observed Ca-dependence of *Aplysia* NOS confirms an earlier hypothesis that the rise of intracellular Ca^{2+} (either following activation of transmembrane Ca-channels or from intracellular stores) might act as a physiological regulator of NO synthesis in the molluscan CNS. In this repect, *Aplysia* neuronal NOS was similar to the NOS described in two representatives of pulmonate molluscs, *Lymnaea stagnalis* [32] and *Helix pomatia* [17]. Interestingly, in *Helix* the level of NOS activity was around 13 times higher than in *Aplysia*, and even three times higher than in the mammalian cerebellum. However, in another marine opisthobranch mollusc, *Pleurobranchaea californica*, NOS activity was about two magnitudes lower [3] than reported here and was shown to be Ca-independent but calmodulin-dependent. Such substantial variations are likely to be related to ecology and the overall metabolic activity of these molluscan species as well as the possible presence of more than one NOS isoform and needs to be investigated in the future.

NOS activity measured in *Aplysia* was around six to seven times lower than the activity detected in the mammalian cerebellum [18], but it was comparable with the average values reported for the insect brain [33,34]. Yet, regions of the insect brain involved in chemosensation and known to be enriched with NOS containing elements express 10–20 times higher levels of NOS activity than we detected in *Aplysia* [35,36] On the other hand, *Aplysia* might contain only about 140–160 centrally located NOS-containing neurons out of ~20,000 cells in the whole CNS (Moroz, Bodnarova unpublished observations).

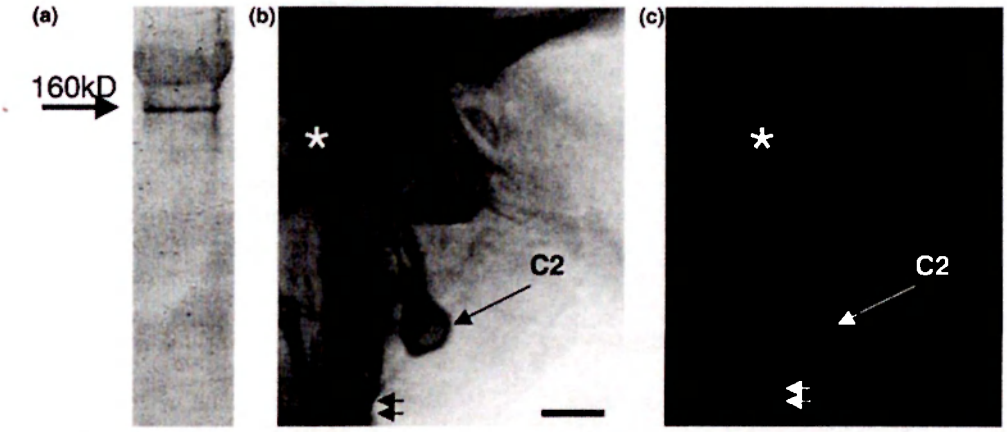

Fig. 5. Western blot and immunostaining in the CNS of *Aplysia*. (a) Partially purified ApNOS is from the CNS cross reacted with a preadsorbed polyclonal antibody to rat neuronal NOS and is recognized as a protein with molecular mass of cca 160 kDa (a). (b) NADPH-diaphorase histochemistry in the lateral part of the cerebral ganglion (E-cluster area); (c) NOS immunoreactivity with rat polyclonal NOS antibodies reveals similar patterns of labeling in the same region of the cerebral ganglion. Large arrows in (b and c) indicate the position of the identified neuron (C2) also know to be nitrergic and located in this area of the cerebral ganglion. Small arrows mark specific labeling in nerves and (*) point out the staining in ganglionic neuropil.

The pharmacological profile of *Aplysia* NOS was similar but not identical to NOS described for other species. The ApNOS showed closest similarity to mammalian neuronal NOS, although selective inhibitors of two other mammalian isoforms (eNOS and iNOS) had a significant suppressive effect as well. L-thiocitrulline was found to be the most potent inhibitor of ApNOS and suppressed the relative NOS activity to a level of less than 5% of its control value, while the widely used competitive NOS inhibitor L-NAME was less effective.

There is relatively little known about the structure of NOS-related proteins in molluscs. For example, partially purified NOS protein from *Aplysia* CNS displayed a band with molecular mass of approximately 160 kDa and a very faint band around 175 kDa. The shorter band is comparable in size with the 150 kDa of denatured rat nNOS protein [37]. The molecular mass of insect NOS protein was around 130–155 kDa [33,34], but, surprisingly, the immunoreactive NOS protein in the mollusc *Helix pomatia* with the highest reported enzymatic activity showed only a band of 60 kDa [17].

The fact that NO induces cGMP synthesis and immunoreactivity through activating soluble guanylyl cyclase has already been shown [38–42] for many species including some molluscs [5,6,43]. However, direct biochemical measurements of soluble guanylyl activity in molluscs has been performed only on a representative of land pulmonates, *Helix pomatia* [27]. Here, we determined the basal levels of cGMP production in the CNS of *Aplysia* and showed that it significantly increased following stimulation with NO donors (~3-fold), and incubation with PDE inhibitors (>20-fold). Importantly, a specific inhibitor of soluble guanylyl cyclase (ODQ) reduced by half the basal level of cGMP in the CNS of *Aplysia* and prevented the rise of cGMP by NO. These results suggest the substantial tonic production of NO in the intact CNS and its link to cGMP pathways.

In summary, we directly showed that enzymatically active Ca-dependent NOS is present in the CNS of *Aplysia californica* and that it can act via cGMP signaling. Biochemical and pharmacological characterization of these two signaling pathways provide a foundation to further examine their interactions and functional role in neuronal networks using *Aplysia* as a model organism.

5. Abbreviations

ApNOS	*Aplysia* nitric oxide synthase
BH4	tetrahydrobiopterin
BSA	bovine serum albumin
CaM	calmodulin
CB G250	coomassie blue
cGMP	cyclic guanosine monophosphate
CNS	central nervous system
DEA/NONOate	or DEA/NO, diethylammonium (Z)-1-(*N*,*N*-diethylamino) diazen-1-ium-1,2-diolate
DMSO	dimethyl sulfoxide
EDTA	*e*thylene*d*iamine*t*etra*a*cetic acid
EGTA	ethylene glycol bis(2-aminoethyl ether)-*N*,*N*,*N*′*N*′-tetraacetic acid
FAD	flavin adenine dinucleotide
FAM	flavin adenine mononucleotide
FSW	filtered seawater
HEPES	*N*-(2-hydroxyethyl)piperazine-*N*′-(2-ethanesulfonic acid)
HAC	acetic acid
IBMX	3-isobutyl-1-methylxanthine
MeOH	methanol
L-NAME	*N*-nitro-L-arginine methyl ester
D-NAME	*N*-nitro-D-arginine methyl ester
NADPH	nicotinamide adenine dinucleotide phosphate, reduced form
NBT/BCIP	nitroblue tetrazolium/ bromochloroindolyl
L-NIL	L-*N*6-(1-iminoethyl)lysine dihydrochloride
NOS	nitric oxide synthase
eNOS	endothelial NOS
iNOS	inducible NOS
nNOS	neuronal NOS
NO	nitric oxide
ODQ	1H-[1,2,4]oxadiazolo[4,3-a] quinoxaline-1-one
PDE	phosphodiesterase
PVDF	polyvinylidene fluoride
RIA	radioimmunoassay
S-Ethyl-ITU	*S*-Ethylisothiourea HBr
SDS	sodium dodecyl sulphate
SDS-PAGE	sodium dodecyl sulphate-polyacrylamide gel electrophoresis
SNAP	*S*-nitroso-*N*-acetylpenicillamine
Tris	Tris(hydroxymethyl)aminomethane
TBS	Tris buffered solution
TTBS	TBS buffer containing Tween 20

Acknowledgements

Supported by NIH and NSF as well as Packard and McKnight Foundation grants to LLM, and by GA ČER 309/02/1139 to PM and MB. Polyclonal antibodies raised against recombinant rat neuronal NOS were kindly provided by Professor Bettie Sue Masters, Department of Biochemistry, University of Texas Health Science Center at San Antonio, Texas, USA.

We thank Mr. James Netherton for critical reading and his comments on the manuscript.

References

[1] L.L. Moroz, Microsc. Res. Techniq. 49 (2000) 557–569.
[2] L.L. Moroz, R. Gillette, J.V. Sweedler, J. Exp. Biol. 202 (1999) 333–341.
[3] L.L. Moroz, D. Chen, M.U. Gillette, R. Gillette, J. Neurochem. 66 (1996) 873–876.
[4] J.W. Jacklet, J. Neurophysiol. 74 (1995) 891–895.
[5] H.Y. Koh, J.W. Jacklet, Eur. J. Neurosci. 13 (2001) 553–560.
[6] H.Y. Koh, J.W. Jacklet, J. Neurosci. 19 (1999) 3818–3826.
[7] J.P. Mothet, P. Fossier, A. Schirar, L. Tauc, G. Baux, Physiol. Res. 45 (1996) 177–183.
[8] J.P. Mothet, P. Fossier, L. Tauc, G. Baux, Proc. Natl. Acad. Sci. USA 93 (1996) 8721–8726.
[9] J.P. Mothet, P. Fossier, L. Tauc, G. Baux, J. Physiol. 493 (1996) 769–784.
[10] A. Meulemans, J.P. Mothet, A. Schirar, P. Fossier, L. Tauc, G. Baux, Neuroscience 69 (1995) 985–995.
[11] P. Fossier, B. Blanchard, C. Ducrocq, C. Leprince, L. Tauc, G. Baux, Neuroscience 93 (1999) 597–603.
[12] A. Katzoff, T. Ben-Gedalya, A.J. Susswein, J. Neurosci. 22 (2002) 9581–9594.
[13] M. Sawada, M. Ichinose, J. Neurosci. Res. 44 (1996) 21–26.
[14] M. Sawada, M. Ichinose, N. Hara, Brain Res. 670 (1995) 248–256.
[15] M. Sawada, M. Ichinose, G.B. Stefano, Brain Res. 740 (1996) 124–130.
[16] M. Sawada, M. Ichinose, G.B. Stefano, J. Neurosci. Res. 50 (1997) 450–456.
[17] S. Huang, H.H. Kerschbaum, E. Engel, A. Hermann, J. Neurochem. 69 (1997) 2516–2528.
[18] D.S. Bredt, S.H. Snyder, Proc. Natl. Acad. Sci. USA 87 (1990) 682–685.
[19] M.M. Bradford, Anal. Biochem. 72 (1976) 248–254.
[20] H. Itoh, H. Hidaka, J. Biochem. 96 (1984) 1721–1726.
[21] E.P. Garvey, J.A. Oplinger, G.J. Tanoury, P.A. Sherman, M. Fowler, S. Marshall, M.F. Harmon, J.E. Paith, E.S. Furfine, J. Biol. Chem. 269 (1994) 26669–26676.
[22] W.M. Moore, R.K. Webber, G.M. Jerome, F.S. Tjoeng, T.P Misko, M.G. Currie, J. Med. Chem. 37 (1994) 3886–3888.
[23] K. Narayanan, O.W. Griffith, J. Med. Chem. 37 (1994) 885–887.
[24] J.A Beavo, J.G. Hardman, E.W. Sutherland, J. Biol. Chem. 245 (1970) 5649–5655.
[25] J. Garthwaite, E. Southam, C.L. Boulton, E.B. Nielsen, K. Schmidt, B. Mayer, Mol. Pharmacol. 48 (1995) 184–188.
[26] D. Morley, C.M. Maragos, X.Y. Zhang, M. Boignon, D.A. Wink, L.K. Keefer, J. Cardiovasc. Pharmacol. 21 (1993) 670–676.
[27] S. Huang, H.H. Kerschbaum, A. Hermann, Brain Res. 780 (1998) 329–336.
[28] U.K. Laemmli, Nature 227 (1970) 680–685.
[29] H. Towbin, T. Staehelin, J. Gordon, Proc. Natl. Acad. Sci. USA 76 (1979) 4350–4354.
[30] L.J. Roman, E.A. Sheta, P. Martasek, S.S. Gross, Q. Liu, B.S. Masters, Proc. Natl. Acad. Sci. USA 92 (1995) 8428–8432.
[31] F.S. Vilim, E.C. Cropper, D.A. Price, I. Kupfermann, K.R. Weiss, J. Neurosci. 16 (1996) 8105–8114.
[32] R. Elofsson, M. Carlberg, L.L. Moroz, L. Nezlin, D. Sakharov, Neuroreport 4 (1993) 279–282.
[33] M.R. Elphick, I.C. Green, M. O'Shea, Brain Res. 619 (1993) 344–346.
[34] M. Regulski, T. Tully, Proc. Natl. Acad. Sci. USA 92 (1995) 9072–9076.
[35] M.R. Elphick, G. Kemenes, K. Staras, M. O'Shea, J. Neurosci. 15 (1995) 7653–7664.
[36] U. Muller, Eur. J. Neurosci. 6 (1994) 1362–1370.
[37] D.J. Stuehr, O.W. Griffith, Adv. Enzymol. Relat. Areas Mol. Biol. 65 (1992) 287–346.
[38] E. Southam, J. Garthwaite, Neuroreport 2 (1991) 658–660.
[39] H.H. Schmidt, S.M. Lohmann, U. Walter, Biochim. Biophys. Acta 1178 (1993) 153–175.
[40] D. Luo, E. Leung, S.R. Vincent, J. Neurosci. 14 (1994) 263–271.
[41] W.P. Arnold, C.K. Mittal, S. Katsuki, F. Murad, Proc. Natl. Acad. Sci. USA 74 (1977) 3203–3207.
[42] H. Aonuma, Zool. Sci. 19 (2002) 969–979.
[43] S. Fujie, H. Aonuma, I. Ito, A. Gelperin, E. Ito, Zool. Sci. 19 (2002) 15–26.

Journal of Neuroscience Methods 149 (2005) 15–25

JOURNAL OF NEUROSCIENCE METHODS

www.elsevier.com/locate/jneumeth

Two-color in situ hybridization in the CNS of *Aplysia californica*

Sami H. Jezzini[a,1], Michaela Bodnarova[a,b,1], Leonid L. Moroz[a,*]

[a] *The Whitney Laboratory for Marine Bioscience and Department of Neuroscience, University of Florida, 9505 Ocean Shore Blvd., St. Augustine, FL 32080, USA*

[b] *Department of Pediatrics, 1st Medical Faculty, Charles University, Prague, Czech Republic*

Received 10 January 2005; received in revised form 4 April 2005; accepted 8 April 2005

Abstract

Aplysia californica is an attractive model organism for cellular and systems neuroscience. Currently, there is a growing body of sequence data from *Aplysia* that includes many interesting genes. To fully exploit this molecular data it must be integrated with the large body of physiological data that are already available for identified neurons in *Aplysia* networks. In situ hybridization is a powerful technique that enables this to be done. Expression patterns of selected mRNA transcripts can be mapped to individual cells in the central nervous system (CNS). Here, we describe a detailed non-radioactive in situ hybridization protocol optimized for whole-mount preparations of *Aplysia* ganglia. The indirect alkaline phosphatase-based chromogenic detection method we employ may be used with one or two colors in order to detect one or two different transcripts in the same preparation. The procedure is also compatible with intracellular dye labeling, making it possible to couple localization of transcripts with electrophysiological studies in positively identified neurons. Double labeling was done for transcripts encoding the neuropeptides FMRFamide and sensorin. The sensitive detection of mRNA and great preservation of CNS morphology makes this method a useful tool for analyzing expression patterns of neuron specific genes in *Aplysia*.

Keywords: FMRFamide; Sensorin; Fasciclin; Potassium channels; Molluscs; Lucifer Yellow

1. Introduction

Molecular mapping is crucial for applying genomic data to the study of brain function. Program efforts are currently ongoing to define the 'molecular neuroanatomy' of specific brain regions by charting patterns of gene expression. While serial analysis of gene expression (SAGE) (Velculescu et al., 1995) and microarray techniques play an important part in molecular mapping efforts (de Chaldee et al., 2003; Lein et al., 2004), results must be validated by in situ hybridization because it is the most accurate method known for localizing transcripts in tissues and cells. From mapping studies, it is clear that morphologically distinct groups of cells within the mammalian CNS present distinct molecular profiles that correlate with functional phenotype. However, one impediment to the application of expression data to functional studies in vertebrate neuronal networks is the inability to reliably obtain electrophysiological recordings from identified pre- and post-synaptic cells.

Aplysia californica's central nervous system contains many large and identifiable neurons that make it a useful model where studies of behavioral phenomena can be carried out on a cellular level. Some areas where identified neurons of *Aplysia* have been utilized include study of the molecular basis of learning and memory (Kandel, 2001; Brembs et al., 2004; Sharma and Carew, 2004), cellular correlates of motivational states (Kupfermann et al., 1991; Prockt and Weiss, 2003; Prockt et al., 2004), nerve injury and regeneration (Bedi and Glanzman, 2001; Sung et al., 2004; Weragoda

Abbreviations: ASW, artificial sea water; CNS, central nervous system; DIG, digoxigenin; EST, expressed sequence tag; FRDB, Fast Red detection buffer; NBD, NBT/BCIP detection buffer; NBT/BCIP, nitro blue tetrazolium chloride/5-bromo-4-chloro-3-indolyl phosphate; PCR, polymerase chain reaction; PBS, phosphate-buffered saline; PBT, 0.1% Triton-X 100, 2 mg/ml bovine serum albumin, in PBS, pH 7.4; PTW, 0.1% Tween 20 in PBS, pH 7.4; SDS, sodium dodecyl sulfate solution; SSC, saline sodium citrate buffer; TEA HCl, triethanolamine hydrochloride solution

* Corresponding author. Tel.: +1 904 461 4020; fax: +1 904 461 4052.
E-mail address: moroz@whitney.ufl.edu (L.L. Moroz).

[1] This author contributed equally to this work.

0165-0270/$ – see front matter © 2005 Elsevier B.V. All rights reserved.
doi:10.1016/j.jneumeth.2005.05.007

et al., 2004), and motor pattern generation and modulation (Cropper et al., 2004). The large body of data regarding functional aspects of neuronal networks in *Aplysia*, combined with a growing body of molecular data, makes *Aplysia* an attractive model for neurogenomic studies. The ability to map expression patterns in identified neurons of *Aplysia* makes it possible to carry out repeatable in vivo analyses of gene function on a synaptic or cellular level that is not possible in vertebrate systems.

Here, we provide a detailed description of a two-color in situ hybridization protocol that has been optimized for use on whole-mount *Aplysia* ganglia. The procedure can be used in conjunction with intracellular dye labeling using Lucifer Yellow, making it possible to directly correlate functional activity in identified neurons with the expression of specific genes.

Several in situ hybridization protocols have previously been applied to the CNS of *Aplysia* (McAllister et al., 1983; Brunet et al., 1991; Ono and McCaman, 1992; Levenson et al., 2000) and related molluscan species (Santama et al., 1993; Smit et al., 1993; Bogdanov et al., 1996) but most were adapted to sectioned tissues or cultured neurons (Moccia et al., 2003). Ono and McCaman (1992) described an alkaline phosphatase-based in situ hybridization method for whole-mount *Aplysia* ganglia; however, the protocol was not able to consistently detect expression of the abundant transcript for the neuropeptide FMRFamide in identified cells such as R2 where it is known to be expressed. The protocol described here differs from previous *Aplysia* protocols in that it is optimized for processing whole ganglia, produces consistent staining for neuropeptides, and is sensitive enough to detect less abundant transcripts.

Expression patterns of two highly abundant neuropeptide transcripts, sensorin (Brunet et al., 1991) and FMRFamide (Price and Greenberg, 1977; Schaefer et al., 1985), and two relatively low abundance transcripts, putative ion channel AcK2p1 (Jezzini and Moroz, 2004) and fasciclin (Bastiani et al., 1987) are shown as illustrative examples. Some parts of this protocol have been published previously (Vilim et al., 2001; Jezzini and Moroz, 2004; Walters et al., 2004).

2. Materials and methods

2.1. Animals and CNS preparation

A. californica weighing 50–70 g were obtained from the National Resource for *Aplysia* at the University of Miami, and *Aplysia* weighing 150–250 g were collected in the wild by Marinus Scientific, Long Beach, California. Animals were anesthetized by injection of 50% (volume/body weight) isotonic $MgCl_2$ (337 mM) prior to surgical removal of the CNS. Ganglia were removed and incubated in 1% Protease IX (Sigma) in artificial sea water (ASW: 460 mM NaCl, 10 mM KCl, 55 mM $MgCl_2$, 11 mM $CaCl_2$, 10 mM HEPES, pH 7.6) at 34 °C for 20–45 min to soften the connective tissue of the neuronal sheath. Following treatment with Protease IX, ganglia were washed in several changes of ASW and pinned into a sylgard-bottomed dish. In preparations where dye injection was done, only the sheath overlying cells of interest was removed using fine forceps and scissors. Ganglia that were not used for dye injection were immediately fixed in 4% formaldehyde in phosphate-buffered saline (PBS: 137 mM NaCl, 27 mM KCl, 10 mM Na_2HPO_4, 2 mM K_2PO_4, pH 7.4) overnight at 4 °C following treatment in Protease IX, and prior to removal of any sheath. After fixation, all ganglia were washed in three 15 min changes of PBS before being placed in fresh PBS for removal of the sheath, or in the case of previously dye injected ganglia, any remaining sheath, using fine forceps and scissors under the dissecting microscope.

2.2. Dye injection

Sensory neurons were impaled with sharp microelectrodes filled with 4% Lucifer Yellow in 0.1% lithium chloride (LiCl). The same type electrodes had resistances of 5–9 MΩ when filled with 3 M potassium acetate and ~25–40 MΩ when filled with 0.1% LiCl. Dye was iontophoretically injected into sensory neurons for ~25 min using a continuous train of −2 to −5 nA current pulses with a 600 ms interpulse interval and a 50% duty cycle. After injection ganglia were fixed by flooding the dish with 4% formaldehyde in PBS and left for at least 4 h, but not longer than overnight at 4 °C. Following fixation the preparations were rinsed and desheathed as described above.

2.3. In situ hybridization

Major steps in the in situ hybridization protocol, which was modified from those previously published (Bogdanov et al., 1996; Ono et al., 2000), are shown in Fig. 1. The method utilizes a non-radioactive chromogenic in situ hybridization protocol based on immunological detection using alkaline phosphatase-conjugated antibodies. We have used this protocol extensively for in situ hybridization utilizing digoxygenin (DIG)-labeled antisense RNA probes with nitro blue tetrazolium chloride/5-bromo-4-chloro-3-indolyl phosphate (NBT/BCIP) as the alkaline phosphatase substrate for detection of single mRNA species. Briefly, DIG-labeled uridine triphosphate (UTP) is incorporated into the antisense RNA probe when it is synthesized. After hybridization of the probe to whole-mount ganglia, the preparations are incubated with alkaline phosphatase-conjugated anti-DIG antibodies. Visualization is done by introducing an alkaline phosphatase substrate to the preparation. Dephosphorylation of such substrates leads to the formation of a colored precipitate; for the NBT/BCIP substrate the precipitate is blue.

The method for two-color in situ hybridization relies on the same basic principles (Jowett and Lettice, 1994; Jowett et al., 1996; Hansen et al., 2000). After hybridization of an antisense RNA probe containing fluorescein-labeled UTP, alkaline phosphatase-conjugated anti-fluorescein antibodies

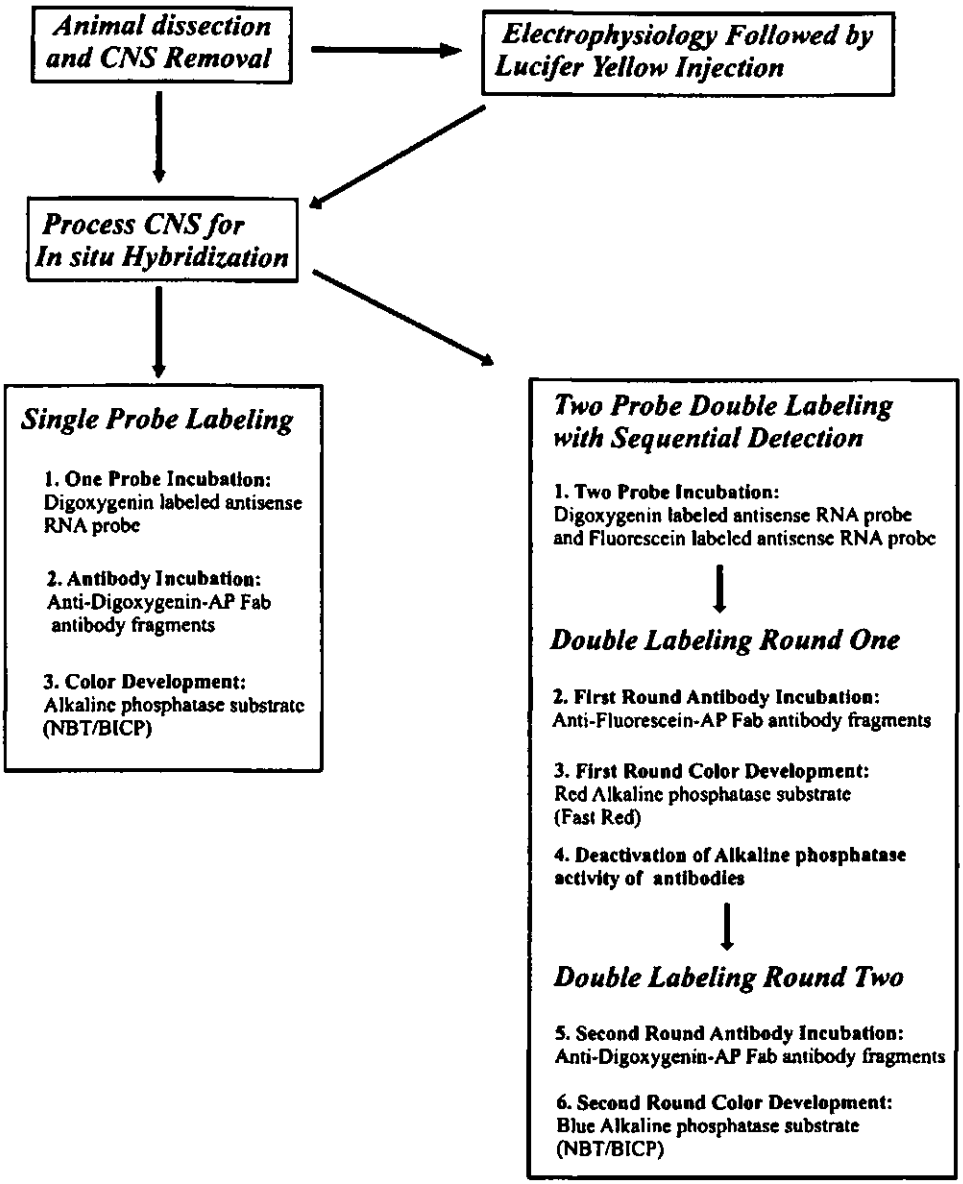

Fig. 1. An overview of the in situ hybridization protocol. The left side outlines the basic steps of the in situ hybridization. Optional variations are shown on the right. Lucifer Yellow may be injected prior to fixation of ganglia to specifically mark neurons after electrophysiological tests. For two-color in situ labeling, two probes are hybridized at the same time and detected separately by sequential antibody incubations and color development reactions on separate days. Each probe and antibody incubation is done overnight, thus the procedure takes at least 3 days to complete for single labeling and 4 days for double labeling.

are employed with the alkaline phosphatase substrate Fast Red. The processing of ganglia is the same whether using a single probe type or two different probe types up until the immunological detection steps (see Fig. 1). In the case of two-color detection, both RNA probe types are added together and hybridized at the same time while the subsequent antibody incubations and color development reactions are done sequentially on separate days.

All procedures described below should be done at room temperature unless stated otherwise. Agitation during any of the incubations or washes is optional, and is usually done only during antibody incubations and washes. Particular attention should be paid to maintaining an RNase-free environment. To help avoid contamination, solutions should be made in small batches in disposable sterile 50 ml plastic centrifuge tubes (Corning Incorporated, NY, USA; Cat. No. 430921), and all incubations are done in disposable sterile 24-well cell culture plates (Corning Incorporated, NY, USA; Cat. No. 3524). Best results are achieved by transferring ganglia one by one into new wells for each solution change. We have concluded from experience that all the solutions are stable for up to three months if stored at 4 °C with the exception of the hybridization and detection buffers, both of which should either be prepared fresh before the experiment or stored in aliquots at −20 °C. Formation of precipitates may be observed in some washing solutions with high salinity such as 5 × saline sodium

citrate buffer (SSC) when stored at 4 °C; however, the solutions may be heated to room temperature or the incubation temperature and precipitates will re-dissolve without any ill affects. Chemicals were obtained from Sigma unless otherwise indicated.

2.3.1. Probe preparation

Digoxygenin-labeled antisense RNA probes are transcribed in vitro using SP6 or T7 polymerases from full-length cDNA clones, ligated into p-GEM T vector (Promega), and linearized with the appropriate restriction endonucleases. Full-length sense probes are used for negative controls. One microliter of the restriction digest should be run on a 1% agarose gel with ethidium bromide staining to check for quality of the reaction and the remainder is purified using a PCR purification kit (Qiagen). Typically, 13 μl of the purified linearized plasmid (approximately, 1 μg of plasmid) is used as a template in the probe synthesis reaction. Probe synthesis is carried out using the DIG RNA Labeling Kit (SP6/T7) (Roche; Cat. No. 1175025) according to the manufacturer's directions (13 μl template, 2 μl NTP labeling mix, 2 μl 10× transcription buffer, 1 μl RNase inhibitor, 2 μl SP6 or T7 RNA polymerase, 37 °C for 2 h). The reactions are stopped with the addition of 2 μl 0.2 M EDTA, pH 8.0. The NTP labeling mix contains either DIG-11-UTPs (DIG RNA Labeling Mix, Roche; Cat. No. 1277073) for synthesis of DIG-labeled probes, or fluorescein-12-UTPs (Fluorescein RNA Labeling Mix, Roche; Cat. No. 1685619) for synthesis of fluorescein-labeled probes. The quality of plasmids, restriction digests, and synthesized probes should be checked on a 1% agrose gel with ethidum bromide staining prior to use. Concentrations of labeled RNA can be more accurately determined using an Agilent 2100 Bioanalyzer equipped with the RNA 6000 Nano Assay LabChip kit (Agilent Technologies, Palo Alto, CA, USA).

Probes up to 1 kb or even longer may be used at full length. Alternatively, probes may be fragmented or "crushed" via alkaline hydrolysis prior to use. To crush the probe 6 μl of 5× crush buffer (0.2 M $NaHCO_3$, 0.3 M Na_2CO_3) is added to 24 μl of probe diluted in water (2–6 μl probe and 18–22 μl water), and incubated at 60 °C for 30–45 min. This is done immediately prior to the hybridization step and the reaction is stopped by adding the entire 30 μl volume into the well containing the processed ganglia in 1 ml of hybridization buffer (see CNS preparation below).

2.3.2. CNS processing and probe hybridization

Fully desheathed, fixed ganglia are transferred to PTW (0.1% Tween 20 in PBS) for 10 min, and subsequently dehydrated in sequential 10 min incubations in 30, 50, and 70% methanol in PTW, followed by placement in 100% methanol. Ganglia are kept overnight or for up to 2 weeks in 100% methanol at −20 °C. Next, the ganglia are rehydrated by sequential 10 min incubations in 70, 50, and 30% methanol in PTW followed by placement into 100% PTW for 15 min. Following rehydration, the ganglia are transferred to a wash of 0.3% Triton X-100 in PBS for 10 min, followed by a wash in PBS for 10 min, and then placed into PTW.

After 5 min in PTW, Proteinase K (Roche Diagnostics) is added to the PTW to make a final concentration of 10 μg Proteinase K per 1 ml PTW (typically around 0.6 μl Proteinase K per 1 ml PTW). The ganglia are incubated at room temperature for 60 min or until they start to appear slightly translucent around the edges. The exact time of Proteinase K incubation depends on the size of the animals and how much the ganglia were digested in the initial Protease IX treatment. An hour is generally sufficient for ganglia from animals weighing from 70 to 150 g, ganglia from larger animals required up to 1.5 h or more. Proteinase K activity is terminated by transferring ganglia to 4% formaldehyde in PBS for 20 min at 4 °C.

Following post-fixation in 4% formaldehyde, the ganglia are washed in two changes of PTW containing 2 mg/ml of glycine (a proteinase K inhibitor), followed by two changes of PTW without glycine, and three changes of TEA HCl (0.1 M Triethanolamine hydrochloride, adjusted to pH 8.0 with sodium hydroxide). With the ganglia in a 1 ml volume of TEA HCl, 2.5 μl of acetic anhydride is added slowly while stirring. After adding the acetic anhydride, the ganglia are left to sit for 5 min before adding an additional 2.5 μl acetic anhydride while stirring, followed by another 5 min incubation.

Next, the ganglia are washed in three changes of PTW before being transferred to hybridization buffer (HB: 50% formamide, 5 mM EDTA, 5× SSC (20× SSC: 3 M NaCl, 0.3 M sodium citrate, pH 7.0), 1× Denhardt solution (0.02% ficoll, 0.02% polyvinylpyrrolidone, 0.02% bovine serum albumin), 0.1% Tween 20, 0.5 mg/ml yeast tRNA (GIBCO BRL)). Prehybridization incubation is then done immediately for 6–8 h at 50 °C, or the ganglia can be left overnight in HB at −20 °C before being incubated for 6–8 h at 50 °C the next day. Next, 2–6 μl of each probe is added (either full length or "crushed") and hybridization allowed to proceed for 12–14 h at 50 °C.

2.3.3. Immunological detection

Immunological detection is performed using either anti-digoxygenin-AP Fab antibody fragments at a dilution of 1:1500 or anti-fluorescein-AP Fab antibody fragments at 1:1000 (both from Roche Diagnostics, Mannheim, Germany). For double labeling the detection has to be performed sequentially, incubating the ganglia first with one antibody followed by development with one of the alkaline phosphatase substrates, and then after deactivating the phosphatase activity of the first antibody, incubation with the second antibody followed by the other alkaline phosphatase substrate.

After probe hybridization, the ganglia are washed in the following solutions: 50% formamide/5× SSC/1% SDS (sodium dodecyl sulfate, Fisher 20% solution BP1311) for 30 min, then 50% formamide/2× SSC/1% SDS for 30 min at 60 °C, and two 30 min changes of 0.2× SSC at 55 °C. Ganglia are then transferred to PBT (0.1% Triton-X 100, 2 mg/ml bovine serum albumin, in PBS; pH 7.4) for 20 min followed

by two additional 20 min changes of PBT at room temperature. Goat serum is added after the third change to make a concentration of 10% by volume and the ganglia are then incubated for 90 min at 4 °C with gentle shaking. After that the ganglia are placed in 1% goat serum in PBT. Alkaline phosphatase-conjugated antibodies are then added and incubation allowed to proceed for 12–14 h at 4 °C with gentle shaking.

2.3.4. Development using the NBT/BCIP alkaline phosphatase substrate: single probe labeling

After incubation with antibody, the ganglia are transferred to PBT at 4 °C and washed in three–five 30 min changes of PBT at 4 °C followed by three 5 min changes of filtered NBT/BCIP detection buffer (NDB: 100 mM NaCl, 50 mM $MgCl_2$, 0.1% Tween 20, 1 mM levamisol, 100 mM Tris–HCl; pH 9.5) at 4 °C. NBT/BCIP stock solution (NBT/BCIP: 18.75 mg/ml nitro blue tetrazolium chloride, 9.4 mg/ml 5-bromo-4-chloro-3-indolyl phosphate toluidine salt in 67% dimethyl sulfoxide, Roche; Cat. No. 1681451) is added to the third change of NDB, in the amount of 20 μl/ml, while stirring thoroughly until completely dissolved.

The ganglia are kept on ice in the dark and monitored every 10–15 min for the development of staining. The developing ganglia should be viewed for only brief intervals to avoid excessive exposure to light. Development should be terminated after cell-specific labeling is clearly visible and before excessive background begins to appear.

Development is terminated by transferring the ganglia to 4% formaldehyde in methanol for 60 min at 4 °C followed by a final transfer into 100% ethanol at 4 °C. Immediately following the final transfer to 100% ethanol, preparations may be washed in two 10 min changes of 100% ethanol at 4 °C, cleared in methylsalicylate (for about 1 min or until they sink to the bottom), and mounted on microscope slides in Permount (Fisher) (see Fig. 2A and B). Preparations may also be imaged immediately while in ethanol (see Figs. 2C and 4A).

Post-fixation in methanol often dissipates all background and should be carefully monitored. Weakly staining ganglia, where cell-specific labeling appears to be fading excessively, may be post-fixed in 4% formaldehyde in methanol for less than 60 min before being rehydrated by 15 min changes of 70, 50, and 30% ethanol in PBS. Following rehydration, ganglia can be cleared in glycerol by 20 min changes of 30, 50, and 75% glycerol in PBS at 4 °C. Preparations can then be kept in 75% glycerol in PBS and either pinned out in sylgard-bottomed dishes or placed on microscope slides for imaging (see Fig. 3B).

2.3.5. Development using the Fast Red alkaline phosphatase substrate: double labeling round one

After incubation with antibody, the ganglia are transferred to PBT at 4 °C and washed in three–five 30 min changes of PBT at 4 °C followed by three 5 min changes of filtered Fast Red detection buffer (FRDB: 0.1% Tween 20, 100 mM Tris–HCl; pH 8.2) at 4 °C. Ganglia are then transferred to FRDB containing the substrate Fast Red (Fast Red TR/naphthol AS-MX, Sigma; Cat. No. F-4523) and development is monitored closely as described above for NBT/BCIP.

The reaction is stopped by transferring the ganglia to PBT for 10 min followed by five changes of PBT for 10 min each. Residual alkaline phosphatase activity is then terminated by incubating ganglia for 10 min in 0.1 M glycine hydrochloride, pH 2.2 followed by another five 10 min washes in PBT. The ganglia are then transferred to 1% goat serum in PBT at 4 °C for overnight incubation in the other antibody.

2.3.6. Development using the NBT/BCIP alkaline phosphatase substrate: double labeling round two

When performing a double labeling experiment, it is beneficial to use NBT/BCIP for the transcript of lesser abundance. It is also beneficial to use NBT/BCIP for development in the second round after using Fast Red in the first round, because alkaline phosphatase activity is lower the second time around and NBT/BCIP tends to give the stronger signal (Hansen et al., 2000).

After the second-round incubation with antibody, the ganglia are washed and developed exactly as described above for NBT/BCIP except that the reactions are stopped by transferring the ganglia to PBT for 10 min instead of 4% formaldehyde in methanol because the Fast Red precipitate will dissolve in alcohol. After 10 min in PBT the ganglia are rinsed in five changes of PBS for 10 min each followed by post-fixation in 4% formaldehyde in PBS for 30 min followed by several more PBS washes. Preparations can be kept in PBS for imaging or cleared and mounted in glycerol as described above for weakly stained ganglia.

2.4. Imaging

Images were acquired digitally with a Nikon DS-L1 camera mounted on an Olympus SZX12 binocular dissecting microscope.

3. Results

3.1. Probe synthesis

Antisense probes were synthesized to four different full-length cDNAs. Two encoded neuropeptides sensorin (X56770) and FMRFamide (gi|155762), one encoded the putative potassium channel *Ac*K2p1 (gi|24528452), and one encoded the protein fasciclin (Bastiani et al., 1987) (gi|20799319). Sensorin is relatively short at 541 bp and encodes a peptide that is specific to mechanosensory neurons (Brunet et al., 1991). The FMRFamide transcript encodes a longer prepropeptide and is ~2.4 kb in length (Schaefer et al., 1985). The coding region of the *Ac*K2p1 RNA transcript is ~2.5 kb and the coding region for the fasciclin transcript is ~2.3 kb.

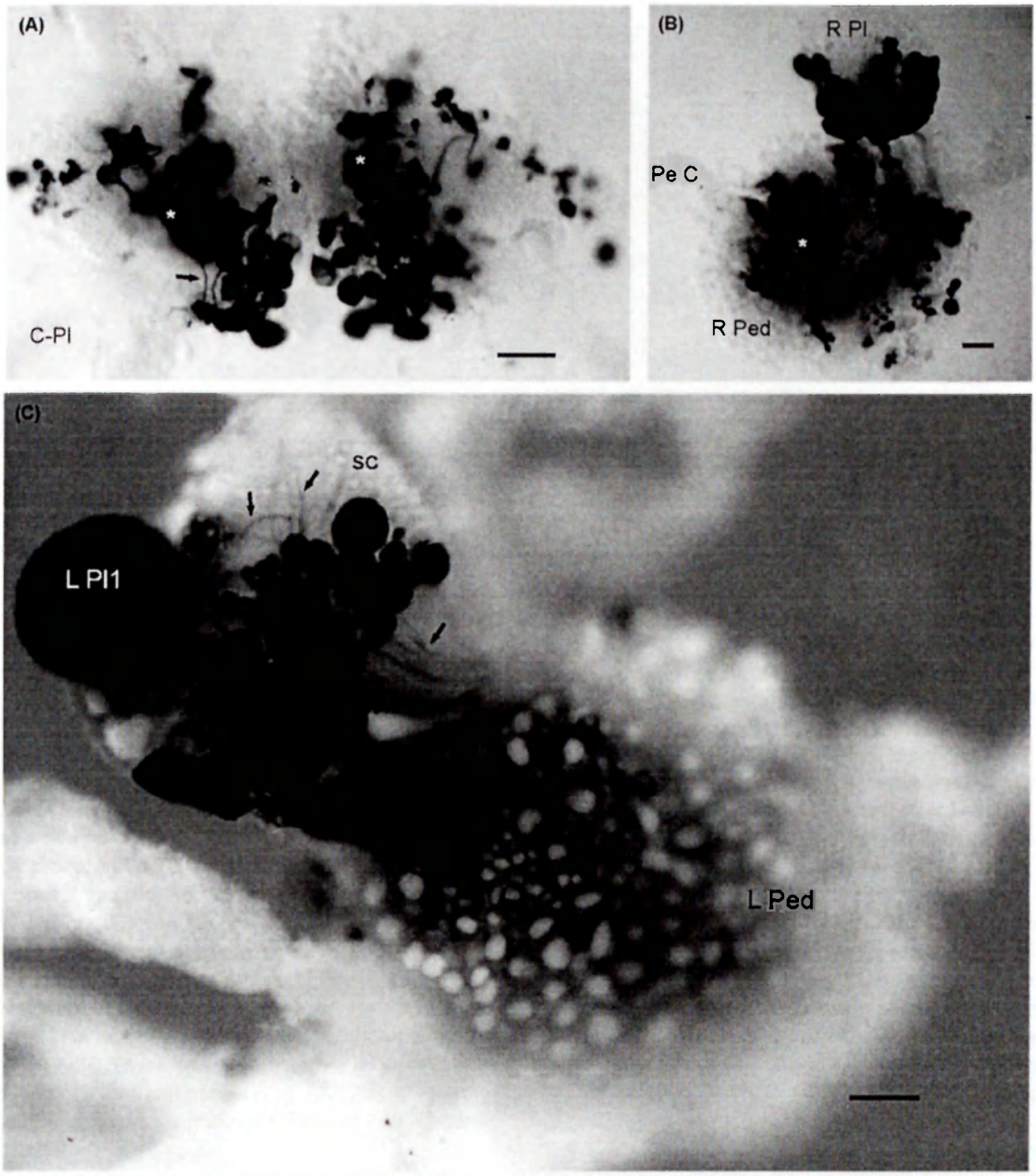

Fig. 2. In situ hybridization to FMRFamide mRNA produced intense and specific labeling throughout the CNS. (A) Dorsal view of the cerebral ganglion. (B) Dorsal view of the right pedal and pleural ganglia. (C) Dorsal view of the left pedal and pleural ganglia. The arrows in (A) and (C) indicate labeled axons. The preparations in (A) and (B) have been cleared in methylsalicylate and mounted in Permount. Asterisks are placed over ventrally located cell clusters. The plane of focus in (A) is more dorsal, and in (B) is more ventral. The preparation in (C) was imaged in a 100% ethanol bath. Morphology is better preserved in (C) than in (A) and (B); however, ventrally located cells are not visible. C-Pl, cerebropleural connective; Pe C, pedal commissure; R Ped, right pedal ganglion; R Pl, right pleural ganglion; L Pl 1, left pleural giant cell; L Ped, left pedal ganglion; L Pl, left pleural ganglion; SC, sensory cluster. Scale bars = 100 μm.

We found it necessary to empirically determine the optimum amount of probe to be used whenever a new probe was synthesized because yields of probe during synthesis and abundance of different transcripts were both variable. It was also necessary to empirically determine whether crushed or uncrushed probe produced more intense cell-specific staining. When probe synthesis reactions produced a bright band on a 1% agrose gel, 2.0 μl of probe per 1.0 ml of hybridization buffer was used for the first test and often produced good results. Such probes typically contained 100–400 ng/μl of labeled RNA. For example the concentration of DIG labeled probes for the neuropeptides used in this study was 115 ng/μl for FMRFamide and 380 ng/μl for sensorin.

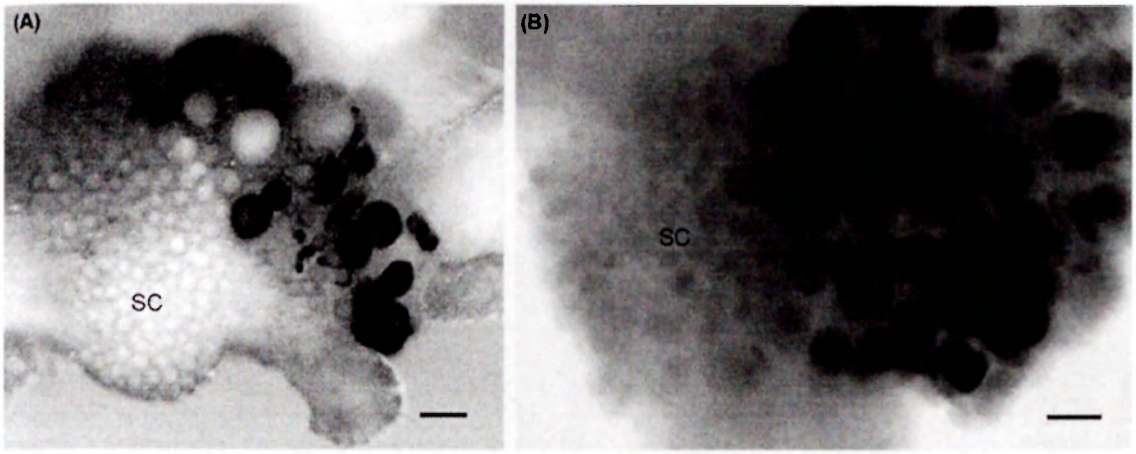

Fig. 3. Chromogenic in situ hybridization allowed detection of low abundance transcripts. (A) Fasciclin expression in the right caudal region of the buccal ganglion imaged in a 100% ethanol bath. (B) Expression of a putative potassium channel transcript (*Ac*K2p1) in the right pleural ganglion. The image in (B) was taken from a preparation mounted on a microscope slide in glycerol. SC, sensory clusters. Scale bars = 100 μm.

3.2. *Single probe labeling*

For all single-probe experiments, DIG-labeled RNA probes were used and hybridization was allowed to proceed for 12–14 h at 50 °C. For both peptides, 2 μl of probe was used per 1 ml of hybridization buffer. The DIG-labeled antisense FMRFamide probe was used at full length without being crushed. The sensorin probe produced the most intense staining after being crushed for 30 min at 60 °C. Development of FMRFamide and sensorin was apparent in as little as 10 min and was terminated after 30–60 min (Fig. 2). The FMRFamide probe produced very dark and highly specific labeling in central ganglia. Some visually identifiable cells such as LPI 1 (Fig. 2C) and R2 (see Fig. 5B) were darkly stained. The overall expression pattern of FMRFamide in the CNS was similar to patterns previously reported for this transcript that were based on in situ hybridization (Ono and McCaman, 1992) or labeling by anti-FMRFamide antibodies (Small et al., 1992). There was also clearly visible FMRFamide labeling of axons and nerves (Fig. 2A and C), which was consistent with previous findings (Ono and McCaman, 1992).

Mapping of the expression of sensorin in the CNS has been reported recently in detail (Walters et al., 2004). Sensorin produced highly specific and intense staining of sensory clusters that was similar in intensity to that seen for FMRFamide (Figs. 4 and 5).

The development of fasciclin-specific labeling took 60–90 min (Fig. 3A). Fasciclin produced clear and specific labeling of many cells in the CNS as seen in the buccal ganglion (Fig. 3A).

Detailed results for the putative potassium channel transcript, *Ac*K2p1, have also been recently described (Jezzini and Moroz, 2004). When we used 2 μl of probe per 1 ml of hybridization buffer for this relatively low abundance transcript, it took as long as 4 h to begin to see specifically labeled cells. When 4–6 μl of probe was used the most intensely staining cells became apparent after 1–2.5 h of development (Fig. 3B). The overall intensity of staining was much lower and less uniform, both within preparations and between preparations, than that seen for the neuropeptides. In preparations with intense overall levels of staining, some cells appeared quite dark and others extremely faint or barely distinguishable from background (Fig. 3B). In preparations with weak levels of staining overall, only the most darkly labeled cells were distinguishable from background. The most intensely staining cells (the darker ones in Fig. 3B) also became apparent during development up to an hour before more weakly staining cells.

3.2.1. *Single probe labeling with Lucifer Yellow labeling*

Because sensorin reliably stains sensory clusters, and because sensory cells comprising the clusters are also visually identifiable, we decided to use them to test whether injected Lucifer Yellow would be retained after the extensive washes of the in situ procedure. Fig. 4 shows Lucifer Yellow and sensorin labeling of two buccal sensory neurons that were injected with Lucifer Yellow prior to fixation. The intensity of the post-in situ hybridization Lucifer Yellow signal was dependent on how much Lucifer Yellow was injected. Iontophoretic injections lasting 20–30 min were adequate for sensory neurons.

3.3. *Double labeling using two probe types*

Double labeling was done using a DIG-labeled sensorin probe and the fluorescein-labeled FMRFamide probe. Two microliters of DIG-labeled antisense sensorin and 2 μl fluorescein-labeled antisense FMRFamide were added at the same time and hybridized at 50 °C for 13 h. The first round of immunological detection was done for FMRFamide using the Fast Red substrate, which produced a distinct and intense signal (Fig. 5). In the second round, sensorin was detected using the NBT/BCIP substrate (Fig. 5). We did not see any

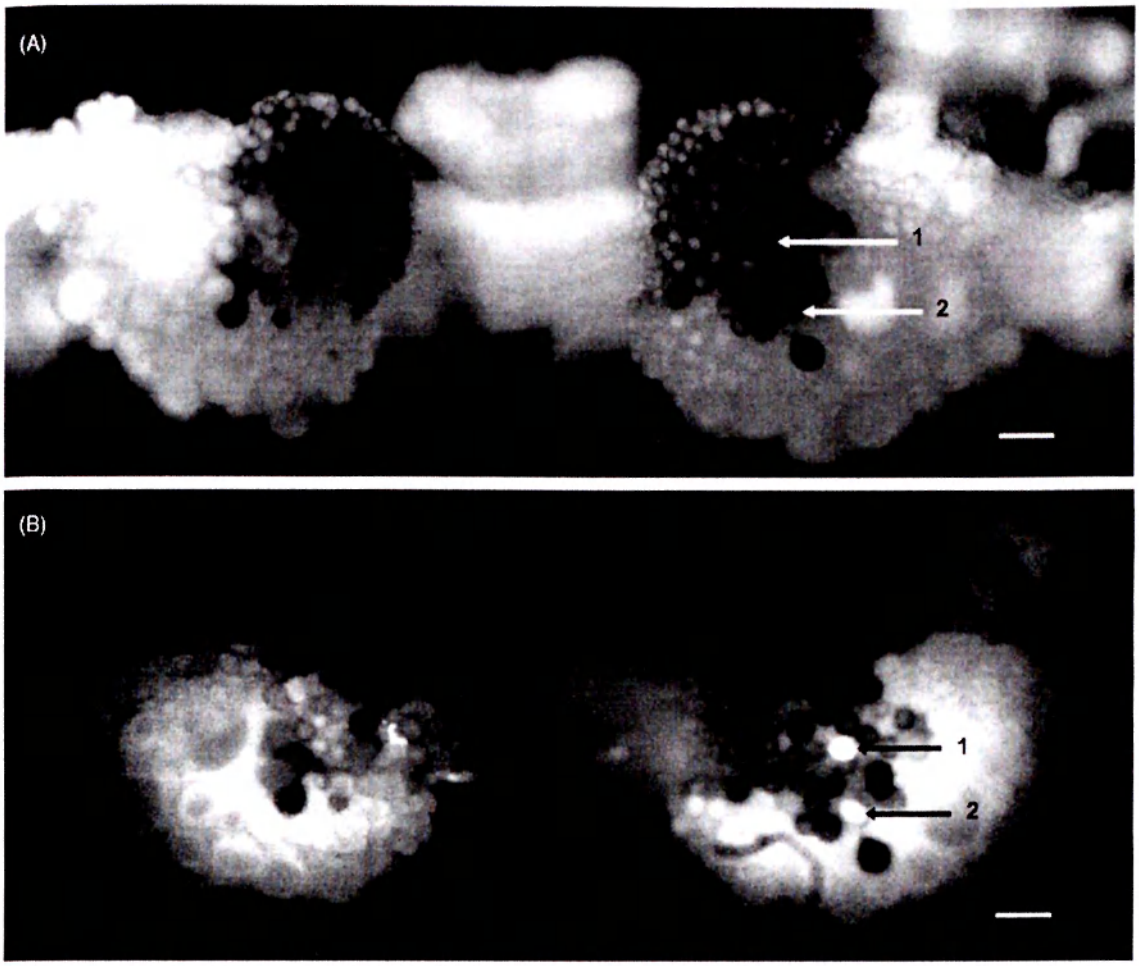

Fig. 4. Lucifer Yellow is retained after in situ hybridization. (A) Sensorin darkly labels sensory clusters of the buccal ganglion. Arrows indicate cells that were labeled with Lucifer Yellow prior to fixation. (B) Fluorescent image of the same preparation as in (A). The white appearance of the Lucifer Yellow injected neurons is due to digital contrast enhancement done in Adobe Photoshop. Scale bars = 100 μm.

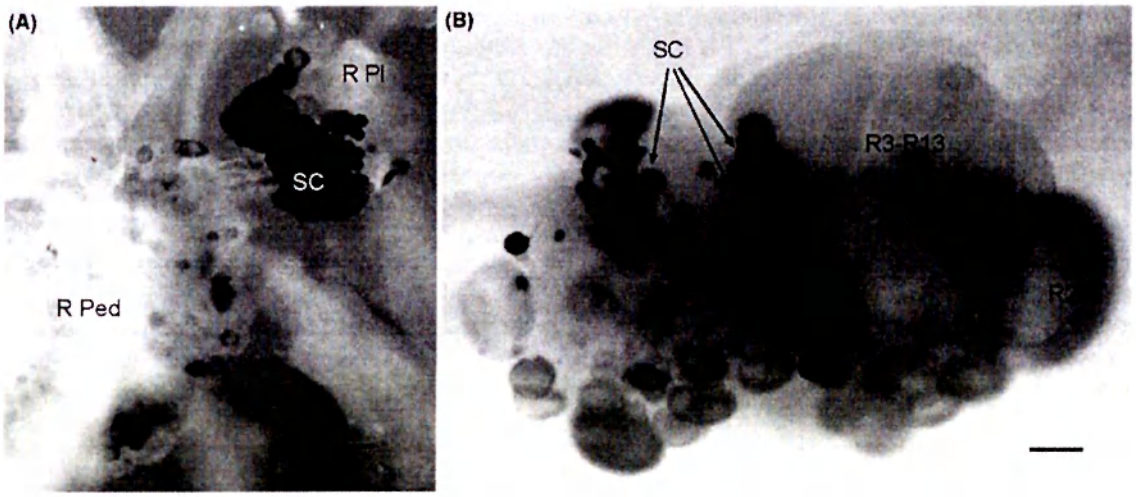

Fig. 5. Double labeling for sensorin (navy) and FMRFamide (red) indicates the respective positions of sensory clusters and cells expressing FMRFamide. (A) Ventral view of the right pedal and pleural ganglia. (B) Dorsal view of the abdominal ganglion. The giant cell R2, which is the contra-lateral homolog of LPl 1 shown in Fig. 2C) is intensely stained while the cluster containing cells R3–R13 is not. The ganglia in (A) and (B) were imaged in a glycerol bath. R Pl, right pleural ganglion; R Ped, right pedal ganglion; SC, sensory clusters. Scale bars = 100 μm. (For interpretation of the references to color in this figure legend, please refer to the web version of the article.)

colocalization between FMRFamide and sensorin; however, it is possible for the dark blue precipitate to mask the lighter red staining (Jowett et al., 1996).

4. Discussion

4.1. Specific labeling

A highly sensitive protocol for double chromophore-labeled in situ hybridization has been developed and optimized for whole-mount preparations of *Aplysia* CNS. It has been successfully used for *Aplysia* from 10 to 300 g. While optimized for *Aplysia*, it has also been used to label peptide-expressing neurons in the molluscs *Lymnaea stagnalis* and *Pleurobranchaea californica* (unpublished observations). This procedure can also be used for molecular mapping of expressed genes in combination with electrophysiological mapping of identified neurons. Lucifer Yellow labeling of specific cells following electrophysiology is retained during in situ hybridization, thus the identity of a cell can be positively matched with any particular gene it may express.

The protocol can be easily adapted to ganglia from different size animals by adjusting the protease digestion times accordingly. It is also readily adaptable to transcripts of different lengths and abundances by empirically determining optimal probe dilution, whether or not to "crush" the probe, and development time. Optimal results are usually obtained after several repetitions of the procedure.

The efficiency and intensity of in situ labeling correlates well with relative abundance of the target mRNAs. The frequency of the chosen model transcripts among randomly collected expressed sequence tags (ESTs) indicates that the neuropeptides are expressed at relatively high abundance, while fasciclin and the potassium channel transcript are expressed at relatively low abundance. Labeling for peptides develops quickly and is intense. The application of this protocol revealed additional (previously unreported) neurons expressing sensorin located on the dorsal side of the cerebral ganglion and in pedal ganglia (Walters et al., 2004). The pattern of expression for FMRFamide is consistent with previous immunolabeling patterns (Brown et al., 1985; Schaefer et al., 1985; Small et al., 1992), but also indicates an approximately 20–30% greater number of FMRFamide-expressing cells. The FMRFamide probe also consistently labels the giant and visually identifiable cells LPl 1 (Fig. 2C) and R2 (Fig. 5B). Low abundance transcripts, such as those for ion channels can be reliably detected (Fig. 3); however, the staining is not as intense or distinct and development times are considerably longer.

4.2. CNS preparation

We found that it is important that the ganglia are not over digested during the initial treatment in Protease IX. When ganglia were over digested with Protease IX, excessive damage can occur during desheathing causing cells to be lost, and the preparations will be prone to over digestion during later treatment with Proteinase K. It is always important to monitor the proteolytic treatment of ganglia with Proteinase K because the actual strength of both proteases can vary from lot to lot and with slight differences in concentration. Over digestion with Proteinase K (one indication of over digestion is that the nerves were starting to dissolve) usually resulted in preparations with high background, poor signal, and mechanical damage.

Contamination by RNase can also cause signal to be low in some cases. For this reason, extra care should be taken to prevent any oils from the skin or fingerprints from contaminating tools or anything else in contact with the dish containing the preparations. One should proceed immediately after desheathing, without delay, from the PBS wash to the methanol/PTW dehydration series because the stability of mRNA is much greater when the tissue is stored in methanol and any RNase will be inactive. Keeping ganglia in methanol for several days also proves advantageous when hybridizing transcripts of low abundance, in part, because the natural yellow pigmentation of the *Aplysia* CNS, which can hinder visualization when staining is weak, is dissipated. An alternative procedure to avoid keeping fixed ganglia in PBS for long periods is to desheath the ganglia right after protease treatment and prior to fixation. Also, it is necessary to remove the entire sheath because even the thinnest remnant of sheath will block penetration of probe.

4.3. Probe synthesis and quality

We found that in most cases, excessive background or an absence of staining was due to poor quality probe. Since the stability of RNA is very sensitive to its environment, care should be taken to ensure that all solutions are clean and sterile and at the correct pH. The labeled RNA probes are also sensitive to freeze–thaw cycles and should be aliquoted and stored at −80 °C. When stored under these conditions probes may be used for up to 1 year but should be checked for degradation before use by running 2 μl on a fresh agarose gel.

The longer the cDNA fragment used for probe preparation, the more specific the binding to mRNA, and the more stable the hybrids that are formed. Therefore, we always use full-length cDNA clones to make the probe. Transcriptionally labeled RNA probes prepared from linearized plasmid vector contain the short poly-cloning site of the plasmid preceding the start of the gene. This short pre-sequence normally does not cause any background problems for any of the full-length genes shown here. However, if only a short fragment of a gene of interest is available the polycloning site can be removed by designing sequence-specific PCR primers with a Sp6 promoter sequence added onto one primer and a T7 promoter sequence on the other. The PCR product may then serve as template for probe transcription.

If an initial test of an "uncrushed" probe not only appears to produce specifically labeled cells but also produces high background, then it should be tested again using the "crush" protocol. For an initial crush test, we always use 30 min at 60 °C for incubation. More or less time may be used; however, varying the crush time seems to influence staining less than varying probe concentration. While it makes intuitive sense that smaller fragments generated by "crushing" the probe should permeate the tissue more effectively, we have no objective data to support this idea. We have seen that relatively long transcripts such as FMRFamide at 2.5 kb penetrate just fine. In some cases, crushing the probe increases specificity, and in some cases it decreases specificity, this is unpredictable and must be empirically determined. We suspect that issues concerning secondary structure of the antisense RNA, or non-specific binding due to specific segments along the total length of the RNA, are more relevant to these effects than length.

4.4. Development and background

We have applied previously developed procedures and criteria used for NADPH-diaphorase histochemistry to the NBT/BCIP in situ development because the former also relies on the formation of a formazan precipitate from NBT and provides excellent results in several invertebrate preparations including opisthobranch molluscs (Moroz, 2000). The NBT/BICP substrate is normally utilized when doing in situ for a single probe type because the signal produced is generally stronger than that produced by the Fast Red substrate. There is also an added advantage that ganglia labeled using NBT/BCIP can be dehydrated in ethanol while Fast Red will dissolve away if exposed to alcohol. Post-fixation in ethanol often dissipates all background, and following dehydration, allows preparations to be cleared in methylsalicylate and mounted permanently (see Fig. 2A and B).

Neuron-specific labeling is most easily distinguished from background when staining for abundant transcripts such as those encoding neuropeptides. Neurons expressing such peptides become very darkly labeled within minutes and the development can be terminated before significant background develops. When such preparations are placed in methanol, labeled neurons should appear dark and distinct while unlabeled ones should appear completely white (Figs. 2 and 4A).

With less abundant transcripts, careful comparisons between negative controls (ganglia incubated with sense probe) and experimental preparations (ganglia incubated with antisense probe) are required. Development of the negative controls should be terminated at exactly the same time as experimental ganglia. After placement in methanol, the negative control should become devoid of any coloration. If color is present, it should be considered background and any comparable level of coloration in the experimental ganglia should also be considered background. Repeating the in situ procedure multiple times is also important in discerning faint cell-specific labeling from diffuse background. A consistent neuron-specific pattern should repeatedly emerge. Interestingly, we have not yet observed any transcripts to have faint, uniform expression throughout the CNS of *Aplysia*. Typically, either labeling is indistinguishable from background, or a neuron-specific pattern emerges.

Positive controls are also extremely useful. If the procedure is being done for the first time with new reagents, or a probe to a rare transcript is being tried for the first time, a positive control using a neuropeptide, such as FMRFamide, should be done in parallel. This controls for hybridization conditions and processing of ganglia. When an initial in situ for a new or rare transcript fails, but the positive control does not, then the procedure should simply be repeated with a higher probe concentration.

Because the alkaline phosphatase continually catalyzes the precipitation of substrate over time, color development continues over time and the signal becomes more intense over time. One consequence of this is that transcripts of low abundance take longer to develop than transcripts of high abundance. It can take an hour or more (in some cases up to 4–6 h) to begin to see any signal from low abundance transcripts. Less intense staining that occurs with low abundance transcripts, or when development is terminated too early, can be significantly diminished or even lost when the ganglia are cleared in methylsalicylate or placed in ethanol for prolonged periods. Thus, it is sometimes necessary to image the ganglia immediately after placement in ethanol or to rehydrate the ganglia and image them in glycerol. The glycerol can clear the preparations without loss of specific labeling, allowing the stain to be seen more easily (see Fig. 3B). Another property of the substrate is that color development can occur independently of alkaline phosphatase activity causing background staining to also develop over time. The alkaline phosphatase-independent development of background staining is particularly sensitive to light and heat, therefore, keeping the developing preparations on ice and in the dark as much as possible will help to keep the signal high and the background to a minimum.

Acknowledgements

We thank Dr. Andrea Kohn for determining the probe concentrations and Dr. Ruslan Sadreyev for earlier work on the protocol development. This work was supported by NIH and NSF grants, and in part by Packard and McKnight Brain research Foundation grants to LLM and GAČR 309/02/1193 to MB.

References

Bastiani MJ, Harrelson AL, Snow PM, Goodman CS. Expression of fasciclin I and II glycoproteins on subsets of axon pathways during neuronal development in the grasshopper. Cell 1987;48(5):745–55.

Bedi SS, Glanzman DL. Axonal rejoining inhibits injury-induced long-term changes in *Aplysia* sensory neurons in vitro. J Neurosci 2001;21(24):9667–77.

Bogdanov YD, Balaban PM, Zakharov IS, Poteryaev DA, Belyavsky AV. Identification of two novel genes specifically expressed in the D-group neurons of the terrestrial snail CNS. Invertebr Neurosci 1996;2(1):61–9.

Brembs B, Baxter DA, Byrne JH. Extending in vitro conditioning in *Aplysia* to analyze operant and classical processes in the same preparation. Learn Memory 2004;11(4):412–20.

Brown RO, Gusman D, Basbaum AI, Mayeri E. Identification of *Aplysia* neurons containing immunoreactive FMRFamide. Neuropeptides 1985;6(6):517–26.

Brunet JF, Shapiro E, Foster SA, Kandel ER, Iino Y. Identification of a peptide specific for *Aplysia* sensory neurons by PCR-based differential screening. Science 1991;252(5007):856–9.

Cropper EC, Evans CG, Hurwitz I, Jing J, Proekt A, Romero A, et al. Feeding neural networks in the mollusc *Aplysia*. Neurosignals 2004;13(1–2):70–86.

de Chaldee M, Gaillard MC, Bizat N, Buhler JM, Manzoni O, Bockaert J, et al. Quantitative assessment of transcriptome differences between brain territories. Genome Res 2003;13(7):1646–53.

Hansen GN, Williamson M, Grimmelikhuijzen CJ. Two-color double-labeling in situ hybridization of whole-mount *Hydra* using RNA probes for five different *Hydra* neuropeptide preprohormones: evidence for colocalization. Cell Tissue Res 2000;301(2):245–53.

Jezzini SH, Moroz LL. Identification and distribution of a two-pore domain potassium channel in the CNS of *Aplysia californica*. Brain Res Mol Brain Res 2004;127(1–2):27–38.

Jowett T, Lettice L. Whole-mount in situ hybridizations on zebrafish embryos using a mixture of digoxigenin- and fluorescein-labelled probes. Trends Genet 1994;10(3):73–4.

Jowett T, Mancera M, Amores A, Yan Y-L. In situ hybridization to embryo whole mounts and tissue sections: mRNA detection and application to developmental studies. In: Clark M, editor. In situ hybridization. Weinheim: Chapman & Hall; 1996. p. 91–121.

Kandel ER. The molecular biology of memory storage: a dialogue between genes and synapses. Science 2001;294(5544):1030–8.

Kupfermann I, Teyke T, Rosen SC, Weiss KR. Studies of behavioral state in *Aplysia*. Biol Bull 1991;180:262–8.

Lein ES, Zhao X, Gage FH. Defining a molecular atlas of the hippocampus using DNA microarrays and high-throughput in situ hybridization. J Neurosci 2004;24(15):3879–89.

Levenson J, Sherry DM, Dryer L, Chin J, Byrne JH, Eskin A. Localization of glutamate and glutamate transporters in the sensory neurons of *Aplysia*. J Comp Neurol 2000;423(1):121–31.

McAllister LB, Scheller RH, Kandel ER, Axel R. In situ hybridization to study the origin and fate of identified neurons. Science 1983;222(4625):800–8.

Moccia RD, Chen V, Lyles E, Kapuya YE, Kalachikov S, Spahn CM, et al. An unbiased cDNA library prepared from isolated *Aplysia* sensory neuron processes is enriched for cytoskeletal and translational mRNAs. J Neurosci 2003;23(28):9409–17.

Moroz LL. Giant identified NO-releasing neurons and comparative histochemistry of putative nitrergic systems in gastropod molluscs. Microsc Res Tech 2000;49(6):557–69.

Ono JK, McCaman RE. In situ hybridization of whole-mounts of *Aplysia* ganglia using non-radioactive probes. J Neurosci Methods 1992;44(1):71–9.

Ono T, Hirano S, Yonezawa S, Aono S, Osaki M, Masaki S, et al. Comparative mapping of seven genes in mouse, rat and Chinese hamster chromosomes by fluorescence in situ hybridization. Cytogenet Cell Genet 2000;89(3–4):209–13.

Price DA, Greenberg MJ. Structure of a molluscan cardioexcitatory neuropeptide. Science 1977;197(4304):670–1.

Proekt A, Brezina V, Weiss KR. Dynamical basis of intentions and expectations in a simple neuronal network. Proc Natl Acad Sci U S A 2004;101(25):9447–52.

Proekt A, Weiss KR. Convergent mechanisms mediate preparatory states and repetition priming in the feeding network of *Aplysia*. J Neurosci 2003;23(10):4029–33.

Santama N, Li KW, Bright KE, Yeoman M, Geraerts WP, Benjamin PR, et al. Processing of the FMRFamide precursor protein in the snail *Lymnaea stagnalis*: characterization and neuronal localization of a novel peptide, 'SEEPLY'. Eur J Neurosci 1993;5(8):1003–16.

Schaefer M, Picciotto MR, Kreiner T, Kaldany RR, Taussig R, Scheller RH. *Aplysia* neurons express a gene encoding multiple FMRFamide neuropeptides. Cell 1985;41(2):457–67.

Sharma SK, Carew TJ. The roles of MAPK cascades in synaptic plasticity and memory in *Aplysia*: facilitatory effects and inhibitory constraints. Learn Memory 2004;11(4):373–8.

Small SA, Cohen TE, Kandel ER, Hawkins RD. Identified FMRFamide-immunoreactive neuron LPL16 in the left pleural ganglion of *Aplysia* produces presynaptic inhibition of siphon sensory neurons. J Neurosci 1992;12(5):1616–27.

Smit AB, Hoek RM, Geraerts WP. The isolation of a cDNA encoding a neuropeptide prohormone from the light yellow cells of *Lymnaea stagnalis*. Cell Mol Neurobiol 1993;13(3):263–70.

Sung YJ, Walters ET, Ambron RT. A neuronal isoform of protein kinase G couples mitogen-activated protein kinase nuclear import to axotomy-induced long-term hyperexcitability in *Aplysia* sensory neurons. J Neurosci 2004;24(34):7583–95.

Velculescu VE, Zhang L, Vogelstein B, Kinzler KW. Serial analysis of gene expression. Science 1995;270(5235):484–7.

Vilim FS, Alexeeva V, Moroz LL, Li L, Moroz TP, Sweedler JV, et al. Cloning, expression and processing of the CP2 neuropeptide precursor of *Aplysia*. Peptides 2001;22(12):2027–38.

Walters ET, Bodnarova M, Billy AJ, Dulin MF, Diaz-Rios M, Miller MW, et al. Somatotopic organization and functional properties of mechanosensory neurons expressing sensorin-A mRNA in *Aplysia californica*. J Comp Neurol 2004;471(2):219–40.

Weragoda RM, Ferrer E, Walters ET. Memory-like alterations in *Aplysia* axons after nerve injury or localized depolarization. J Neurosci 2004;24(46):10393–401.

THE JOURNAL OF COMPARATIVE NEUROLOGY 471:219–240 (2004)

Somatotopic Organization and Functional Properties of Mechanosensory Neurons Expressing Sensorin-A mRNA in *Aplysia californica*

EDGAR T. WALTERS,[1]* MICHAELA BODNAROVA,[2] ALLEN J. BILLY,[1,3] MICHAEL F. DULIN,[1,4] MANUEL DÍAZ-RÍOS,[5,6] MARK W. MILLER,[5] AND LEONID L. MOROZ[2]

[1]Department of Integrative Biology and Pharmacology, University of Texas-Houston Medical School, Houston, Texas 77030

[2]The Whitney Laboratory, Department of Neuroscience, University of Florida, St. Augustine, Florida 32080

[3]Program in Basic Health Sciences, School of Health Sciences, British Columbia Institute of Technology, Burnaby, British Columbia V5G 3H2, Canada

[4]Harrisburg Family Physicians, Harrisburg, North Carolina 28075

[5]Department of Anatomy and Institute of Neurobiology, University of Puerto Rico, Medical Sciences Campus, San Juan, Puerto Rico 00901

[6]Neurobiology and Behavior, Cornell University, Ithaca, New York 14853

ABSTRACT

A previous study reported that a peptide, sensorin-A, is expressed exclusively in mechanosensory neurons having somata in central ganglia of *Aplysia*. The present study utilized in situ hybridization, staining by nerve back-fill and soma injection, and electrophysiological methods to characterize the locations, numbers, and functions of sensorin-A-expressing neurons and to define the relationships between soma locations and the locations of peripheral axons and receptive fields. Approximately 1,000 cells express sensorin-A mRNA in young adult animals (10–30 g) and 1,200 cells in larger adults (100–300 g). All of the labeled somata are in the CNS, primarily in the abdominal LE, rLE, RE and RF, pleural VC, cerebral J and K, and buccal S clusters. Expression also occurs in a few sparsely distributed cells in most ganglia. Together, receptive fields of all these mechanosensory clusters cover the entire body surface. Each VC cluster forms a somatotopic map of the ipsilateral body, a "sensory apl unculus." Cells in the pleural and cerebral clusters have partially overlapping sensory fields and synaptic targets. Buccal S cells have receptive fields on the buccal mass and lips and display notable differences in electrophysiological properties from other sensorin-A-expressing neurons. Neurons in all of the clusters have relatively high mechanosensory thresholds, responding preferentially to threatening or noxious stimuli. Synaptic outputs to target cells having defensive functions support a nociceptive role, as does peripheral sensitization following noxious stimulation, although additional functions are likely in some clusters. Interesting questions arise from observations that mRNA for sensorin-A is present not only in the somata but also in synaptic regions, connectives, and peripheral fibers. J. Comp. Neurol. 471:219–240, 2004.

Indexing terms: nociceptor; receptive field; axon; neuropeptide; defensive reflex; sensory map

Grant sponsor: National Institutes of Health (NIH); Grant number: NS35979 (E.T.W.); Grant number: NS35882 (E.T.W.); Grant sponsor: NIH; Grant number: NS39103; Grant number: MH60261 (L.L.M.); Grant number: P50G002806 (L.L.M.); Grant sponsor: the David and Lucile Packard Foundations (L.L.M.); Grant sponsor: the Evelyn F. McKnight Brain Research Grant Program (L.L.M.); Grant sponsor: NIH; Grant number: NS07464 (M.W.M.); Grant number: MH048190 M-RISP (M.W.M.); Grant number: GM08224 MBRS (M.W.M.); Grant sponsor: NIH; Grant number: RR10294.

*Correspondence to: Edgar T. Walters, Department of Integrative Biology and Pharmacology, University of Texas-Houston Medical School, 6431 Fannin Blvd. MSB 4.116, Houston, TX 77030. E-mail: edgar.t.walters@uth.tmc.edu

Received 18 August 2003; Revised 19 November 2003; Accepted 5 December 2003

DOI 10.1002/cne.20042

Published online the week of February 16, 2004 in Wiley InterScience (www.interscience.wiley.com).

The gastropod mollusc *Aplysia californica* has proved to be a useful species for exploring mechanisms of neural plasticity related to learning and memory (see, e.g., Kandel, 2001) and injury (see, e.g., Ambron and Walters, 1996). Much of this utility comes from experimental advantages offered by mechanosensory neurons, whose readily identifiable somata are clustered in the animal's central ganglia. The sensory clusters that have been utilized most extensively by neurobiologists are the left E (LE) cluster in the abdominal ganglion (Castellucci et al., 1970; Byrne et al., 1974), the ventrocaudal (VC) clusters in the pleural ganglia (Walters et al., 1983), and the J and K clusters in the cerebral ganglia (Rosen et al., 1979; see Fig. 1). These sensory populations were shown to innervate, respectively, the siphon, the tail, and the head, although none of these studies systematically examined the entire surface of the body for receptive fields. Mechanosensory neurons displaying morphological and response properties similar to those of these three groups of cells were also found in the abdominal ganglion right E (RE), right F (RF), and rostral LE (rLE) clusters (Byrne et al., 1974; Byrne, 1980; Dubuc and Castellucci, 1991) and in the buccal ganglion S_1 and S_2 clusters (Fiore and Geppeti, 1981). All of the abdominal ganglion clusters innervate structures in the mantle cavity, whereas the buccal ganglion S clusters appear to innervate the buccal mass.

By using a differential screening approach, Brunet and colleagues (1991) identified an mRNA encoding a potential neuropeptide precursor that was expressed in pleural VC clusters. Physiological experiments demonstrated that sensorin-A, a nonapeptide (ARYRVGYMF-NH_2) cleaved from this precursor, could act as an inhibitory cotransmitter at VC cell synapses. In situ hybridization with an antisense probe to the sensorin mRNA and immunohistochemistry with an antibody that recognized sensorin-A and its propeptide indicated that sensorin-A is selectively expressed in all of the known mechanosensory clusters in the central ganglia of *Aplysia*. Moreover, sensorin-A expression appeared to be absent from all other cells of the CNS (Brunet et al., 1991). Selective probes for sensorin-A and its mRNA offer powerful tools that have been exploited to study axonal regeneration (Steffensen et al., 1995a), changes in gene expression after nerve injury (Noel et al., 1995), and expression and stability of neuropeptide mRNA during synapse formation and synaptic plasticity (Santarelli et al., 1996; Schacher et al., 1999; Sun et al., 2001; Hu et al., 2002). However, except for the brief, preliminary description of sensorin-A staining in previously defined mechanosensory clusters by Brunet et al. (1991), probes for sensorin-A have not yet been used to examine systematically the topographic organization of the mechanosensory systems expressing this neuropeptide.

The discrete but distributed population of neurons defined by the expression of sensorin-A raises basic questions that are addressed herein. How many sensorin-A-expressing neurons are there in *Aplysia* and what is their detailed central distribution? How are the locations of the central sensorin-A-expressing somata related to the distribution of their peripheral axons and the locations of their mechanosensory receptive fields? Are all of the sensorin-A-expressing clusters actually mechanosensory in function? In this paper, we describe the central and peripheral organization of these cells and show that the receptive fields of the sensorin-A-expressing clusters cover the entire surface of the animal's body. Furthermore, by documenting receptive fields of the buccal S cells, we confirm that all of the sensorin-A-expressing clusters in *Aplysia* contain mechanosensory neurons and show that these cells, like neurons in the cerebral, pleural, and abdominal clusters, have relatively high mechanosensory thresholds.

Materials and Methods

Animals

Aplysia californica (10–300 g) were supplied by Alacrity Marine Biological Services (Redondo Beach, CA), Marinus (Long Beach, CA), and the NIH *Aplysia* Resource Facility (Miami, FL). Animals were housed in aquaria containing artificial seawater (ASW; Instant Ocean, Burlington, NC) at 15–18°C on a 12:12-hour light:dark cycle for up to 3 weeks before use. Constant body weight was maintained on a diet of live *Gracilaria* seaweed or dried seaweed laver. Animals weighed 10–30 or 100–300 g. The smaller animals were probably young adults, as indicated by the presence of bag cell clusters, but they may have included some animals transitioning from the last juvenile stage to adulthood (Kriegstein, 1977a,b; Cash and Carew, 1989). Prior to dissection, animals were anesthetized by injecting a volume of isotonic $MgCl_2$ (337 mM) equivalent to 50–60% of their weight.

In situ hybridization protocol

All in situ hybridization experiments were performed using whole-mount preparations of the CNS of *A. californica*. Ganglia (Fig. 1) were isolated, and before fixation they were pinned to a Sylgard dish in artificial seawater (ASW: 460 mM NaCl, 10 mM KCl, 55 mM $MgCl_2$, 11 mM $CaCl_2$, 10 mM HEPES, pH 7.6). Plasmids containing the sequence of full-length *A. californica* sensorin (GeneBank accession number gi:5589) subcloned in pGEM-T vector (Promega, Madison, WI) were obtained during EST sequencing from the CNS and sensory cells of *A. californica* (Moroz et al., 2002). The plasmid (JM-109 in *Escherichia coli*) was extracted, purified, and sequenced to obtain the orientation of the gene. The plasmid was linearized with specific endonucleases (NotI for the antisense probe using T7 polymerase, NcoI for the sense probe with Sp6 polymerase) and used as a template for the preparation of specific antisense and sense digoxigenin (DIG)-labeled sensorin RNA probes following the Roche protocol for probe preparation with a DIG RNA labeling kit (Sp6/T7). Control experiments (six preparations) using sense probes and identical labeling protocols and conditions did not produce specific staining in the CNS.

Our in situ hybridization protocol was based on previously published reports (Bogdanov Yu et al., 1996), with several modifications. Briefly, dissected central ganglia from *Aplysia* were treated with 1% trypsin (Sigma, St. Louis, MO) in filtered sea water (FSW) for 45–60 minutes at 34°C, rinsed for 5 minutes in FSW, and incubated with 1% trypsin inhibitor for 15 minutes in FSW at room temperature. The ganglia were fixed overnight in 4% paraformaldehyde in 0.2 M phosphate-buffered saline (PBS; pH 7.2) at 4°C. Preparations were washed in PBS, and connective tissues of the ganglionic sheath were carefully removed from all ganglia. The ganglia were washed in PTW (0.1% Tween 20 in PBS) three times for 5 minutes each, followed by a 10-minute incubation in increasing

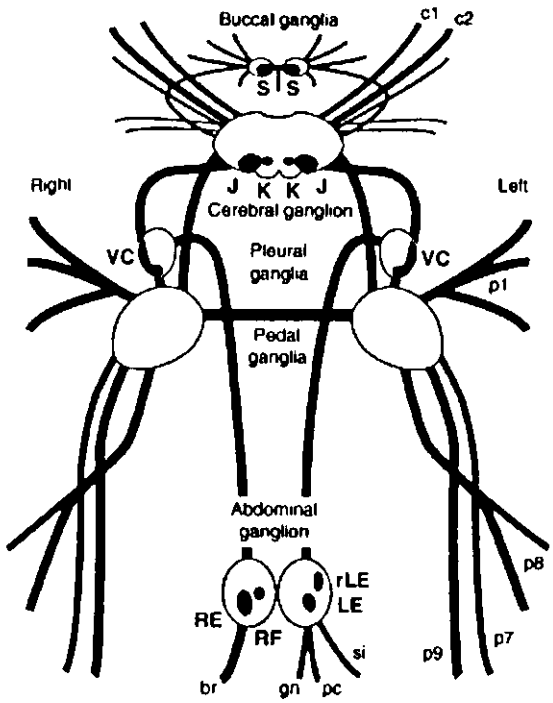

Fig. 1. Schematic diagram of the ventral side of the *Aplysia* CNS, with the sensorin-A-expressing mechanosensory clusters indicated by black shading (bilateral buccal S; bilateral cerebral J and K; bilateral pleural VC; and abdominal rLE, LE, RF, and RE clusters). The following nerves are labeled: c1 (superior labial), c2 (anterior tentacular), p1 (anterior pedal), p7 (middle parapodial), p8 (middle pedal), p9 (posterior pedal), si (siphon), pc (pericardial), gn (genital), br (branchial).

amounts of methanol (3:1 PTW:MetOH, 1:1, 1:3, and 100% MetOH), in which the ganglia were preserved for up to 1 week. In most experiments, ganglia were transferred back to PTW in the same fashion by repetitive substitution of methanol by PTW (10-minute washes with 1:3 PTW/MetOH, 1:1, 3:1, PTW, followed by a 10-minute wash with 0.3% Triton in PBS, PTW for 5 minutes). After incubation with proteinase K (10 μg/ml) in PTW at room temperature for 1 hour, the ganglia were postfixed with 4% paraformaldehyde in PBS for 20 minutes at 4°C and washed (2 × 5 minutes) in each of the following solutions: glycine (2 mg/ml PTW), PTW, 0.1 M triethanolamine hydrochloride (TEA HCl; pH 8.0), and anhydrous acetate (2.5 μl/ml) in TEA HCl. Next, the ganglia were repeatedly washed in PTW and incubated at −20°C in hybridization buffer (50% formamide, 5 mM EDTA, 5× SSC, 1× Denhardt solution [0.02% ficoll, 0.02% polyvinylpyrrolidone, 0.02% bovine serum albumin (BSA)], 0.1% Tween 20, 0.5 mg/ml yeast tRNA (Gibco BRL) overnight. All subsequent steps until detection (including the 6–8-hour prehybridization at 60°C) were peformed with moderate shaking. DIG-labeled RNA probes (2 μl/ml) were added, and ganglia were incubated for a further 6–8 hours. Hybridization was followed by 30 minutes of washing at 60°C in 50% formamide/5× SSC/1% sodium dodecyl sulfate (SDS), then 50% formamide/2× SSC/1% SDS, then 0.2× SSC, twice for 30 minutes at 55°C. After three washes in PBT (1× PBS, 0.1% Triton X-100, 2 mg/ml BSA), ganglia were treated with 10% normal goat serum in PBT at 4°C for up to 90 minutes and left overnight with a 1:1,350 dilution of alkaline phosphatase-conjugated DIG antibodies (Boehring, Indianapolis, IN) in 1% goat serum in PBT at 4°C. Unbound antibodies were washed out in several PBT incubations at 4°C (at least 2–3 hours total). After two 5-minute incubations in detection buffer (100 mM NaCl, 50 mM $MgCl_2$, 100 mM NaCl, 100 mM Tris Cl, pH 9.5, 0.01% Tween 20, 1 mM levamisol), NBT/BCIP color substrates (DIG Nucleic Acid Detection Kit; Boehringer) were added to detect the hybridized probes. At this stage, ganglia were kept at 4°C in the dark with periodic visual assessment of the staining intensity. After the detection procedure (usually 30–60 minutes), ganglia were postfixed in 4% paraformaldehyde in methanol for up to 1 hour and washed twice in 100% ethanol. Permanent preparations were produced by incubating ganglia in methylsalycilate and embedding in Permount (Fisher, Fair Lawn, NJ) on microscopic slides. Examination and analysis of staining were conducted on an upright Nikon Optiphot-2 or an Olympus SZX 12 dissecting microscope. Images were acquired with a Nikon Coolpix 4500 digital camera and initially saved as JPEG files.

Electrophysiological properties and receptive field mapping

Receptive fields and peripheral axon distributions of individual cells in sensorin-A-expressing clusters were studied in semiintact or excised ganglia preparations while recording intracellularly from sensory neuron somata. All recordings were made at room temperature (18–22°C). Semiintact preparations used to map receptive fields were modified from those shown to provide access to most of the body surface (Hening et al., 1979; Walters et al., 1983; Billy and Walters, 1989a) or to optimize access to either the mantle organs (Dubuc and Castellucci, 1991; Illich and Walters, 1997) or the head and buccal mass (Rosen et al., 1979; Teyke et al., 1989; Miller et al., 1994). Most commonly, the body remained intact, except for dorsal and ventral incisions to expose the circumesophageal ganglia. The esophagus was cut, tied off, pulled out from the circumesophageal ganglia, and pinned to the Sylgard substrate out of the way. In other cases, all of the viscera and different parts of the body were removed. Margins of the foot and parapodia, or other body parts (depending on the preparation), were stretched taut with numerous restraining pins. Selected ganglia were then pinned tightly to the substrate. During surgical procedures, the ganglia were bathed in a solution containing equal amounts of ASW and isotonic $MgCl_2$. After desheathing, the $MgCl_2$ was washed from the bath with large volumes of buffered ASW at least 1 hour before recording. $MgCl_2$ was washed out of peripheral tissues by injecting 60–120 ml of buffered ASW into the sinus between the skin and the underlying muscle layer. The effectiveness of washout was indicated by the return of spontaneous movements and of local and centrally mediated withdrawal reflexes in the injected region (see, e.g., Walters et al., 1983; Billy and Walters, 1989b; Krontiris-Litowitz et al., 1989; Illich and Walters, 1997). The buffered ASW contained (in mM) NaCl, 460; $CaCl_2$, 11; KCl, 10; $MgCl_2$, 30; $MgSO_4$, 25; and Tris buffer, 10 (pH 7.6). Neuronal clusters in the ganglia of interest were sketched in detail, and a life-sized diagram of the available body surface was made on graph paper by

using dividers for precise transfer of each measurement (Billy and Walters, 1989a).

Intracellular recordings from neuronal somata were made with glass microelectrodes filled with 3 M potassium acetate and 6 mM fast green dye (Sigma; electrode resistance 10–30 MΩ). Electrophysiological evidence for the presence of an axon in a peripheral nerve was obtained when electrical stimulation of a nerve (2–5-msec pulses through suction electrodes placed 1–3 cm from the appropriate ganglion) reliably evoked all-or-none depolarizing potentials when the ganglion was bathed in ASW containing 1% normal [Ca^{2+}] (0.1 mM, substituting $MgCl_2$ for 11 mM $CaCl_2$) to block synaptic transmission. Injection of the same solution into peripheral tissue blocked spontaneous contractions and local contractions evoked by local or distant tactile stimulation. Evidence for an axon was usually the elicitation of overshooting action potentials, but all-or-none blocked spikes were occasionally elicited (see Fig. 9D; see also Clatworthy and Walters, 1993a). Because spikes are not evoked by synaptic inputs to VC cells, most of the receptive field mapping of this cluster was performed in ASW, although a few receptive fields of VC cluster and S cluster neurons were tested with the periphery bathed in 1% [Ca^{2+}] solution in order to block peripheral synaptic transmission. Excitatory receptive fields were mapped by systematically tapping peripheral tissue with a stiff von Frey hair (bending pressure 60 g/mm^2; Stoelting, Chicago, IL) and transferring the perimeter measurements to graph paper with dividers. Mechanical threshold was defined as the lowest pressure from a standard, ascending series of von Frey hairs that activated the cell when the von Frey hair bent. Mechanosensory threshold and receptive field area were determined using the same methods and von Frey hairs utilized in previous studies (Billy and Walters, 1989a; Illich and Walters, 1997). In a few experiments, synaptic potentials from pleural and cerebral sensory neurons to cerebral motor neurons were tested using conventional methods in a bath containing elevated divalent cation concentrations (121 mM Mg^{2+} and 14 mM Ca^{2+}) to reduce polysynaptic contributions (Liao and Walters, 2002). In some cases, soma excitability was assessed by injecting a 2-second, 2-nA depolarizing pulse and counting the evoked spikes.

Nerve back-fills and dye injections

The biotin-avidin protocol followed the methods of Xin et al. (1999), with modifications based on Díaz-Ríos et al. (1999). The ganglion of interest was excised from a small animal (20–30 g) and pinned out near a small vaseline well that was formed on the Sylgard surface. The nerve of interest was cut near the periphery and drawn into the well. Care was taken to avoid contact between the end of the nerve and the vaseline. The tip of the nerve was cut one more time, and then the ASW inside the well was withdrawn and replaced with a saturated aqueous solution (1.6 mg/30 μl) of biocytin (Sigma). The walls of the well were then built up with successive layers of vaseline, forming an "igloo" that effectively isolated the biocytin pool from the ASW surrounding the ganglion. The preparation was covered and incubated overnight at 14°C. The well was then removed, and ganglia were washed three to five times in ASW, repinned, and fixed in paraformaldehyde as described above. The fixed ganglia were transferred to microcentrifuge tubes, washed five times (30 minutes each) with PTA solution, and incubated overnight (room temperature, with shaking) in rhodamine$_{600}$ avidin D (Vector, Burlingame, CA) diluted 1:3,000 in PTA (24–48 hours, room temperature).

Carboxyfluorescein injections were achieved by iontophoresis from microelectrode tips (10–30 MΩ) filled with 4% carboxyfluorescein dissolved in 0.5 M KCl, 50 mM Tris (pH 7.6). The electrode shafts were filled with 2 M KCl. Depolarizing current pulses (1–2 nA, 0.5 seconds, 1 Hz, 10–30 minutes) were used to eject the dye. This procedure did not alter the resting potential of the injected neuron. Preparations were left at room temperature for 5–10 minutes to allow material to diffuse from the injection site in the soma into small and distant processes. They were then repinned if necessary and photographed under a Nikon (Optiphot) fluorescent microscope.

Pressure injection was used for staining of individual neurons with horseradish peroxidase (HRP). A solution of 4% HRP in 1 mM KCl and 6 mM fast green was ejected from micropipettes pulled to a resistance of 3–5 MΩ (Nazif et al., 1991; Steffensen et al., 1995a). A Picospritzer II (General Valve) delivered two or three pulses at 20–25 psi to the back-filled electrode while the injected cell was monitored visually. Ganglia were left in culture medium at 4°C for 20–24 hours, fixed in a solution containing 2.5% glutaraldehyde and 30% sucrose in 0.1 M PBS (pH 7.3) for 1 hour, washed with PBS, and placed in a solution containing diaminobenzidine (Vector). Tissue was then reacted using 0.003% peroxide for 15 minutes, dehydrated in a graded series of EtOH concentrations (25%, 50%, 75%, and 95%), and cleared in methyl salicylate. Whole-mount preparations in Permount were viewed on an Olympus BH-2 microscope and photographed with Tmax 100 (Kodak) black-and-white film.

Statistical analysis

Statistical comparisons of receptive field area and mechanosensory threshold were made with one-way analysis of variance (ANOVA), followed by Newman-Keuls post-hoc tests. Other comparisons utilized unpaired *t*-tests. A probability of <0.05 was considered significant.

Results

Central distribution and number of sensorin-A-expressing somata

Abdominal ganglion. Sensorin-A-expressing somata were usually absent from the dorsal surface of the abdominal ganglion in small (10–30 g) and large (100–300 g) animals, although up to three cells were sometimes seen just beneath the surface in the region of the deep RF cluster (Fig. 2A1, arrow). On the ventral surface (Fig. 2A2,A3), groups of cells in locations corresponding generally to the previously defined LE, rLE, and RE clusters (Fig. 1) were labeled intensely by probes for sensorin-A mRNA. Although labeled cells were concentrated in the regions expected for these clusters, the boundaries of the clusters were not well defined. Because of the overlap of the edges of the RE and RF clusters and of the LE and rLE clusters, no attempt was made to sort the cells by cluster. Rather, we simply counted the total number of sensorin-A-expressing cells in the left and right hemiganglia (Tables 1, 2). Some of the cells in the rLE cluster were obscured by larger, overlying cells (cf. Fig. 2A2 and Fig. 2A3). Most of the RF cells were obscured, because they are

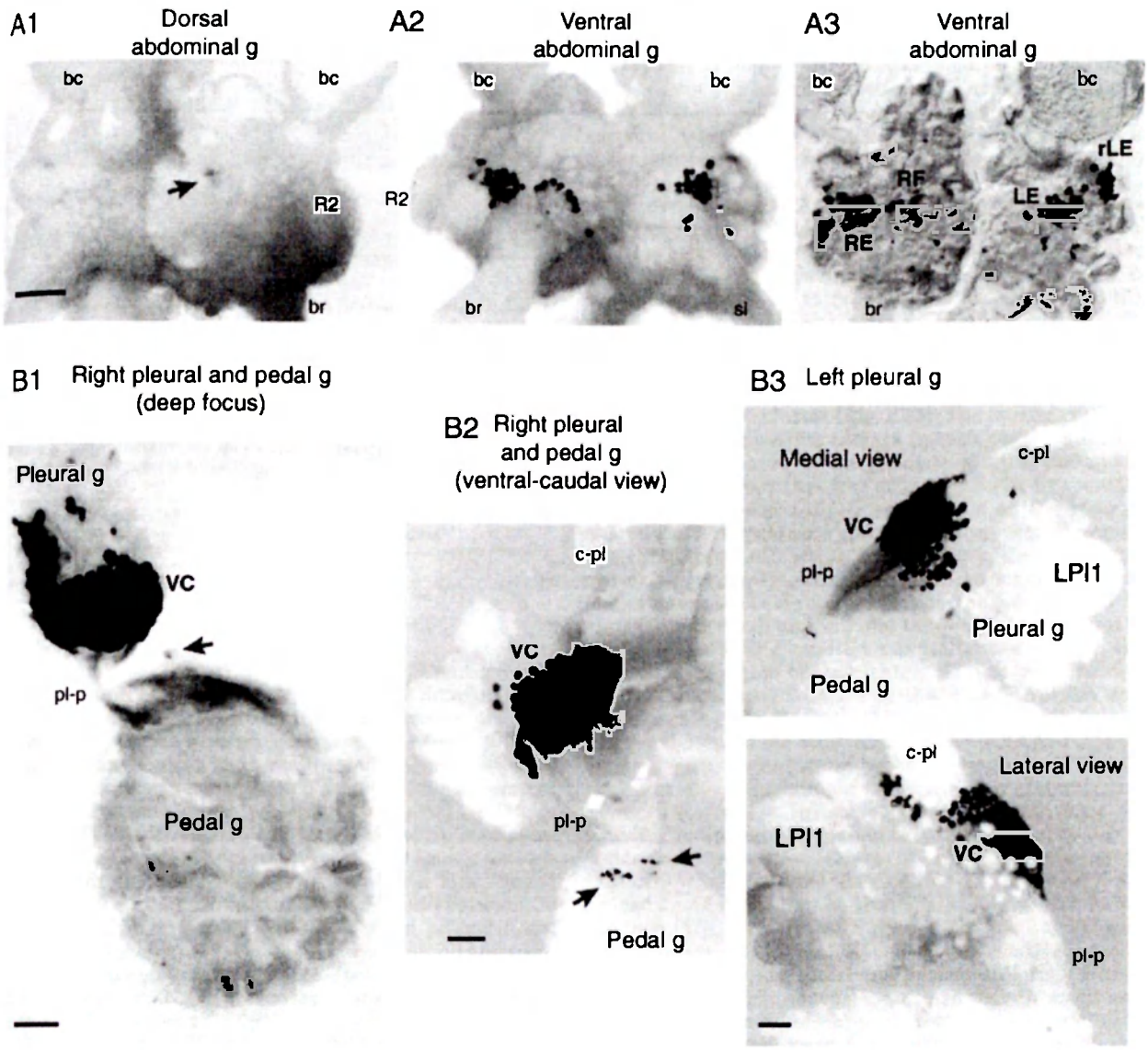

Fig. 2. Somata in abdominal, pleural, and pedal ganglia labeled by in situ hybridization with antisense probe to sensorin-A mRNA. **A1:** Dorsal surface of abdominal ganglion from a 100-g animal. The arrow indicates labeling of three neurons in the RF cluster. These are partially obscured by overlying unlabeled cells. The giant cell, R2, bag cells (bc), and the branchial nerve (br) are shown for reference. **A2:** Ventral surface of the same ganglion. The siphon nerve (si) is also shown for reference. Although many superficial cells are labeled with the antisense probe, several are obscured by unlabeled cells. **A3:** The same view of the same ganglion after clearing and embedding to reveal the rLE cluster. The RE, RF, LE, and rLE mechanosensory clusters are labeled, and several previously obscured cells, including most of the rLE cluster, can now be seen. **B1:** Relatively deep focus on a whole-mount preparation of the right pleural and pedal ganglia from a 30-g animal after clearing and embedding. This revealed labeled cells throughout the VC cluster and a smaller, more lightly labeled cell in the pedal ganglion (arrow). Note the intense labeling of neurites in the pleural–pedal connective (pl-p) and the neuropil throughout the pedal ganglion. **B2:** Right pleural and pedal ganglia in a 100-g animal. The cerebral–pleural connective (c-pl) is shown for reference. In addition to the VC cluster, 11 small cells are labeled in the pedal ganglion (arrows). **B3:** Two views of the left pleural ganglion, showing opposite edges of the VC cluster, which curves around the ganglion. Scale bar in A1 = 200 μm (applies to A1–A3); 200 μm in B1–B3.

located deep in the right hemiganglion, close to both the ventral and the dorsal sides of the commissure (Byrne, 1980). The deep cells were revealed by pushing the larger overlying somata aside or by adjusting the plane of focus in cleared preparations (not shown). Because of the possibilities that some of the deep cells were missed and that a few cells could have been lost during desheathing or processing of the ganglia, a conservative estimate of the number of sensorin-A-expressing cells in the ganglion is the greatest number of cells counted in any of the prepara-

TABLE 1. Highest Counts of Sensorin-A-Expressing Somata

Ganglion	Side	Number
Abdominal	L	85
	R	66
Pedal	L	11
	R	9
Pleural	L	231
	R	223
Cerebral	L	126
	R	122
Buccal	L	176
	R	152
Total		1,201

TABLE 2. Increase in Number of Sensorin-A-Expressing Somata in Larger Animals

	Small animals			Large animals[1]			
Ganglia	Mean	SEM	N[2]	Mean	SEM	N	P[3]
Abdominal	94	6	7	79	4	5	0.190
Pedal (L + R)	9	1	7	9	2	6	0.870
Pleural (L + R)	355	9	3	438	4	3	0.001*
Cerebral	203	8	6	234	6	3	0.045*
Buccal	246	7	6	294	14	4	0.008*

[1]Small animals weighed 10–30 g and large animals 100–300 g.
[2]N indicates number of animals examined for each type of ganglion.
[3]P indicates probability of a significant difference between soma numbers from large and small animals (unpaired *t*-test).
*$P < 0.05$.

tions examined (Table 1, N = 6–12 for different ganglia; see also Table 2). No qualitative differences between small and large animals were noted in the positions or arrangement of any of the sensorin-A-expressing cells in the abdominal ganglion (or in the other ganglia). The average number of sensorin-A-expressing somata in the abdominal ganglion was not significantly different in small and large animals (Table 2). Soma size, as measured by maximum diameter, showed no apparent differences among sensory clusters in the abdominal ganglion. Soma size ranged between 20 and 50 μm in small animals and between 30 and 60 μm in larger animals. In cleared preparations, sensorin-A labeling could be seen in the neuropil and roots of the siphon and branchial nerves (not shown), indicating that sensorin mRNA is present in axons as well as somata (see also Brunet et al., 1991).

Pedal ganglia. We failed to find sizable clusters of sensorin-A-expressing somata in pedal ganglia from large or small animals (Fig. 2B), which is consistent with the lack of previous reports of mechanosensory neurons in the pedal ganglia. Labeled fibers were found, however, throughout much of the pedal ganglion. These fibers appeared to come largely from cells in the pleural ganglion (see below). We observed, in 20 of 22 pedal ganglia examined, a small and highly variable number (2–11) of labeled somata (arrows in Fig. 2B1,B2; see Tables 1, 2). No significant difference in the number of sensorin-A-expressing neurons was seen between smaller and larger animals. Most of these cells were found near the root of the pleural–pedal (pl-p) connective (Fig. 2B2) and were about half the diameter (20–40 μm) of the nearby sensory neuron somata in the pleural VC cluster. We recorded intracellularly from three small cells in this region of the pedal ganglion, in a 150-g animal, that had the same visual appearance as the VC sensory neurons. The somata of these cells displayed electrophysiological properties characteristic of those of the VC neurons on the other side of the connective, i.e., lack of spontaneous action potentials or postsynaptic potentials and clear spike accommodation in response to long depolarizing current pulses. Although we have not yet looked for peripheral axons or receptive fields of these cells, the general similarity of the small sensorin-A-expressing neurons in each pedal ganglion to other sensorin-A-expressing neurons suggests that they may also be mechanosensory neurons.

Pleural ganglia. As predicted by earlier descriptions of the pleural VC clusters, we found that these bilateral clusters have the largest number of sensorin-A-expressing cells and that these cells are tightly packed into a strikingly uniform cluster in each pleural ganglion (Fig. 2B), which appeared quite similar in small and large animals. Nevertheless, every ganglion had a few cells separated from the main cluster. Because each VC cluster curves around the pleural ganglion, two images were needed to display the entire cluster (Fig. 2B3). The average number of sensorin-A-expressing somata in each pleural ganglion (Table 1) was similar to the estimate of about 200 mechanosensory neurons that was originally made by counting cells that had been defined as VC cells on the basis of shared visual appearance and electrophysiological properties (Walters et al., 1983). Interestingly, the number of sensorin-A-expressing somata increased significantly in larger animals (Table 2). Soma size ranged between 30 and 60 μm in small animals and between 40 and 80 μm in larger animals. The smallest somata tended to be in the anterolateral region of the cluster, close to the cerebral–pleural connective. Because of the distinctive size and dense packing of cells in the VC cluster, we were able to observe that all of the cells in the cluster exhibited intense labeling with the antisense probe for sensorin-A. We observed extensive labeling of fibers in the pl-p connective, as was reported by Brunet et al. (1991), and these extended into the pedal ganglion (Fig. 2B1,B2).

Cerebral ganglion. Most of the cells expressing sensorin-A mRNA were located in the previously described J and K clusters on the ventral side of each hemiganglion (Fig. 3A1). As with cells in the pleural VC sensory clusters, the J and K cells were relatively small (30–60 μm soma diameter) and packed uniformly within each cluster, which appeared quite similar in small and large animals. In addition, a number of very small cells (~20 μm diameter) were distributed on the dorsal and ventral surfaces, near the middle of each cerebral hemiganglion. On the dorsal surface (Fig. 3A2), these cells appeared to be part of the D clusters (Jahan-Parwar and Fredman, 1976). Caudal to these cells on the dorsal surface of each hemiganglion was a single stained cell (60–70 μm diameter) with a prominently stained initial axon segment. The cells within the J and K clusters consistently exhibited more intense labeling than the smaller cells located outside of these clusters. As found in the pleural ganglia, the number of sensorin-A-expressing somata in the cerebral ganglion increased significantly in larger animals (Table 2). Average soma diameter was also about 50% larger in larger animals. Labeling of sensorin-A mRNA was also found in the neuropil and roots of the connectives (Fig. 3A1) and roots of cerebral nerves (not shown).

Buccal ganglia. Large clusters of sensorin-A-expressing somata, corresponding to the S clusters of Fiore and Meunier (1975), were found to curve over the dorsal surface of each hemiganglion, extending from the

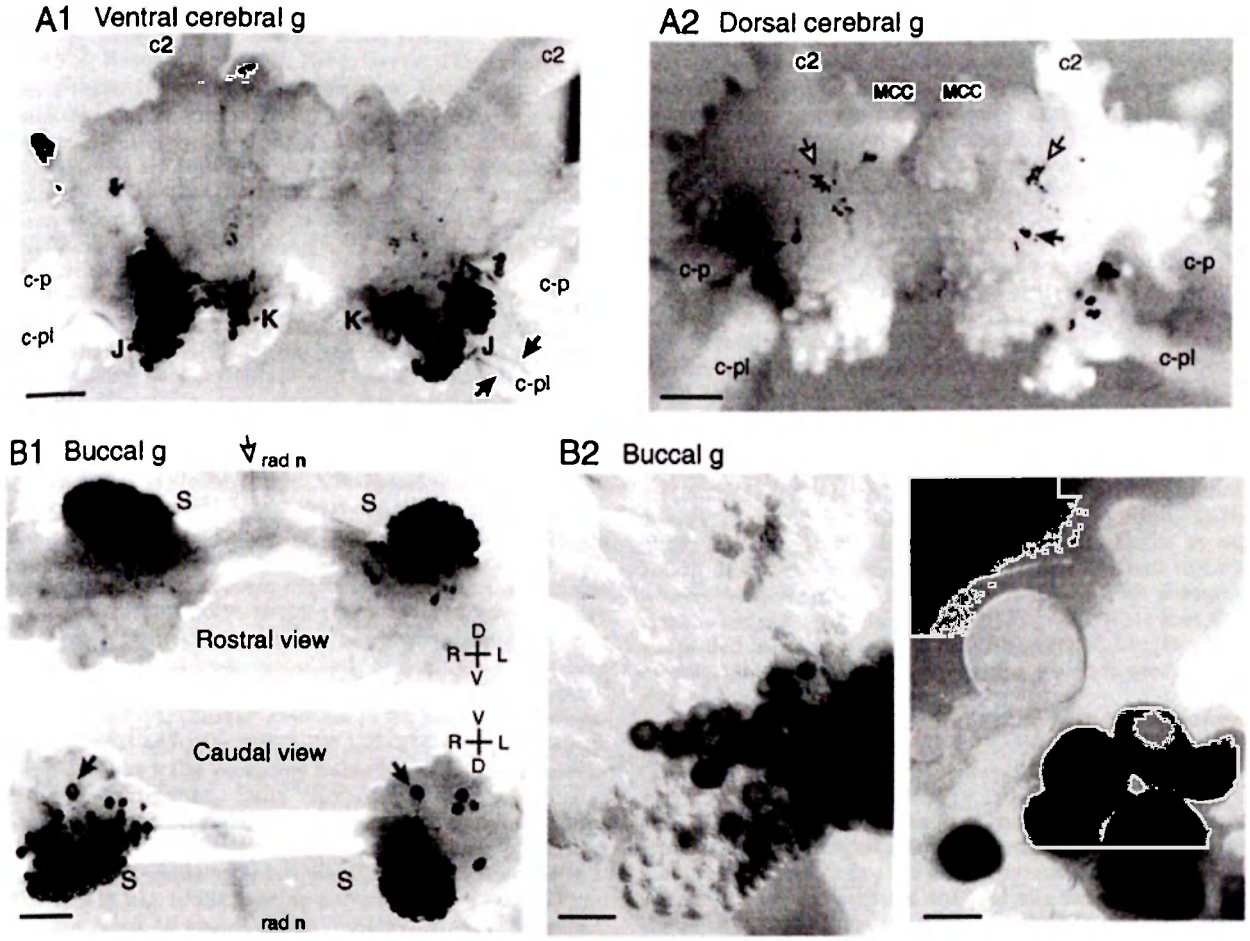

Fig. 3. Sensorin-A-expressing neurons in the cerebral and buccal ganglia. **A1:** Ventral view of cerebral ganglion in a 100-g animal, showing intense labeling of J and K mechanosensory clusters. Landmarks are the anterior tentacular nerve (c2), and cerebral–pedal (c-p) and c-pl connectives. Note the labeled fibers in the left c-pl connective (red arrows). **A2:** Dorsal view of cerebral ganglion. Additional landmarks are the giant metacerebral cells (MCC). The red arrows indicate a pair of large labeled neurons with prominent axons that are invariably found in these locations. Anterior to these are small cells labeled within the D clusters (yellow arrows). Labeled cells near the roots of the c-pl connectives are from the J clusters. **B1:** Rostral and caudal views of the buccal ganglia from a 25-g animal, showing labeling of the S clusters. Red arrows (bottom) indicate larger cells reliably labeled on the ventral-caudal surface of the ganglia. Notice the variation in labeling intensity and cell size. Yellow arrow (top) indicates labeled axons in the radula nerve. **B2:** Nomarski high-resolution images from buccal ganglion illustrating the variation in labeling intensity and cell size in a 30-g animal. Scale bars = 500 μm in A1,A2; 200 μm in B1; 50 μm in B2 (left); 25 μm in B2 (right).

caudal to the rostral side (Fig. 3B1). Compared with clusters in the other ganglia, the buccal clusters showed considerable heterogeneity in soma size and sensorin mRNA labeling intensity (Fig. 3B2). We failed to see in many animals a distinct division between subclusters that would correspond to the S_1 and S_2 dichotomy, so we simply use the term *S cluster* to describe the core group of small (20–30 μm diameter in small animals), intensely labeled somata. Ventral to each S cluster was a group of 15–20 larger (40–60 μm) sensorin-A-expressing neurons, additional small neurons with a sparser distribution, and a distinctive larger ventral cell (arrow in Fig. 3B1) that was separated from the others. As found in the pleural and cerebral ganglia, the number of sensorin-A-expressing somata in the buccal ganglia increased significantly in larger animals (Table 2). Average soma size was also ~50% larger in larger animals. In cleared preparations, labeling for sensorin-A could be seen in fibers in the neuropil, buccal commissure, and roots of the buccal nerves (see the buccal commissure and radula nerve in Fig. 3B1).

Periphery. No sensorin-A-expressing neuronal somata were found outside the central ganglia in adult animals. In juvenile animals (<2 g), two or three sensorin-A-expressing neurons have been observed in mantle tissue (Moroz and Bodnarova, unpublished observations), which might be a site of neurogenesis (McAllister et al., 1983; Hickmott and Carew, 1991).

Peripheral targets of the sensorin-A-expressing clusters

Detailed descriptions of the receptive field properties and peripheral axon distributions of sensorin-A-

expressing sensory clusters in the abdominal ganglion and cerebral ganglia have already been published (Byrne et al., 1974; Rosen et al., 1979, 1982; Byrne, 1980; Dubuc and Castellucci, 1991; Illich and Walters, 1997). For the abdominal LE, RE, and rLE clusters, we have confirmed the general locations and typical sizes of receptive fields that were previously reported on the siphon and mantle (data not shown). The receptive field locations, peripheral axon distributions, and newly described physiological properties found in some of the other sensorin-A-expressing clusters are described below.

Receptive fields of pleural VC clusters. When the present studies began, it was known that the mantle organs, head, and buccal mass are innervated by sensorin-A-expressing sensory clusters in the abdominal, cerebral, and buccal ganglia, respectively. The remaining sensorin-A-expressing clusters, the two pleural VC clusters, had been shown to have receptive fields on the tail and posterior parapodia (Walters et al., 1983), but only a small part of each VC cluster had been mapped. When combined, all the documented receptive fields of sensorin-A-expressing neurons left much of the foot, parapodia, midbody, and posterior neck uncovered. We predicted that the remaining parts of the body surface are covered by receptive fields of VC mechanosensory neurons whose receptive fields had not yet been examined.

To test this hypothesis, we investigated the receptive fields of 287 VC cluster neurons in 25 semiintact preparations from animals weighing 115–275 g (mean 185 g). Figure 4 shows the receptive fields found in six representative experiments. Cells throughout the VC cluster showed electrophysiological properties that appeared indistinguishable from those in the previously described subset of VC sensory neurons that innervates the tail (Walters et al., 1983): resting potentials between −40 and −55 mV, lack of spontaneous activity or synaptic input, bursts of action potentials lacking prepotentials during receptive field stimulation (Fig. 4, inset), action potential amplitudes between −85 and −105 mV (during good impalements), lack of excitatory postsynaptic potentials (EPSPs) during receptive field stimulation, and (sometimes) slow hyperpolarizing responses to stimulation outside the excitatory receptive field. Excitatory receptive fields were found over the entire surface of the body ipsilateral to each VC cluster (Fig. 4). As noted previously for receptive fields on the tail (Billy and Walters, 1989a), very few receptive fields in other regions extended across the midline. The highest incidence of crossover was on the ventral surface of the foot (Fig. 4B2), where 16 of 110 midline fields (15%) extended over to the contralateral side. In contrast, only 1 of 24 (4%) crossed over on the dorsal surface of the head, and 0 of 26 crossed over on the neck.

Receptive field sizes in this study ranged from 0.1 to 12 cm^2. Although receptive field size varied considerably within each part of the body, receptive fields on the tentacles, head, and anterior foot (propodium) were significantly smaller than those on more posterior parts of the body (Fig. 5A; one-way ANOVA, $P < 0.0001$, with $P < 0.05$ for each post-hoc comparison using the Newman-Keuls test). No significant differences among regions were found in mechanosensory thresholds (Fig. 5B); the median threshold in all regions was 35 g/mm^2, except for the tentacles, where the median threshold was 45 g/mm^2.

Somatotopic organization of the pleural VC clusters. It was originally noted by Walters et al. (1983) that the VC cluster is organized at least partially in a somatotopic fashion, because all the somata of neurons with receptive fields on the tail are grouped on the medial side of the cluster. In the receptive field study just described (N = 287 VC cells in 25 animals), we confirmed this localization of the somata of tail sensory neurons to the medial side of the cluster and found that cells with receptive fields on the head were restricted to the opposite (anterolateral) side of the cluster. Cells with receptive fields in the middle of the body were generally found in the central part of the VC cluster. Thus, each VC cluster (Fig. 6B) forms a crude somatotopic map of the ipsilateral surface of the body (Fig. 6A) or, in effect, a "sensory aplunculus" (see Discussion).

Additional information about the somatotopic organization of the VC sensory neurons came from investigating the distribution of these cells' axons in peripheral nerves. Previous studies have shown the approximate sensory and motor fields (which are largely coextensive) of peripheral nerves in *Aplysia* (Jahan-Parwar and Fredman, 1976, 1978; Kandel, 1979; Walters et al., 1983; Dulin et al., 1995), and these provide a guide to the general regions where receptive fields of sensory neurons with axons in specific nerves would be expected (Fig. 7A). Note that this simplified map does not show the marked overlap that exists at the boundaries of the fields, which is most extensive in the head and neck.

We used electrical stimulation of peripheral nerves, combined with intracellular recording from VC somata (Fig. 7, inset), to relate peripheral axon distribution to soma location. Figure 7B shows the position of the VC cluster when the left pleural ganglion is pinned out in our standard experimental conformation. In this position, the medial side (containing tail sensory neurons) is completely visible. However, because the VC cluster winds around the lateral side of the ganglion (Fig. 2B3), the anterolateral edge of the cluster is hidden when the medial edge is visible. The inset shows the complete cluster as it would appear if it were unwound from the ganglion. Results from a single experiment in which 102 sensory neurons were sampled while brief stimuli were delivered to ipsilateral pedal nerves p9, p8, p1, and the cerebral–pleural connective (c-pl) revealed that somata with apparent axons in nerve p9 were largely on the medial side of the VC cluster, that somata with axons in nerve p1 or the c-pl connective were largely in the anterolateral region, and that somata with axons in nerve p8 were primarily in the central region of the cluster (Fig. 7C1). Figure 7C2 summarizes 22 experiments, showing the approximate locations of all the somata responding with action potentials to stimulation of pedal nerves p1, p4, p5, p6, p7, p8, p9 (excluding the anterior branch, p9a, which innervates the posterior parapodium), p9a, or the c-pl connective. Somata in the VC cluster are organized so that cells with axons projecting toward the anterior of the animal are primarily in the anterolateral region of the cluster, cells with axons projecting to the middle of the animal are primarily in the central region of the cluster, and cells with axons projecting to the posterior of the animal are primarily in the medial region of the cluster. Part of this study has been described in abstract form (Billy and Walters, 1987).

The maximum numbers of VC cells found in a single preparation having apparent axons in specific nerves are shown in Table 3. As indicated by action potentials evoked

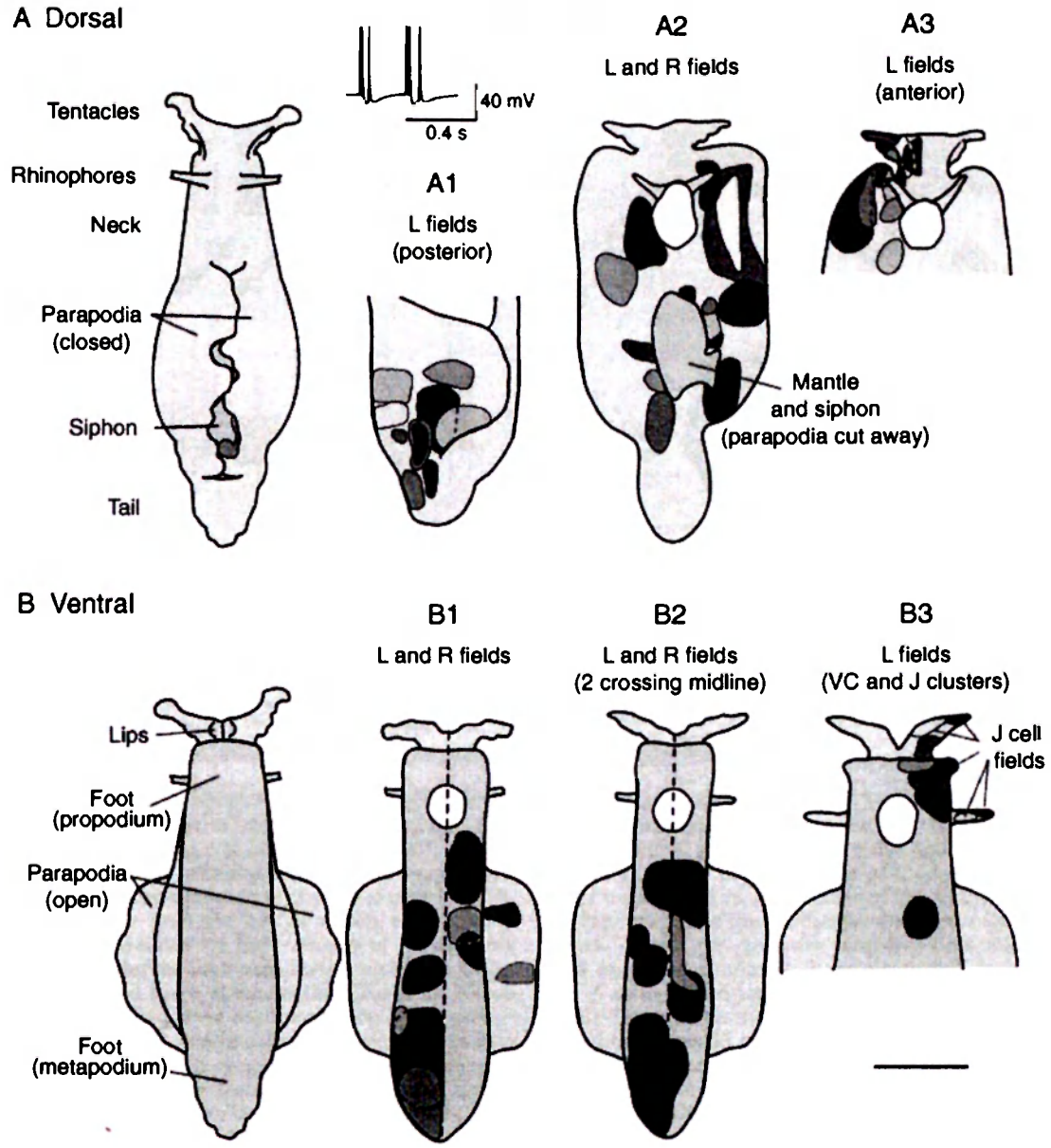

Fig. 4. Examples of receptive fields of mechanosensory neurons in the pleural VC and cerebral J clusters. For reference, schematic drawings of dorsal and ventral views of intact *Aplysia* are presented in the left-most panels. The **inset** shows an example of action potential discharge evoked by a brief (~0.5-second) poke of the left parapodium by the stiff (60 g/mm^2) von Frey hair used to map the receptive fields. **A1:** Dorsal fields of cells in left VC cluster. The anterior half of the animal was discarded and Lp7, Lp8, and Lp9 nerves were intact. **A2:** Dorsal fields of cells in right and left VC clusters. Except for the excised parapodia and incisions above and below the circumesophageal ring ganglia, all of the body was intact. No fields were found on the mantle or siphon. Tonic contractions of the base of each cut parapodium obscured the mantle floor, which was not tested in this animal. **A3:** Dorsal fields of cells in the left VC cluster on the head and neck. **B1:** Ventral fields of cells in the left and right VC clusters that fail to cross the midline on the foot. **B2:** Ventral fields (red) that cross the midline of the foot. No VC fields in any animal were completely contralateral. **B3:** Ventral fields of VC and J cells (see red lines) from left pleural and cerebral ganglia. Scale bar = 4 cm.

by stimulating different nerves, dual axons were uncommon, being found in only 3% (17 of 550) of cells tested. The highest incidence of dual axons occurred in the posterior and anterior branches of p9 (p9p and p9a). In the two experiments in which the two major branches of this nerve were stimulated together, 5 of 63 cells (8%) had axons in both branches. The next highest incidence was in p6 and p7, where 6 of 114 cells tested in seven experiments had dual axons (5%). Dual axons were also implicated in p8 and p9 (twice), p7 and p8 (twice), p6 and p8 (once), and,

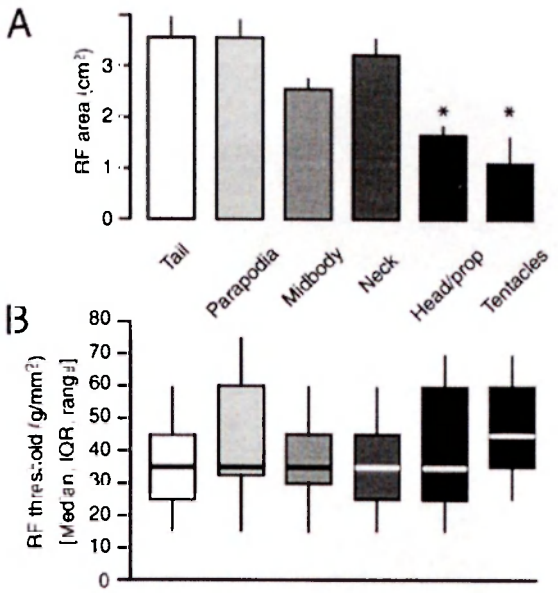

Fig. 5. Areas and thresholds of VC cell receptive fields in different regions of the body. **A:** Significantly smaller receptive fields in the head/propodium region and anterior tentacles than in more posterior regions (*$P < 0.05$). **B:** Lack of significant differences in mechanosensory threshold in different regions. In each case the central line indicates the median, the box the interquartile range (i.e., between the 25th and 75th percentiles), and the bars the total range.

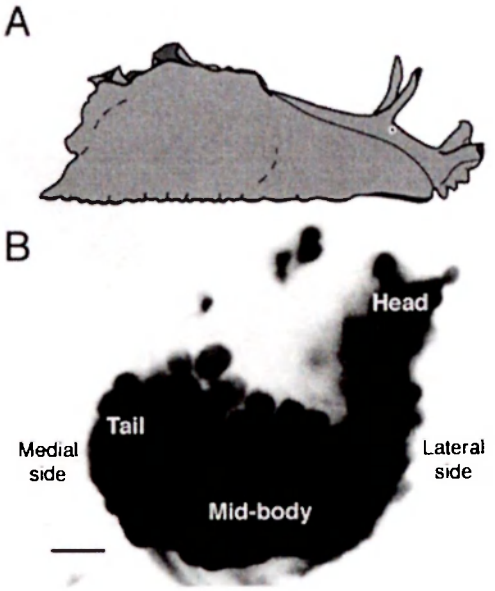

Fig. 6. Somatotopic representation of mechanosensory receptive fields in the VC cluster. **A:** Drawing of the right side of an *Aplysia* facing the right. **B:** A micrograph of the right VC cluster as revealed by in situ hybridization of a probe for sensorin-A mRNA. The regions within the cluster having somata with receptive fields on the head, midbody, and tail are indicated. The anterior side of the cluster is at the top of the image, and the medial and lateral sides are indicated (see Figs. 2, 7). Scale bar = 100 μm.

surprisingly, p1 and p9 (once). We found in separate experiments (see below) that VC cells with axons in nerve p1 often have an axon in the c-pl connective as well.

Back-fill experiments provided complementary evidence for the somatotopic organization of the VC cluster (Fig. 8). These experiments and the nerve shock experiments yielded similar estimates for the numbers of VC neurons with axons in the nerves that were tested with both methods: p9, p8, p1, and the c-pl connective (Table 3). Nerve back-fills also provided clear documentation of the grouping of somata having axons in different major nerves into different regions of the VC cluster. Figure 8A shows cells with axons in the posterior pedal nerve (p9) concentrated in the medial portion of the VC cluster, whereas cells with axons in the anterior pedal nerve (p1) or in the c-pl connective or anterior tentacular nerve (c2) are concentrated in the anterolateral part of the cluster (Fig. 8C–E), and cells with axons in the middle pedal nerve (p8) are concentrated in the central region of the cluster (Fig. 8B). Similar findings were described in a preliminary report on nickel-lysine and cobalt back-fills of nerves p7, p8, and p9 and the c-pl connective (Zhang et al., 1993).

Receptive fields of the cerebral sensory clusters. We have extended previous studies by showing that receptive fields of some J cells are located on the ipsilateral rhinophore and propodium, in addition to the previously reported fields on the anterior tentacle, lip region, and dorsal surface of the head (Rosen et al., 1979, 1982). In a sample of 11 J cells (in three preparations), five receptive fields were on the tentacle, two were on the lips near the midline, two were on the propodium, and two were on the rhinophore (Fig. 4B3). All receptive fields were ipsilateral to the sampled cells. Because the preparations were pinned ventral side up, we were not able to sample receptive fields on the dorsal surface of the head. No receptive fields were found in the middle of the body, even though the innervation of the parapodia and entire foot remained intact. We did not quantify receptive field sizes, but the sizes appeared similar to those previously described for J and K cells on the tentacles and lips (Rosen et al., 1979, 1982). The median mechanosensory threshold of the sampled J cells was 35 g/mm^2, with a range of 15–45 g/mm^2. This median threshold was the same as that found previously with the same calibrated von Frey hairs for tail (Billy and Walters, 1989a) and siphon (Illich and Walters, 1997) sensory neurons.

Intersecting functions of cerebral J/K cells and pleural VC cells. Back-filling the anterior tentacular nerve (c2) stains somata in both the J/K and the VC clusters (Fig. 8E), and the excitatory receptive fields of cells in the J/K clusters and cells in the anterolateral region of the ipsilateral VC cluster show extensive overlap on the tentacles and anterior foot (Fig. 4). Moreover, receptive fields of J/K cells and VC cells in this general region display the same range of mechanosensory thresholds. These observations suggest that many of the cerebral and pleural sensory neurons share one or more common functions. A likely function is to sense threatening or noxious stimuli and trigger appropriate defensive responses, such as the head-withdrawal reflex (Walters and Erickson, 1986; Teyke et al., 1989). This function is supported by our observation that VC cells with receptive fields on the anterior part of the body, such as the anterior foot (Fig.

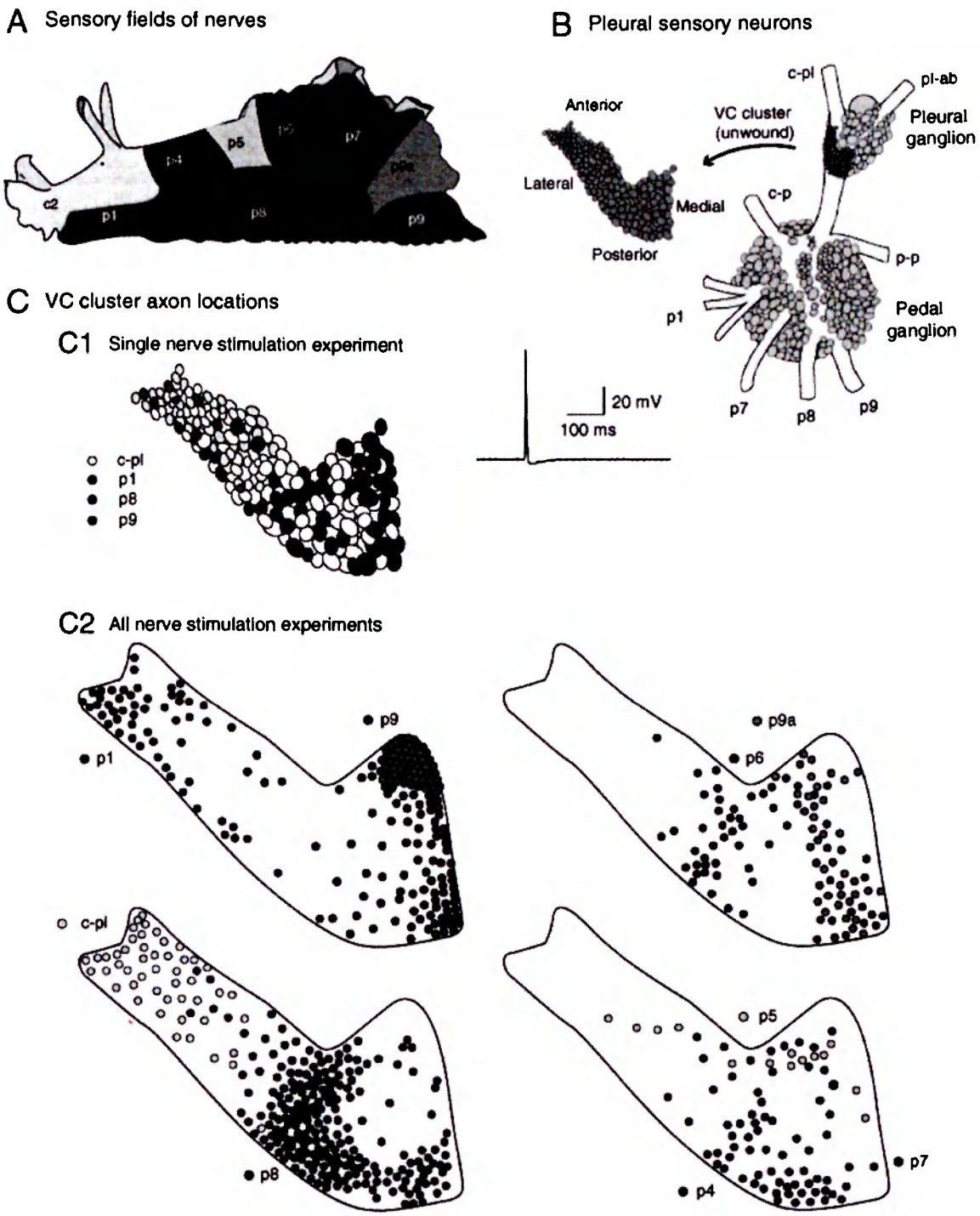

Fig. 7. Relationship between positions of the somata in the VC cluster and axonal projections into peripheral nerves. **A:** Simplified map of the major sensory fields of left pedal nerves and a left cerebral nerve, c2 (anterior tentacular nerve). The extensive overlap of different fields is not indicated on this map. **B:** Schematic drawing of VC cluster in left pleural ganglion. The entire cluster is represented two-dimensionally by unwinding it (left) from the cylindrical tract extending from the pl-p to the c-pl connectives. The right VC cluster is very similar (not shown). **C:** The inset shows a spike evoked by a 2-msec shock delivered to nerve p9. **C1:** Positions and relative sizes recorded in a single experiment of cells in left VC cluster that responded with spikes to stimulation of axons in the indicated nerves. **C2:** Summary of results from all nerve stimulation experiments (N = 22). Dots represent locations (not size of soma) of all cells responding to stimulation of the indicated nerves in all the experiments.

TABLE 3. Axon Distribution of Pleural VC Cluster

Nerve	Target	Maximum number of cells with axons[1]	
		Shock N (preps)	Back-fill N (preps)
p9	Tail	28 (14)	30 (4)
p9a	Posterior PP[2]	15 (3)	
p8	Midfoot	30 (13)	30 (2)
p7	Mid-PP	20 (11)	
p6	Anterior PP	15 (12)	
p5	Posterior neck	7 (3)	
p4	Anterior neck	9 (2)	
p1	Anterior foot	25 (10)	35 (4)
c-pl	Head	22 (2)	20 (2)
c2	Head		12 (1)

[1]Presence of an axon is defined by the occurrence of an action potential in the soma evoked by electric shock delivered to the indicated nerve, or by filling of the soma after delivery of dye to the indicated nerve. The maximum number of cells corresponds to the greatest number with axons observed in any one of the indicated number of preparations (preps).
[2]Parapodia.

9A) and tentacle (Fig. 9B), evoke EPSPs in the Bn motor neurons, which mediate the head-withdrawal reflex (Teyke et al., 1989). Figure 9C shows an example of an EPSP in a cerebral Bn motor neuron evoked by a single action potential in a pleural VC cell having a receptive field on the propodium. The EPSP appeared to be monosynaptic, because it was evoked in a solution containing 2.2 × normal $[Mg^{2+}]$ and 1.25 × normal $[Ca^{2+}]$. We found that 9 of 10 sensory neurons (in two animals) sampled in the region of the VC cluster innervating the anterior part of the body had connections to Bn motor neurons, with the mean amplitude being 5 mV and the range 2–9 mV. In one case, three Bn neurons were sampled, and all received EPSPs from the same VC cell. This small sample suggests that most VC cells with receptive fields on the head connect to most Bn neurons, as is true for the J/K cells (Teyke et al., 1989).

Back-filling the c-pl connective in smaller animals (20–30 g) revealed about 20 VC cells with axons projecting to the cerebral ganglion (Fig. 8D). About 12 cells projected an axon into c2, the anterior tentacular nerve, as revealed by separate back-fills of this nerve (Fig. 8E). Dye fills of individual VC cells demonstrated that at least some of the VC cells project axons into both the cerebral ganglion and the pedal ganglion (Fig. 10). In the three filled cells having dual axons, the axon projecting into the c-pl connective was substantially thinner than the axon projecting into the pleural–pedal connective. This morphology was consistent with electrophysiological responses of the VC cells that responded to electrical stimulation of both nerve p1 and the c-pl connective. In all five cases, single, brief p1 stimuli invariably evoked normal overshooting spikes, whereas, in three of five cases, single, brief stimuli to the c-pl connective evoked small, all-or-none depolarizing potentials that had the properties of blocked spikes. The small spikes summed at high frequency to initiate a full action potential in the VC cell soma (Fig. 9D). In this same study, two VC cells responded to p1 stimulation but not to c-pl connective stimulation, and one VC cell responded to tentacle stimulation but not to p1 stimulation. Extending earlier reports (Rosen et al., 1979; Clatworthy and Walters, 1994), 6 of 10 sampled J/K cells responded with all-or-none action potentials to electrical stimulation of the c-pl connective, and three of these also responded to p1 stimulation, indicating that some of the J/K cells innervate the anterior foot via axons that project via this pedal nerve.

Receptive fields of the buccal S clusters. Of all the sensorin-A-expressing clusters in *Aplysia*, the least studied have been the S clusters in the buccal ganglia. To our knowledge, there has only been a single report about the receptive fields of buccal S cells, in a review article that stated only that these cells can respond to mechanical stimulation of "specific muscular or epithelial regions in the buccal mass" even when synaptic transmission in the tissue is reduced by quadrupling extracellular $[Mg^{2+}]$ (Fiore and Geppeti, 1981). Although a comprehensive investigation of the S cells is beyond the scope of this paper, we wished to extend this earlier report by identifying general regions of the body that have S cell receptive fields and by describing basic electrophysiological properties of the S cells.

Dye fills of S cell somata (not shown) and back-fills of nerves and connectives indicated that many of these cells project axons into buccal nerves, but only a few project into the esophageal nerve (approximately six cells) and none into the cerebral–buccal connective. Back-fills of the ventral buccal nerve (b1; Fig. 11A) revealed 14–16 S cell somata in the ipsilateral cluster and two in the contralateral cluster. Back-fills of the lateral buccal nerve (b2; Fig. 11B) revealed 45–55 S cell somata in the ipsilateral cluster and six to eight in the contralateral cluster. In contrast, the dorsal buccal nerve (b3; Fig. 11C) revealed a preponderance of S cell axons from contralateral somata: there were 5 to 10 filled cells in the rostral half of the contralateral S cluster vs. two cells in the rostral half of the ipsilateral cluster and 25–30 cells in the caudal half of the contralateral cluster vs. five cells in the caudal half of the ipsilateral cluster. Back-fills of the radula nerve revealed the largest number of S cell axons, filling approximately 120 S cell somata, evenly divided between the left and the right hemiganglia, but with a larger number of somata on the rostral than caudal side of the cluster. In our clearest back-fill of the radula nerve (Fig. 11D), there were 36 filled cells in the rostral half of the left S cluster, 38 cells in the rostral half of the right cluster, 24 cells in the caudal half of the left cluster, and 20 cells in the caudal half of the right cluster. These observations agree generally with previous results obtained with cobalt back-fills (Scott et al., 1991) and with the original claim that the S cells "send axons to the periphery through all the buccal nerves" (Fiore and Geppeti, 1981). This suggests that the S cells have receptive fields on or in most of the buccal mass and perhaps in the perioral area and part of the esophagus.

All S cells sampled with intracellular electrodes (N = 21 cells in three animals) were silent in the absence of peripheral stimulation and showed no evidence of spontaneous synaptic input or of evoked EPSPs during stimulation of peripheral receptive fields (Fig. 12A,B). Basic electrophysiological properties were assessed in the nine cells showing the best impalements, as judged by the most negative resting potentials and largest action potential amplitudes. Mean resting potential was −51.1 ± 1.8 mV. Mean action potential amplitude was 98.6 ± 1.6 mV. Both of these values are similar to those of other sensorin-A-expressing sensory neurons. However, three properties were different. Compared with VC, J/K, or LE cells (see, e.g., Walters et al., 1991; Clatworthy et al., 1994; Clatworthy and Walters, 1994; Illich and Walters, 1997), mean spike afterhyperpolarization (15.9 ± 0.7 mV) was about three times larger, mean spike duration (6.4 ± 0.4 msec at

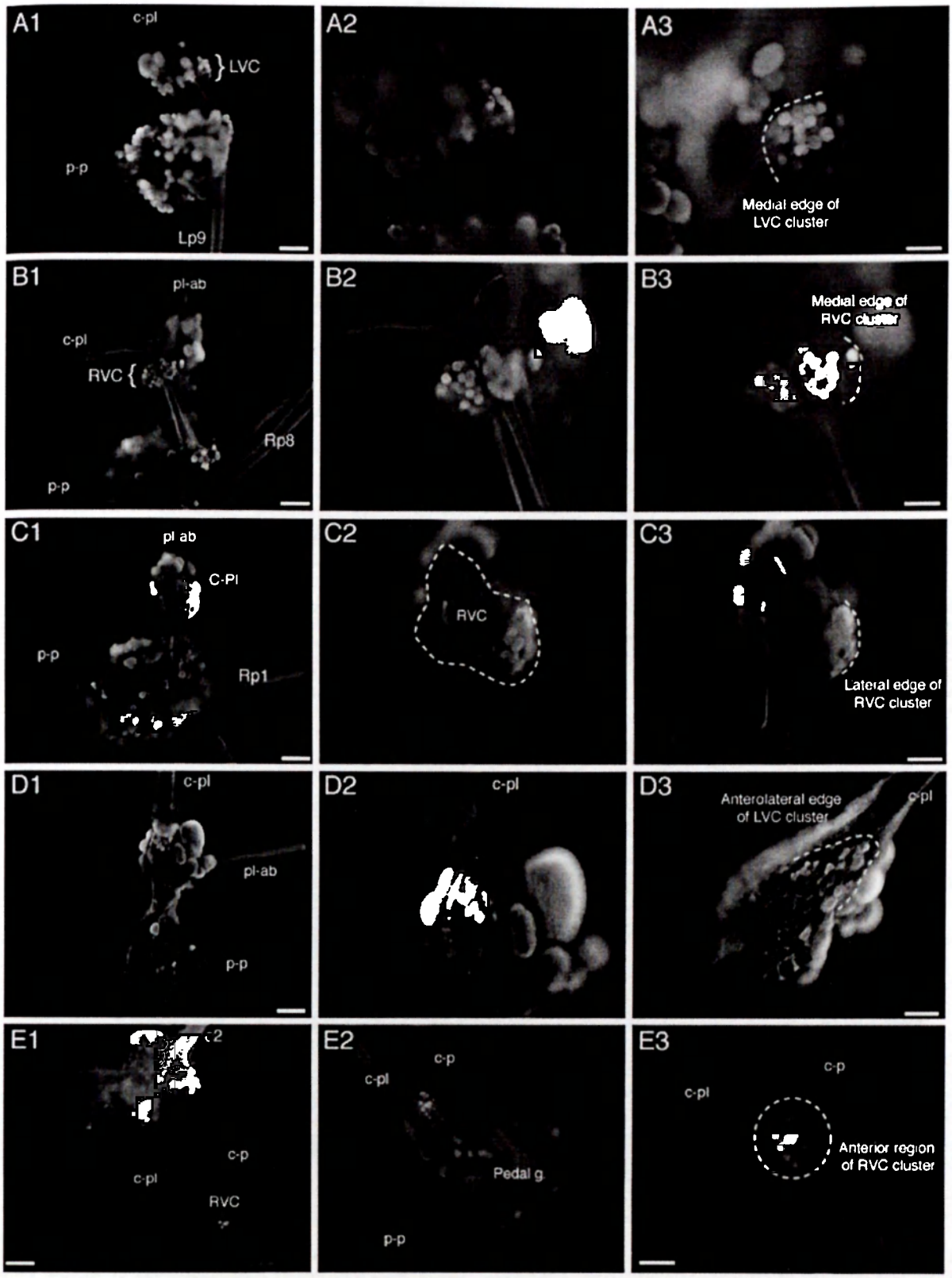

Fig. 8. Somata in pleural VC clusters stained by nerve back-fills (biotin-avidin protocol). Columns on the right show higher magnifications and partially rotated views of each preparation. **A1–A3:** Cells stained by p9 back-fill are concentrated in the medial region of the VC cluster. **B1–B3:** Cells stained by p8 back-fill are found throughout the middle of the VC cluster. **C1–C3:** Cells stained by p1 back-fill are concentrated in the anterolateral region of the VC cluster. **D1–D3:** Cells stained by c-pl connective back-fill also are concentrated in the anterolateral region of the VC cluster. **E1–E3:** Cells stained by c2 back-fill also are concentrated in the anterolateral region of the VC cluster. Note that cerebral ganglion cells in the J/K and B cluster areas are also stained. Scale bars = 200 μm in A1–E1; 100 μm in A3–E3 (applies to A2–E2, A3–E3).

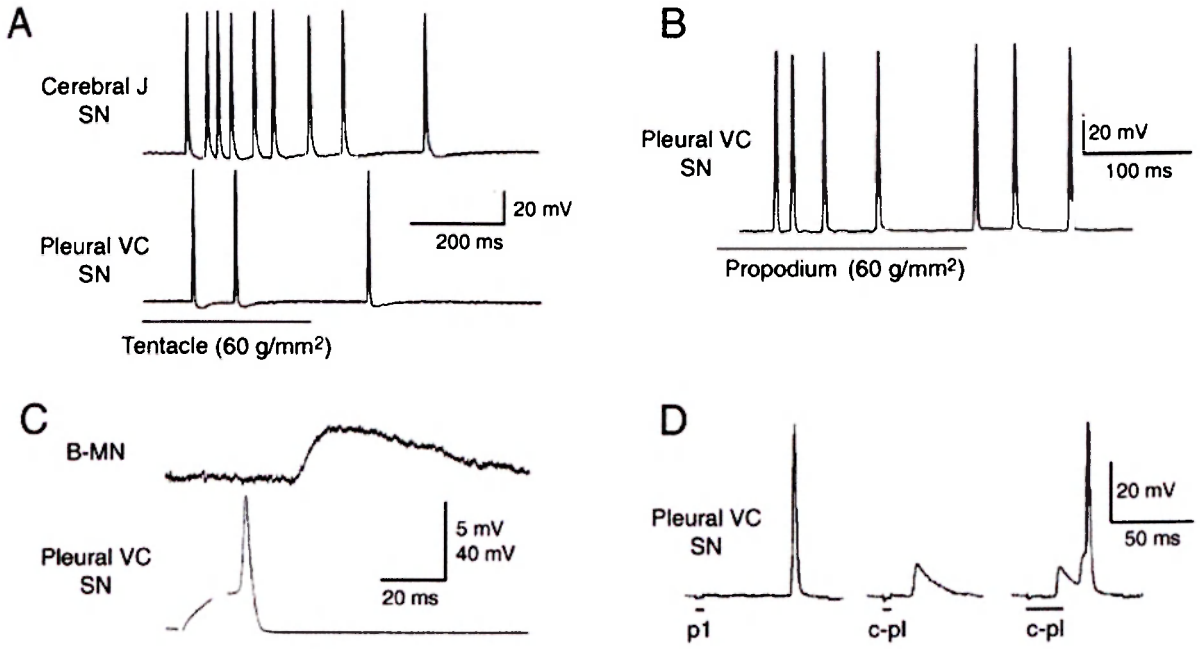

Fig. 9. Evidence for shared functions of cerebral J cells and anterolateral pleural VC cells. **A:** Simultaneous activation of a J sensory neuron (SN) and VC sensory neuron by brief von Frey hair stimulation of the ipsilateral tentacle. **B:** Activation of an anterolateral VC cell by von Frey stimulation of the ipsilateral anterior foot (propodium). **C:** Probable monosynaptic EPSP produced in ipsilateral B motor neuron (MN) by intracellular activation of anterolateral VC cell. Elevation of divalent cation concentrations minimized possible activation of interneurons. **D:** Evidence for dual axons with different conduction properties in anterolateral VC cell. Brief shock of anterior pedal nerve (p1) activates an overshooting spike. Brief shock to c-pl connective evokes an 8-mV, all-or-none depolarization. Longer shock to the connective evokes two small depolarizations, which sum to activate an overshooting spike in the soma (see text). Recordings were made in saline containing elevated divalent cation concentrations.

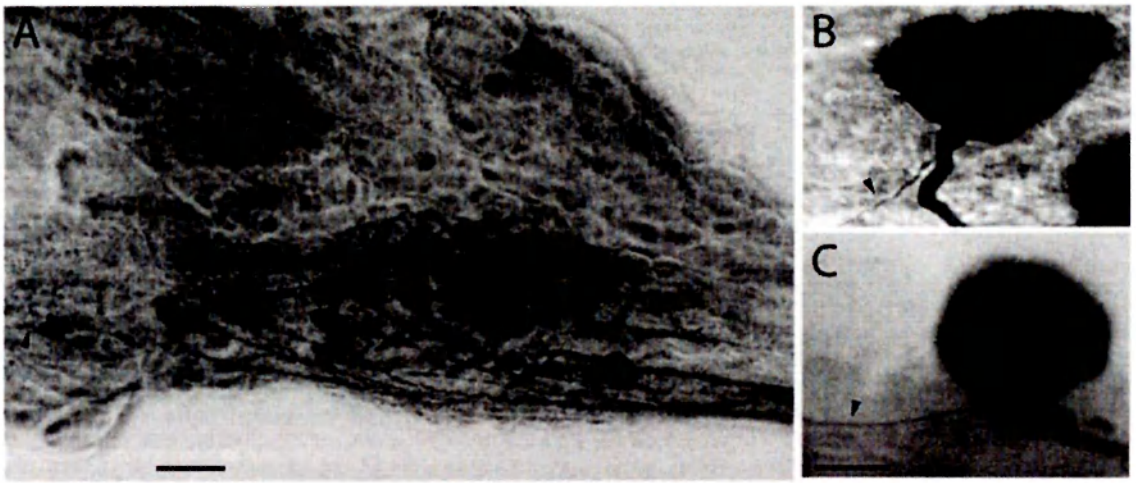

Fig. 10. Morphological evidence for dual axons in anterolateral VC sensory neurons. **A:** Low-magnification view of cells injected with horseradish peroxidase (HRP) in the middle and anterolateral regions of the left VC cluster. Most axons project to the right, into the pl-p connective. Arrowheads indicate two axons projecting to the left, toward the c-pl connective. **B:** Close-up view showing a thin process (arrowhead) projecting toward the c-pl connective, whereas the major axon projects toward the pl-p connective. Direct inspection through the microscope (adjusting the focal plane) confirmed that the thin process came from the large axon and traveled into the c-pl connective. **C:** Example from another preparation showing a thin process projecting toward the c-pl connective and a thick process (out of the focal plane) projecting toward the pl-p connective. Scale bar = 100 μm in A; 25 μm in C (applies to B,C).

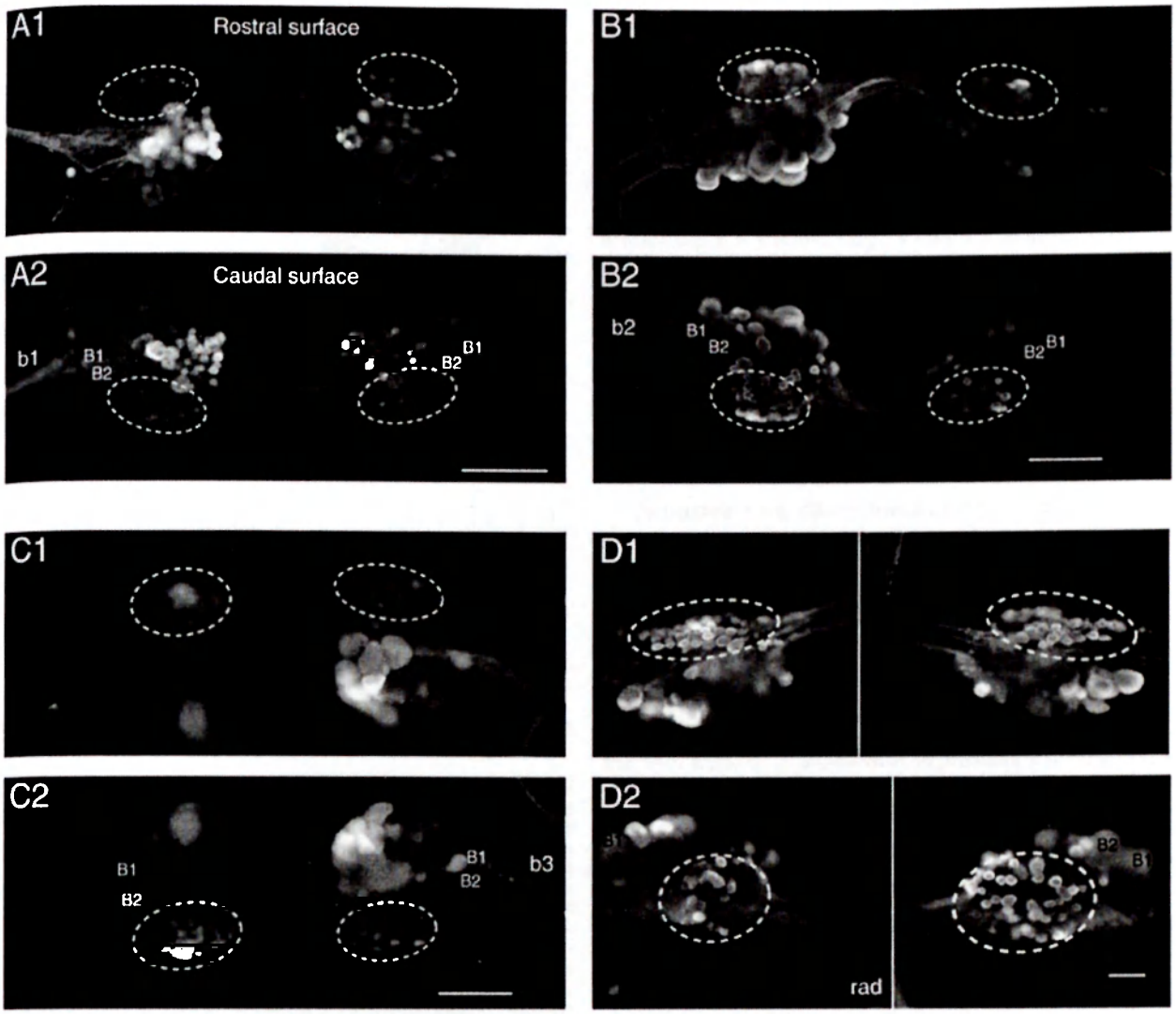

Fig. 11. Somata in buccal S clusters stained by nerve back-fills (biotin-avidin protocol). In each part, the right and left S clusters are encircled. Identified cells B1 and B2 are shown as landmarks on each caudal surface. The nerve back-filled (b1, b2, b3, or the radula nerve) is labeled in each pair of images. **A1,A2:** Cells on rostral and caudal surfaces stained by ventral buccal nerve (b1) back-fill. **B1,B2:** Cells stained by lateral buccal nerve (b2) back-fill. **C1,C2:** Cells stained by dorsal buccal nerve (b3) back-fill. **D1,D2:** Cells stained by radula nerve back-fill. Scale bars = 200 μm.

the base of the spike) was 50–100% longer, and the cells showed remarkably little spike accommodation during prolonged depolarizations (Fig. 12A,C). Our standard 2-second, 2-nA test pulse evoked 38.0 ± 3.9 spikes, and, in every case, spikes were generated until the end of the 2-second pulse. No afterdischarge was observed following the intracellular test pulse.

Receptive fields were sampled using three semiintact preparations, each of which maintained most buccal, cerebral, and anterior pedal nerve connections to the buccal mass, esophagus, oral veil/tentacle region, and anterior foot. In the first preparation, the buccal mass was left intact (precluding stimulation of internal structures, such as the radula and odontophore), and the radula nerve was cut. Six of nine S cells recorded were found to have receptive fields, all ipsilateral: five on the muscular outer surface of the buccal mass and one on the perioral zone and lip, near the propodium. The mechanosensory thresholds of the cells innervating the buccal mass ranged between 30 and 65 g/mm^2. The threshold of the cell innervating the perioral zone/lip (Fig. 12A–C) was 20 g/mm^2. No responses were evoked by concentrated NaCl solutions or NaCl crystals dropped on the skin. In the second preparation, a midline incision was made in the caudal/dorsal surface of the buccal mass to expose its internal structures, and the radula nerve remained intact. Three of five recorded cells had receptive fields: two on the external surface of the radula (with thresholds of 45 and 60 g/mm^2), and one on the perioral zone/lip (threshold 20 g/mm^2). All S cells displayed responses that were graded with the intensity of

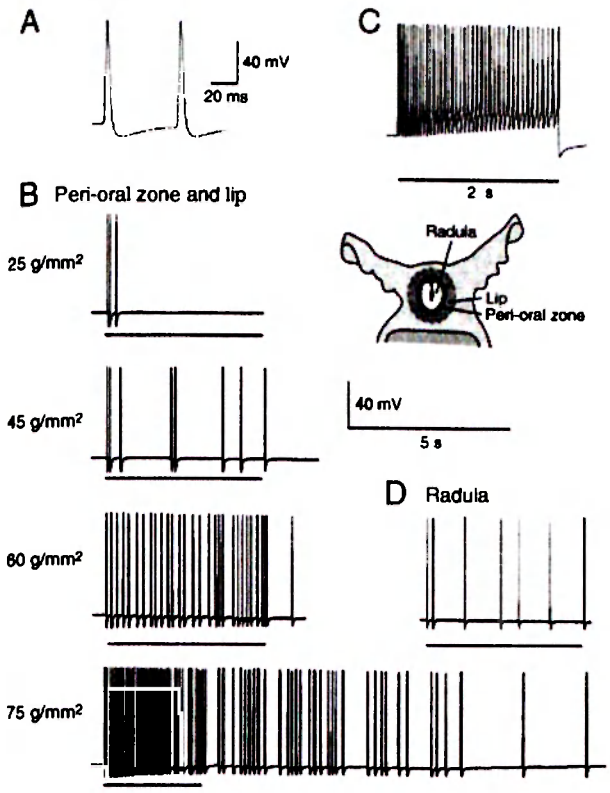

Fig. 12. Electrophysiological properties of buccal S cells. Inset: Diagram of the mouth region, with the radula exposed during feeding behavior. A: Examples of action potentials in the soma evoked by peripheral tap to perioral zone. Note the relatively long spike duration (7 msec at the base of the spike) and large afterhyperpolarization (14 mV). B: Graded responses of the same cell to increasingly stiff von Frey hairs. Note the near-absence of response accommodation. At 75 g/mm², prolonged afterdischarge follows the termination of the stimulus. C: Limited spike accommodation in the same cell during intracellular injection of a prolonged depolarizing pulse (2 nA) into the soma. D: Relatively weak response of another S cell to a stiff von Frey hair (60 g/mm²) applied to the surface of the radula (compare with the corresponding response in B).

the mechanical stimulus, and strong mechanical stimuli often evoked an afterdischarge that could persist for several seconds after stimulus offset (Fig. 12B). A given pressure evoked more spikes in the cells innervating the perioral zone/lip than in cells innervating the radula (Fig. 12B,D). Except at the lowest stimulus pressures, mechanosensory responses (like the responses to soma stimulation) showed very little accommodation (Fig. 12B). In the third preparation, a midline incision was made in the ventral surface of the buccal mass. Two receptive fields were found on the lumenal surface of the wall of the buccal cavity adjacent to the radula (thresholds 35 g/mm²). One was found in the perioral zone. This cell initially had a threshold between 25 and 30 g/mm², but, after repeated testing, the threshold fell to 15 g/mm², and the cell then fired sporadically for several minutes in response to brief taps at this lower pressure. This suggests that the S cells, like the VC cells and LE cells (Billy et al., 1989; Illich and Walters, 1997), can exhibit peripheral sensitization. Receptive field sizes were not measured systematically, but, in both preparations, receptive fields appeared smaller than the average size of those of cerebral J/K cells or pleural VC cells innervating the head. The responses to perioral zone/lip stimulation persisted after the cerebral–buccal connectives were transected, indicating that the S cell axons traveled in a buccal nerve. Recordings from two of these cells showed that mechanosensory responses persisted after the receptive field was injected with saline containing 2 × normal [Mg^{2+}] and 0.1 × normal [Ca^{2+}], indicating that the responses do not require peripheral chemical synaptic transmission. Although this blocked all behavioral indications of local synaptic transmission (see Materials and Methods), we cannot exclude the possibility that mechanical stimulation activates the peripheral terminals of the S cells indirectly, by electrical synapses or highly encapsulated chemical synapses from other cells.

Discussion

Number and distribution of sensorin-A-expressing neurons

In adult *Aplysia*, all of the somata labeled by sensorin-A antisense probes in our whole-mount preparations were in central ganglia; none was in peripheral ganglia or other tissues. The labeled somata correspond to previously described mechanosensory clusters in the abdominal, pleural, cerebral, and buccal ganglia. This agrees with observations of sensorin-A expression in serial sections of the ganglia by Brunet et al. (1991). Our counts indicate that the total number of sensorin-A-expressing neurons in the body is about 1,200 in reproductively mature animals (100–300 g) and 1,000 in small animals (10–30 g). Thus, sensorin-A-expressing neurons represent 5–10% of all the neurons in the CNS (Cash and Carew, 1989; Kandel, 2001). The small animals we examined probably included young adults and individuals transitioning from the last juvenile stage to adulthood (Kriegstein, 1977b; Cash and Carew, 1989). Significant increases in the number of sensorin-A-expressing cells with animal size were seen in the pleural, cerebral, and buccal ganglia but not in the abdominal or pedal ganglia (Table 2).

An interesting question concerns the source of the additional sensorin-A-expressing neurons counted in the larger animals. One possibility is that the numbers in small and large animals are actually the same but that we found fewer sensorin-A-expressing cells in smaller animals because accidental cell loss during surgical desheathing was greater in these animals or because the labeled cells were more likely to be obscured by overlying cells in smaller animals. Neither of these explanations seems likely to us, but we cannot rule them out. A second possibility is that some cells in these mechanosensory clusters begin to express sensorin-A at detectable levels only after the animal has reached a relatively large size or advanced stage of adult development. This would be consistent with indirect observations suggesting that the adult complement of sensory neurons may be largely complete by the early adult stage (Marcus et al., 1988; Cash and Carew, 1989). The wide range of labeling intensities observed in some clusters (especially the buccal clusters) might reflect different stages of development of sensorin-A expression in different neurons. A third possibility is that new sensorin-A-expressing neurons continue to be gener-

ated in adulthood. Although addition of new neurons in adult mollusks has not, to our knowledge, been reported, such a mechanism might be useful to maintain complete coverage of the body surface by receptive fields of central mechanosensory neurons during the extraordinary growth of these animals. Adult *Aplysia* exhibit over a 100-fold increase in weight and volume, growing from <30 g to >3,000 g within several months (Carefoot, 1987). The substantial variation in numbers of sensorin-A-expressing cells observed in animals within the same size range (Table 2) might also reflect accidental cell loss during microsurgery, differences in developmental onset of sensorin-A expression, and/or differences in late generation of sensorin-A-expressing neurons across animals.

Somatotopic organization of sensorin-A-expressing neurons

The present report completes the macroscopic map of the peripheral receptive fields of sensorin-A-expressing cell clusters. Figure 13 shows the combined receptive fields of cells in each of the abdominal clusters (LE, rLE, RE, and RF), the cerebral J and K clusters, the buccal S clusters, and the pleural VC clusters. Our study confirms earlier descriptions of receptive fields in *Aplysia* (Byrne et al., 1974; Rosen et al., 1979, 1982; Byrne, 1980; Fiore and Geppeti, 1981; Walters et al., 1983; Billy and Walters, 1989a; Dubuc and Castellucci, 1991; Illich and Walters, 1997) and provides new information about coverage of the midbody and anterior body by the pleural VC clusters, of the rhinophores and propodium by the cerebral J clusters, and of the lip region and buccal mass by the buccal S clusters. When all of this information is combined, sensorin-A-expressing cells are seen to provide a centrally distributed map of the entire surface of the body (Fig. 13).

The receptive fields of the sensorin-A-expressing clusters exhibit modest cephalization, with the head having the smallest, most densely packed fields. Receptive fields of pleural VC cells are significantly smaller on the head than on other parts of the body (Fig. 5B). In the perioral/lip region, the receptive fields of the J/K cells (Rosen et al., 1979, 1982) and the buccal S cells (see Results) appear to be particularly small and numerous. The head is unique in showing overlap of fields from clusters in three different ganglia: the buccal S, cerebral J/K, and pleural VC clusters, and of course there is also extensive overlap of receptive fields among cells within each cluster. The other part of the body showing extensive overlap of receptive fields from different clusters is the mantle cavity, where all four of the clusters in the abdominal ganglion (LE, rLE, RE, and RF) innervate some parts of the mantle and branchial cavity (Dubuc and Castellucci, 1991). Perhaps reflecting evolutionary pressures similar to those responsible for cephalization, the anterior part of the mantle and siphon tip display the smallest receptive fields found in the mantle region (Dubuc and Castellucci, 1991).

Because of their large number, straightforward identification, easy accessibility, and apparently uniform properties, the pleural VC neurons have been utilized extensively for studies of neuronal plasticity in *Aplysia*. However, little was known about the locations of the receptive fields of the VC neurons. We have now shown that axons from each VC cluster project into all of the pedal nerves (after passing through the pl-p connective) and into at least one of the cerebral nerves (c2, after passing through the c-pl connective) and that body regions supplied by each pedal nerve contain receptive fields of VC neurons. Only the mantle organs and the floor of the mantle cavity were found to lack VC cell receptive fields, and no VC cell axons were found in the pl-ab connective. Although in most regions of the body the VC cell receptive fields were restricted to the ipsilateral side (see also Billy

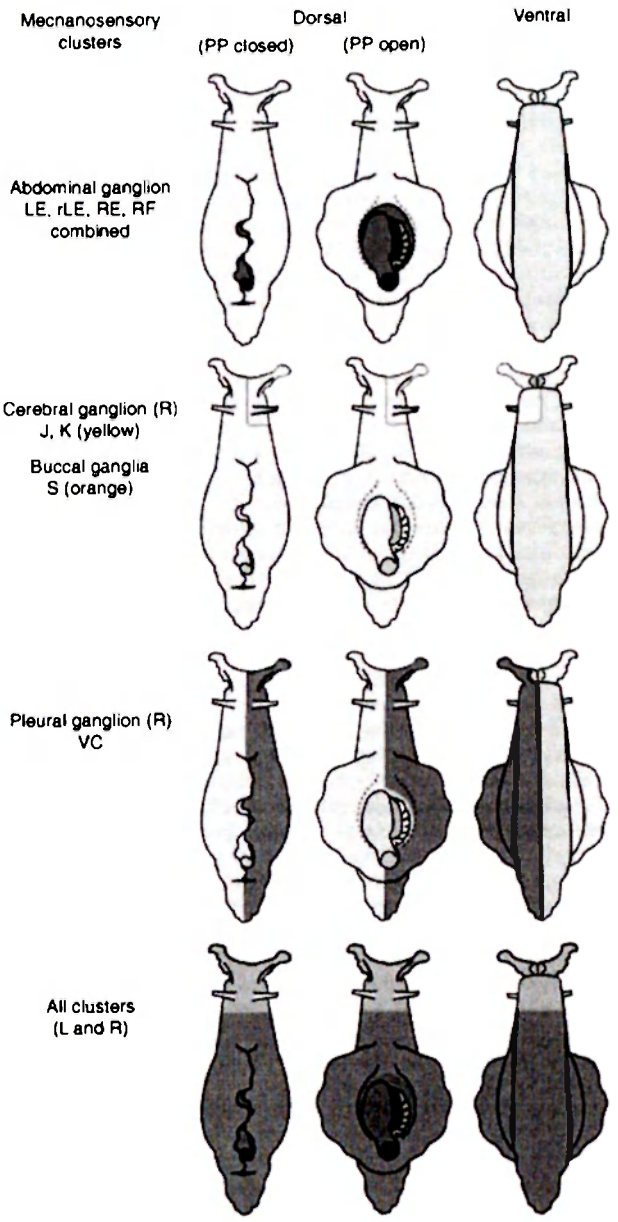

Fig. 13. Sensorin-A-expressing clusters form a macroscopic map of the entire surface of *Aplysia*. The dorsal views show the parapodia (PP) closed (left) and open (right), to reveal the mantle organs. The ventral views show the foot and perioral/lip area. Clusters are grouped by ganglion and their fields color coded as indicated. When all the clusters' fields are combined (bottom row), the fields cover the whole body. Overlap of the cerebral J/K fields (yellow) and pleural VC fields (blue) is indicated by green.

and Walters, 1989a), about 15% of the receptive fields on the foot crossed the midline (Fig. 4B2). Several VC cells were found to have dual axons, with the greatest incidence of dual axons in cells in the anterolateral region of the cluster, where cells often send one axon to the anterior foot through nerve p1 and the pl-p connective and a second through the c-pl connective to synapse with B motor neurons in the cerebral ganglion and/or to innervate the ipsilateral tentacle (Figs. 4, 8, 9). These anterolateral VC cells are probably a major source of sensory neurons with dual axons that are used in studies of synapse-specific plasticity in dissociated cell culture (see, e.g., Martin et al., 1997; Schacher et al., 1999).

A clear (albeit rough) topographic relationship was demonstrated between the location of each sensory neuron soma in the VC cluster and both the location of its peripheral receptive field (Fig. 6) and the nerve carrying its primary axon (Fig. 7; see also Zhang et al., 1993). Thus, each VC cluster forms a somatotopic map of most of the ipsilateral body surface. Although somatotopic mapping of the body surface onto topographically organized populations of central neurons (e.g., the sensory homunculus in sensory cortex) is a common feature of mammalian sensory systems, and somatotopic organization of afferent terminals is well known in arthropods (see, e.g., Murphey, 1981; Peterson and Weeks, 1988), this remains the only somatotopic mapping of peripheral receptive fields onto a discrete cluster of central neuronal somata of which we know in an invertebrate (Walters et al., 1983). Interesting questions arise about the functional significance, if any, of this "sensory aplunculus" in each pleural ganglion and the developmental mechanisms responsible for its formation.

None of the other sensorin-A-expressing clusters has revealed distinct somatotopic maps of their peripheral targets. However, more investigation is needed of the organization of the receptive fields of the buccal S clusters. Our nerve back-fills (Fig. 12) revealed intriguing differences in the mapping of soma position to axon location among the major buccal nerves. One surprise was that somata filled from the dorsal buccal nerve (b3) were contralateral to the back-filled nerve, in contrast to the ipsilateral patterns produced by filling the ventral and lateral buccal nerves (b1 and b2; see also Scott et al., 1991). The significance of these observations must await detailed studies on the locations, sizes, and overlap of the S cell receptive fields. Our preliminary observations on S cell receptive fields were intended only to establish that S cells are mechanosensory in function and that they have fields on the buccal mass and perioral region. The fact that separate back-fills of the major buccal nerves (b1, b2, b3, and the radula nerve) appeared to stain all of the cells in the S clusters (Fig. 12; see also Scott et al., 1991) suggests that all of the S cells may have receptive fields in the regions supplied by these nerves. The observation that different back-fills stained nearly all the cells in some overlapping regions of the buccal clusters suggests that some S cells send at least two axons to the periphery through different nerves.

Functions of sensorin-A-expressing neurons

Is the expression of sensorin-A associated with unique neuronal functions? Little light is shed on this question by the initial physiological effect reported for sensorin-A; application of the peptide hyperpolarized a subset of the postsynaptic target neurons, suggesting that it can function as an inhibitory cotransmitter (Brunet et al., 1991). However, the most prominent synaptic effect of sensorin-A-expressing neurons is rapid excitation, probably mediated by release of glutamate (Dale and Kandel, 1993; Trudeau and Castellucci, 1993; Gapon and Kupfermann, 1996; Levenson et al., 2000). On the other hand, the degree of sensorin-A expression in dissociated cell cultures has correlated well with the presence and strength of excitatory synapses onto motor neuron targets (Santarelli et al., 1996; Schacher et al., 1999; Sun et al., 2001; Hu et al., 2002). This suggests that sensorin-A has functions related to synaptic transmission or synaptic plasticity, although the paucity of hyperpolarizing responses reported for sensory neuron stimulation and the lack of depolarizing responses to exogenous sensorin-A application means that sensorin-A is unlikely to function like a classical neurotransmitter. Axotomized sensory neurons, cut off from peripheral receptive fields but still maintaining central synapses, display a decrease in sensorin-A mRNA expression, whereas contralateral, intact sensory neurons display a simultaneous increase in expression (Noel et al., 1995). If sensorin had an immediate inhibitory effect, the observed facilitation of EPSPs from regenerating tail sensory neurons (Walters et al., 1991) might be due to disinhibition resulting from a decrease in tonic release of sensorin-A from sensory neurons after axotomy. However, exogenous sensorin-A failed to inhibit these same synapses onto tail motor neurons (Brunet et al., 1991). Recent evidence from dissociated cell culture indicates that sensorin may act as a growth factor, contributing to synapse formation and long-term synaptic facilitation (Hu et al., 2003). It is interesting that sensorin-A is also present in coiled sensory terminals (Steffensen and Morris, 1996) located in muscle layers distant from known synapses of these cells. This suggests additional, nonsynaptic functions of sensorin-A, perhaps related to mechanoreception or nociception.

The most notable feature of sensorin-A is its close association with cells known to be mechanosensory neurons. Our studies have strengthened and extended this association by confirming the original patterns of expression reported by Brunet et al. (1991) and by demonstrating a sensory function of the buccal S cells (Fig. 12), the only previous evidence for which had been largely undocumented (Fiore and Geppeti, 1981). Although all the sensorin-A-expressing clusters in *Aplysia* have demonstrated sensory functions, we do not know whether all sensorin-A-expressing neurons do. Indeed, the present study has revealed small numbers of sparsely distributed sensorin-A-expressing neurons in novel locations (pedal ganglia, dorsal surface of the cerebral ganglion, ventral-caudal region of the buccal ganglia). These are often smaller than the cells in the sensorin-A-expressing sensory clusters, although a few are somewhat larger than cells in the clusters. Possible sensory functions of these newly discovered cells remain to be tested. On the other hand, extensive investigations of the LE clusters (Byrne et al., 1974, 1978a; Dubuc and Castellucci, 1991; Illich and Walters, 1997) and VC clusters (this paper; see also Walters et al., 1983; Walters, 1987; Billy and Walters, 1989a,b; Clatworthy and Walters, 1993b) indicate strongly that all of the cells in the LE and VC clusters have peripheral mechanosensory fields.

What types of mechanosensory function are associated with sensorin-A expression? Mechanosensory function in

TABLE 4. Synaptic Targets of Sensorin-A-Expressing Clusters

Ganglion and cluster	Target[1]	Cell type[2]	Cell number[3]	PSP types[4]	Mono-test[5]	Target functions[6]	Original references
Abdominal							
LE	L7	MN, gill	1	fE	TEA	GWR, SWR	Castellucci et al., 1970; Castellucci and Kandel, 1974
	L16	IN, inh	1	fE		GWR, SWR	Castellucci and Kandel, 1974; Hawkins et al., 1981a
	LDG	MN, gill	2	fE	hi-di	GWR	Byrne et al., 1978b; Frost et al., 1997
	L9	MN, gill	2	fE		GWR	Byrne et al., 1978b
	RDG	MN, gill	1	fE		GWR	Byrne et al., 1978b
	L24	IN, multi	1	fE, sI		?	Byrne and Koester, 1978
	L14	MN, ink	3	fE	hi-di	Ink	Byrne, 1980
	R18	IN, exc	1	fE		Ink	Byrne, 1980
	L22	IN, exc	3	fE		GWR	Hawkins et al., 1981a
	L23	IN, exc	1	fE		GWR	Hawkins et al., 1981a
	L28	IN, multi	1	fE, sI		GWR	Hawkins et al., 1981a,b
	L29	IN, multi	5	fE		GWR	Hawkins et al., 1981a,b
	L30	IN, inhib	3	fE		GWR	Hawkins et al., 1981a
	Periph	MN, siphon	50	fE	hi-di	SWR	Bailey et al., 1979
	LFS	MN, siphon	7	fE		SWR	Carew et al. 1981; Frost et al. 1988
	L34	IN, exc	2	fE	hi-di	SWR	Trudeau and Castellucci, 1992; Frost and Kandel, 1995
	LDS	MN, siphon	1	fE		SWR	Frost and Kandel, 1995
rLE	L7	MN, gill	1	fE		GWR	Dubuc and Castellucci, 1991
	LFS	MN, siphon	7	fE		SWR	Dubuc and Castellucci, 1991
RE	L14	MN, ink	3	fE	hi-di	Ink	Byrne, 1980
RF	L14	MN, ink	3	fE	hi-di	Ink	Byrne, 1980
	L7	MN, gill	1	fE	hi-di	GWR	Byrne, 1981
Pleural							
VC	P5/6/7	MN, tail	6	fE	hi-di	TWR	Walters et al., 1983
	LP117	IN, exc	2	fE		TWR, SWR, GWR	Cleary and Byrne, 1993
	RP14	IN, inh	2	fE		TWR	Xu et al., 1994
	Bn	MN, head	60–70	fE	hi-di	HWR	This paper
Cerebral							
J/K	Bn	MN, head	60–70	fE	hi-di	HWR	Rosen et al., 1979, 1982; Teyke et al., 1989
	B4/5	SN, IN, MN, multi	4	fE	hi-di	Ingestion, egestion	Rosen et al., 1982
	MCC	IN, multi	2	fE	hi-di	Feeding	Rosen et al., 1982
	VC	SN	440	sE, sI, fE, fI		Defense	Raymond and Byrne, 1994
	LP117	In, exc	2	fE, sE		TWR, SWR, GWR	Raymond and Byrne, 1994
Buccal							
S	B4/5	SN, IN, MN, multi	4	fE	hi-di	Ingestion, egestion	Fiore and Meunier, 1975; Susswein and Byrne, 1988
	S	SN	320	fE	TEA	?	Fiore and Meunier, 1975

[1]Periph, peripheral siphon motor neurons; MCC, metacerebral giant cell. Some uniquely identified cells have been combined with highly similar individuals (P5/6/7 = P5, P6, and P7; B4/5 = B4 and B5).
[2]MN, motor neuron; IN, interneuron; SN, sensory neuron; exc, excitatory interneuron; inh, inhibitory interneuron; multi, multiaction (with at least two of the following actions on the same or different follower neurons: excitation, inhibition, or modulation with little or no change in potential).
[3]Number is for the entire animal (i.e., double the number for individual paired ganglia).
[4]fE, fast EPSP; sE, slow EPSP; fI, fast IPSP; sI, slow IPSP.
[5]Test for monosynapticity; hi-di, high divalent cation solution; TEA, presynaptic TEA injection; blanks indicate no reported tests.
[6]Behavioral functions documented; GWR, gill-withdrawal reflex; SWR, siphon-withdrawal reflex; TWR, tail-withdrawal reflex; HWR, head-withdrawal reflex.

Aplysia does not require sensorin-A, insofar as other centrally located mechanosensory neurons have been described in *Aplysia* that fail to express this peptide, including giant neurons R1 and L1 in the abdominal ganglion (Cobbs and Pinsker, 1978), proprioceptive multiaction neurons B4 and B5 in the buccal ganglion (Jahan-Parwar et al., 1983), the proprioceptive modulatory neuron C2 in the cerebral ganglion (Weiss et al., 1986a–c), and rostral clusters of radula mechanoafferents in the buccal ganglion. The latter are distinguished from adjacent S cells by the presence of peptides SCP_A and SCP_B and a lack of sensorin-A (Miller et al., 1994; Borovikov et al., 2000; Rosen et al., 2000). In addition, indirect evidence suggests the existence of unidentified mechanosensory populations having peripherally located somata (Kupfermann et al., 1974; Peretz et al., 1976; Walters et al., 1983; Xin et al., 1995; Frost et al., 1997; Hickie et al., 1997; Walters and Cohen, 1997; Croll, 2001). We found no evidence of sensorin-A expression in peripheral somata of adult animals. One difference between the other central mechanosensory neurons and the sensorin-A-expressing neurons is that the former are much more likely to show substantial fast excitation from synaptic inputs and thus appear to have interneuronal (and sometimes motor) as well as sensory functions. In contrast, fast PSPs from other neurons have not been reported for most of the sensorin-A-expressing clusters (Table 4). The major exception is the buccal S cells, which receive fast EPSPs (~1 mV) from many other S cells (Fiore and Meunier, 1975). In addition, ~4% of cells in the cerebral J cluster evoke very small EPSPs (<1 mV) in pleural VC cells (Raymond and Byrne, 1994). Another difference is that most of the other central and at least some of the peripheral mechanosensory neurons are sensitive to very weak, innocuous stimuli. In contrast, we have now shown that sensorin-A-expressing neurons in all of the ganglia have relatively high thresholds to mechanical stimulation. J/K cells, VC cells, and S cells tested with the same set of von Frey hairs all showed mean response thresholds of 30–35 g/mm^2, as did LE cells and VC cells in previous studies (Billy and Walters, 1989a; Illich and Walters, 1997), and the thresholds ranged between 15 and 65 g/mm^2. At pressures of 25–35 g/mm^2, the siphon skin begins to be perforated (Illich and Walters, 1997). If the threshold for tissue in-

jury in other regions is also within this range, then cells in these clusters are tuned to mechanical stimuli that produce or threaten tissue damage; i.e., sensorin-A expression is likely to be associated with a nociceptive function.

Further insight into the functions of sensorin-A-neurons comes from the known synaptic connections of these cells. The connections reported to be direct are listed in Table 4, which reveals that neurons in every sensorin-A-expressing cluster produce fast EPSPs in specific motor neurons (e.g., Fig. 9C) as well as other types of neurons. In most cases, the identified target neurons have defensive functions, which include driving the release of ink and withdrawal of the gill, siphon, tail, or head (Table 4). Subsets of both the pleural VC cells and the cerebral J/K cells contribute jointly to head- and tentacle-withdrawal reflexes, because some of their receptive fields overlap and they often excite the same Bn motor neurons (Fig. 9C; see also Raymond and Byrne, 1994). In addition, the VC cells (Billy and Walters, 1989a,b; Clatworthy and Walters, 1993b), LE cells (Illich and Walters, 1997), and perhaps S cells (see Results) display nociceptive sensitization of their peripheral receptive fields. Peripheral sensitization following intense activation appears to be a sensory property that is unique to nociceptors; other sensory neurons usually show adaptation instead (Light, 1992). Taken together, the synaptic outputs of the sensorin-A-expressing neurons and their capacity for peripheral sensitization provide additional evidence for defensive and nociceptive functions of many of these cells.

The functions of the buccal S cells, however, remain mysterious. These cells not only excite each other (Table 4) but excite and sometimes inhibit many other buccal ganglion neurons (Fiore and Meunier, 1975, 1979), many of which participate in controlling ingestive and egestive behaviors of the buccal mass. In addition to their unusual synaptic interconnections, the S cells exhibit several other features that distinguish them from most of the other sensorin-A-expressing neurons, suggesting that the S cells may have some unique functions in the animal. For example, whereas the somata of most sensorin-A-expressing neurons show rapidly accommodating responses to prolonged depolarizing pulses (see, e.g., Klein et al., 1986; Walters et al., 1991; Clatworthy and Walters, 1994), the buccal S cells show very little spike accommodation in the soma (Fig. 12C) as well as little accommodation during mechanosensory responses (Fig. 12B). Compared with other sensorin-A-expressing neurons, the S cells also have spike durations that are about twice as long, and afterhyperpolarizations that are three times the amplitude of those in the VC, J/K, and LE neurons (cf. Hochner et al., 1986; Baxter and Byrne, 1990; Walters et al., 1991; Clatworthy and Walters, 1994; Gunstream et al., 1995; Illich and Walters, 1997; Ungless et al., 2002). These unusual features of the S cells may reflect unique biomechanical properties or functions of the highly complex buccal mass, or its location inside the body (the other clusters innervate tissues near the surface of the body). We have recorded from too few S cells to know whether the properties found in this preliminary study are characteristic of the entire cluster or whether subpopulations exist with different properties and sensory functions. Given the diversity of tissues in the buccal mass/lip region that can evoke spikes in S cells (including buccal muscle, lip/perioral tissue, hard radula, and soft tissues lining the buccal cavity), it would be surprising if all functional properties were expressed uniformly across all the sensorin-expressing neurons in the buccal ganglia. Moreover, although the other sensorin-A-expressing clusters share many physiological properties, all of their properties are not identical. For example, subsets of the sensory cells in the cerebral and abdominal clusters show different responses to the same neuromodulators, including serotonin and FMRFamide (Rosen et al., 1989; Storozhuk and Castellucci, 1998), and no systematic studies have yet been performed on pleural VC clusters to examine patterns of response to endogenous neuromodulators across the entire VC cell population.

Although much remains to be learned about the functions of sensorin-A and the neurons that express this peptide, the availability of well-defined populations of mechanosensory neurons in *Aplysia* that express sensorin-A along with other mechanosensory populations that fail to express the peptide means that powerful comparative methods can be used to elucidate such functions. This power will be increased if the comparisons can be extended to mechanosensory neurons in other molluscan species. Sensorin-A-expressing neurons have been found in the snail *Lymnaea stagnalis* (Steffensen et al., 1995b), and it will be interesting to see whether some of the mechanosensory populations described in other gastropod molluscs also express sensorin-A (see, e.g., Getting, 1976; Spray et al., 1980; Elliott and Benjamin, 1989; Inoue et al., 1996; Malyshev et al., 2002). Among the functional questions that will be important to address is why the mRNA for sensorin-A is expressed so widely within the cell, being found not only in the soma but in dendritic and axonal regions within ganglia and connectives (Figs. 2B1, 3A1,B1; Brunet et al., 1991), in neurites and synaptic terminals in dissociated cell culture (Santarelli et al., 1996; Schacher et al., 1999), and in peripheral axons (Fig. 3B1).

ACKNOWLEDGMENTS

Some of the animals were supplied by the National Center for Research Resources, National Resource for *Aplysia*, at the University of Miami.

LITERATURE CITED

Ambron RT, Walters ET. 1996. Priming events and retrograde injury signals: a new perspective on the cellular and molecular biology of nerve regeneration. Mol Neurobiol 13:61–79.

Bailey CH, Castellucci VF, Koester J, Kandel ER. 1979. Cellular studies of peripheral neurons in siphon skin of *Aplysia californica*. J Neurophysiol 42:530–557.

Baxter DA, Byrne JH. 1990. Differential effects of cAMP and serotonin on membrane current, action-potential duration, and excitability in somata of pleural sensory neurons of *Aplysia*. J Neurophysiol 64:978–990.

Billy AJ, Walters ET. 1989a. Long-term expansion and sensitization of mechanosensory receptive fields in *Aplysia* support an activity-dependent model of whole-cell sensory plasticity. J Neurosci 9:1254–1262.

Billy AJ, Walters ET. 1989b. Modulation of mechanosensory threshold in *Aplysia* by serotonin, small cardioactive peptideB (SCPB), FMRFamide, acetylcholine, and dopamine. Neurosci Lett 105:200–204.

Bogdanov Yu D, Balaban PM, Zakharov IS, Poteryaev DA, Belyavsky AV. 1996. Identification of two novel genes specifically expressed in the D-group neurons of the terrestrial snail CNS. Invert Neurosci 2:61–69.

Borovikov D, Evans CG, Jing J, Rosen SC, Cropper EC. 2000. A proprioceptive role for an exteroceptive mechanoafferent neuron in *Aplysia*. J Neurosci 20:1990–2002.

Brunet JF, Shapiro E, Foster SA, Kandel ER, Iino Y. 1991. Identification of a peptide specific for *Aplysia* sensory neurons by PCR-based differential screening. Science 252:856–859.

Byrne JH. 1980. Neural circuit for inking behavior in *Aplysia californica*. J Neurophysiol 43:896–911.

Byrne JH. 1981. Comparative aspects of neural circuits for inking behavior and gill withdrawal in *Aplysia californica*. J Neurophysiol 45:98–106.

Byrne JH, Koester J. 1978. Respiratory pumping: neuronal control of a centrally commanded behavior in *Aplysia*. Brain Res 143:878–105.

Byrne JH, Castellucci V, Kandel ER. 1974. Receptive fields and response properties of mechanoreceptor neurons innervating siphon skin and mantle shelf in *Aplysia*. J Neurophysiol 37:1041–1064.

Byrne JH, Castellucci VF, Carew TJ, Kandel ER. 1978a. Stimulus-response relations and stability of mechanoreceptor and motor neurons mediating defensive gill-withdrawal reflex in *Aplysia*. J Neurophysiol 41:402–417.

Byrne JH, Castellucci VF, Kandel ER. 1978b. Contribution of individual mechanoreceptor sensory neurons to defensive gill-withdrawal reflex in *Aplysia*. J Neurophysiol 41:418–431.

Carefoot T. 1987. *Aplysia*: its biology and ecology. Oceanogr Mar Biol Annu Rev 25:167–284.

Carew TJ, Walters ET, Kandel ER. 1981. Associative learning in *Aplysia*: cellular corelates supporting a conditioned fear hypothesis. Science 211:501–504.

Cash D, Carew TJ. 1989. A quantitative analysis of the development of the central nervous system in juvenile *Aplysia californica*. J Neurobiol 20:25–47.

Castellucci VF, Kandel ER. 1974. A quantal analysis of the synaptic depression underlying habituation of the gill-withdrawal reflex in *Aplysia*. Proc Natl Acad Sci U S A 71:5004–5008.

Castellucci V, Pinsker H, Kupfermann I, Kandel ER. 1970. Neuronal mechanisms of habituation and dishabituation of the gill-withdrawal reflex in *Aplysia*. Science 167:1745–1748.

Clatworthy AL, Walters ET. 1993a. Activity-dependent depression of mechanosensory discharge and excitability in *Aplysia*. J Neurophysiol 70:1195–1209.

Clatworthy AL, Walters ET. 1993b. Rapid amplification and facilitation of mechanosensory discharge in *Aplysia* by noxious stimulation. J Neurophysiol 70:1181–1194.

Clatworthy AL, Walters ET. 1994. Comparative analysis of hyperexcitability and synaptic facilitation induced by nerve injury in two populations of mechanosensory neurones of *Aplysia californica*. J Exp Biol 190: 217–238.

Cleary LJ, Byrne JH. 1993. Identification and characterization of a multifunctional neuron contributing to defensive arousal in *Aplysia*. J Neurophysiol 70:1767–1776.

Cobbs JS, Pinsker HM. 1978. In vivo responses of paired giant mechanoreceptor neurons in *Aplysia* abdominal ganglion. J Neurobiol 9:121–141.

Croll RP. 2001. Catecholamine-containing cells in the central nervous system and periphery of *Aplysia californica*. J Comp Neurol 441:91–105.

Dale N, Kandel ER. 1993. L-glutamate may be the fast excitatory transmitter of *Aplysia* sensory neurons. Proc Natl Acad Sci U S A 90:7163–7167.

Díaz-Ríos M, Suess E, Miller MW. 1999. Localization of GABA-like immunoreactivity in the central nervous system of *Aplysia californica*. J Comp Neurol 413:255–270.

Dubuc B, Castellucci VF. 1991. Receptive fields and properties of a new cluster of mechanoreceptor neurons innervating the mantle region and the branchial cavity of the marine mollusk *Aplysia californica*. J Exp Biol 156:315–334.

Dulin MF, Steffensen I, Morris CE, Walters ET. 1995. Recovery of function, peripheral sensitization, and sensory neurone activation by novel pathways following axonal injury in *Aplysia*. J Exp Biol 198:2055–2066.

Elliott CJ, Benjamin PR. 1989. Esophageal mechanoreceptors in the feeding system of the pond snail, *Lymnaea stagnalis*. J Neurophysiol 61: 727–736.

Fiore L, Geppeti L. 1981. Neural control of buccal mass activity of *Aplysia*. In: Salanki J, editor. Neurobiology of invertebrates. London: Pergamon Press. p 201–223.

Fiore L, Meunier JM. 1975. A network of synaptic relations in the buccal ganglia of *Aplysia*. Brain Res 92:336–340.

Fiore L, Meunier JM. 1979. Synaptic connections and functional organization in *Aplysia* buccal ganglia. J Neurobiol 10:13–29.

Frost WN, Clark GA, Kandel ER. 1988. Parallel processing of short-term memory for sensitization in *Aplysia*. J Neurobiol 19:297–334.

Frost L, Kaplan SW, Cohen TE, Henzi V, Kandel ER, Hawkins RD. 1997. A simplified preparation for relating cellular events to behavior: contribution of LE and unidentified siphon sensory neurons to mediation and habituation of the *Aplysia* gill- and siphon-withdrawal reflex. J Neurosci 17:2900–2913.

Frost WN, Kandel ER. 1995. Structure of the network mediating siphon-elicited siphon withdrawal in *Aplysia*. J Neurophysiol 73:2413–2427.

Gapon S, Kupfermann I. 1996. Evidence for transmitter similarity of two classes of mechanoreceptor neurons in the cerebral ganglion of *Aplysia*. Neurosci Lett 205:157–160.

Getting PA. 1976. Afferent neurons mediating escape swimming of the marine mollusc, *Tritonia*. J Comp Physiol 110:271–286.

Gunstream JD, Castro GA, Walters ET. 1995. Retrograde transport of plasticity signals in *Aplysia* sensory neurons following axonal injury. J Neurosci 15:439–448.

Hawkins RD, Castellucci VF, Kandel ER. 1981a. Interneurons involved in mediation and modulation of gill-withdrawal reflex in *Aplysia*. I. Identification and characterization. J Neurophysiol 45:304–314.

Hawkins RD, Castellucci VF, Kandel ER. 1981b. Interneurons involved in mediation and modulation of gill-withdrawal reflex in *Aplysia*. II. Identified neurons produce heterosynaptic facilitation contributing to behavioral sensitization. J Neurophysiol 45:315–328.

Hawkins RD, Abrams TW, Carew TJ, Kandel ER. 1983. A cellular mechanism of classical conditioning in *Aplysia*: activity-dependent amplification of presynaptic facilitation. Science 219:400–405.

Hening WA, Walters ET, Carew TJ, Kandel ER. 1979. Motorneuronal control of locomotion in *Aplysia*. Brain Res 179:231–253.

Hickie C, Cohen LB, Balaban PM. 1997. The synapse between LE sensory neurons and gill motoneurons makes only a small contribution to the *Aplysia* gill-withdrawal reflex. Eur J Neurosci 9:627–636.

Hickmott PW, Carew TJ. 1991. An autoradiographic analysis of neurogenesis in juvenile *Aplysia californica*. J Neurobiol 22:313–326.

Hochner B, Klein M, Schacher S, Kandel ER. 1986. Action-potential duration and the modulation of transmitter release from the sensory neurons of *Aplysia* in presynaptic facilitation and behavioral sensitization. Proc Natl Acad Sci U S A 83:8410–8414.

Hu JY, Meng X, Schacher S. 2002. Target interaction regulates distribution and stability of specific mRNAs. J Neurosci 22:2669–2678.

Hu JY, Wu F, Meng X, Wang D, Schacher S. 2003. Release of sensorin peptide is required for synapse formation and long-term synaptic facilitation in *Aplysia*. Soc Neurosci Abstr 478.4.

Illich PA, Walters ET. 1997. Mechanosensory neurons innervating *Aplysia* siphon encode noxious stimuli and display nociceptive sensitization. J Neurosci 17:459–469.

Inoue T, Takasaki M, Lukowiak K, Syed NI. 1996. Identification of a putative mechanosensory neuron in *Lymnaea*: characterization of its synaptic and functional connections with the whole-body withdrawal interneuron. J Neurophysiol 76:3230–3238.

Jahan-Parwar B, Fredman SM. 1976. Cerebral ganglion of *Aplysia*: cellular organization and origin of nerves. Comp Biochem Physiol A54:347–357.

Jahan-Parwar B, Fredman SM. 1978. Pedal locomotion in *Aplysia californica*—I. Sensory and motor fields of pedal nerves. Comp Biochem Physiol 60A:459–465.

Jahan-Parwar B, Wilson AH Jr, Fredman SM. 1983. Role of proprioceptive reflexes in control of feeding muscles of *Aplysia*. J Neurophysiol 49: 1469–1480.

Kandel ER. 1979. Behavioral biology of *Aplysia*. San Francisco: W.H. Freeman & Co.

Kandel ER. 2001. The molecular biology of memory storage: a dialogue between genes and synapses. Science 294:1030–1038.

Klein M, Hochner B, Kandel ER. 1986. Facilitatory transmitters and cAMP can modulate accommodation as well as transmitter release in *Aplysia* sensory neurons: evidence for parallel processing in a single cell. Proc Natl Acad Sci USA 83:7994–7998.

Kriegstein AR. 1977a. Development of the nervous system of *Aplysia californica*. Proc Natl Acad Sci U S A 74:375–378.

Kriegstein AR. 1977b. Stages in the post-hatching development of *Aplysia californica*. J Exp Zool 199:275–288.

Krontiris-Litowitz JK, Cooper BF, Walters ET. 1989. Humoral factors

released during trauma of *Aplysia*. I. Body wall contraction, cardiac modulation, and central reflex suppression. J Comp Physiol B159:211–223.

Kupfermann I, Carew TJ, Kandel ER. 1974. Local, reflex, and central commands controlling gill and siphon movements in *Aplysia*. J Neurophysiol 37:996–1019.

Levenson J, Sherry DM, Dryer L, Chin J, Byrne JH, Eskin A. 2000. Localization of glutamate and glutamate transporters in the sensory neurons of *Aplysia*. J Comp Neurol 423:121–131.

Liao X, Walters ET. 2002. The use of elevated divalent cation solutions to isolate monosynaptic components of sensorimotor connections in *Aplysia*. J Neurosci Methods 120:45.

Light AR. 1992. The initial processing of pain and its descending control: spinal and trigeminal systems. Basel: Karger.

Malyshev AY, Balaban PM. 2002. Identification of mechanoafferent neurons in terrestrial snail: response properties and synaptic connections. J Neurophysiol 87:2364–2371.

Marcus EA, Schuerman G, Stopfer M, Carew TJ. 1988. Development of tail sensory neurons in the pleural ganglia of *Aplysia*. Soc Neurosci Abstr 14:481.

Martin KC, Casadio A, Zhu H, Yaping E, Rose JC, Chen M, Bailey CH, Kandel ER. 1997. Synapse-specific, long-term facilitation of *Aplysia* sensory to motor synapses: a function for local protein synthesis in memory storage. Cell 91:927–938.

McAllister LB, Scheller RH, Kandel ER, Axel R. 1983. In situ hybridization to study the origin and fate of identified neurons. Science 222:800–808.

Miller MW, Rosen SC, Schissel SL, Cropper EC, Kupfermann I, Weiss KR. 1994. A population of SCP-containing neurons in the buccal ganglion of *Aplysia* are radula mechanoafferents and receive excitation of central origin. J Neurosci 14:7008–7023.

Moroz LL, Iannuccilli B, Si K, Sathyanarayanan PV, Sadreyev R, Edwards J, Panchin Y, Meleshkevich E, Nguyen T, Farmerie W, Ju J, Kandel ER. 2002. *Aplysia* EST project: from the CNS to neuronal and synaptic transcriptome. Soc Neurosci Abstr 376.13.

Murphey RK. 1981. The structure and development of a somatotopic map in crickets: the cercal afferent projection. Dev Biol 88:236–246.

Nazif FA, Byrne JH, Cleary LJ. 1991. cAMP induces long-term morphological changes in sensory neurons of *Aplysia*. Brain Res 539:324–327.

Noel F, Frost WN, Tian L-M, Colicos MA, Dash PK. 1995. Recovery of the tail-elicited siphon-withdrawal reflex following unilateral axonal injury is associated with ipsi- and contralateral changes in gene expression in *Aplysia californica*. J Neurosci 15:6926–6938.

Peretz B, Jacklet JW, Lukowi K. 1976. Habituation of reflexes in *Aplysia*: contribution of the peripheral and central nervous systems. Science 191:396–399.

Peterson BA, Weeks JC. 1988. Somatotopic mapping of sensory neurons innervating mechanosensory hairs on the larval prolegs of *Manduca sexta*. J Comp Neurol 275:128–144.

Raymond JL, Byrne JH. 1994. Distributed input to the tail-siphon withdrawal circuit in *Aplysia* from neurons in the J cluster of the cerebral ganglion. J Neurosci 14:2444–2454.

Rosen SC, Weiss KR, Kupfermann I. 1979. Response properties and synaptic connections of mechanoafferent neurons in cerebral ganglion of *Aplysia*. J Neurophysiol. 42:954–974.

Rosen SC, Weiss KR, Cohen JL, Kupfermann I. 1982. Interganglionic cerebral-buccal mechanoafferents of *Aplysia*: receptive fields and synaptic connections to different classes of neurons involved in feeding behavior. J Neurophysiol 48:271–288.

Rosen SC, Susswein AJ, Cropper EC, Weiss KR, Kupfermann I. 1989. Selective modulation of spike duration by serotonin and the neuropeptides, FMRFamide, SCPB, buccalin and myomodulin in differennt classes of mechanoafferent neurons in the cerebral ganglion of *Aplysia*. J Neurosci 9:390–402.

Rosen SC, Miller MW, Cropper EC, Kupfermann I. 2000. Outputs of radula mechanoafferent neurons in *Aplysia* are modulated by motor neurons, interneurons, and sensory neurons. J Neurophysiol 83:1621–1636.

Santarelli L, Montarolo P, Schacher S. 1996. Neuropeptide localization in varicosities of *Aplysia* sensory neurons is regulated by target and neuromodulators evoking long-term synaptic plasticity. J Neurobiol 31:297–308.

Schacher S, Wu F, Panyko JD, Sun ZY, Wang D. 1999. Expression and branch-specific export of mRNA are regulated by synapse formation and interaction with specific postsynaptic targets. J Neurosci 19:6338–6347.

Scott ML, Govind CK, Kirk MD. 1991. Neuromuscular organization of the buccal system in *Aplysia californica*. J Comp Neurol 312:207–222.

Spray DC, Spira ME, Bennett MV. 1980. Peripheral fields and branching patterns of buccal mechanosensory neurons in the opisthobranch mollusc, *Navanax inermis*. Brain Res 182:253–270.

Steffensen I, Morris CE. 1996. Coiled mechanoreceptors in *Aplysia* revealed by sensorin immunofluorescence and confocal microscopy. Invert Neurosci 2:129–134.

Steffensen I, Dulin MF, Walters ET, Morris CE. 1995a. Peripheral regeneration and central sprouting of sensory neurone axons in *Aplysia californica* following nerve injury. J Exp Biol 198:2067–2078.

Steffensen I, Syed NI, Lukowiak K, Bulloch AGM, Morris CE. 1995b. Sensorin-A immunocytochemistry reveals putative mechanosensory neurons in *Lymnaea* CNS. Invert Neurosci 1:207–213.

Storozhuk MV, Castellucci VF. 1998. The synaptic junctions of LE and RF cluster sensory neurones of *Aplysia californica* are differentially modulated by serotonin. J Exp Biol 202:115–120.

Sun ZY, Wu F, Schacher S. 2001. Rapid bidirectional modulation of mRNA expression and export accompany long-term facilitation and depression of *Aplysia* synapses. J Neurobiol 46:41–47.

Susswein AJ, Byrne JH. 1988. Identification and characterization of neurons initiating patterned neural activity in the buccal ganglia of *Aplysia*. J Neurosci 8:2049–2061.

Teyke T, Weiss KR, Kupfermann I. 1989. A subpopulation of cerebral B cluster neurones of *Aplysia californica* is involved in defensive head withdrawal but not appetitive head movements. J Exp Biol 147:1–20.

Trudeau LE, Castellucci VF. 1992. Contribution of polysynaptic pathways in the mediation and plasticity of *Aplysia* gill and siphon withdrawal reflex: evidence for differential modulation. J Neurosci 12:3838–3848.

Trudeau LE, Castellucci VF. 1993. Excitatory amino acid neurotransmission at sensory-motor and interneuronal synapses of *Aplysia californica*. J Neurophysiol 70:1221–1230.

Unglese MA, Gasull X, Walters ET. 2002. Long-term alteration of S-type potassium current and passive membrane properties in *Aplysia* sensory neurons following axotomy. J Neurophysiol 87:2408–2420.

Walters ET. 1987. Multiple sensory neuronal correlates of site-specific sensitization in *Aplysia*. J Neurosci 7:408–417.

Walters ET, Cohen LB. 1997. Functions of the LE sensory neurons in *Aplysia*. Invert Neurosci 3:15–25.

Walters ET, Erickson MT. 1986. Directional control and the functional organization of defensive responses in *Aplysia*. J Comp Physiol A159: 339–351.

Walters ET, Byrne JH, Carew TJ, Kandel ER. 1983. Mechanoafferent neurons innervating tail of *Aplysia*. I. Response properties and synaptic connections. J Neurophysiol 50:1522–1542.

Walters ET, Alizadeh H, Castro GA. 1991. Similar neuronal alterations induced by axonal injury and learning in *Aplysia*. Science 253:797–799.

Weiss KR, Chiel HJ, Koch U, Kupfermann I. 1986a. Activity of an identified histaminergic neuron, and its possible role in arousal of feeding behavior in semi-intact *Aplysia*. J Neurosci 6:2403–2415.

Weiss KR, Chiel HJ, Kupfermann I. 1986b. Sensory function and gating of histaminergic neuron C2 in *Aplysia*. J Neurosci 6:2416–2426.

Weiss KR, Shapiro E, Kupfermann I. 1986c. Modulatory synaptic actions of an identified histaminergic neuron on the serotonergic metacerebral cell of *Aplysia*. J Neurosci 6:2393–2402.

Xin Y, Weiss KR, Kupfermann I. 1995. Distribution in the central nervous system of *Aplysia* of afferent fibers arising from cell bodies located in the periphery. J Comp Neurol 359:627–643.

Xin Y, Hurwitz I, Perrins R, Evans CG, Alexeeva V, Weiss KR, Kupfermann I. 1999. Actions of a pair of identified cerebral–buccal interneurons (CBI-8/8) in *Aplysia* that contain the peptide myomodulin. J Neurophysiol 81:507–520.

Xu Y, Cleary LJ, Byrne JH. 1994. Identification and characterization of pleural neurons that inhibit tail sensory neurons and motor neurons in *Aplysia*: correlation with FMRFamide immunoreactivity. J Neurosci 14:3565–3577.

JOURNAL OF EXPERIMENTAL ZOOLOGY (MOL DEV EVOL) 306B:551-566 (2006)

Thyroid Hormone Metabolism and Peroxidase Function in Two Non-chordate Animals

ANDREAS HEYLAND[1,3*], DAVID A. PRICE[1], MICHAELA BODNAROVA-BUGANOVA[1], AND LEONID L. MOROZ[1,2*]
[1]*The Whitney Laboratory for Marine Bioscience, University of Florida, Florida 32080*
[2]*Department of Neuroscience and McKnight Brain Institute, University of Florida, Florida 32080*
[3]*Friday Harbor Laboratories, University of Washington, Washington 98250*

ABSTRACT In mammals, thyroid hormone (TH) signaling is essential for metabolic control, differentiation and homeostasis. These hormones are also involved in the regulation of metamorphosis in amphibians and lampreys and a role in basal chordates has been suggested. Increasing evidence supports TH-related function not only in basal chordates such as urochordates and cephalochordates but also in other invertebrate groups. However, the regulatory mechanisms underlying TH function including the mechanisms of endogenous synthesis of hormones in these groups are essentially unknown. Our data provide evidence for endogenous TH synthesis in the sea hare *Aplysia californica* and the sea urchin *Lytechinus variegatus* based on thin layer chromatography. Pharmacological experiments show that these hormones accelerate development to metamorphosis and specifically affect the formation of juvenile skeletal structures in the sea urchin. Furthermore, we identified two new peroxidase genes (LvTPO from *L. variegatus* and AcaTPO from *A. californica*) showing high sequence similarity with peroxidasin and thyroid peroxidases (the critical TH synthesis enzymes found in all vertebrates). Spatial and temporal expression patterns of these transcripts suggest a role of LvTPO and AcaTPO in a variety of processes such as development to metamorphosis and the regulation of the animal's energetics. We discuss our new findings in the context of evolution of TH synthesis and TH signaling in non-chordate animals. *J. Exp. Zool. (Mol. Dev. Evol.) 306B:551-566, 2006.*

The importance of thyroid hormone (TH; please note that we use the term TH for invertebrates as an abbreviation for thyroid hormone-like compounds throughout because these hormones still await identification using mass spectrometry and other analytical, non-antibody-based methods) signaling for diverse processes such as cell differentiation, growth and metabolism has been well-documented for all vertebrate species investigated to date (*reviewed in* McNabb, '92; Yen, 2001). One critical component of the TH signaling pathway is the synthesis of the hormone. The vertebrate thyroid is a highly specialized organ that is able to concentrate the limited iodine from the environment (Venturi et al., 2000; Truesdale and Bailey, 2002). Subsequently, tyrosine residues present on a thyroglobulin scaffold are iodinated by a series of reactions catalyzed by thyroid peroxidase (TPO) (McLachlan and Rapoport, '92; Taurog, 2000).

The endostyle of basal chordates, a pharyngeal organ involved in filter feeding, is generally accepted as the thyroid homolog and evolutionary predecessor of thyroid glands found in vertebrates (Ogasawara et al., '99; Ruppert et al., '99; Ogasawara, 2000). As a confirmation of this

This article contains supplementary material available via the internet at http://www.mrw.interscience.wiley.com/suppmat/1552-5007/suppmat
Grant sponsor: NIH; Grant sponsor: NSF; Grant sponsor: Swiss National Science Foundation Post-doctoral Grant; Grant sponsor: Link Fellowship; Grant number: 643; Grant sponsor: Packard and McKnight Brain Research Foundation Grants.

Abbreviations: Explanation TH, thyroid hormone; TPO, thyroid peroxidase; MFSW, millipore-filtered seawater; 0.2μm; T4, thyroxine; SW125 MFSW with I125; T3 (3,3″, 5-triiodo-L-thyronine); TR, thyroid hormone receptor; SULT, sulfotransferase.

*Correspondence to: Drs. A. Heyland and L.L. Moroz, The Whitney Laboratory, University of Florida, 9505 Ocean Shore Blvd., St. Augustine, FL 32080-8610.
E-mail: aheyland@ufl.edu, moroz@whitney.ufl.edu

Received 29 August 2005; Accepted 21 March 2006
Published online 31 May 2006 in Wiley InterScience (www.interscience.wiley.com). DOI: 10.1002/jez.b.21113.

hypothesis, recent investigations revealed the presence of this enzyme in the endostyle of three basal chordates, the ascidians *Ciona intestinalis* and *Halocynthia roretzi* (Ogasawara et al., '99) and the cephalochordate *Brachiostoma belcheri* (Ogasawara, 2000). However, no conclusive evidence on endogenous TH synthesis outside of the chordate clade exists. Moreover, there is little information about the presence of TPO-related genes outside the chordates. Here we provide evidence that endogenous TH synthesis evolved within the echinoderms and within the lophotrochozoans suggesting that this character is not a chordate synapomorphy. Additionally, we propose a new model of TH synthesis via TPO-related peroxidases from the animal peroxidase superfamily.

Several critical components of TH signaling have been investigated in a variety of metazoan taxa except ctenophores, nematodes and echiurans (Fig. 1, *all data compiled from* Eales, '97). For example, several insect species have been shown to incorporate iodine into THs (*reviewed in* Eales, '97). In the polychaete *Eisenia foeta*, radioiodine is incorporated into the central nervous system (CNS) specifically between neurosecretory cells and the neuropile fibers (Davoli et al., '91). Moreover, thyroglobulin-like immunoreactivity was detected in the nervous system of this species (Marcheggiano et al., '85). The gorgonian coral *Leptogorgia irgulata* contains a thyroxine (T4)-like substance which appears to be involved in Ca^{2+} metabolism (Kingsley et al., 2001). Another cnidarian, the jellyfish *Aurelia*, responds to THs by strobilation and it has been further suggested that this cnidarian can synthesize TH precursors endogenously (Spangenberg, '67, '71, '74). More examples are reviewed in Eales ('97) and summarized in Figure 1.

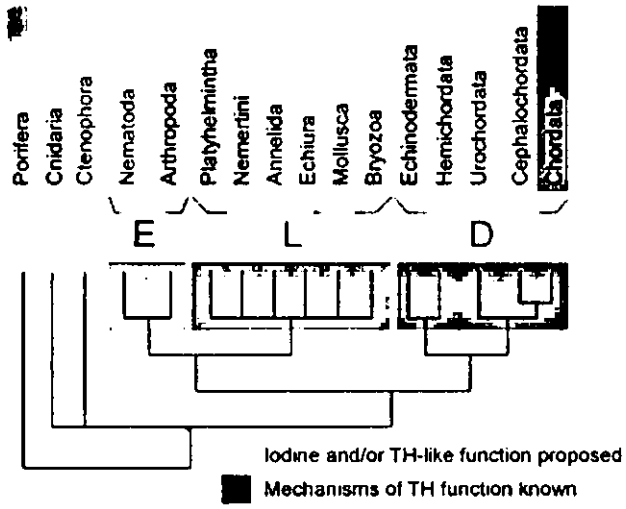

Fig. 1. Thyroid hormone-like function has been proposed for a variety of metazoan phyla but its mechanisms are poorly investigated in the majority of taxa except chordates. We identified two peroxidases potentially involved in thyroid hormone synthesis from the opisthobranch mollusc *Aplysia californica* (AcaTPO) and the echinoderm *Lytechinus variegatus* (LvTPO). Cladogram shows metazoan phylogeny (modified from Peterson and Eernisse, 2001): Except Ctenophores, Nematodes and Echiurans, all metazoan taxa appear to have Iodine and/or TH-like functions (data compiled from Eales et al., 1997 and Heyland et al., 2005). E: Ecdysozoa; L: Lophotrochozoa; D: Deuterostomata; The presence of TH and mechanistic basis of TH action however is only known in chordates (dark shading).

In several echinoids and one sea star, exogenous T4 (one TH) accelerates larval development (Chino et al., '94; Johnson and Cartwright, '96; Hodin et al., 2001; Heyland and Hodin, 2004) and leads subsequently to an earlier metamorphosis (Heyland and Hodin, 2004). The source of endogenous hormone however remains controversial. Several authors have hypothesized that TH or TH-like compounds may primarily originate from unicellular algae in feeding sea urchin larvae (larval type in echinoderms that needs to feed on phytoplankton in order to reach metamorphosis; Chino et al., '94; Heyland and Hodin, 2004; Heyland and Moroz, 2005; Heyland et al., 2005). In contrast, we provided preliminary evidence that feeding larvae of two sand dollar species, *Dendraster excentricus* and *Clypeaster rosaceus* may synthesize thyroid hormone-like compounds endogenously, additionally to the exogenous source (Heyland and Hodin, 2004; Heyland et al., Personal Communication). Moreover, Saito et al. ('98) showed that the lecithotrophic Japanese sand dollar species *Peronella japonica* contains small but detectable amounts of T4 and T3. In all of these studies, the vertebrate goitrogen thiourea inhibited metamorphosis, suggesting the involvement of TPO-related enzymes in thyroid hormone synthesis in non-chordate deuterostomes as well.

Iodine incorporation and the ability to metabolize exogenous THs have been demonstrated for some bivalve and gastropod Molluscs (Antheunisse and Lever, '56; Tong and Chaikoff, '61) but endogenous hormone synthesis and TH-related signaling has not further been investigated in this and other lineages of lophotrochozoan animals. Here, we present evidence for TH-related function in the sea urchin *Lytechinus variegatus* and the marine opisthobranch Mollusc *Aplysia californica*. We show that both *Aplysia* and *Lytechinus* contain THs (T4 and T3) and provide evidence that

these hormones are synthesized from incorporated iodine using thin layer chromatography (TLC). Moreover, we show that T4 accelerates spicule formation and development to metamorphosis in the sea urchin. Finally, we partially sequenced two new peroxidase genes from *Aplysia* and *Lytechinus* that are closely related to peroxidasin of human (PERDSN: HUMAN; Genbank accession number BAA13219), *Drosophila* (PERDSN:DROME, Genbank accession number S46224) and *C. elegans* (PERDSN1:CELE, Genbank accession number CAA91994) and fall into a sister clade to TPOs. The gene product of PERDSN:DROME has been previously shown to synthesize THs in vitro (Nelson et al., '94). Moreover, the expression patterns of AcaTPO and LvTPO suggest roles in development and metabolism in larvae and adults. Their functional involvement in endogenous TH synthesis in Molluscs and echinoderms however remains to be elucidated.

MATERIALS AND METHODS

Animal maintenance and larval culturing

For testing TH and TH metabolite effects on sea urchin development and metamorphosis, we collected adult *L. variegatus* at Jupiter inlet Florida (26°57′28.41″N; 80°04′40.03″W) in October and November 2002 at low tide and from the Keys marine Laboratory on Long Key, Florida in February and October 2003. Upon collection, animals were maintained in the laboratory at 21–24°C in flow-through seawater. We received juvenile and adult *A. californica* from the experimental hatchery in Miami (The University of Miami Experimental Hatchery of the Rosenstiel School of Marine and Atmospheric Science).

To obtain sea urchin larval cultures, we induced spawning by injection of 1 ml 0.55 M KCl solution in the gonad of adult urchins. Eggs were collected in millipore-filtered seawater (MFSW; 0.2 μm) and sperm were collected dry. After eggs had settled, excess water was replaced once with fresh MFSW and a 1:10,000 solution of concentrated sperm was added. About 1 min later, eggs were viewed under the compound microscope to check for fertilization envelopes. Fertilization success was estimated by counting the number of successfully fertilized eggs out of 50 randomly sampled eggs. We only considered the fertilization as successful if fertilization success was more than 95% (successfully fertilized/50). Larvae were maintained in gallon jars filled with 3.8 l MFSW at a concentration of 1 larva/5 ml MFSW. Hatching occurred within 12 hr after fertilization. Larvae were then fed 4 cells/μl of the unicellular alga *Rhodomonas lens* or 12 cells/ul *T-iso*. Water in cultures was changed every 2 days by reverse filtration (see Strathmann, '87). At each water-change, fresh food was added.

TH, TH metabolite and thiourea effects on larval development and metamorphosis

In order to estimate T4 effects on development to metamorphosis and metamorphic competence, larvae in cultures were exposed to four concentrations of T4 and the control (no T4) 2 days after fertilization until metamorphosis. Primary T4 stocks [L-Thyroxin (Sigma, St. Louis, MO); T-1776] were prepared at a concentration of 10^{-6}, 10^{-7}, 10^{-8} and 10^{-9} M (Heyland and Hodin, 2004) and then diluted 1:10^4 for the final concentrations of 10^{-10}, 10^{-11}, 10^{-12} and 10^{-13} M (THYROXINE 10^{-10} M; THYROXINE 10^{-11} M; THYROXINE 10^{-12} M; THYROXINE 10^{-13} M) in the culture jars (note that for this experiment we used 1 l glass jars filled with 800 ml MFSW). We monitored development in larvae by removing replicate larvae from culture jars and determining their developmental stage on living specimens. When larvae were considered competent for metamorphosis (for definition of metamorphic competence see Heyland and Hodin, 2004), water in 1 l jars was reduced to 100 ml by reverse filtration (Strathmann, '87) and 4 ml of 1 M KCl was added resulting in 40 mM excess final KCl concentration. Jars were screened for metamorphosed *L. variegatus* after 4 hr. This procedure was repeated 4 times every 2 days. We estimated timing to metamorphic competence in larvae by calculating the cumulative percentage of metamorphosis for the dates listed above. Once the threshold of 20% cumulative percentage metamorphosis was overcome, we consider larvae in a replicate metamorphically competent.

For a broad comparison of the effects of the TH metabolite and TH synthesis inhibitor thiourea in development of morphological structures, we cultured larvae to the developmental stage when the juvenile rudiment was clearly flattened and juvenile spicules were present (see also Chino et al., '94). About 24 hr before exposure, we reared larvae in the complete absence of food to drain the stomachs of any algal diet. We then distributed larvae into individual wells of 12-well plates filled with 4 ml of MFSW and exposed them to one of the following treatments: CONTROL (no chemicals added), THYROXINE [10^{-10} M thyroxine (Sigma:

T-1776)], RESCUE (10^{-10}M thyroxine+10^{-3}M thiourea), THIOUREA (10^{-3}M thiourea), L-TYROSINE (2×10^{-10}M L-tyrosine [Sigma: T9040-9]), NaI (4×10^{-10}M NaI [Sigma: S2179]), L-TYROSINE+NaI (2×10^{-10}M L-tyrosine+4×10^{-10}M NaI), NaCl (4×10^{-10}M NaCl). At this point we took two images from each individual larva that was mounted alive on a microscope slide with sufficient MFSW. Each image was taken at a different magnification (10×, 20×) in order to be later able to measure stomach size (SS) and rudiment size (RS), respectively. Note that each treatment was replicated 12 times (i.e., one entire well-plate per treatment). On April 15, we removed each individual larva carefully from the well plate and photographed it in the same way as on April 11. On April 16, we removed larvae from the well plate and flattened larvae underneath cover slides and imaged larval and juvenile skeletal structures. All images were analyzed using imageJ software (http://rsb.info.nih.gov/ij/). We measured postoral arm length (PO), postdorsal arm length (PD), the SS and RS. SS and RS were calculated as the square root of the cross-sectional area of an ellipsoid (using stomach length, stomach width and rudiment length, rudiment width, respectively, as the axes of the ellipsoid).

Iodine incorporation and TH synthesis

We exposed larvae at the developmental stage when adult spicules had formed (see also above) for 8 hr in 12-well plates to experimental treatments. Note that before this exposure we cultured larvae for 24 hr in the complete absence of food to drain the stomachs from any algal food. We placed 50 randomly chosen larvae into each well, containing 4 ml of solution (10^{-3}M thiourea and the control, respectively). All solutions were made up in SW^{125} (MPFSW with I^{125} at 51,937 dpm; Carrier-free specific activity of I^{125} was 642.8 GBq/mg). For each treatment we used 6 wells. After the exposure, larvae from three wells were pooled together in one test tube resulting in two independent replicates per treatment (150 larvae per replicate). Specimens were washed 5 times with fresh MFSW until the radioactivity in the supernatant was below 30 dpm (counted on ssMPD instrument see below). Between each wash larvae were centrifuged at 1,980*g* for 3 min and kept on ice. *A. californica* juveniles were processed in a similar way except that we used 10^{-2}M thiourea in the inhibitor treatment.

To test whether I^{125} that the larvae had incorporated was built into T4, we prepared samples for TLC. We added 1 ml of ice-cold MeOH to each sample after the sample was counted (samples containing I^{125} were counted on a ssMPD instrument [BioTraces, Inc., Herndon, VA] in standard mode. In standard mode, digital signal processing is used to distinguish the I^{125} decay-specific characteristics from those of background events to give a background equivalent to 5 DPM of I^{125} with about 45% efficiency) and let it stand at 4°C overnight. After vortexing all samples at full strength for 2 min, we centrifuged them at 1,980*g* for 10 min and collected the supernatant. Then we spiked the samples with 100 µl non-radioactive 10^{-4}M T4 (thyroxine; Sigma-Aldrich T-1774) and T3 (3,3″,5-triiodo-L-thyronine; Sigma: T2877) and then concentrated in a speed-vac to complete dryness. The dry pellet was redissolved in 30 µl 0.01 N NaOH. Note that usually not all the salt crystals redissolved. All 30 µl (excluding the crystals) were loaded on a TLC plate (Whatman LK5D silica gel 150A with fluorescence marker; Whatman #4851-840) and run for 1.5 hr in a 2-methylbutanol/*t*-butyl alcoholy/25%NH3/acetone, 7:14:14:56, vol/vol solvent. We visualized the cold T4 and T3 markers under UV light on a BioRad™ Flour-S Multilmager system and radioactive bands on a Molecular Dynamics™ Phosphorimager SI. Overlaying the UV image with the one from the phosphor imager allowed us to compare the radioactive bands to our THs standards.

TH measurements in sea urchin larvae and Aplysia hemolymph

We collected *Aplysia* hemolymph samples and sea urchin larval samples (40 larvae per sample). In case samples were not immediately processed we kept them at −80°C. Note that samples were never kept longer at −80°C than 2 months. Then we defrosted samples on ice, and added 5 volumes of 100% ice-cold MeOH. Extraction was done at 4°C overnight. We then centrifuged samples at 3,000 rpm for 10 min at 4°C. We decanted the liquid upper phase and kept the pellet for protein analysis. The upper phase was brought to complete dryness in a Speed-Vac™ and then resuspended in 50 µl 0.01 N NaOH. The pellet was redissolved in 100 µl 1 N HCl at 60°C for 1 hr and then vortexed at full strength for 1 min per sample.

For TH analysis we used the ELISA KIT (Total Thyroxine (Total T4) ELISA Kit Alpha Diagnostic International, Inc.; TX, USA) following the

manufacturer's instructions. Note that in addition to the standards provided in the kit we used our own standards made up in 0.01 N NaOH for better comparison. For Protein analysis we used Pierce™ micro-BCA kit using manufacturer's instructions.

Gene cloning and in situ hybridizations

Two pools of double-stranded cDNA from the sea urchin *L. variegatus* larval stages and *A. californica* cerebral ganglia were isolated and amplified following protocols of the Clontech Smart-PCR cDNA synthesis kit (Clontech Laboratories, Mountain View, CA, USA) as described in (Matz, 2003). We ligated cDNA to double-stranded adaptors (Marathon cDNA Amplification Kit, Clontech). For cloning of LvTPO (*L. variegatus* TPO), we selected conserved amino acid sequences among peroxidases to choose the sites for PCR primers. We choose sense [TPO-F: ACIGCIGCITT(TC)(CA)GITT(TC)GGICA, corresponding to the amino acid sequence TAAFRFGH] and the antisense [TPO-R: GGIA(AG)ICC(AG)TG(AG)TCIC(GT)ICCIC(GT)(TC)TG, corresponding to the amino acid sequence QRGRDHGLP] degenerate primers based on (Ogasawara et al., '99). For AcaTPO (*A. californica* TPO), we then used rapid amplification of cDNA ends (RACE) to generate 5′ and 3′ PCR products following procedures previously described in Matz et al. (2003). We cloned Gel purified PCR products into the pT-Adv Vector (Clontech TA cloning) and sequenced it at the Whitney Laboratory, St. Augustine, FL.

We fixed organismal samples in 100 mM HEPES, pH 6.9, 2 mM $MgSO_4$, 1 mM EGTA for 24–48 hr and dehydrated them in 50% ethanol, then 80% ethanol (30 min each) and stored at −20°C in 80% ethanol until used for in situ hybridizations. We synthesized digoxigenin labeled (DIG) antisense probes from linearized plasmids according to the protocols supplied with the DIG RNA Labeling kit (Roche Molecular Biochemicals, Indianapolis, IN). Whole-mount in situ hybridizations were performed by a similar protocol to that of Swalla et al., ('94). We washed samples with phosphate buffered saline with 0.1% Tween 20 (PBT) then treated with 10 mg/ml Proteinase K in PBT at 37°C for 10 min. We stopped the reaction in 2 mg/ml glycine in PBT, and washed with PBT. Samples were post-fixed in 4% paraformaldehyde in PBS, washed with PBT and treated with 0.25% anhydrous acetic acid in 0.1 M triethanolamine (pH 8.0) prepared just before use. We hybridized samples overnight at 45°C with LvTPO antisense full length probe and used the sense probe as a negative control. We then washed with 2 × SSC at 45°C and treated with 20 mg/ml RNase at 37°C. Samples were blocked in 0.1% blocking reagent in PBT, then incubated in 1/2,000 anti-DIG-AP in PBT, both from the DIG Nucleic Acid Detection Kit (Roche Molecular Biochemicals). AP detection buffer contained levamisole and NBT/BCIP. After the desired staining was reached, samples were rinsed in PBS. Samples were then mounted in benzyl alcohol:benzyl benzoate after being dehydrated through a series of ethanol washes: 30%, 50%, 80%, 90%, 100% along with two washes in benzyl alcohol:benzyl benzoate 1:1. Note that for all these procedures we cultured larvae for 24 hr in the complete absence of food to drain the stomachs from any algal food (cDNA synthesis and sample fixation). All in situ hybridizations were replicated 3 times independently (i.e., on three different days using three new probes).

Phylogenetic analysis

Amino acid sequences of the peroxidases catalytic domains were aligned using default settings in ClustalX (Thompson et al., '94). No manual adjustment of the alignment was necessary (Appendix A). For a complete list of sequences see Table 1. Phylogenetic analysis was performed using maximum-likelihood, parsimony and Bayesian inference. For the maximum-likelihood analysis we used Tree-Puzzle software (Schmidt et al., 2002). JTT model of amino acid evolution (Jones et al., 1992) was used for maximum-likelihood distance calculation (parameters estimated from the dataset), gamma distribution of sites variability was assumed (alpha parameter estimated from the dataset) and 10,000 puzzling steps were done to obtain support values. For the parsimony analysis, we used PAUP* 4.0b10 for Windows (Sinauer Associates, Inc., Sunderland, MA, USA). All characters were equally weighted and unordered. Gaps were treated as missing data. The analysis was performed using 10,000 random addition sequence replicates, holding 10 trees at each step and TBR branch swapping algorithm. Clade support was estimated with 1,000 bootstrap replicates (100 replicates of random addition with 10 trees held at each step). Bayesian inference was carried out using MrBayes, ver. 3.0B4 (Huelsenbeck and Ronquist, 2001). We used

TABLE 1. Genes used for phylogenetic analyses

Abbreviation	Protein name	Organism	Database ID	Length	Domain
PERT:HALOR	Thyroid peroxidase	*Halocynthia roretzi* (Ascidian)	BAA76689 (gb)	918	214–716
PERT:HUMAN	Thyroid peroxidase	Human	P07202 (sp)	933	201–711
PERT:MOUSE	Thyroid peroxidase	Mouse	P35419 (sp)	914	195–699
PERT:CIONA	Thyroid peroxidase	*Ciona intestinalis* (Ascidian)	BAA76688 (gb)	909	200–703
PERT:RAT	Thyroid peroxidase	*Rat*	P14650 (sp)	914	195–699
PERT:PIG	Thyroid Peroxidase	*Pig*	P09933 (sp)	926	201–709
PERS:MOSQ1	Salivary peroxidase	*Anopheles albimanus* (Mosquito)	AAD22196 (gb)	591	75–568
RIBON:XENLA	Polysomal ribonuclease 1	*Xenopus laevis* (Frog)	AAC94959 (gb)	713	195–689
PERNT:PACL	Peroxinectin	*Pacifastacus leniusculus* (Signal crayfish)	JC4397 (pir)	818	293–787
PERDSN:HUMAN	Peroxidasin homolog	*Human*	BAA13219 (gb)	1,496	808–1,308
PERDSN:DROME	Peroxidasin homolog	*D. melanogaster* (Fruit fly)	S46224 (gb)	1,535	831–1,329
PERDSN1:CELE	Peroxidasin homolog	*C. elegans*	CAA91994 (gb)	1,328	719–1,225
PERH2N:CELE	Peroxidase homolog 3N	*C. elegans*	CAA88963 (gb)	1,490	205–676
AcaTPO	Peroxidase homolog	*Aplysia californica* (Sea hare)	AAT90333 (gb)	560	1–560
PERH:MOSQ1	Peroxidase homolog	*Aedes aegypti* (Yellow fever fly)	AAC97504 (gb)	683	138–642
LvTPO	Peroxidase homolog	*Lytechinus variegatus* (Sea urchin)	AAT90332 (gb)	678	49–548
PERH:BRANB	Peroxidase homolog	*Branchiostoma belcheri* (Lancelet)	BAA83376 (gb)	764	231–738
PERH:DROME	Peroxidase homolog	*D. melanogaster* (Fruit fly)	Q01603 (sp)	690	150–652
PERH:PSEDA	Peroxidase homolog	*Pseudomonas alcaligenes* (Bacterium)	AAC83355 (gb)	913	100–614
PIOX:TABAC	Pathogen induced oxygenase	*Nicotiana tabacum* (Tabaco)	CAA07589 (gb)	643	130–623
PERO:HEMP	Ovoperoxidase	*Hemicentrotus pulcherrimus* (Sea urchin)	BAA19738 (gb)	814	194–686
PERM:HUMAN	Myeloperoxidase	Human	P05164 (sp)	745	223–720
PERM:MOUSE	Myeloperoxidase	Mouse	P11247 (sp)	718	197–694
PERI:SEPO	Melanogenic peroxidase	*Sepia officinalis* (Cuttlefish)	CAA72331 (gb)	926	369–852
PERI:EUPS	Light organ peroxidase	*Euprymna scolopes* (Squid)	AAA16244 (gb)	894	337–820
PERL:BOVIN	Lactoperoxidase	Bovine	P80025 (sp)	712	188–686
PERL:HUMAN	Lactoperoxidase	Human	P22079 (sp)	712	188–686
PERE:MOUSE	Eosinophil peroxidase	Mouse	CAI25724 (gb)	716	196–692
PERE:HUMAN	Eosinophil peroxidase	Human	P11678 (sp)	715	195–691
PGH2:HUMAN	Cyclooxygenase-2	Human	P35354 (sp)	604	156–568
PGH1:HUMAN	Cyclooxygenase-1	Human	P23219 (sp)	599	169–581

The first column corresponds to the name used in the phylogenetic tree and the alignment (Fig. 4B; Appendices A and B). The second column is a characterization of the peroxidase. Column three describes the organism from which the gene originates. Column four is the database accession number (sp: SwissProt; gb: Genbank; pir: Protein Information Resource). Column five indicates the number of amino acids of the gene and column 6 indicates the region in which the catalytic domain was identified and used for the phylogenetic analysis.

a fixed JTT model for amino acid evolution (Jones et al., 1992). Each Markov chain was started from a random tree and run for 2×10^6 generations, sampling every 100th generation from the chain. Each run comprised four differently heated chains. The analysis resulted in the accumulation of 60,000 trees. The first 30,000 generations of data (i.e., 3,000 trees) were discarded ("burned") for the posterior probabilities calculation. Three independent runs were performed. For parsimony and maximum-likelihood analyses we used the following four taxa as outgroups: PERH:PSEDA, PIOX:TABAC, PGH2:HUMAN and PGH1:HUMAN. For Bayesian analysis we used PIOX:TABAC (Pathogen induced oxygenase from *Nicotiana tabacum* Genbank accession number (CAA07589)).

Data analysis

Data were organized and analyzed in Excel™ and SPSS™. Statistical comparisons between the experimental treatments and the controls were done using student's *t*-test, ANOVA with simple contrast or MANOVA. For all analyses we used SPSS™. Results are presented as: mean difference (treatment value minus control value) ± 1SE; *P*-value. If the mean difference is positive this means that the value in the experimental treatment was larger than the value in the control. All *P*-values are from null hypotheses testing that the mean difference mentioned above equals 0. Information on *A. californica* ESTs was derived from the *Aplysia* neuronal transcriptome (Moroz et al., unpublished data). EST and genomic information

from the sea urchin *Strongylocentrotus purpuratus* was derived from NCBI.

RESULTS

Iodine incorporation and TH synthesis in two invertebrate species is inhibited by thiourea

We exposed larval sea urchins and juvenile *Aplysia* to I^{125} in order to test whether (1) iodine is incorporated into these organisms and (2) incorporated iodine is used for TH synthesis (T4 and triiodotyrosine). Sea urchin larvae incorporated I^{125} (Fig. 2A and B). Thiourea, a TPO inhibitor, blocked iodine uptake in a dose-responsive manner in the sea urchin (Fig. 2A). However, $KClO_4$, known as a competitive inhibitor of the sodium iodine symporter (Dai et al., '96; Eskandari et al., '97), did not have any effects on iodine incorporation in sea urchins (Fig. 2B).

Our results from the TLCs confirm that both the sea urchin larvae and *Aplysia* juveniles used incorporated I^{125} to make THs (Fig. 2C and D). Interestingly, *Lytechinus* larvae predominately synthesize T4 (Fig. 2C) while *Aplysia* juveniles primarily synthesize T3 (Fig. 2D). Thiourea inhibited TH synthesis in both *Aplysia* and sea urchins (Fig. 2C and D).

Finally, we were able to detect T4 and T3 in sea urchin larvae and hemolymph of adult *Aplysia* (Fig. 2E) using ELISA. Note that all measurements are standardized to the protein content of the samples.

THs accelerate development to metamorphosis in sea urchin larvae while thiourea acts in an inhibitory manner

First, we tested T4 effects on pre-metamorphic stages and attainment of metamorphic competence of the sea urchin *L. variegatus* (Fig. 3A and B). Secondly, we tested whether iodine, tyrosine, thiourea (a TPO inhibitor) and T4 result in morphological changes in sea urchin larvae (Fig. 3C, D). T4 significantly accelerated occurrence of juvenile spines (Fig. 3A) and attainment of metamorphic competence (Fig. 3B) in larvae that were continuously exposed to the hormone during development. The number of adult skeletons was significantly higher in the THYROXINE 10^{-10}M (6.46 ± 1.91; $P = 0.001$) AND THYROXINE 10^{-11}M ($4.05 + 1.91$; $P = 0.038$) treatment 9 days after fertilization compared to the control using ANOVA with simple contrast (Fig. 3A).

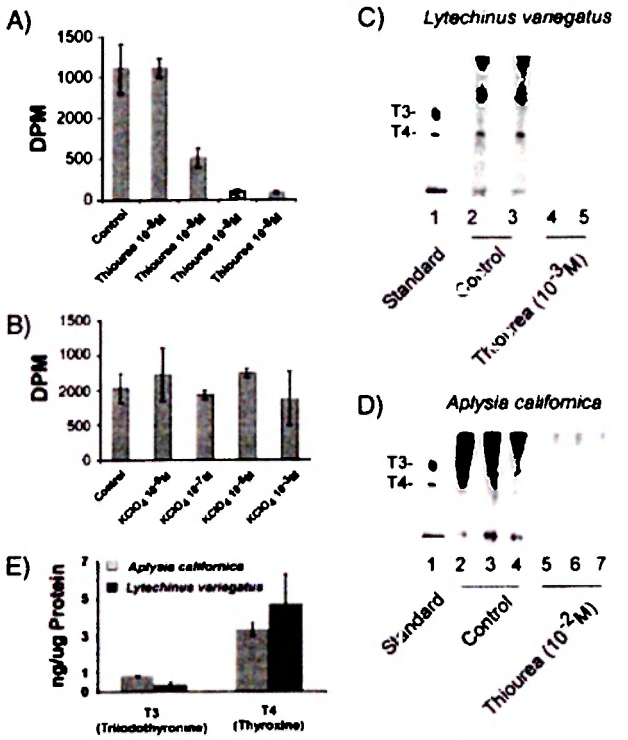

Fig. 2. *Lytechinus variegatus* larvae and *Aplysia californica* juveniles incorporate I^{1+0} (radioactively labeled iodine) and synthesize iodinated tyrosines (i.e., T4 and T3). (**A**) Thiourea inhibits iodine (I^{125}) uptake in *Lytechinus* variegates; (**B**) $KClO_4$ (another thyroid hormone synthesis inhibitor, inhibiting the Na/I symporter in vertebrates, for details see text) has no effect on iodine uptake. (**C**) Incorporated iodine is used to synthesize thyroxine (T4) in *Lytechinus variegatus* (Control; lanes 2 and 3, standard in lane 1); (**D**) Incorporated iodine is used to synthesize T3 in *Aplysia californica* (Control, lanes 2–4, standard in lane 1). (**E**) We measured T4 and T3 in sea urchin (*Lytechinus*) larvae and *Aplysia* juveniles using ELISA and found both hormones present in both species in comparable concentrations. Note that all measurements are standardized to the protein content of the samples. T4 was present at higher concentrations in both species. DPM: decays per minute. In both *Aplysia* and *Lytechinus* neither T4 nor T3 was detected when larvae and juveniles were exposed to thiourea before extraction.

Metamorphic competence was reached significantly earlier (approximately 15%) in the THYROXINE 10^{-10}M treatment compared to the control (-3.50 ± 1.45 days; $P = 0.03$) (Fig. 3B). Note that we used a threshold value of 20% competence for this analysis (data not shown).

We then tested the effects of various THs and TH metabolites on larval and juvenile morphology using well-plate experiments (for experimental design see materials and methods). T4 lead to a significantly stronger relative reduction of SS (-0.21 ± 0.09; $P = 0.02$), and absolute reduction

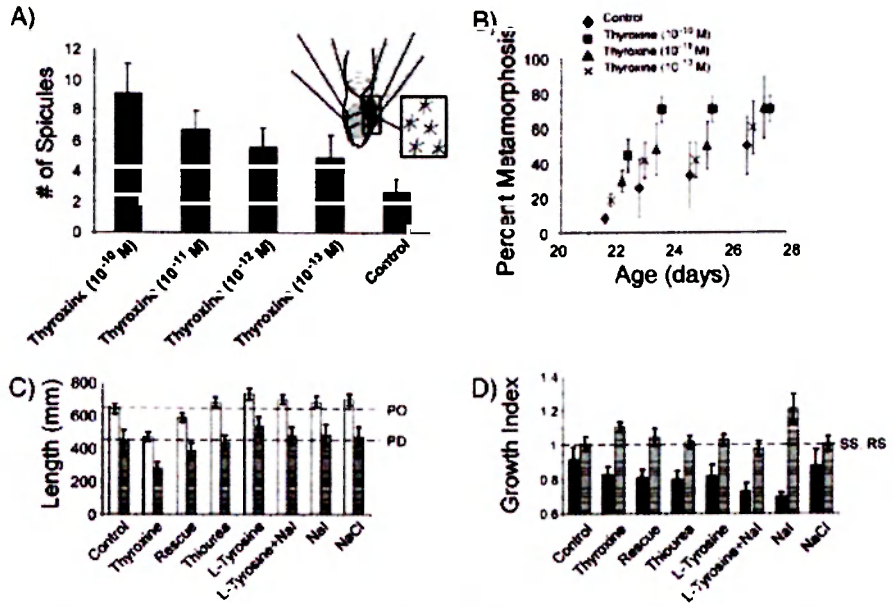

Fig. 3. Thyroxine (T4) accelerates larval development (A) and development to metamorphosis (B). (A) Larvae of *Lytechinus variegatus* were treated with different concentrations of T4 during larval development ranging from 10^{-10} to 10^{-13} M. We observed a significant increase in number of spicules that formed in the adult rudiment. We showed earlier that this spicule formation is a good indicator for juvenile development in pluteus larvae (see Heyland and Hodin, 2004). (B) T4 also significantly accelerated development to metamorphosis (analysis see text) measured in the time it takes larvae to reach metamorphic competence threshold of 20% (please note that measurements were done at the same time points 22, 23, 25, 27 days after fertilization). (C,D) We exposed larvae to seven different treatments and the control in order to test whether iodine and/or tyrosine simulate the effect of T4 on larval characters (C), the stomach (D) and the juvenile rudiment (D) and whether thiourea has an inhibitory effect on these structures as it was found in other echinoid larvae. Thiourea did not have any effects on larval and juvenile structures while T4 did. The rescue treatment (T4+thiourea) however was not significantly different from the control either. We conclude from these findings that thiourea has an opposite effect on morphological characters than T4. We also found that NaI significantly decreases stomach size and so does T4 (for details on statistical analysis see text). No shading in (C): postoral arm length; horizontal shading in (C): posterodorsal arm length; no shading in (D): stomach size; horizontal shading in (D): rudiment size. Growth index indicates SS or RS after experimental exposure divided by SS or RS before exposure, respectively. Dashed lines indicate the o-change isoclines. For PO and PD arm length this corresponds to the length of the arms in the CONTROL while it corresponds to 1 for stomach size and rudiment size (indicating no change).

of PO arm length (-168.98 ± 43.17; $P < 0.001$) and PD arm length ($-169.90 + 74.20$; $P = 0.02$) and a significant relative increase in juvenile size ($0.21 + 0.07$; $P = 0.005$) all relative to the control. We did not find however any significant difference between the THIOUREA treatment (10^{-3} M thiourea) and the CONTROL and the RESCUE treatment (RESCUE [10^{-10} M T4+10^{-3} M thiourea]) and the CONTROL indicating an inhibition of T4 effects by thiourea in terms of larval morphology. Furthermore, we did find a significant relative decrease of SS ($-0.19 + 0.09$; $P = 0.04$) in the NaI treatment. In summary, we found that T4 treatment results in decreased growth and development of larval structures and an increase in juvenile structures. These effects of T4 are reversed by the addition of the thyroid hormone synthesis inhibitor thiourea to our cultures.

Cloning of peroxidases from echinoderms and Molluscs and phylogenetic analysis

As a first step to elucidate the mechanisms of TH synthesis in non-chordate animals, we searched for TPO orthologous genes using degenerate primers and database screens. We cloned two partial sequences of peroxidases closely related to peroxidasin and TPO from *A. californica* (AcaTPO: AY605096) and the sea urchin *L. variegatus* (LvTPO: AY605095; Fig. 1C). Both sequences were submitted to Genbank.

Figure 4A is a schematic representation of the domain structure derived from the complete alignment of *Drosophila melanogaster* peroxidasin and several TPOs. The alignment with details on conserved residues can be found in Appendix A. The sequenced portion of LvTPO encodes 703

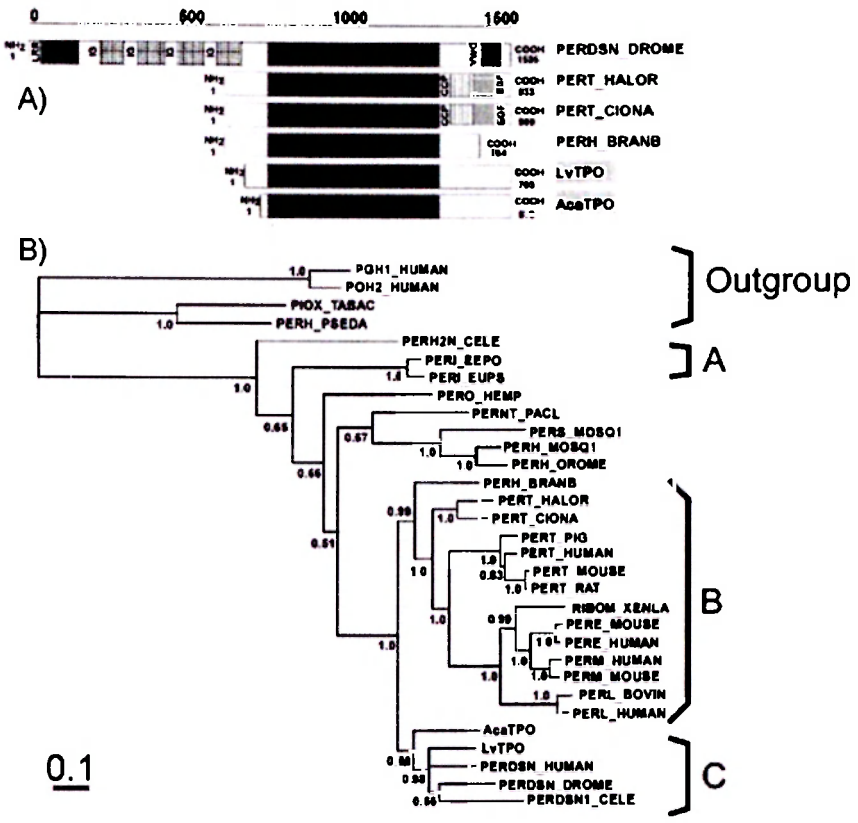

Fig. 4. (A) Schematic result of sequence alignment with putative domain structure. Partial sequences of AcaTPO and LvTPO and their alignment with other peroxidases are represented in Appendix 1. Schadings in the schematic alignment indicate conserved motifs and are from 5′ to 3′: LRR: Leucine-rich repeats; IG: Immunoglobulin domain cell adhesion molecule (cam) subfamily; An-peroxidase: animal haem domain; CCP: complement control proteins; EGF: Calcium-binding EGF-like domain; VWC: von Willebrand factor type C domain B) Bayesian analysis using amino acid sequence of catalytic domains confirms AcaTPO and LvTPO as peroxidases closely related to peroxidasins (Clade C). Clade C represents a sister clade to thyroid- myelo-, lacto-, eosinophil-peroxidases (Clade B). All peroxidases used for the alignment are summarized in Table 1. Note that parsimony and maximum likelyhood analyses (see Appendix 2) resulted in similar tree topology as the bayesian analysis shown here. Values underneath branches represent posterior probabilities.

amino acid residues. The catalytic domain extends from position 74 to 574 and includes all residues necessary for peroxidase function and critical for thyroid hormone synthesis. These are proximal and distal histidine (110, 356), arginine (259) and asparagine (440). The Ca^{2+}-binding domain appears to be only partially conserved in *L. variegatus* [residues T(189), Y(191), D(193), S(195)]. While three residues are completely conserved [T(189), D(193) and S(195)] position 191 is Y in the sea urchin, instead of F as in other TPO genes described. AcaTPO is 576 amino acids long and has also all major domains necessary for peroxidase function conserved. These are proximal and distal histidine in positions 25 and 273, Ca^{2+} binding domain in positions 104 (T), 106 (F), 108 (D) and 110 (S). Finally arginine is found in position 77 and asparagines in position 357. In the sequenced portion of LvTPO and AcaTPO, we were not able to detect any of the complement control protein (CCP) modules (also known as short consensus repeats (SCRs) or SUSHI repeats) towards the 3′ end of the gene as they can be found in human (PERT:HUMAN) and *C. intestinalis* (PERT: CIONA) TPOs. Furthermore, we were not able to find a second calcium-binding EGF-like domain in the partial sequence of LvTPO and AcaTPO.

In order to evaluate the phylogenetic position of AcaTPO and LvTPO among other peroxidases, we performed three different analyses: parsimony, maximum-likelihood and Bayesian. Amino acid sequences used in the phylogenetic analysis are summarized in Table 1. The tree resulting from the Bayesian analysis is presented in Figure 4B. The alignment of the catalytic domain is provided in Appendix A, and the same alignment in nexus

format is provided in Appendix C. For parsimony analysis all characters were weighted equally and gaps were treated as missing values. From a total of 599 characters, 108 were parsimony uninformative and were excluded. This analysis resulted in two maximum parsimony trees (L = 4,732; CI = 0.65; RI = 0.61). All trees showed very similar results. Bayesian and tree puzzle analysis found significant support for Clades A–C, while parsimony did not identify peroxidasins, LvTPO and AcaTPO as a monophyletic group. Clade A consists of melanogenic peroxidase from the cuttlefish *Sepia officinalis* and light organ peroxidase from the squid *Euprymna scolopes*. Clade B consists of lacto-, myelo-, eosinophil and TPOs. The position of polysomal ribonuclease 1 from the frog *Xenopus laevis* and a peroxidase ortholog from the lancelet *B. belcheri* are consistent between maximum-likelihood and Bayesian but not compared to parsimony. Clade C consists of LvTPO and AcaTPO together with peroxidasins from *Drosophila*, *C. elegans* and humans. Trees resulting from the maximum likelihood and parsimony analyses are presented in Appendix B.

Thus, AcaTPO and LvTPO can be characterized as peroxidases based on their conserved residues. Based on their sequence similarities and topology of the phylogenetic tree, we suggest that both AcaTPO and LvTPO can be classified as peroxidasin orthologs.

Temporal and spatial transcription pattern of TPO orthologs in Aplysia and sea urchin

We used probes from partial sequences to characterize expression patterns of LvTPO in sea urchin larvae (Fig. 5A–F) and of AcaTPO in the CNS of *Aplysia* (Fig. 5G–I).

Figure 5A and D presents a planktonic larva of *L. variegatus* 7 days after fertilization and Figure 5B and E is a pre-metamorphic stage of *L. variegatus* 11 days after fertilization. In both stages we detected expression of LvTPO in distinct cell clusters around the mouth region (M), in the stomach (St) and the ectoderm of the juvenile rudiment (R). At later developmental stages (Fig. 5B) we also detected transcription in the pedicellariae (Pe), characteristic skeletal structures that start forming during late larval development and are maintained in the adult sea urchin. No staining was detected in control larvae where we used LvTPO sense probe (Fig. 5C). Note however that some control larvae showed background staining in the arms and very weak staining in the stomach region (not shown). Figure 5F summarizes the transcription patterns resulting from the antisense probe schematically.

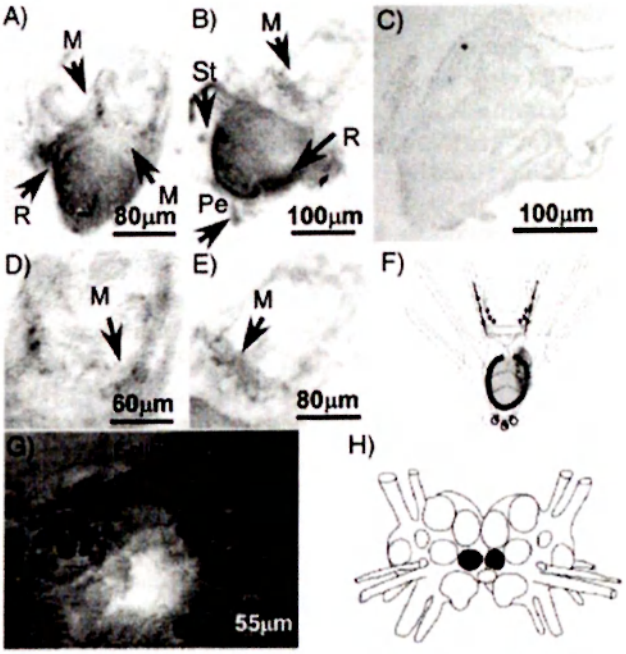

Fig. 5. We performed in situ hybridizations on *Lytechinus variegatus* larval stages (**A–F**) and the central nervous system of *Aplysia californica* (**G** and **H**) using LvTPO and AcaTPO RNA probes, respectively. We detected ubiquitous expression of LvTPO throughout development in the stomach region and the mouth region, the ectoderm of the juvenile rudiment and the stomach. Some of the more specific and pronounced expression occurs in specific cell clusters around the mouth as shown in the close-up images presented in (D,E). (C) Control (sense probe) larvae presented in (C) do not show any staining. Note however that some control larvae showed background staining in the arms and very weak staining in the stomach region (not shown); larva in (A,D) is 7 days old, larva in (B,E) is 11 days old. (F) summarizes schematically the transcription patterns found in (A,B). (G) Neurons of two symmetrical F-clusters (a proposed neuroendocrine center located in the cerebral ganglia of *Aplysia*) stain positive in in situ hybridization with antisense probe (localization of cluster within the cerebral ganglion is schematically represented in (H). (J) AcaTPO sense probe did not produce any positive staining (data not shown). R: juvenile rudiment; M: mouth; PE: Pedicelaria; St: stomach. The arrows in the figure showing larvae of *Lytechinus variegatus* and the cerebral ganglia of *Aplysia californica* are pointing anterior. The cerebral ganglia of *Aplysia californica* are shown from the dorsal side.

In the *Aplysia* CNS, expression of the AcaTPO was detected in the cerebral ganglia, specifically in the area of neurosecretory F-cluster (Fig. 5G). No staining was detected in the control (not shown). The overall morphology of the cerebral ganglion and the F-cluster are depicted in Figure 5H.

Database analysis

We screened EST and genomic databases of *S. purpuratus* (NCBI) for TH signaling-related transcripts. We cloned three new transcripts from the sea urchin potentially involved in TH signaling. These are sulfotransferase (Sp_SULT; DQ176319), retinoic X receptor (Sp_RXR; DQ176321 same sequence as XM_779153) and a new isoform of chicken ovalbumin upstream promoter (Sp_COUP01; DQ176320). Finally, several components of the TH signaling pathway have now been annotated from the newly released *S. purpuratus* genome. These are: thyroid hormone receptor (TR) (gb XP_79257), TR-associated and interacting proteins (XP_795219, XP_780945, XP_786427, XP_796020, XP_781449, XP_791710, XP_785120, XP_791710, XP_790753, XP_795235, XP_790569, XP_790999, XP_792847, XP_789723, XP_784390, XP_780593, XP_787043, XP_780442, XP_780362, XP_783595), thyrotropin receptor precursor (XP_782262).

DISCUSSION

Data presented here provide evidence for thyroid hormone-related signaling in the Mollusc *A. californica* (sea hare) and the echinoderm *L. variegatus* (sea urchin). Our analysis shows that THs affect the development to metamorphosis in sea urchins significantly and that both the sea hare and the sea urchin can synthesize THs endogenously. Furthermore, we cloned two new peroxidases from these two species and the expression patterns in larvae and adults suggest a possible role of these genes in development and metabolism. Together, this new evidence provides support for the hypothesis that endogenous TH synthesis is not a synapomorphy of chordates. Finally we propose a new model of endogenous TH synthesis via peroxidases among non-chordate metazoa.

Endogenous TH synthesis in the sea hare and sea urchin

Numerous reports have been published on TH-related function in various invertebrate phyla (Fig. 1, *reviewed in* Eales, '97). However, the mechanisms and specific TH signaling pathways are presently unknown. Recent studies have documented TH-like signaling among Echinodermata (Chino et al., '94; Johnson and Cartwright, '96; Suyemitsu et al., '97; Johnson, '98; Saito et al., '98; Suyemitsu, 2000; Hodin et al., 2001; Heyland and Hodin, 2004) a sister taxon to chordates. These data suggest that TH-like compounds play a critical role in echinoderm larval development and metamorphosis including preliminary evidence for endogenous hormone synthesis (Chino et al., '94; Saito et al., '98; Heyland and Hodin, 2004), involvement of TH signaling in the phenotypic plastic response to food of echinoid larvae (Heyland and Hodin, 2004) and the timing of attaining metamorphic competence of echinoderm larvae (Chino et al., '94; Suyemitsu et al., '97; Saito et al., '98; Suyemitsu, 2000; Hodin et al., 2001; Heyland and Hodin, 2004).

Our TLC analysis reveals that the sea urchin and the sea hare incorporate iodine into TH similar to T4 and T3, respectively, which we interpret as evidence for endogenous TH synthesis. These findings are further backed up by ELISA measurements of THs in larvae and adult of these organisms. Intriguingly the synthesis of THs is inhibited by the TPO inhibitor thiourea. It is not clear though on what level the synthesis of these molecules is inhibited. Since thiourea treatment not only decreases the amount of hormone synthesized but also decreases the intensity of the non-specifically incorporated iodine, it is possible that other processes involved in iodine uptake and/or binding are affected by the inhibitor. The fact that $KClO_4$ does not affect the uptake of iodine tells us that iodine uptake/concentration mechanisms in echinoderms are different from those found in vertebrates. $KClO_4$ is a potent competitive inhibitor of iodine uptake into the thyroid gland that is mediated via the sodium-iodine symporter. In fact it is conceivable that in marine invertebrate larvae, iodine uptake from seawater occurs via epithelial diffusion as it is well known from the gut epithelium of humans and other vertebrates.

Thiourea effects on sea urchin larvae from this study were very different from effects that we previously described on larvae of the sand dollar *D. excentricus* (Heyland and Hodin, 2004). While thiourea had a significant effect on arm length, SS and RS in *D. excentricus* larvae (Heyland and Hodin, 2004), these effects were either absent and/or much weaker in the sea urchin. We interpret this as evidence that endogenous sources of hormones are more important for sand dollar larval development than for sea urchin larval development. These findings are particularly interesting in the context of our previously stated hypothesis that feeding larvae from different echinoderm clades have different abilities to

synthesize THs endogenously and that feeding larvae with an increased capacity for endogenous TH synthesis can be found specifically in clades in which non-feeding development evolved frequently (Heyland and Hodin, 2004; Heyland et al., 2005). However, alternatively this difference could also be explained by the difference in experimental design between the two studies. While we exposed sand dollar larvae continuously to thiourea in the presence of algal food, sea urchin larvae in the present study were exposed to the inhibitor in the absence of food over a limited period of time. The advantage of the design used in this study is that indirect effects of inhibitor on algae can be excluded and in fact it could be such effects that are ultimately responsible for the differences seen between sand dollar and sea urchin larvae. We propose to use the design used in this study for future experiments to exclude the indirect effects described above.

Iodine simulates the effects of T4 on rudiment and stomach morphogenesis in the sea urchin. Both iodine and THs can originate from exogenous sources. Chino et al. ('94) first emphasized the presence of THs in unicellular algae that are commonly used as larval nutrition. Our recent study confirmed measurements of THs in algae (Heyland and Moroz, 2005). Furthermore, the ability of endogenous hormone synthesis, although present, appears to be reduced in feeding larvae, suggesting that some of the hormone may be supplied from exogenous sources such as algae. Iodine concentration is generally much higher in marine than in terrestrial environments, but even in the oceans, iodine concentrations can vary significantly (Truesdale and Bailey, 2002). The potentially dual source of hormone and/or iodine on development is reflected in the expression patterns of LvTPO in the stomach and the adjacent surface of the juvenile rudiment. These are also candidate structures through which iodine and THs could be incorporated into the larva.

THs as developmental and metabolic regulators

The effects of T4 on *L. variegatus* are well in line with these previous findings in that we were able to confirm an acceleration of development in the sea urchin that is very similar to the sand dollar *D. excentricus*. This acceleration is not only represented in an earlier attainment of metamorphic competence but also in the earlier appearance of spine precursors in the juvenile rudiment.

Pharmacological effects of THs on *A. californica* have been previously shown: A sodium-phosphate and sodium-sulfate symporter in the *Aplysia* foregut epithelium was stimulated by triiodothyronine (T3) (Gerencser et al., 2002a,b) suggesting that TH may play a role in phosphate and sulfate homeostasis. Our data indicate that in contrast to *L. variegatus* larvae, *Aplysia* juveniles primarily synthesize T3 and not T4. This result suggests that TH signaling in *A. californica* is likely not mediated via TRs. TRs have a very high affinity to T3 and in vertebrates the pre-hormone T4 is converted to T3 only in the target cell which is a crucial mechanism to ensure the specificity of the hormone. In addition to their genomic action, THs can act via a variety of non-genomic pathways that include, for example, MAPK transduction pathways (Davis and Davis, '96). A number of such non-genomic actions are equally responsive to T4 and T3 (Davis and Davis, '96; Hulbert, 2000). Finally, some preliminary recent evidence suggests the presence of a TR ortholog in the sea urchin genome (Genbank accession number XM_784395). Our search of the *Aplysia* neuronal transcriptome (Moroz et al., unpublished data) did not reveal a TR ortholog.

TH signaling in the nervous system

The transcription of AcaTPO in the cerebral ganglion of *A. californica* implies the exciting possibility that THs signal on the level of the CNS in non-chordate deuterostomes. Although we did not establish a functional link between the peroxidase we cloned and TH function it is worth mentioning that the areas of F- and C-clusters of the *Aplysia* CNS, where AcaTPO is expressed, are part of the neurosecretory center that is able to synthesize insulin-like peptides, cerebrin and possibly other peptide hormones yet to be identified (Rubakhin et al., '99). If AcaTPO is in fact involved in TH synthesis, these hormones could be critical players in this neuroendocrine network that integrates information from the environment with internal signals in order to fine tune feeding behavior and metabolic functions. Intriguingly, some expression domains of LvTPO are linked to the larval nervous system. Specific cell clusters in the mouth region and later in development in the pedicellariae (defensive structures of larvae and adults) are both elements of the larval nervous system (Burke, '80, '83) which also express nitric

oxide synthase (Bishop and Brandhorst, 2001). Finally the function of TH-related transcripts on the level of the nervous system has been reported in polychaetes (Marcheggiano et al., '85; Davoli et al., '91). *E. foeta* incorporates radioactive iodine, traces of which were detected in the CNS of the worm specifically between neursecretory cells and the neuropile fibers (Davoli et al., '91). Marcheggiano ('85) also detected thyroglobulin-like immunoreactivity in the nervous system of *Eisenia* which had a distinct expression pattern from cholinesterase a protein that has high sequence similarity to one thyroglobulin subunit.

The detection of THs in hemolymph of *Aplysia* finally indicates that these hormones may also act as circulatory hormones with non-neuronal functions related to metabolism and homeostasis. It is therefore crucial to further elucidate the role of THs in *Aplysia* metamorphosis using an experimental approach as we have successfully applied it to various echinoid larvae (Heyland and Hodin, 2004; Heyland et al., 2004).

Have peroxidases been co-opted for thyroid hormone synthesis?

AcaTPO and LvTPO fall into one clade together with peroxidasin from human, *Drosophila* and *C. elegans*. Our phylogenetic analysis shows that this peroxidasin clade is a sister clade to animal peroxidases (*sensu* Taurog, 1999) that have been only identified in chordates and includes genes coding for thyroid, myelo and lactoperoxidases. *Drosophila* peroxidasin shows many important similarities to vertebrate peroxidases as has been shown by Nelson et al. ('94). In fact, this peroxidase has been shown to synthesize THs in vitro (Nelson et al., '94). Furthermore, we were able to identify proximal and distal histidines in LvTPO and AcaTPO. In vertebrate TPOs, these residues are located on opposite sides of the heme and participate in the heterolytic cleavage of the O–O bond, an essential step for the formation of compound I (Poulos and Fenna, '94). This step is necessary for the oxidation of iodide, critical in thyroid hormone synthesis. In fact, the lack of the proximal histidine in an alternatively spliced form of TPO (TPO-2) has been hypothesized to be the cause why this enzyme cannot synthesize T4 (Niccoli et al., '97). Finally, another site critical for TH synthesis, the Ca^{2+} binding domain, is also well conserved in AcaTPO and LvTPO.

The synthesis of THs via TPOs is generally viewed as a synapomorphy of chordates. Two new TPO orthologs that were recently cloned from two ascidian species (urochordata) provide additional support for this hypothesis (Ogasawara et al., '99). Our new findings suggest however that TH synthesis is not restricted to the chordates. Our search for TPO-related genes in these two clades using degenerate PCR and database searches (*A. californica* neuronal transcriptome, Moroz et al., unpublished data) and genomic databases (*S. purpuratus* genome Genbank) however did not reveal any TPO orthologous genes in these clades. We argued recently that various peroxidases could have been co-opted independently in different metazoan lineages for thyroid hormone synthesis (Heyland and Moroz, 2005) due to the presence of specific conserved residues in the catalytic domain of these genes which are necessary for tyrosine cross-linking and iodination (Taurog and Howells, '66; Nelson et al., '94). Moreover, the oxidation of iodide to iodine is a critical step for scavenging reactive oxygen species that could do potential damage to the cell (Venturi et al., 2000; Heyland and Moroz, 2005). The reaction of iodine with tyrosine residues removes potentially poisonous iodine from the cell. It has therefore been proposed that the production of iodine and the subsequent iodination of tyrosines via peroxidase action represent a mechanism that primarily evolved as a cellular response to deal with iodine from the environment (Venturi et al., 2000; Heyland and Moroz, 2005). It will be therefore interesting for future studies to investigate the hypothesis that various invertebrate peroxidases are involved in TH synthesis and/or metabolism.

EST and genomic screening for TH-related transcripts in Molluscs and echinoderms

Apart from vertebrates, the first molecular insight in understanding TH signaling in basal chordates has been obtained from the sequenced genome of the urochordate *C. intestinalis*. A whole battery of molecules was found that is potentially involved in TH function (Dehal et al., 2002). Moreover *C. intestinalis* possesses an endostyle, the hypothesized homolog to the vertebrate thyroid gland. Ogasawara et al. ('99) have previously provided evidence for the presence of a TPO orthologous gene that is expressed in a specific zone of the ascidian endostyle and could be involved in TH synthesis. We were able to identify and clone several transcripts potentially involved in TH function from the sea urchin

(*S. purpuratus*) genome. The newly released *S. purpuratus* genome furthermore reveals several TH-signaling-related transcripts including TR orthologous genes. Although further analysis is required to confirm the molecular identity of these transcripts, we will here outline some implications of the presence of such elements in Molluscs and echinoderms.

THs signal via TR, factors that regulate transcription upon binding of ligand (TH). These transcription factors recruit various co-regulators for proper regulation of transcription. TRs heterodimerize with retinoic X receptor which we were also able to identify from *S. purpuratus* (DQ176321, see also XP_792571). One putative repressor of TR is chicken ovalbumin upstream promoter (Zhang and Dufau, 2004) that has been previously identified from sea urchins (Chan et al., '92; Kontrogianni-Konstantopoulos et al., '96). We identified a new form of this orphan receptor from *S. purpuratus* (DQ176320). The *S. purpuratus* genome also reveals several TR interacting proteins which might act as co-activators or repressors of TH signaling in echinoderms. In addition to the genomic mode of action of THs via TRs, non-genomic modes of TH action have also been described (Davis and Davis, '96; Brent, '99; Hulbert, 2000) in which T4, T2 or rT3 can have significantly stronger effects than T3. These signaling pathways are usually characterized by the absence of de novo protein synthesis and a much faster mode of action, properties particularly critical for signaling in the nervous system and circulatory system (*for a recent review see* Hulbert, 2000). These non-genomic modes of TH action should be further investigated in non-vertebrate animals.

Deiodinases transform T4 to T3 which in vertebrates then binds to TRs with high affinity (see above). Another pathway that controls the availability of active T3 involves sulfotransferases (SULTs). These enzymes can transform T4 to rT3 but also have high affinity to various other THs (for review see Visser, '94). We did not identify any deiodinases in *Aplysia* and the sea urchin. However, we were able to retrieve the full-length sequence of a SULT from *S. purpuratus* (DQ176319) that shows high sequence similarity to phenol preferring SULTs belonging to subfamily 1A. Enzymes from this family have high affinity to THs (Strott, 2002). Such SULTs could be involved in the regulation of active THs in echinoid and other marine invertebrate larvae by regulating the iodination state of di-tyrosines.

These preliminary data on TH-related transcripts in *Aplysia* and the sea urchin provide a first step towards identification of TH-related genes in marine invertebrates. In situ hybridizations and RNAi will help to understand whether and how these genes are involved in TH-related function in these species.

ACKNOWLEDGMENTS

We would like to thank Drs. Billie Swalla and Yale Passemaneck for their generous help in the initial steps of this study. Furthermore we would like to thank Drs. Svetlana Maslakova, David Julian, Louis Guillette, Charles Wood, Gustav Paulay, Craig Osenberg, Jason Hodin, Cory Bishop and three anonymous reviewers for their help in improving earlier versions of this manuscript. We would also like to acknowledge the help of Dr. Michael Matz in performing the phylogenetic analysis. Additionally we would like to thank the Whitney Laboratory, the Smithsonian Marine Station at Fort Pierce and The Friday Harbor Laboratories for providing research space for this study. This research was supported by NIH, NSF, Swiss National Science Foundation Post-doctoral Grant to A.H., Link Fellowship to A.H. (contribution number 643) and in part by Packard and McKnight Brain Research Foundation Grants.

LITERATURE CITED

Antheunisse LJ, Lever J. 1956. I^{131}-accumulation in some invertebrates. KNAW 59:562–565.

Bishop CD, Brandhorst BP. 2001. NO/cGMP signaling and HSP90 activity represses metamorphosis in the sea urchin *Lytechinus pictus*. Biol Bull 201:394–404.

Brent GA. 1999. Thyroid hormone action: down novel paths—focus on "Thyroid hormone induces activation of mitogen-activated protein kinase in cultured cells". Am J Physiol Cell Physiol 276:C1012–C1013.

Burke RD. 1980. Neural control of echinoid metamorphosis. Am Zool 20:911.

Burke RD. 1983. Neural control of metamorphosis in *Dendraster excentricus*. Biol Bull 164:176–188.

Chan SM, Xu N, Niemeyer CC, Bone JR, Flytzanis CN. 1992. SpCOUP-TF: a sea urchin member of the steroid/thyroid hormone receptor family. Proc Natl Acad Sci USA 89: 10568–10572.

Chino Y, Saito M, Yamasu K, Suyemitsu T, Ishihara K. 1994. Formation of the adult rudiment of sea-urchins is influenced by thyroid-hormones. Dev Biol 161:1–11.

Dai G, Levy O, Carrasco N. 1996. Cloning and characterization of the thyroid iodide transporter. Nature 379:458.

Davis PJ, Davis FB. 1996. Nongenomic actions of thyroid hormone. Thyroid 6:497–504.

Davoli C, Marcheggiano A, Ravagnan G, Minu M, Serafino A, Iannoni C. 1991. Iodination activity in *Eisenia foetida* (Annelida, Oligochaeta). Cell Tissue Res 264:9-14.

Dehal P, Satou Y, Campbell RK, Chapman J, Degnan B, De Tomaso A, Davidson B, Di Gregorio A, Gelpke M, Goodstein DM, Harafuji N, Hastings KE, Ho I, Hotta K, Huang W, Kawashima T, Lemaire P, Martinez D, Meinertzhagen IA, Necula S, Nonaka M, Putnam N, Rash S, Saiga H, Satake M, Terry A, Yamada L, Wang HG, Awazu S, Azumi K, Boore J, Branno M, Chin-Bow S, DeSantis R, Doyle S, Francino P, Keys DN, Haga S, Hayashi H, Hino K, Imai KS, Inaba K, Kano S, Kobayashi K, Kobayashi M, Lee BI, Makabe KW, Manohar C, Matassi G, Medina M, Mochizuki Y, Mount S, Morishita T, Miura S, Nakayama A, Nishizaka S, Nomoto H, Ohta F, Oishi K, Rigoutsos I, Sano M, Sasaki A, Sasakura Y, Shoguchi E, Shin-i T, Spagnuolo A, Stainier D, Suzuki MM, Tassy O, Takatori N, Tokuoka M, Yagi K, Yoshizaki F, Wada S, Zhang C, Hyatt PD, Larimer F, Detter C, Doggett N, Glavina T, Hawkins T, Richardson P, Lucas S, Kohara Y, Levine M, Satoh N, Rokhsar DS. 2002. The draft genome of *Ciona intestinalis*: insights into chordate and vertebrate origins. Science 298:2157–2167.

Eales JG. 1997. Iodine metabolism and thyroid-related functions in organisms lacking thyroid follicles: are thyroid hormones also vitamins? Proc Soc Exp Biol Med 214:302–317.

Eskandari S, Loo DD, Dai G, Levy O, Wright EM, Carrasco N. 1997. Thyroid Na^+/I^- symporter. Mechanism, stoichiometry, and specificity. J Biol Chem 272:27230–27238.

Gerencser GA, Cornette KM, Zhang J. 2002a. Thyroid-hormone-induced phosphate absorption in *Aplysia californica* gut is mediated through protein synthesis. Can J Physiol Pharmacol 80:1195–1198.

Gerencser GA, Levin R, Zhang JL. 2002b. Sulfate absorption in *Aplysia californica* gut: thyroid hormone stimulation. Can J Zool 80:964–966.

Heyland A, Hodin J. 2004. Heterochronic developmental shift caused by thyroid hormone in larval sand dollars and its implications for phenotypic plasticity and the evolution of nonfeeding development. Evolution 58:524–538.

Heyland A, Moroz LL. 2005. Cross-kingdom hormonal signaling: an insight from thyroid hormone functions in marine larvae. J Exp Biol 208:4355–4361.

Heyland A, Reitzel AM, Hodin J. 2004. Thyroid hormones determine developmental mode in sand dollars (Echinodermata: Echinoidea). Evol Dev 6:382–392.

Heyland A, Hodin J, Reitzel AM. 2005. Hormone signaling in evolution and development: a non-model system approach. Bioessays 27:64–75.

Hodin J, Hoffman J, Miner BJ, Davidson BJ. 2001. Thyroxine and the evolution of lecithotrophic development in echinoids. In: Barker MF, editor. Proceedings of the 10th International Echinoid Conference, Dunedin, New Zealand.

Huelsenbeck JP, Ronquist F. 2001. Mrbayes: Bayesian inference of phylogenetic trees. Bioinformatics 17:754–755.

Hulbert AJ. 2000. Thyroid hormones and their effects: a new perspective. Biol Rev 75:519–631.

Johnson LG. 1998. Stage-dependent thyroxine effects on sea urchin development. N Z J Mar Fresh 32:531–536.

Johnson LG, Cartwright CM. 1996. Thyroxine-accelerated larval development in the crown-of-thorns starfish, *Acanthaster planci*. Biol Bull 190:299–301.

Jones DT, Taylor WR, Thornton JM. 1992. The rapid generation of mutation data matrices from protein sequences. Comput Appl Biosci 8:275–282.

Kingsley RJ, Corcoran ML, Krider KL, Kriechbaum KL. 2001. Thyroxine and vitamin D in the gorgonian *Leptogorgia virgulata*. Comp Biochem Physiol A 129:897–907.

Kontrogianni-Konstantopoulos A, Vlahou A, Vu D, Flytzanis CN. 1996. A novel sea urchin nuclear receptor encoded by alternatively spliced maternal RNAs. Dev Biol 177: 371–382.

Kriegstein AR. 1977. Stages in the post-hatching development of *Aplysia californica*. J Exp Zool 199:275–288.

Marcheggiano A, Iannoni C, Davoli C. 1985. Thyroglobulin-like immunoreactivity in the nervous system of *Eisenia foetida* (Annelida, Oligochaeta). Cell Tissue Res 241:429–433.

Matz MV. 2003. Amplification of representative cDNA pools from microscopic amounts of animal tissue. Methods Mol Biol 221:103–116.

Matz MV, Alieva NO, Chenchik A, Lukyanov S. 2003. Amplification of cDNA ends using PCR suppression effect and step-out PCR. Methods Mol Biol 221:41–49.

McLachlan SM, Rapoport B. 1992. The molecular biology of thyroid peroxidase: cloning, expression and role as autoantigen in autoimmune thyroid disease. Endocr Rev 13:192–206.

McNabb FMA. 1992. Thyroid hormones. Englewood Cliffs: Prentice-Hall.

Nelson RE, Fessler LI, Takagi Y, Blumberg B, Keene DR, Olson PF, Parker CG, Fessler JH. 1994. Peroxidasin: a novel enzyme-matrix protein of *Drosophila* development. EMBO J 13:3438–3447.

Niccoli P, Fayadat L, Panneels V, Lanet J, Franc JL. 1997. Human thyroperoxidase in its alternatively spliced form (TPO2) is enzymatically inactive and exhibits changes in intracellular processing and trafficking. J Biol Chem 272: 29487–29492.

Ogasawara M. 2000. Overlapping expression of amphioxus homologs of the thyroid transcription factor-1 gene and thyroid peroxidase gene in the endostyle: insight into evolution of the thyroid gland. Dev Genes Evol 210: 231–242.

Ogasawara M, Di Lauro R, Satoh N. 1999. Ascidian homologs of mammalian thyroid peroxidase genes are expressed in the thyroid equivalent region of the endostyle. J Exp Zool 285:158–169.

Peterson KJ, Eemisse DJ. 2001. Animal Phylogeny and the Ancestry of Bilaterians: Inferences From Morphology and 18s Rdna Gene Sequences. Evolution & Development. 3: 170–205.

Poulos TL, Fenna RE. 1994. Peroxidases: structure, function, and engeneering. In: Siegel H, Siegel A, editors. New York: Marcel Dekker, Inc. p 22–75.

Rubakhin SS, Li LJ, Moroz TP, Sweedler JV. 1999. Characterization of the *Aplysia californica* cerebral ganglion F cluster. J Neurophysiol 81:1251–1260.

Ruppert EE, Cameron CB, Frick JE. 1999. Endostyle-like features of the dorsal epibranchial ridge of an enteropneust and the hypothesis of dorsal-ventral axis inversion in chordates. Invertebr Biol 118:202–212.

Saito M, Seki M, Amemiya S, Yamasu K, Suyemitsu T, Ishihara K. 1998. Induction of metamorphosis in the sand dollar *Peronella Japonica* by thyroid hormones. Dev Growth Differ 40:307–312.

Schmidt HA, Strimmer K, Vingron M, von Haeseler A. 2002. TREE-PUZZLE: maximum likelihood phylogenetic analysis using quartets and parallel computing. Bioinformatics 18: 502–504.

Spangenberg DB. 1967. Iodine induction of metamorphosis in *Aurelia*. J Exp Zool 165:441–449.

Spangenberg DB. 1971. Thyroxine induced metamorphosis in *Aurelia*. J Exp Zool 178:183–189.

Spangenberg DB. 1974. Thyroxine in early strobilation in *Aurelia aurita*. Am Zool 14:825–831.

Strathmann MF. 1987. Reproduction and larval development of marine invertebrates of the northern Pacific Coast. Seattle: University of Washington Press.

Strott CA. 2002. Sulfonation and molecular action. Endocr Rev 23:703–732.

Suyemitsu T. 2000. Thyroid hormones and metamorphosis of Sea Urchin Larvae. Zygote 8:S52–S53.

Suyemitsu T, Saito M, Ishihara K. 1997. Thyroid hormones and metamorphosis of sea urchins. In: Kawashima S, Kikuyama S, editors. Advances in comparative endocrinology. Proceedings of the 13th international congress of comparative endocrinology. Monduzzi editore s.p.a, Bologna, Italy. p 381–386.

Swalla BJ, White ME, Zhou J, Jeffery WR. 1994. Heterochronic expression of an adult muscle actin gene during ascidian larval development. Dev Genet 15:51–63.

Taurog A. 2000. Hormone synthesis: thyroid iodine metabolism. In: Braverman LE, Utiger RD, editors. The Thyroid, 8th edition. Philadelphia: Lippincott Williams & Wilkins. p 61–85.

Taurog A, Howells EM. 1966. Enzymatic iodination of tyrosine and thyroglobulin with chloroperoxidase. J Biol Chem 241: 1329–1333.

Thompson JD, Higgins DG, Gibson TJ. 1994. CLUSTAL W: improving the sensitivity of progressive multiple sequence alignments through sequence weighting, position specific gap penalties and weight matrix choice. Nucleic Acids Res 22:4673–4680.

Tong W, Chaikoff IL. 1961. I^{131} utilization by aquarium snail and cockroach. Biochim Biophys Acta 48:347–349.

Truesdale VW, Bailey GW. 2002. Iodine distribution in the Southern Benguela system during an upwelling episode. Cont Shelf Res 22:39–49.

Venturi S, Donati FM, Venturi A, Venturi M. 2000. Environmental iodine deficiency: a challenge to the evolution of terrestrial life? Thyroid 10:727–729.

Visser TJ. 1994. Role of sulfation in thyroid hormone metabolism. Chem Biol Interact 92:293–303.

Yen PM. 2001. Physiological and molecular basis of thyroid hormone action. Physiol Rev 81:1097–1142.

Zhang Y, Dufau ML. 2004. Gene silencing by nuclear orphan receptors. Vitam Horm 68:1–48.

Structural basis of hereditary coproporphyria

Dong-Sun Lee*, Eva Flachsová†, Michaela Bodnárová†, Borries Demeler‡, Pavel Martásek†, and C. S. Raman*§

*Department of Biochemistry and Molecular Biology, University of Texas Medical School, Houston, TX 77030; †Department of Pediatrics, Center of Applied Genomics, First School of Medicine, Charles University, 121 09 Prague, Czech Republic; and ‡Department of Biochemistry, University of Texas Health Science Center, San Antonio, TX 78229

Communicated by Ferid Murad, University of Texas-Houston Health Science Center, Houston, TX, August 1, 2005 (received for review March 12, 2004)

Hereditary coproporphyria is an autosomal dominant disorder resulting from the half-normal activity of coproporphyrinogen oxidase (CPO), a mitochondrial enzyme catalyzing the antepenultimate step in heme biosynthesis. The mechanism by which CPO catalyzes oxidative decarboxylation, in an extraordinary metal- and cofactor-independent manner, is poorly understood. Here, we report the crystal structure of human CPO at 1.58-Å resolution. The structure reveals a previously uncharacterized tertiary topology comprising an unusually flat seven-stranded β-sheet sandwiched by α-helices. In the biologically active dimer ($K_D = 5 \times 10^{-7}$ M), one monomer rotates relative to the second by ~40° to create an intersubunit interface in close proximity to two independent enzymatic sites. The unexpected finding of citrate at the active site allows us to assign Ser-244, His-258, Asn-260, Arg-262, Asp-282, and Arg-332 as residues mediating substrate recognition and decarboxylation. We favor a mechanism in which oxygen serves as the immediate electron acceptor, and a substrate radical or a carbanion with substantial radical character participates in catalysis. Although several mutations in the CPO gene have been described, the molecular basis for how these alterations diminish enzyme activity is unknown. We show that deletion of residues (392–418) encoded by exon six disrupts dimerization. Conversely, harderoporphyria-causing K404E mutation precludes a type I β-turn from retaining the substrate for the second decarboxylation cycle. Together, these findings resolve several questions regarding CPO catalysis and provide insights into hereditary coproporphyria.

coproporphyrinogen oxidase | oxidative decarboxylation | mitochondria | x-ray crystallography

The terminal three steps of heme biosynthesis occur within the mitochondria (1, 2). First, coproporphyrinogen III is converted to protoporphyrinogen IX in the intermembrane space (3, 4) by coproporphyrinogen oxidase (CPO) (5, 6). Thus, CPO contains an unusually long (110 residues) N-terminal targeting sequence, required for its import into the mitochondria (7, 8). The substrate for CPO is generated in the cytosol (9) by uroporphyrinogen decarboxylase, and the precise mechanism by which it enters the mitochondria remains to be elucidated. Second, protoporphyrinogen oxidase mediates the six electron oxidation of protoporphyrinogen to protoporphyrin IX. This enzyme is localized to the cytoplasmic side of the inner mitochondrial membrane. Third, ferrochelatase inserts the ferrous iron to generate heme within the matrix of the mitochondria. Hence, the heme biosynthetic pathway is not only partitioned between mitochondria and cytosol, but the last three enzymes are compartmentalized within the mitochondria.

Partial deficiency of CPO leads to hereditary coproporphyria (HCP), an acute hepatic porphyria inherited in an autosomal dominant fashion (10–12). The disease is characterized by abdominal pain, neuropsychiatric symptoms, and/or cutaneous photosensitivity (13). If diagnosed early, HCP can be treated with a high carbohydrate diet and i.v. administration of heme in the form of heme arginate (14). In the majority of heterozygous HCP patients, CPO activity is reduced to ~50% (15–17), resulting in the excretion of coproporphyrin in urine and stool. In rare homozygous cases, enzyme activity decreases to <10% (18–20). Other factors, including drugs, alcohol, stress, or infection, can precipitate HCP in susceptible individuals (21). Since the cloning of human CPO gene (22, 23), several mutations that diminish enzyme activity have been identified (24).

CPO is an extraordinary enzyme of particular interest to chemistry and medicine. As a homodimer (25), it catalyzes the oxidative decarboxylation of propionic acid side chains of rings A and B of coproporphyrinogen III (refs. 26–29 and Fig. 1*A*) without using metals (25, 27, 35), reducing agents, thiols, prosthetic groups, organic cofactors, or modified amino acids (36). Whereas the stereochemistry of this reaction has been worked out (31, 32), the molecular oxygen consumption presents an interesting mechanistic puzzle. From a clinical standpoint, a well defined correlation between the genotype and severity of disease is lacking (34). Thus, unlike other hepatic porphyrias, heterozygotes carrying mutations known to cause HCP in homozygotes have the propensity to develop disease.

Here, we describe the high-resolution crystal structure of human CPO and provide molecular mechanisms to explain how disease-causing mutations suppress enzyme activity. We also offer a detailed picture of the active site residues and elaborate on catalytic mechanism(s).

Materials and Methods

Protein Preparation, Crystallization, and Structure Determination. Human CPO was expressed and purified as described (25). Several attempts to crystallize this protein failed because of time-dependent proteolytic cleavage (Fig. 1*B*). Therefore, we devised a cross-seeding strategy to obtain diffraction-quality crystals, details of which are described in *Supporting Text*, which is published as supporting information on the PNAS web site. The structure was determined by experimental phasing using selenomethionine-substituted crystals. The crystallographic data statistics are shown in Table 1, which is published as supporting information on the PNAS web site.

Equilibrium Analytical Ultracentrifugation. One hundred twenty microliters of wild-type human CPO was sedimented to equilibrium at two different loading concentrations (A_{280} of 0.32 and 0.4), five different speeds (18.0, 22.1, 23.4, 26.2, and 28.0 krpm), and at 4°C in a double-sector, epon-filled centerpieces by using an AN60 TI rotor in a Beckman Optima XL-A analytical ultracentrifuge. Scans were taken at 280 nm, once equilibrium was established, by scanning with 20 averages at a 0.001-cm radial step size setting. A detailed account of the methods used in data analysis is provided in *Supporting Text*.

This work was presented at the Gordon Conference on Chemistry and Biology of Tetrapyrroles, July 25–30, 2004, Salve Regina University, Newport, RI, and also in part at the Porphyrins and Porphyrias Meeting, September 21–24, 2003, Prague, Czech Republic [Mikula, I., Bodnárová, M., Lee, D.-S., Flachsová, E., Rosipal, R., Zeman, J., Moroz, L., Raman, C. S. & Martásek, P. (2003) *Physiol. Res.* 52, 18S (abstr.)].

Freely available online through the PNAS open access option.

Abbreviations: HCP, hereditary coproporphyria; CPO, coproporphyrinogen oxidase.

Data deposition: The atomic coordinates and structure factors have been deposited in the Protein Data Bank, www.pdb.org (PDB ID code 2AEX).

§To whom correspondence should be addressed. E-mail: c.s.raman@uth.tmc.edu.

www.pnas.org/cgi/doi/10.1073/pnas.0506557102

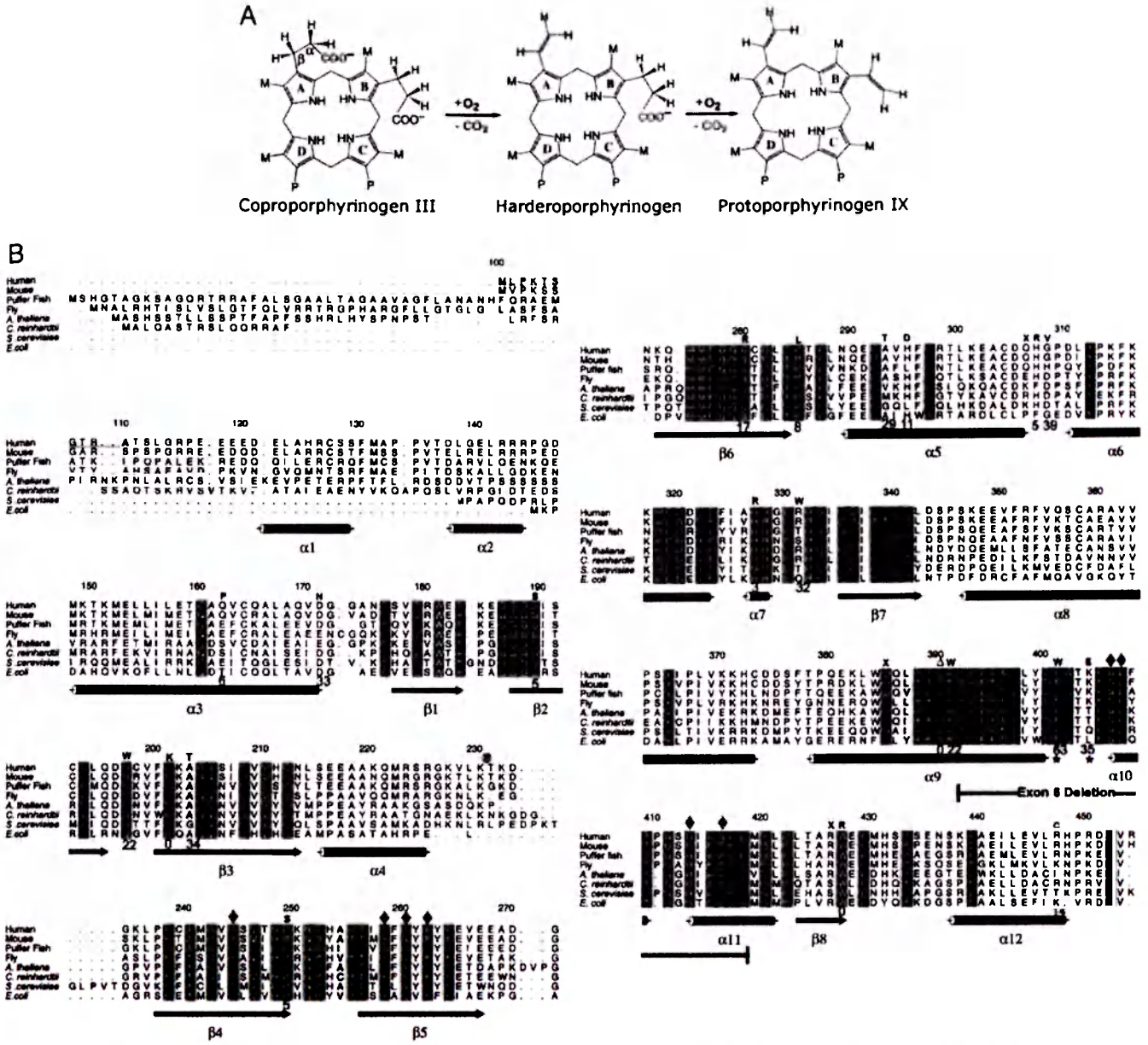

Fig. 1. CPO chemistry and sequence conservation. (*A*) Reaction catalyzed by CPO involves both oxidation and decarboxylation (5). CPO sequentially decarboxylates (26, 30) the propionates attached to A and B rings without affecting those on C and D rings. A hydrogen atom from the β-position of the propionate side chain also is removed at each step (31, 32). The chemical identity of the oxidation end product(s) remains to be elucidated. M = CH_3 and P = $CH_2.CH_2.COO^-$. (*B*) Sequence alignment, secondary structure, and location of HCP-causing mutations in human CPO. The first 110 amino acids are absent in the mature enzyme, for they are part of a mitochondrial targeting signal that is cleaved upon import. In the alignment (generated by using AMPS and ALSCRIPT) red represents absolute identity over all sequences present in that part of the alignment. Database of Secondary Structure of Proteins-derived (33) secondary structural assignments are shown directly below the alignment with cylinders indicating α-helices and arrows denoting β-strands. Mutations known to cause HCP are indicated by one letter codes above the human sequence. The enzymatic activity of these variants (24, 34) are shown in blue (% relative to native enzyme). An asterisk denotes residues that affect the second decarboxylation step. Residues that make contact with citrate are indicated by diamonds. ∞, proteolytic cleavage site.

Results and Discussion

Quality of the Crystal Structure. The electron density for the CPO structure is continuous and well defined. The real space correlation coefficient (37) is excellent, and there are no residues in disallowed regions of the Ramachandran plot. An example electron-density map is shown in Fig. 2*A*. Some indicators of model quality are detailed in Table 1.

The Protein Fold. CPO assumes a previously unknown tertiary topology characterized by a large seven-stranded β-sheet that is flanked on both sides by α-helices (Fig. 2*B*). The up-and-down β-strands are similar to porins, but the β-sheet in CPO is flat (Fig. 2*C*) and does not form a barrel. The T fold, which was predicted to share structural similarities with CPO (38), also has some resemblance to porins because of the long β-strands, but the β-sheet in the T fold is curved as in porin. Moreover, the T fold has helices on one side of the sheet, but these helices are in a long collapsed hairpin β-α-α-β motif, whereas the connectivity is completely different in CPO.

The flatness of the up-and-down β-sheet in CPO is striking (Fig.

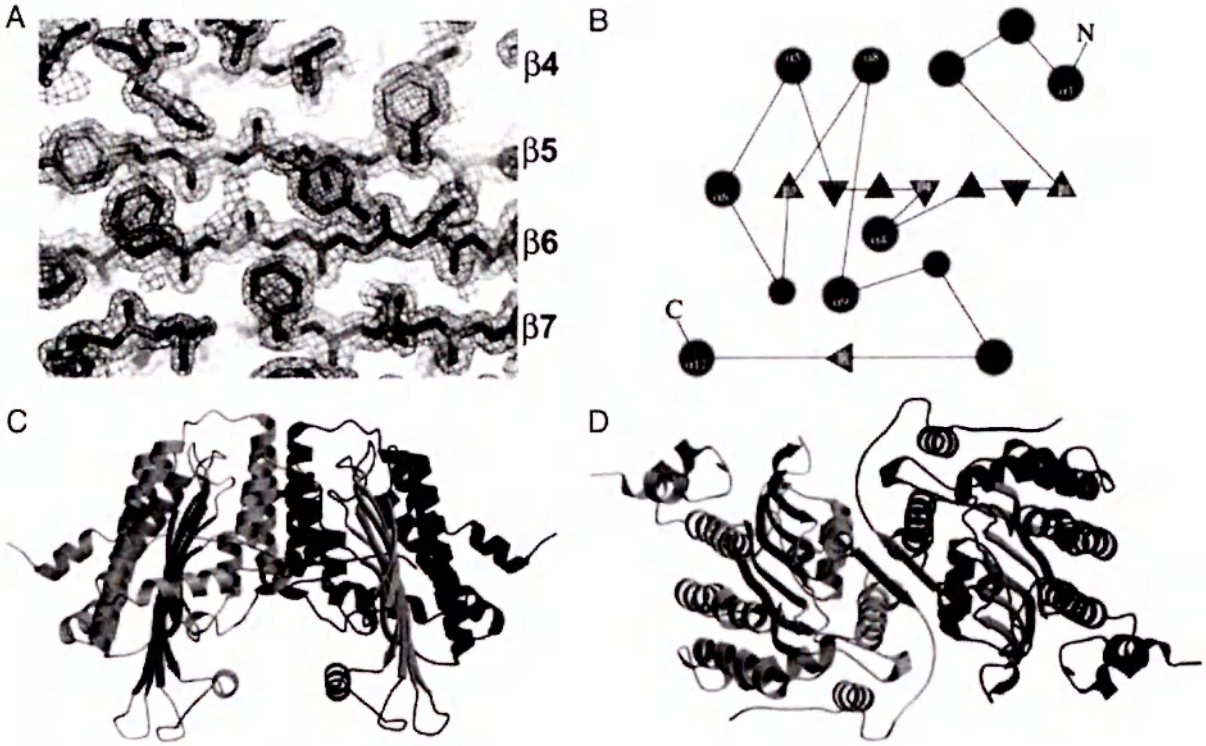

Fig. 2. Structure of human CPO. (*A*) $2F_o - F_c$ electron density map (contoured at 1.5 σ) at 1.58 Å with a final model in place. The identity of the β-strands are shown on the right. (*B*) Topology diagram illustrating the organization of secondary structural elements in human CPO. Filled circles and triangles represent α-helices and β-strands, respectively. (*C*) Tertiary topology and quaternary structure. (*D*) Dimer interface.

2*C*). In contrast, seven-stranded β-sheet-containing enzymes usually contain a twisted (TauD; ref. 39) or highly curved (thiol ester dehydrase; ref. 40) β-sheet whose convex or the apolar concave side, respectively, is flanked by helices. Furthermore, in the dehydrase, eight β-bulges contribute effectively toward introducing strong curvature into the sheet. There are only three β-bulges in CPO. The flatness of the CPO sheet is very likely enabled by the abundance of Gly residues found within the β-strands (β2, β3, β4, β6, and β7). In this regard, Richardson and Richardson (41) have noted that high glycine content helps allow either very high or very low curl or twist of β-sheets.

CPO Functions as a Homodimer. The dimensions of the dimer are ≈80 × 60 × 60 Å. The two subunits of the CPO homodimer are related by an ≈40° rotation of one monomer relative to another (Fig. 2*D*). This rotation is a hinge-like motion about the crystallographic 2-fold axis located roughly parallel to the β-sheet. A dimeric protein the size of CPO (M_r 78,000) is expected to have an accessible surface area (ASA) of ~28,000 Å^2 on the basis of a survey of water-soluble oligomeric proteins (42). Consistent with this prediction, calculations with a 1.4-Å probe reveal that the CPO dimer has an ASA of 28,800 Å^2. Roughly 1,300 Å^2 per subunit are buried in the dimer interface that is relatively flat (planarity, rms = 2.4 Å) and circular-shaped (length/breadth ratio = 0.92). Twenty-two residues (70% evolutionarily conserved) that comprise this interface hail from five different segments of the polypeptide chain (see Fig. 6, which is published as supporting information on the PNAS web site). Interestingly, β8 is not part of the flat β-sheet, but instead pairs up in an antiparallel fashion, with the corresponding β-strand from the second subunit to generate key contacts at the dimer interface (Fig. 2*D*). Overall, the interface is made up of 64% nonpolar atoms and 36% polar atoms. Ten intersubunit H bonds also contribute to the dimer stability (Fig. 6). Salt bridges and water-bridged interactions are absent. Taken together, the interacting surface on the CPO monomer is a hydrophobic patch. All of the parameters we have used to describe the CPO interface are in excellent agreement with those found in other homodimers (43, 44). Thus, it is extremely unlikely that CPO will function as a monomer. To quantitatively assess the solution stability of CPO, we have performed analytical ultracentrifugation. The CPO equilibrium distribution fit well to a monomer-dimer-tetramer equilibrium (see Fig. 7 and Table 2, which are published as supporting information on the PNAS web site) with a dissociation constant of 0.5 μM (see *Supporting Text*) at 277 K (ΔG_{diss} of ≈8 kcal·mol^{-1}). Consistent with this finding, yeast (45), human (25), and *Escherichia coli* (46) proteins are all dimers in solution. Thus, we conclude that the homodimer is the biologically relevant form of CPO.

CPO Structure Lacks a Transition Metal Center. Although it has been established that human CPO is not a metalloprotein (25, 27, 35), a recent work suggests that Mn^{2+} ion, coordinated tetrahedrally by His residues, participates in catalysis (47). We have screened for metal ions bound to CPO by recording anomalous dispersion effects (48). We subjected both human and bacterial CPO crystals to fluorescence energy scans at the x-ray absorption edge of Cu, Fe, Mn, and Zn. Furthermore, we have grown CPO crystals in the presence of these metal salts and have collected complete anomalous data sets at the maximal f'' values of the absorption edges. Neither the energy scans nor the native anomalous difference Fourier maps provide evidence for bound transition metal ions in CPO. More importantly, the invariant His residues are far apart (14–22 Å) and, therefore, cannot serve as ligands.

The Active Site. During structure refinement, we serendipitously discovered that an electropositive cleft (Fig. 3*A*) near the dimer interface had a molecule of citrate (Fig. 3 *B* and *C*; see also Fig. 8, which is published as supporting information on the PNAS web site) bound to it. This finding is reminiscent of citrate binding to Src SH2

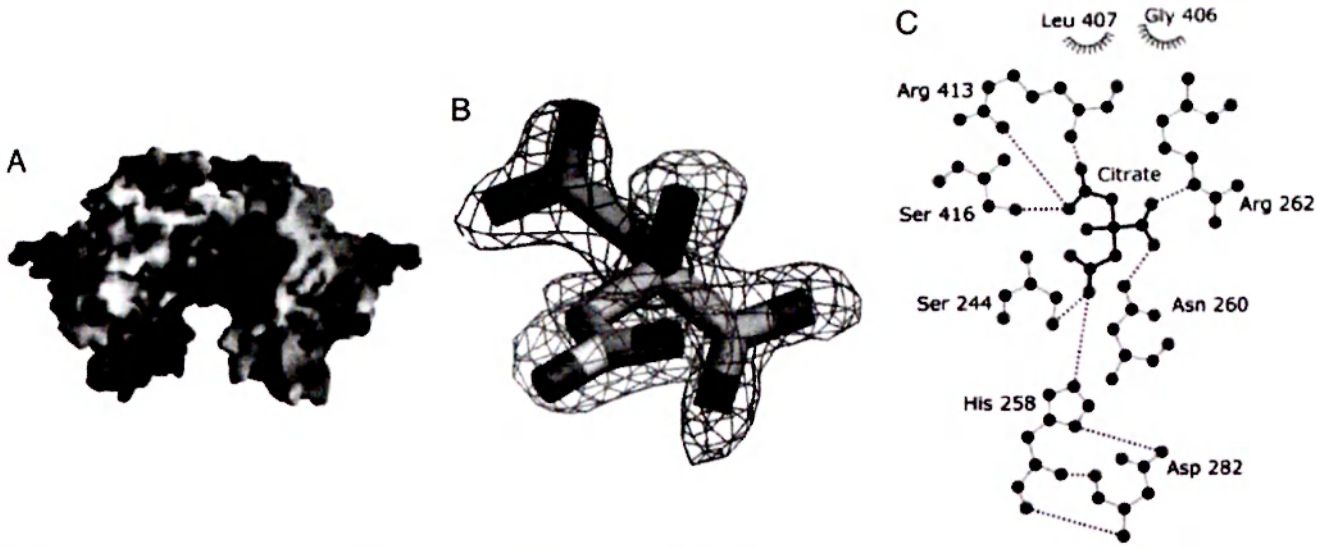

Fig. 3. Active site of human CPO. (*A*) Electrostatic potential mapped on to the molecular surface. The electropositive active site cleft is readily visible. The blue and red contours represent positive and negative potential (full saturation = 10 kT), respectively (figure was generated by using GRASP; ref. 49). (*B*) $F_o - F_c$ omit electron density of citrate bound at the active site. (*C*) Schematic illustration of the amino acid residues that make direct contact with the bound citrate. Dashed lines indicate H bonds, and nonbonded contacts are represented by an arc with spokes radiating toward the ligand atoms (figure was generated by using LIGPLOT; ref. 50).

domain, a fortuitous finding that spearheaded new drug design strategies to treat osteoporosis (51, 52). As in the SH2 case, we too benefited from the use of citrate as a crystallization additive, and it is worth noting that tricarboxylic acid is an elegant mimic of the carboxylate groups in coproporphyrinogen III. In proteins, arginine residues are prime candidates for carboxylate recognition (53), and by comparing >500 unique sequences of CPO (>350 of these sequences are from the environmental samples of the Sargasso Sea; ref. 54), we have identified that Arg-262, Arg-328, Arg-332, and Arg-389 are invariant. In addition, there are no conserved Lys residues. Arg-262 forms a key ionic interaction with citrate and Arg-332 is within striking distance. Other hydrogen-bonded (Gly-411 not shown) and ionic interactions are depicted in Fig. 3*C*. Thus, where coproporphyrinogen III and harderoporphyringen are concerned, we conclude that Arg-262 mediates substrate recognition. His-258 donates a proton in the form of a hydrogen bond from Nδ1 to O1 of Asp-282 and is likely to function as a diad in a manner common to that of many active-site histidines. The H bond of Nδ1 also positions the imidazole ring rather precisely. Thus, we predict that His-258 is in the correct tautomeric state and optimal orientation for catalysis in the free enzyme. Our assignment of a catalytic role for His-258 is supported by two additional observations: (*i*) the His-Asp diad configuration results in a basic lone pair of electrons on Nε2 of His-258, and (*ii*) His258Ala substitution completely abolishes the enzyme activity of mouse CPO (55). Interestingly, the type of residues interacting with citrate and the location of His-Asp/Arg-Ser pairs in CPO is similar to that found in aconitase (56). With the exception of Arg-413 and Ser-416, all of the residues that interact with citrate (Fig. 3*C*) are strictly conserved and reside in strands β4, β5, and β6. Together they form the decarboxylation corridor, the active site region in charge of substrate recognition and catalysis (Fig. 9, which is published as supporting information on the PNAS web site). The invariant Gly-406 and Leu-407, located in close proximity to a region that affects the second step of CPO catalysis (*vide infra*), also make nonbonded contacts with citrate. This part of the active site plays an important role in properly orienting the substrate.

Catalytic Mechanism. CPO catalyzes an unusual metal- and cofactor-independent oxidative decarboxylation. It is well established that CPO abstracts the *pro-S* hydrogen from the methylene group adjacent to the pyrrole ring (Fig. 1*A*), leading to the generation of a vinyl group from the remaining three hydrogens and two carbons without rearrangement (31, 32). Such strong stereoselectivity indicates that CPO strictly constrains the orientation of the substrate in the active site, and our structure provides insights into how this result can be achieved (*vide supra*). However, the precise mechanism for hydrogen abstraction is unknown. Similarities between CPO and urate oxidase have been invoked (38), but the substrate for the latter resembles flavin (57) and, therefore, a well-known redox chemistry is used in catalysis. Because hydride transfer is not an option for CPO, a tyrosyl radical has been proposed in catalysis (36), but substituting conserved Tyr residues (322 and 392) did not affect the activity of the *E. coli* enzyme (47).

We believe that CPO fits in well with the family of metal- and cofactor-free oxygenases, overlooked by other workers in this field, that capitalize on substrate reactivity to generate radical and/or cabanionic intermediates that react rapidly with molecular oxygen (58). Therefore, we favor a mechanism in which molecular oxygen serves as the immediate electron acceptor (D. Arigoni, personal communication) (Fig. 4). Here, the reaction is likely to proceed in two steps, each of which involve a single electron transfer or radical recombination. In the initial step, oxygen diradical removes an electron from the pyrrole nitrogen, resulting in the generation of a substrate radical cation, **2**. Next, superoxide anion reacts with **2** and abstracts the Cβ-H. The "2-center 3-electron" bond (59) shown in **3** provides a rationale for the increased acidity of Cβ-H. A second electron transfer step ensues, resulting in production of the azafulvene cation **4** and H_2O_2. Now, the decarboxylation can proceed readily in light of the electron sink afforded by the positively charged pyrrole ring of **4**. Precedents for this process can be found in pyridoxal-dependent decarboxylases. However, to accommodate Sano's β-hydroxypropionic acid intermediate (60), a Michael addition step **5**, analogous to that of enoyl-CoA hydratase (61), is included. We propose that His-258 is localized next to the pyrrole ring A to assist with the formation of substrate cation.

In our alternate mechanism, a strong base abstracts the Cβ-H proton of coproporphyrinogen III to generate a carbanion intermediate that could react directly with molecular oxygen, through sequential single electron steps, to generate superoxide and a

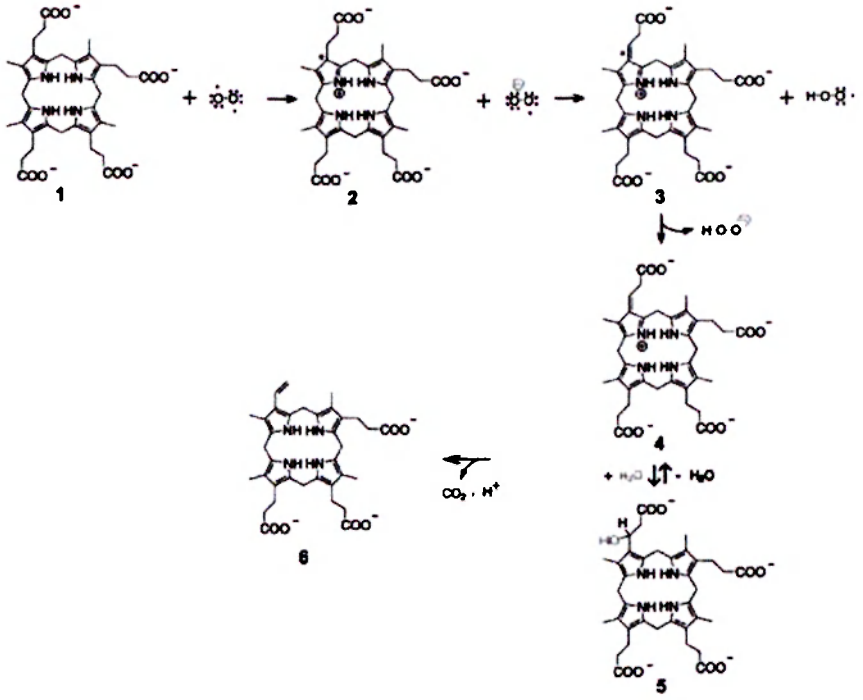

Fig. 4. Catalytic mechanism. Only the first decarboxylation step is shown; the second step is expected to occur in exactly the same manner after the tricarboxylate intermediate undergoes a 90° counterclockwise rotation at the active site (ref. 26 and D. Arigoni, personal communication).

carbon-centered radical. This species would then recombine to yield the hydroperoxide adduct (Cβ-OOH) and can be eliminated with the loss of CO_2. His-258 or Ser-244 (as the alkoxide) can serve as a base. Indeed, there are precedents for Ser/Thr functioning as a base in aconitase (56) and urate oxidase (62). It can be argued that there is no sizeable acidity to Cβ-H ($pK_a \approx 35$), making proton removal from this site difficult. However, precedents exist for deprotonating an unactivated carbon (63) and also for stabilizing high-energy anionic intermediates through nondelocalization mechanisms (64). The ability of O_2 to accept electrons from a singlet carbanion is questionable, for it would result in a high-energy triplet excited state (58). In this regard, we would like to draw a corollary between the oxygenase activities of carbanion-forming enzymes and CPO (65, 66). Spin inversion required for the reaction between a triplet oxygen and a singlet substrate can be facilitated by the formation of a caged radical pair or by activation of the carbanion to the triplet state through geometric distortion (67). In light of their interrupted conjugation, porphyrinogens are well known for adopting an 1,3-alternate conformation characterized by substantial nonplanarity. Furthermore, based on the studies with calixpyrroles (68), anion coordination by the pyrrole nitrogens will generate a cone conformation for the macrocycle. Analogously, H bond interactions between the pyrrole NH groups and a protein carboxylate (69) can provide the geometric distortion required to impart triplet character to a carbanion. We posit that the invariant Asp-400 in CPO is uniquely positioned to help introduce such distortion. Both the free-radical and carbanion mechanisms should yield one equivalent of H_2O_2 for each decarboxylation step. Although CO_2 production has been quantified (30), there is no literature on the stoichiometry of H_2O_2 generation during CPO catalysis.

Structural Basis of Disease. There are >20 naturally occurring HCP mutations (Fig. 1*B* and refs. 24 and 34) and a majority of these mutations lead to substitution of amino acid residues within the structural framework of CPO (Fig. 5). For example, Gln162Pro will disrupt helix α3, and Gly189Ser is expected to perturb strand β2. However, we have found that several mutations distant from the active site can generate dimeric CPO, albeit with little to no activity. Therefore, we will confine our discussion to those mutations for which meaningful insights can be provided solely by inspecting the structure of the native enzyme. First, deletion of the region encoded by exon six, comprising residues 392–418, has been reported in a heterozygous patient, and the resulting protein will be unable to dimerize (Fig. 6). Indeed, we have confirmed this prediction by expressing the variant in *E. coli*. Trp-427, located on strand β8, makes intersubunit interactions, and, therefore, W427R mutation will also affect dimerization. Second, H327R and R328C will perturb the interaction between helix α7 and the dimerization helix

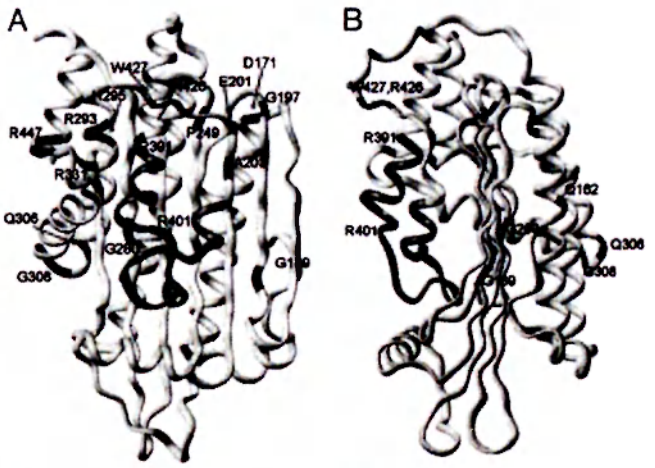

Fig. 5. Residues and structural regions affected by HCP mutations are shown with two different views of the structure. The polypeptide encoded by exon six is shown in cyan. Regions in blue represent mutation sites.

α9 (Fig. 10, which is published as supporting information on the PNAS web site). Third, R331W variant retains sufficient activity to support life in a homozygous setting but can also produce HCP in a heterozygote. Twelve different amino acids are tolerated at position 331 but aromatic residues are not. R331W substitution will abolish the hydrogen bonds between the guanidinium group and the carbonyl of Leu-446 and Arg-447. Interestingly, R447C mutation also results in diminished activity. Finally, K404E causes harderoporphyria, a disease with symptoms unrelated to HCP (34, 70–73). This mutation affects the region that separates helices α9 and α10. Lys-404 is not conserved, and the favored residue at this position is Leu. In the human CPO structure, K404 is part of a type I β-turn. Whereas a positively charged residue at this position is not essential for the second decarboxylation step, introducing a negative charge will produce electrostatic repulsion (or steric hindrance), and the enzyme will lose its ability to hold on to harderoporphyrinogen. From a catalytic standpoint, three key observations illustrate that CPO can function without Lys-404: (*i*) Individuals who are homozygous for K404E do not suffer from acute attacks diagnostic of HCP, (*ii*) harderoporphyrinogen is a good substrate for CPO, and (*iii*) Lys-404 is not evolutionarily conserved. Equally interesting is the R401W mutation that causes atypical HCP in a heterozygous setting. Heterologous expression reveals that this variant, like its K404E counterpart, is defective in the second decarboxylation step. Arg-401 is highly conserved in nearly all CPOs with the exception of *Cytophaga hutchinsoni*, in which a Lys takes its place. Given the strict conservation of a positive charge at this position, the enzyme most likely prevents the release of the intermediate by an ionic interaction with a propionate group that does not undergo decarboxylation (ring C or D). Thus, the primary role for the 401–405 segment is to deter the premature release of intermediate. It does not participate in substrate recognition or decarboxylation. In sum, our work has revealed the identity of active site residues in CPO and has provided previously uncharacterized insights to understand HCP at the molecular level.

Note. While this manuscript was under review, the crystal structure of yeast CPO was reported (74). Consistent with the independent crystallographic results reported here for human CPO, the yeast enzyme crystallized as a dimer and has a similar tertiary topology.

We thank Gerry McDermott (Advanced Light Source, BL 5.0.2) for help with multiwavelength anomalous diffraction data collection; Pierre Nioche for performing the final refinement steps; Sudha Veeraraghavan and Pierre Nioche for figures; Gerard Bricogne for providing BUSTER and Clemens Vonrhein for assistance with using the program; and the Stanford Synchrotron Radiation Laboratories and the Advanced Light Source for generous access to beam time. C.S.R. acknowledges stimulating discussions with Vernon Anderson, Duilio Arigoni, Liisa Holm, Vladimir Kral, Huiying Li, Jane Richardson, Seiyo Sano, John Schloss, Peter Shoolingin-Jordan, Peter Tipton, Sudha Veeraraghavan, and Christopher Walsh and thanks Suzanne Fetzner and Christopher Walsh for sharing their results before publication. This work is supported by the Pew Charitable Trusts through a Pew Scholar Award (to C.S.R.), Robert A. Welch Foundation Grant AU-1574 (to C.S.R.), and Ministry of Education, Youth, and Sports of the Czech Republic Grant 1M 6837805002 (to E.F., M.B., and P.M.). The development of the ULTRASCAN software is supported by National Science Foundation Grant DBI-9974819 (to B.D.).

1. Sano, S., Inoue, S., Tanabe, Y., Sumiya, C. & Koike, S. (1959) *Science* **129**, 275–276.
2. Dailey, H. A. (2002) *Biochem. Soc. Trans.* **30**, 590–595.
3. Elder, G. H. & Evans, J. O. (1978) *Biochem. J.* **172**, 345–350.
4. Grandchamp, B., Phung, N. & Nordmann, Y. (1978) *Biochem. J.* **176**, 97–102.
5. Sano, S. & Granick, S. (1961) *J. Biol. Chem.* **236**, 100–107.
6. Battle, A. M., Del, C., Benson, A. & Rimington, C. (1965) *Biochem. J.* **97**, 731–740.
7. Delfau-Larue, M. H., Martasek, P. & Grandchamp, B. (1994) *Hum. Mol. Genet.* **3**, 1325–1330.
8. Susa, S., Daimon, M., Ono, H., Li, S., Yoshida, T. & Kato, T. (2002) *Tohoku J. Exp. Med.* **55**, 346–353.
9. Shoolingin-Jordan, P. M. (2003) in *The Porphyrin Handbook*, eds. Kadish, K. M., Smith, K. M. & Guilard, R. (Elsevier Science, New York), Vol. 12, pp. 33–74.
10. Berger, H. & Goldberg, A. (1955) *Br. Med. J.* **2**, 85–88.
11. Martasek, P. (1998) *Semin. Liver Dis.* **18**, 25–32.
12. Nordmann, Y. & Puy, H. (2002) *Clin. Chim. Acta* **325**, 17–37.
13. Elder, G. H., Hift, R. J. & Meissner, P. N. (1997) *Lancet* **349**, 1613–1617.
14. Tenhunen, R., Tokola, O. & Linden, I. B. (1987) *J. Pharm. Pharmacol.* **39**, 780–786.
15. Elder, G. H., Evans, J. O., Thomas, N., Cox, R., Brodie, M. J., Moore, M. R., Goldberg, A. & Nicholson, D. C. (1976) *Lancet* **308**, 1217–1219.
16. Nordmann, Y., Grandchamp, B., Phung, N., de Verneuil, H., Grelier, M. & Noire, J. (1977) *Lancet* **309**, 140.
17. Grandchamp, B. & Nordmann, Y. (1977) *Biochem. Biophys. Res. Commun.* **74**, 1089–1095.
18. Grandchamp, B., Phung, N. & Nordmann, Y. (1977) *Lancet* **310**, 1348–1349.
19. Martasek, P., Nordmann, Y. & Grandchamp, B. (1994) *Hum. Mol. Genet.* **3**, 477–480.
20. Kuhnel, A., Gross, U. & Doss, M. O. (2000) *Clin. Biochem.* **33**, 465–473.
21. Anderson, K. E., Sassa, S., Bishop, D. F. & Desnick, R. J. (1999) in *The Metabolic and Molecular Bases of Inherited Disease*, eds. Scriver, C. R., Beaudet, A. L., Sly, W. S. & Valle, D. (McGraw-Hill, New York), Vol. II, pp. 2961–3062.
22. Martasek, P., Camadro, J. M., Delfau-Larue, M.-H., Dumas, J.-B., Montagne, J. J., de Verneuil, H., Labbe, P. & Grandchamp, B. (1994) *Proc. Natl. Acad. Sci.* **91**, 3024–3028.
23. Taketani, S., Kohno, H., Furukawa, T., Yoshinaga, T. & Tokunaga, R. (1994) *Biochim. Biophys. Acta* **1183**, 547–549.
24. Rosipal, R., Lamoril, J., Puy, H., Da Silva, V., Gouya, L., De Rooij, F. W. M., Te Velde, K., Nordmann, Y., Martasek, P. & Deybach, J. C. (1999) *Hum. Mutat.* **13**, 44–53.
25. Martasek, P., Camadro, J.-M., Raman, C. S., Lecomte, M. C., Le Caer, J. P., Demeler, B., Grandchamp, B. & Labbe, P. (1997) *Cell. Mol. Biol. (Noisy-le-Grand)* **43**, 47–58.
26. Elder, G. H., Evans, J. O., Jackson, J. R. & Jackson, A. H. (1978) *Biochem. J.* **169**, 215–221.
27. Yoshinaga, T. & Sano, S. (1980) *J. Biol. Chem.* **255**, 4722–4726.
28. Lash, T. D., Mani, U. N., Drinan, M. A., Zhen, C., Hall, T. & Jones, M. A. (1999) *J. Org. Chem.* **64**, 464–477.
29. Akhtar, M. (2003) in *The Porphyrin Handbook*, eds. Kadish, K. M., Smith, K. M. & Guilard, R. (Elsevier Science, New York), Vol. 12, pp. 69–86.
30. Elder, G. H. & Evans, J. O. (1978) *Biochem. J.* **169**, 205–214.
31. Zaman, Z., Abboud, M. M. & Akhtar, M. (1972) *J. Chem. Soc. Chem. Commun.* 1263–1264.
32. Battersby, A. R., Baldas, J., Collins, J., Grayson, D. H., James, K. J. & McDonald, E. (1974) *J. Chem. Soc. Chem. Commun.* 1265–1266.
33. Kabsch, W. & Sander, C. (1983) *Biopolymers* **22**, 2577–2637.
34. Lamoril, J., Puy, H., Whatley, S. D., Martin, C., Woolf, J. R., Da Silva, V., Deybach, J. C. & Elder, G. H. (2001) *Am. J. Hum. Genet.* **68**, 1130–1138.
35. Medlock, A. E. & Dailey, H. A. (1996) *J. Biol. Chem.* **271**, 15765–15770.
36. Yoshinaga, T. & Sano, S. (1980) *J. Biol. Chem.* **255**, 4727–4731.
37. Reddy, V., Swanson, S. M., Segelke, B., Kantardjieff, K. A., Sacchettini, J. C. & Rupp, B (2003) *Acta Crystallogr. D* **59**, 2200–2210.
38. Colloc'h, N., Mornon, J. P. & Camadro, J. M. (2002) *FEBS Lett.* **526**, 5–10.
39. O'Brien, J. R., Schuller, D. J., Yang, V. S., Dillard, B. D. & Lanzilotta, W. N. (2003) *Biochemistry* **42**, 5547–5554.
40. Leesong, M., Henderson, B. S., Gillig, J. R., Schwab, J. M. & Smith, J. L. (1996) *Structure (London)* **4**, 253–264
41. Richardson, J. S. & Richardson, D. C. (1989) in *Prediction of Protein Structure and the Principles of Protein Conformation*, ed. Fasman, G. D. (Plenum, New York), pp. 1–98.
42. Miller, S., Lesk, A. M., Janin, J. & Chothia, C. (1987) *Nature* **328**, 834–837.
43. Jones, S. & Thornton, J. M. (1995) *Prog. Biophys. Mol. Biol.* **63**, 31–65.
44. Valdar, W. S. J. & Thornton, J. M. (2001) *Proteins Struct. Funct. Genet.* **42**, 108–124
45. Camadro, J. M., Chambon, H., Jolles, J. & Labbe, P. (1986) *Eur. J. Biochem.* **156**, 579–587.
46. Macieira, S., Martins, B. M. & Huber, R. (2003) *FEMS Microbiol. Lett.* **226**, 31–37.
47. Breckau, D., Mahlitz, E., Sauerwald, A., Layer, G. & Jahn, D. (2003) *J. Biol. Chem.* **278**, 46625–46631.
48. Hendrickson, W. A., Smith, J. L. & Sheriff, S. (1985) *Methods Enzymol.* **115**, 41–55.
49. Nicholls, A., Sharp, K. & Honig, B. (1991) *Proteins* **11**, 281–296.
50. Wallace, A. C., Laskowski, R. A. & Thorton, J. M. (1995) *Protein Eng.* **8**, 127–134.
51. Shakespeare, W., Yang, M., Bohacek, R., Cerasoli, F., Stebbins, K., Sundaramoorthi, R., Azimioara, M., Vu, C., Pradeepan, S., Metcalf, C., III, Haraldson, C., Merry, T., *et al.* (2000) *Proc. Natl. Acad. Sci.* **97**, 9373–9378.
52. Bohacek, R., Dalgarno, D., Hatada, M., Jacobsen, V., Lynch, B., Macek, K., Taylor, M., Metcalf, C., Narula, S., Sawyer, T., *et al.* (2001) *J. Med. Chem.* **44**, 660–663
53. Raman, C. S., Martasek, P. & Masters, B. S. S. (2000) in *The Porphyrin Handbook*, eds. Kadish, K. M., Smith, K. M. & Guilard, R. (Academic, New York), Vol. 4, pp. 293–339.
54. Venter, J. C., Remington, K., Heidelberg, J. F., Halper, A. L., Rusch, D., Eisen, J. A., Wu, D., Paulsen, I., Nelson, K. E., Nelson, W., Fouts, D. E., Levy, S., *et al.* (2004) *Science* **304**, 66–74.
55. Kohno, H., Furukawa, T., Tokunaga, R., Taketani, S. & Yoshinaga, T. (1996) *Biochim. Biophys. Acta* **1292**, 156–162.
56. Beinert, H., Kennedy, M. C. & Stout, C. D. (1996) *Chem. Rev.* **96**, 2335–2373.
57. Kahn, K. & Tipton, P. A. (1998) *Biochemistry* **37**, 11651–11659.
58. Fetzner, S. (2002) *Appl. Microbiol. Biotechnol.* **60**, 243–257.
59. Hiberty, P. C., Humbel, S. & Archirel, P. (1994) *J. Phys. Chem.* **98**, 11697–11704.
60. Sano, S. (1966) *J. Biol. Chem.* **241**, 5276–5283.
61. Bahnson, B. J., Anderson, V. E. & Petsko, G. A. (2002) *Biochemistry* **41**, 2621–2629
62. Imhoff, R. D., Power, N. P., Borrok, M. J. & Tipton, P. A. (2003) *Biochemistry* **42**, 4094–4100
63. Smith, D. M., Buckel, W. & Zipse, H. (2003) *Angew. Chem.* **42**, 1867–1870
64. Begley, T. P. & Ealick, S. E. (2004) *Curr. Opin. Chem. Biol.* **8**, 508–515.
65. Abell, L. M. & Schloss, J. V. (1991) *Biochemistry* **30**, 7883–7887.
66. Chen, H., Tseng, C. C., Hubbard, B. K. & Walsh, C. T. (2001) *Proc. Natl Acad. Sci. USA* **98**, 14901–14906.
67. Andres, J., Safont, V. S. & Tapia, O. (1993) *J. Phys. Chem.* **97**, 7888–7894.
68. Sessler, J. L. & Gale, P. A. (2000) in *The Porphyrin Handbook*, eds. Kadish, K. M., Smith, K. M. & Guilard, R. (Academic, New York), Vol. 6, pp. 257–278.
69. Lovie, G. V., Brownlie, P. D., Lambert, R., Cooper, J. B., Blundell, T. L., Wood, S. P., Warren, M. J., Woodcock, S. C. & Jordan, P. M. (1992) *Nature* **359**, 33–39
70. Nordmann, Y., Grandchamp, B., de Verneuil, H. & Phung, L. (1983) *J. Clin. Invest.* **72**, 1139–1149.
71. Doss, M., von Tiepermann, R. & Kopp, W. (1984) *Lancet* **323**, 292.
72. Lamoril, J., Martasek, P., Deybach, J.-C., da Silva, V., Grandchamp, B. & Nordmann, Y. (1995) *Human Mol. Genet.* **4**, 275–278.
73. Lamoril, J., Puy, H., Gouya, L., Rosipal, R., da Silva, V., Grandchamp, B., Foint, T., Bader-Meunier, B., Dommergues, J. P., Deybach, J.-C. & Nordmann, Y. (1998) *Blood* **91**, 1453–1457.
74. Phillips, J. D., Whitby, F. G., Warby, C. A., Labbe, P., Yang, C., Pflugrath, J. W., Ferrara, J. D., Robinson, H., Kushner, J. P. & Hill, C. P. (2004) *J. Biol. Chem.* **279**, 38960–38968.

Supporting Text

Materials and Methods

Crystallization. Human coproporphyrinogen oxidase (CPO) homodimer (subunit M_r 39,248) underwent time-dependent proteolytic cleavage at residue K230 (Fig. 1*B*, indicated by a ⊗), resulting in two fragments of M_r 13,000 and 26,000 and thus precluding its crystallization. To overcome this problem, we devised a cross-seeding strategy. First, we grew crystals of a bacterial CPO (*Chloroflexus aurantiacus*, a thermophilic phototroph). These crystals were obtained via sitting drop vapor diffusion setups at 22°C from a reservoir buffer containing 30% methylene propanediol (MPD) and 100 mM Tris·HCl, pH 6.5. Crystals obtained under these conditions belong to the hexagonal space group with cell dimensions 205.53 × 205.53 × 85.92 Å, $\alpha = 90°$, $\beta = 90°$, $\gamma = 120°$, and easily diffract X-rays to a Bragg spacing of 1.9 Å. Second, seed stocks of *C. aurantiacus* CPO crystals were prepared and used to streak seed into preequilibrated solutions containing fresh human CPO (40 $mg \cdot ml^{-1}$), 20% MPD, 0.05 M Tris·HCl pH 7.5, and 10 mM sodium citrate as an additive. Cubic-shaped crystals appeared after 48 h. We used the same strategy to grow crystals of human selenomethionine (Se-Met)-substituted CPO that, on their own, were incapable of nucleation. Mature crystals were stabilized in a glycerol-containing cryoprotectant before flash freezing in liquid nitrogen. The crystals belong to space group P23 with unit cell dimensions of $a = b = c = 112.72$ Å. There is one molecule in the asymmetric unit corresponding to a solvent content of ≈60%.

Structure Determination. Data from a native crystal were collected to a Bragg spacing of 1.5Å by using an ADSC (Poway, CA) Quantum-315 detector at beam line 9-2 of the Stanford Synchrotron Radiation Laboratory. Multiwavelength data on Se-Met human CPO crystals were collected on an ADSC Quantum-4 CCD detector at beamline 5.0.2 of the Advanced Light Source, Berkeley, CA. All data sets were integrated and scaled by using the HKL2000 package, and the statistics are reported in Table 1. Human CPO contains seven methionine residues, and we were able to identify four of these in native

Bijvoet Patterson maps before solving the structure. All seven selenium sites, however, were readily interpreted by using $F_{PH} - F_P$ coefficients as input to the direct methods option of SHELXS. Heavy-atom parameters were refined and phases were calculated at 1.9 Å resolution by using SHARP. Solvent flattening with SOLOMON and phase extension to 1.58 Å resolution against structure factor amplitudes from the native crystal produced an electron density map into which majority of residues could be built unambiguously by using the program O. The first couple of key refinement steps were performed by using the program BUSTER. This program was a *sine qua non* for modeling four loop regions that had no electron density when refined with CNS. All subsequent refinement calculations, however, were performed with CNS. After the addition and verification of water molecules, the model was further refined with REFMAC5 by using maximum-likelihood target and the translation-liberation-screw (TLS) refinement option. Statistics are reported in Table 1. The current model includes residues 119–454, one molecule of citrate, and 364 water molecules.

Equilibrium Analytical Ultracentrifugation. All data were analyzed with the ULTRASCAN software (10). Monte Carlo analysis was performed on a Linux Beowulf cluster and was used to determine 95% confidence intervals of all parameter estimates as described in ref. 11. All scans were fitted to a global model describing either a single ideal species, or a reversibly self-associating monomer-dimer or monomer-dimer-tetramer system. The generalized model is described by Eq. 1:

$$A_{280,r} = B + \sum_{i=1}^{n} \frac{i C_{ref,m} K_i}{(\epsilon_{280} l)^{i-1}} \exp\{i\sigma\} \quad [1]$$

where A_{280} is the observed optical density at 280 nm at some radius r in the cell, B is a baseline offset, i is the association state, n is the maximum association state, $C_{ref,m}$ is the concentration of the monomer at a reference radius r_{ref}, K_i is the equilibrium constant for the association of the *ith* state, ε_{280} is the molar extinction coefficient of CPO at 1 cm pathlength, l is the pathlength of the epon-filled centerpiece, and σ is given by:

$$\sigma = \frac{M\omega^2(1-\nu\rho)(r^2-r_{ref}^2)}{2RT} \quad . \quad [2]$$

Here, M is the monomer molecular weight, ω is the radial velocity, ν is the partial specific volume of CPO, ρ is the density of the buffer, R is the gas constant, and T is the temperature. Models with $n = 1$, 2, and 4 were fitted, and the variance, molecular weight, and equilibrium constants were determined. Hydrodynamic corrections for buffer conditions were made in ULTRASCAN according to data published by Laue *et al.* (12). The partial specific volume of CPO was estimated according to the method by Cohn and Edsall (13), and was found to be 0.7272 ccm/g. The molar extinction coefficient was estimated for 280 nm from the sequence of the denatured protein by the method of Gill and von Hippel (14).

Results

The results of the fitted equilibrium experiments are shown in Table 2. All three models suggest that in the examined concentration range, the protein is present almost exclusively in the dimeric form of CPO. The best variance, random residuals, and most accurate monomer molecular weight was observed when the data were fitted to a monomer-dimer-tetramer model. In this model, the monomer molecular weight was in excellent agreement with the molecular weight predicted from the protein sequence. The concentration distributions of the equilibrium scans and the monomer-dimer-tetramer fit and the combined residuals are shown in Fig. 7. The equilibrium constant for the monomer-dimer association suggested monomer only present in the low nanomolar range, whereas a slight amount of tetramer was predicted only for the highest concentrations examined in the equilibrium experiment. This small signal contribution of the tetramer species not unexpectedly translated into a low confidence for the monomer-tetramer equilibrium constant, which was confirmed by the Monte Carlo analysis.

1. Stura, E. A. & Wilson, I. A. (1990) *Methods* **1**, 38–49.

2. Otwinowski, Z. & Minor, W. (1997) *Methods Enzymol.* **276,** 307–325.

3. Sheldrick, G. M. (1997) *Methods Enzymol.* **276,** 628–641.

4. de La Fortelle, E. & Bricogne, G. (1997) *Methods Enzymol.* **276,** 472–494.

5. Abrahams, J. P. & Leslie, A. G. W. (1996) *Acta Crystallogr. D* **52,** 30–42.

6. Jones, T. A., Zou, J. Y., Cowan, S. W. & Kjeldgaard, M. (1991) *Acta Crystallogr. A* **47,** 110–119.

7. Bricogne, G. (1997) *Methods Enzymol.* **276,** 361–423.

8. Brunger, A. T., Adams, P. D., Clore, G. M., DeLano, W. L., Gros, P., Grosse-Kunstleve, R. W., Jiang, J. S., Kuszewski, J., Nilges, M., Pannu, N. S., *et al.* (1998) *Acta Crystallogr. D* **54,** 905–921.

9. Winn, M. D., Isupov, M. N. & Murshudov, G. N. (2001) *Acta Crystallogr. D* **57,** 122–133.

10. Demeler, B. (2004) ULTRASCAN (Department of Biochemistry, Univ. of Texas Health Science Center at San Antonio), Version 6.2.

11. Lambert, L. J., Schirf, V., Demeler, B., Cadene, M. & Werner, M. H. (2001) *EMBO J.* **20,** 7149–7159.

12. Laue, T. M., Shah, B. D., Ridgeway, T. M. & Pelletier, S. L. (1992) *Computer-Aided Interpretation of Analytical Sedimentation Data for Proteins: Analytical Ultracentrifugation in Biochemistry and Polymer Science,* eds. Harding, S. E., Rowe, A. J. & Horton, J. C. (R. Soc. Chem., Cambridge, U.K.), pp. 90–125.

13. Cohn, E. J. & Edsall, J. T. (1943) *Proteins, Amino Acids, and Peptides as Ions and Dipolar Ions* (Reinhold, New York).

14. Gill, S. C. & von Hippel, P. H. (1989) *Anal. Biochem.* **182,** 319–326.

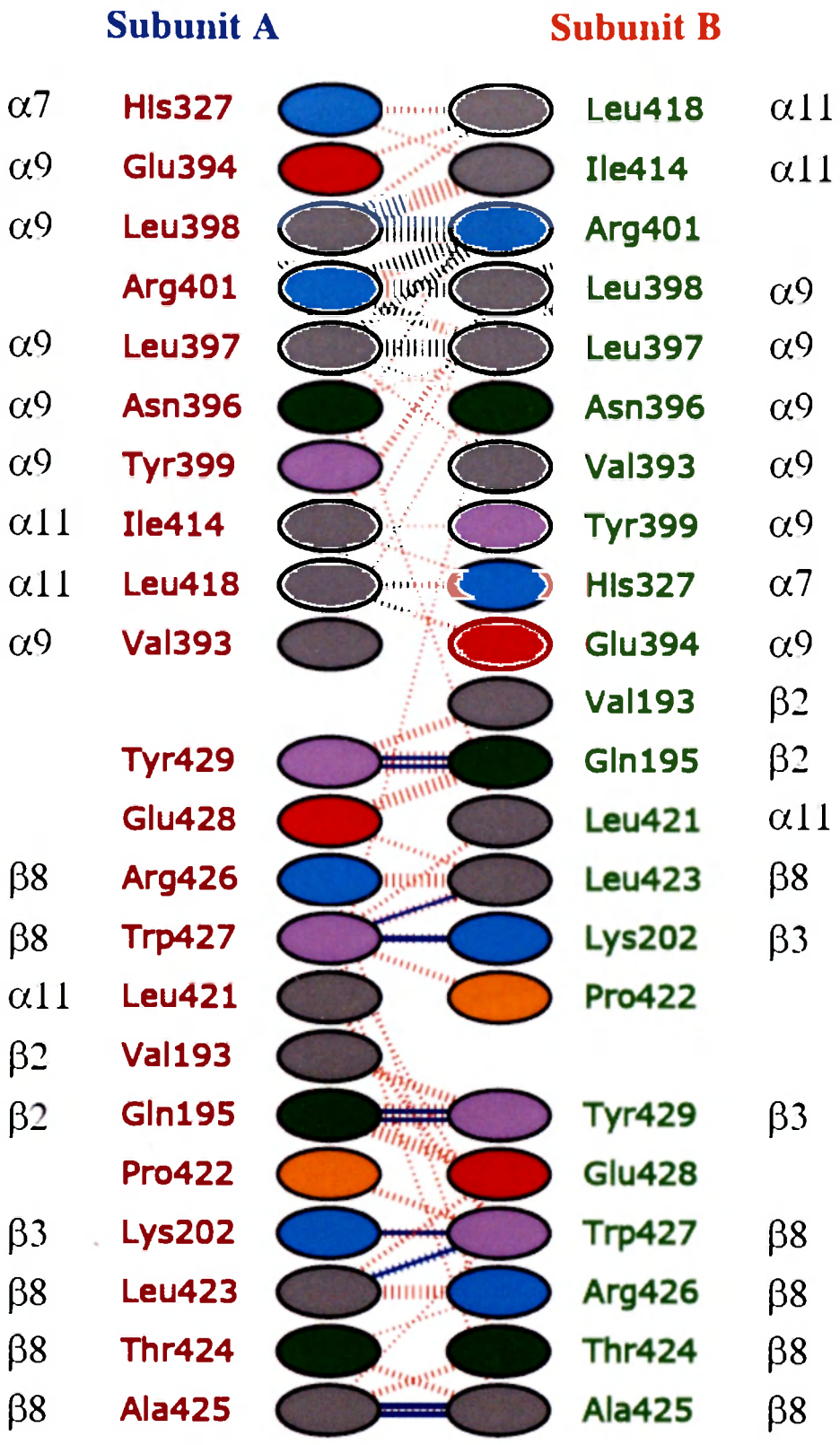

Fig. 6.

Residue interactions across the CPO dimer interface. Hydrogen bonds between any two residues are shown as blue lines. Each line represents one H bond. Nonbonded contacts are shown as red-striped lines whose width is proportional to the number of atomic contacts. The identity of the secondary structural element that harbors each residue is also shown.

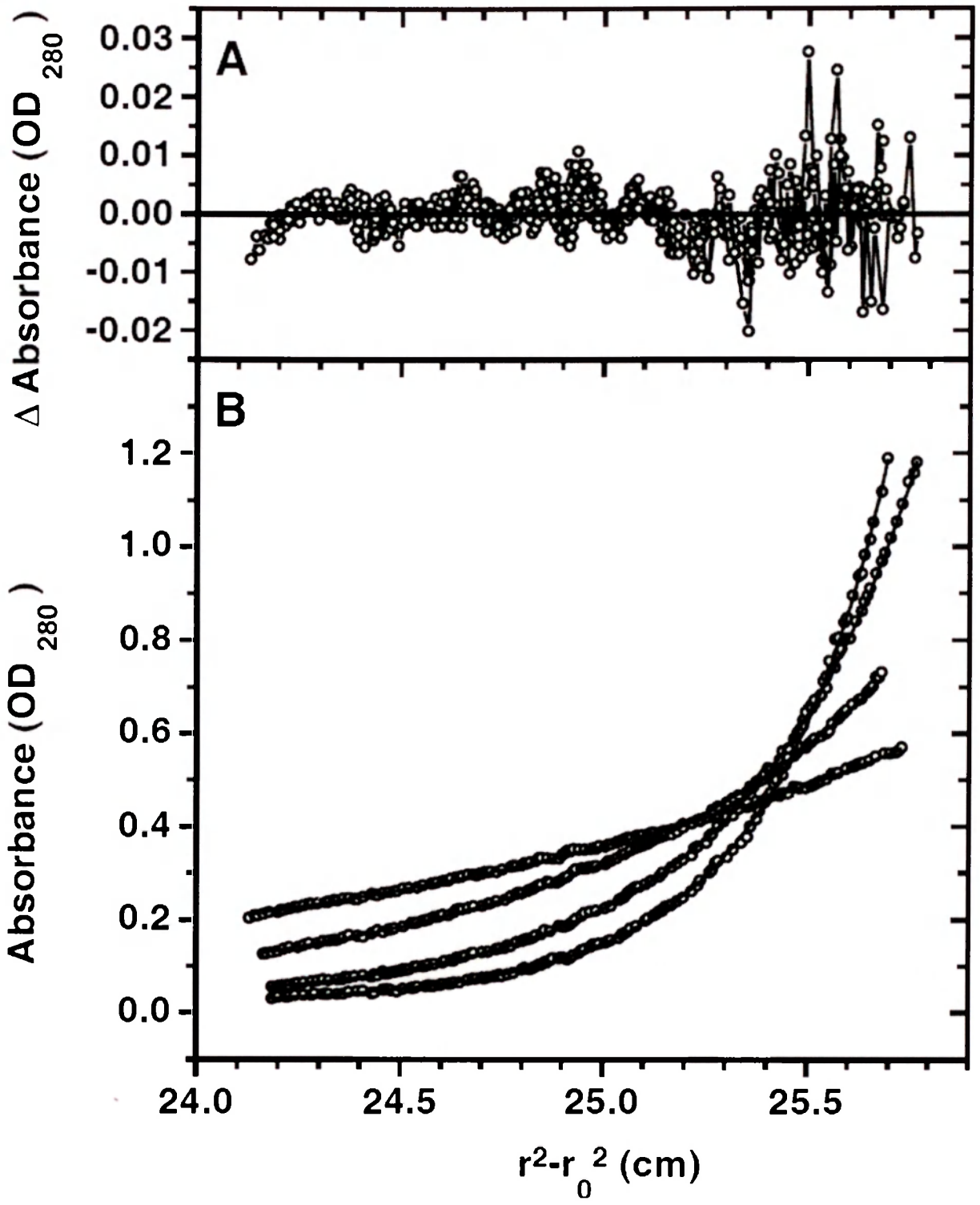

Fig. 7.

Human CPO is a homodimer in solution. Equilibrium scans at 280 nm are shown in *B* (gray circles) with the fitted model (monomer-dimer-tetramer, solid lines) overlaid. The best fit curve from a global analysis of two different starting concentrations at five different speeds yields a K_D = 0.5 μM. The combined residuals to all fitted scans are shown in *A*. The relative monomeric molecular mass of 39,370 determined from the equilibrium analysis is in excellent agreement with that calculated from the sequence, 39,248.

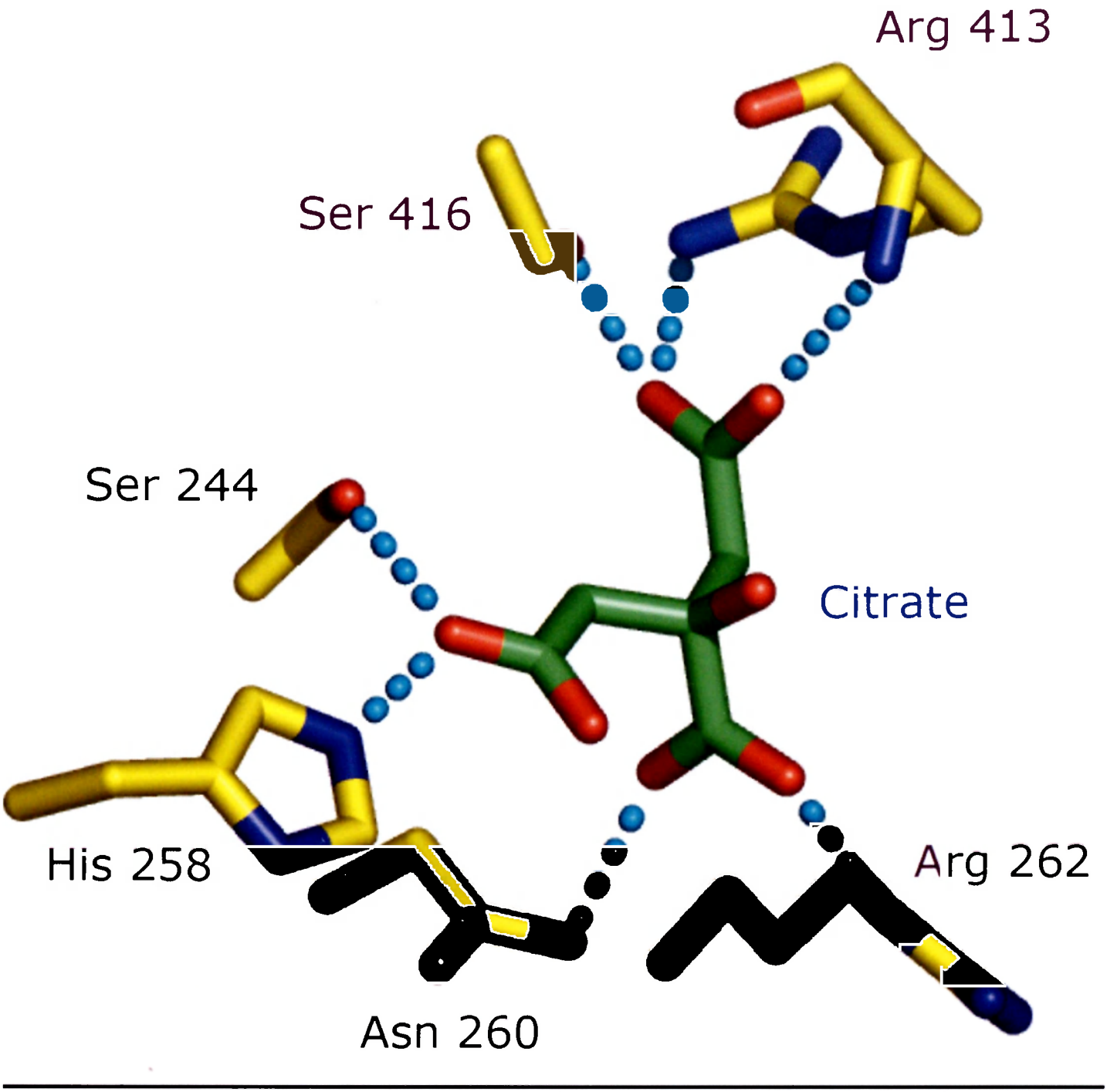

Fig. 8.

A three-dimensional view of citrate bound at the active site. Dotted lines (cyan) indicate hydrogen bonds.

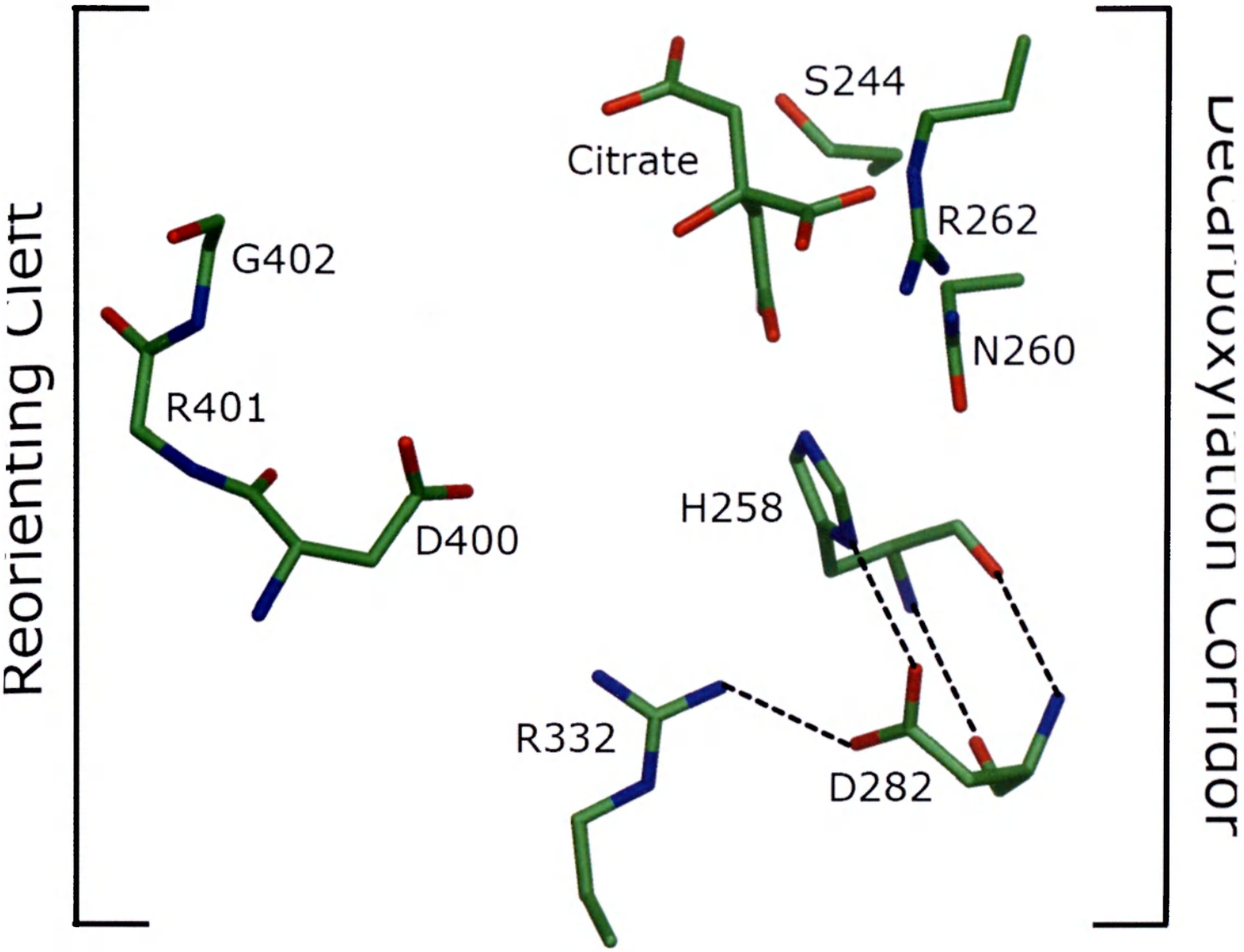

Fig. 9.

Configuration of the CPO active site. Residues identified in the decarboxylation corridor are invariant in >500 unique CPO sequences.

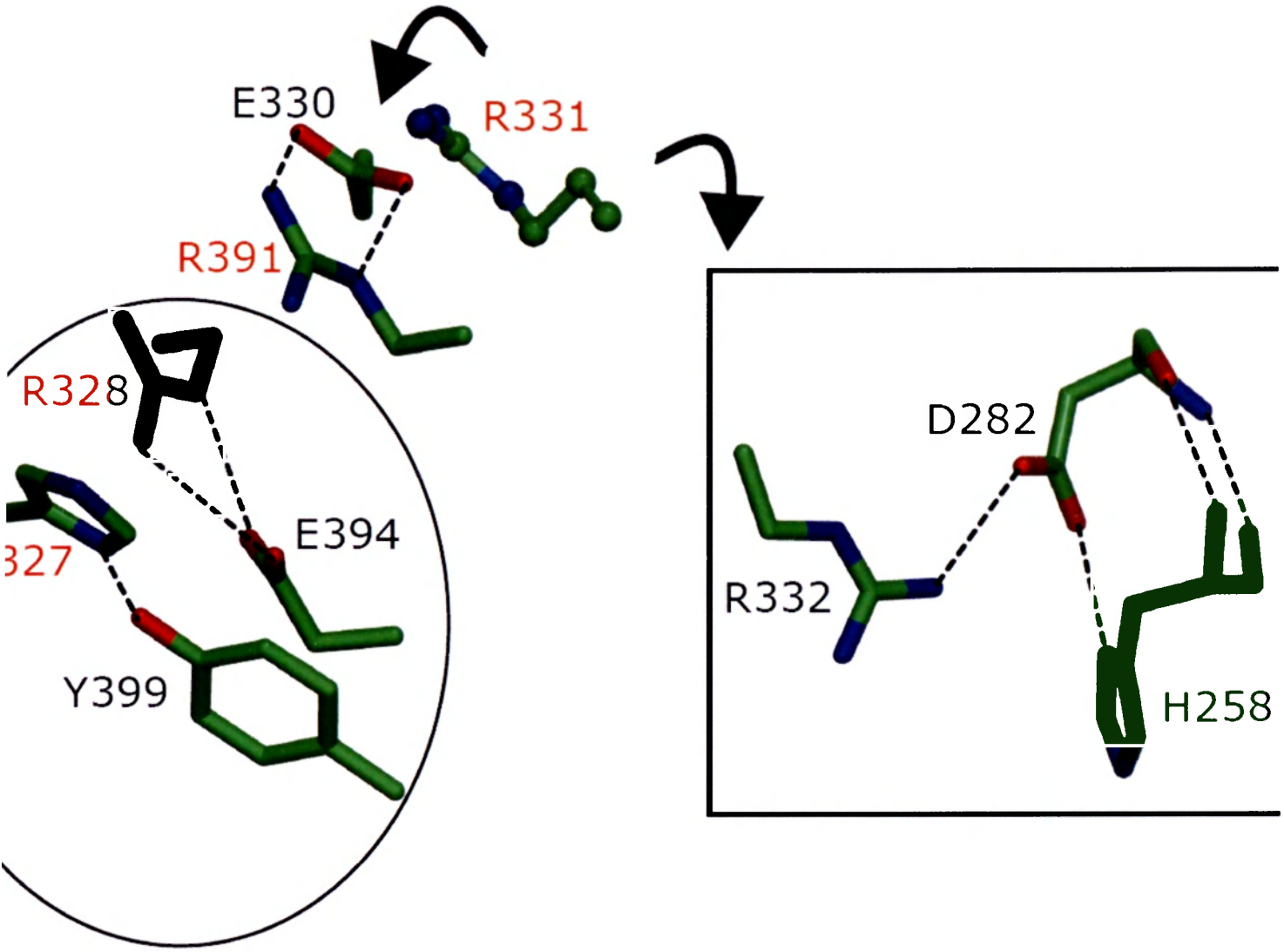

Fig. 10.

ıctural consequences of H327R, R328C, R331W, and R391W. Residues altered by HCP mutations shown in red.

Table 1. Data collection and crystallographic statistics

X-ray data				
Source	BL 9-2, SSRL	MAD phasing, BL 5.0.2, ALS		
Wavelength, Å	0.9536Å	0.9795Å	0.9796Å	0 9537Å
Space group	P23	P23		
Cell dimensions, Å	*a* = *b* = *c* = 112.720	*a* = *b* = *c* = 112.696		
Resolution, Å	1.58	1.9	1.9	1.9
Measured reflections	415,420	455,649	455,312	455,407
Unique reflections	65,081	37,254	37,201	37,188
Average *I* / σ(*I*) (last shell)	41.9 (2.5)	32.8 (2.2)	30.3(2.1)	27.4 (1.9)
Completeness *I* / σ(*I*) > 0, % (last shell)	99.5 (98.3)	99.6 (96.9)	98.9 (96.3)	98.6 (96.3)
R_{sym}* (last shell)	0.050 (0.670)	0.047 (0.563)	0.049 (0.593)	0.051 (0.592)
No. of selenium sites	7			
Figure of merit (sharp)	0.48			
Refinement				
Resolution range, Å	32.0–1.58			
Reflections used, |*F* / σ|*F*| > 0, working/test	61,774/3,293			
R_{cryst}† buster and refmac5 (outer shell)	0.186 (0.230)			
R_{free}‡ buster and refmac5 (outer shell)	0.210 (0.245)			
Average *B* factors, Å²				
Protein (2,880 atoms)	28.3§			
Citrate (12 atoms)	34.2			
rms deviation from ideality				
Bond lengths, angle distances, Å	0.011, 0.024			
Bond, torsion, and improper torsion angles, °	1.36, 22.3, 0.87			
Bonded B factors, Å² (main chain, side chain)	1.1, 1.6			
Ramanchandran plot, % (most favored, allowed)	93.8, 6.2			

SSRL, Stanford Synchotron Radiation Laboratory; ALS , Advanced Light Source.

*$R_{sym} = \Sigma | I - \langle I \rangle | / \Sigma \langle I \rangle$, where I and $\langle I \rangle$ are the measured and averaged symmetry-related intensities, respectively, of the same reflection.

†

$R_{cryst} = \Sigma | F_o - F_c | / \Sigma F_o$, where F_o and F_c are the observed and calculated structure factors, respectively.

‡

R_{free} is computed with 5% of the total reflections chosen randomly and unused throughout the refinement.

§

Wilson plot of the observed intensities versus resolution yields a B factor of 24.0.

Table 2. Equilibrium fitting results

Model	Variance	Monomer MM	Kd (1-2)	Kd (1-4)
Single ideal species	2 04 × 10^{-5}	77.7	N/A	N/A
Monomer-dimer	1.72 × 10^{-5}	49.5 (42.5, 56.5)	6.71 × 10^{-6} (1.55 × 10^{-6}, 2.92 × 10^{-5})	N/A
Monomer-dimer-tetramer	1.31 × 10^{-5}	37.6 (32.6, 42.6)	4.31 × 10^{-7} (1.13 × 10^{-7}, 1.25 × 10^{-6})	1.39 × 10^{-17} (4.36 × 10^{-19}, 4.44 × 10^{-16})

Eight equilibrium scans were globally fitted to the indicated models. Variance, monomer molecular mass (MM in kilodaltons), and dissociation constants are reported. Values in parentheses represent 95% confidence intervals from a 5,000-iteration Monte Carlo analysis of the fit. The single ideal species model did not fit well enough to warrant Monte Carlo analysis. Kd (1-2) refers to the monomer-dimer dissociation constants, which is reported in molar concentration units, whereas Kd (1-4) refers to the monomer-tetramer dissociation constant, which is reported in molar^3 concentration units.